ELECTROSTATIC ATOMIZATION OF VISCOUS LIQUIDS AND CERAMIC SUSPENSIONS

A thesis submitted for the degree of Doctor of Philosophy

by

Suwan Nalin Jayasinghe

Department of Materials

Queen Mary, University of London

Mile End Road

London E1 4NS

United Kingdom

ABSTRACT

The research carried out in this thesis describes the processing of liquids and ceramic suspensions, having a viscosity >100mPa s, using electrostatic atomization, mainly in the stable cone-jet mode.

Electrostatic atomization, also called electrospraying, refers to a process where a liquid or a suspension is made to flow through a needle. The liquid or suspension is subjected to a high voltage maintained between the needle and a ground electrode. Two major physical properties, namely electrical conductivity and viscosity, affect electrostatic atomization in the stable cone-jet mode and the investigations described in this thesis focussed on the latter.

Firstly, a set of liquid mixtures were prepared using distilled water and glycerol. The dc electrical conductivity of these mixtures were kept constant and the viscosity was varied. The mixtures were subjected to electrostatic atomization and in each case the mode of atomization, the cone/jet characteristics and relic sizes were studied as a function of viscosity. The effect of applied voltage on the cone-jet mode electrostatic atomization of glycerol having a viscosity of 1338mPa s was also investigated.

Secondly, the possibilities of electrostatically atomizing ceramic suspensions were studied in detail. Several alumina suspensions were used including one containing a high volume fraction of solids (20 vol.% - the highest filler loading attempted to date using any jet-based processing route). Applied voltage – flow rate – atomization mode maps were constructed for this suspension incorporating even pico-flow rate regimes. This is a new input into the aerosol science and engineering literature. This section also highlights the importance of controlling the applied voltage and flow rate as these parameters affect the jet diameter and relic/droplet size generated. The effect of the geometry of the ground electrode used for electrostatic atomization was also investigated. In particular, the use of a point-like ground electrode was studied for the very first time.

The third and most innovative facet of this research was the discovery of ceramic electrostatic atomization printing (CEAP) and the use of electrostatic atomization to produce ceramic foams. In CEAP a point-like ground electrode is used to focus the spray which was printed as characters, collection of characters and single tracks. This investigation was extended to explore the printing of multiple tracks produced with the aid of several needles and ground electrodes which worked simultaneously.

A ring shaped ground electrode was used to electrospray ceramic droplets onto a polyurethane template and this paved the way for the development of a new method to prepare open-cell ceramic foams with a very high porosity. This method was extended to prepare ceramic structures and complex components.

TABLE OF CONTENTS

ACKNOWLEDGEMENTS

A PhD is not complete without saying thank you to those who have firstly, given me the opportunity to read for my PhD but also who have taken the time to discuss and listen to all my ideas which they have in some form or another helped to bring alive.

I am very grateful to Queen Mary, University of London for providing me with a PhD fees scholarship.

I take this opportunity to thank not only an internationally well known researcher but also a sincere friend, he is none other than my research adviser Professor Mohan Edirisinghe. Thank you for your genuine, professional and personal advise given to me during my doctorate. The endless discussions and resulting arguments have brought about some explosive research and findings.

I sincerely thank Professor Steven Abbott of Autotype International Ltd who not only has helped me by providing materials for this research but by also allowing me to use the analytical laboratories at Autotype.

It is with lots of love that I thank my parents, Shirani and Ronnie for funding my first and second degrees in Mechanical Engineering at Brunel University, Uxbridge. I thank my father for the advice and motivation; which has driven me to innovate new things to benefit mankind. A thank you also goes out to both my brothers Anil and Ramesh for the pocket money and for bring my mother's home cooked food, which was always appreciated.

A thank you also goes out to Susan Gowler, who took on the task of listening and advising me on a lot of important issues and making my stay with her a very pleasant one.

Last but not least I like to thank Dr Martin Blissett, Dr Zofia Luklinska, Sandra Wells, Cath Pedley, John Caulfield, Steve Brooks, Michael Elliot, Vince Ford, Mick Willis, Robert Whitenstall in the Department of Materials and Ray Crundwell (Audio Visual) who have helped me more than the word thank you can ever mean.

Thank you all as I couldn't have done it without you,

Suman.

This research is dedicated to both my mother (Shirani Ardyne Jayasinghe) and father (Ronald Langston Jayasinghe) for their endless and unconditional love for me.

LIST OF TABLES AND FIGURES

Tables **Page**

Figures **Page**

PUBLICATIONS AND AWARDS

1. S.N.Jayasinghe and M.J.Edirisinghe, Relic and droplet sizes produced during electrostatic atomization of ceramic suspensions - *in preparation.*

2. S.N.Jayasinghe, M.J.Edirisinghe and S.Abbott, Electrostatic atomization of a ceramic suspension at pico-flow rates - *in preparation.*

3. S.N.Jayasinghe and M.J.Edirisinghe, A novel method of freeforming multiple tracks from concentrated suspensions. Journal of Materials Research Innovations, *in press.*

4. S.N.Jayasinghe and M.J.Edirisinghe, A novel method of forming open cell ceramic foam. Journal of Porous Materials, *in press.*

5. S.N.Jayasinghe and M.J.Edirisinghe, Obtaining fine droplet relics by electrostatic atomization of viscous liquids. Journal of Materials Science Letters, 2002, **21,** pp.371-373.

6. S.N.Jayasinghe, M.J.Edirisinghe and T.De Wilde, A novel ceramic printing technique based on electrostatic atomization of a suspension. Journal of Materials Research Innovations, 2002, **6**, pp.92-95.

7. S.N.Jayasinghe and M.J.Edirisinghe, Effect of viscosity on the size of relics produced by electrostatic atomization. Journal of Aerosol Science, 2002, **33**, pp.1379-1388.

8. S.N.Jayasinghe and M.J.Edirisinghe, Ceramic forming by electrostatic atomization. Proceedings of ILASS 2002, pp.389-394.

9. The 2002 De Montfort Medal for "Excellence in Science, Engineering and Technology"- by a younger scientist, for a poster presentation at the Houses of Parliament, United Kingdom.

10. The 2002 Leonardo Da Vinci Medal for "Excellence in Engineering" – by a younger engineer, for a poster presentation at the Houses of Parliament, United Kingdom.

CHAPTER 1

Introduction

1.1 Electrostatic Atomisation

Electrostatic atomization also known as electrospraying refers to a process where a liquid jet breaks up into droplets under the influence of an electrical force. The process can take place in many spray modes, e.g. cone-jet where a single jet evolves from the apex of a cone, multi-jet where several jets are observed (Jaworek *et al.,* 1996, 1998), and is influenced by many parameters such as liquid properties (mainly electrical conductivity and viscosity), liquid flow rate, the applied voltage and the geometry of the electrode system used to apply the voltage (Taylor 1964 and Jaworek *et al.,* 1999).

The spray mode of great interest to this research is the cone-jet mode, sometimes loosely referred to as the Taylor cone. This mode evolves as liquid passing through a needle at a controlled flow rate is exposed to an applied voltage held between the needle and a ground electrode. As a result of the electric stress, droplets forming at the tip of the needle are transformed to a conical shape. The applied electric field accelerates the surface charge to the apex of the cone and when the surface tension forces are overcome a jet appears at the tip of the cone (Cloupeau *et at.,* 1989, 1990, 1994, Grace *et al.,* 1994, Hartman *et al.,* 1997, Jaworek *et al.,* 1998, 1999).

Within a liquid the charge carriers are mainly ions. These ions collide with the liquid molecules, which results in the acceleration of the surrounding liquid. This

activity gives rise to a narrow liquid jet emerging at the apex of the cone. This jet can break up into a number of primary droplets with a narrow size distribution and a number of smaller secondary droplets and satellites (Cloupean *et al.*, 1989, Ganan-Calvo *et al.*, 1994, Gomez *et al.*, 1994 and Chen *et al.*, 1995).

The number of secondary droplets can be of the same order of magnitude as the number of the primary droplets. However, the total volume of these secondary droplets is much less than the volume of the primary droplets. Due to the excess of surface charge in the liquid cone and jet, the droplets are highly charged (Ganan-Calvo *et al.*, 1994 and Hartman *et al.*, 1999a, 2000).

The droplet size and charge depend mainly on the liquid flow rate, applied voltage and liquid properties such as electrical conductivity, viscosity, surface tension, electrical permittivity and density (Hartman *et al.*, 1999b).

Hartman *et al.*, (2000) reported that depending on the droplet production parameters, the primary droplet size ranges from nanometers (with production frequencies of the order of 10^8 Hz) to hundreds of micrometers (with production frequencies of approximately 10^4 Hz). A spray is found to evolve soon after the droplet production process is initiated. Electrical interactions between highly charged droplets and their differences in inertia are the main cause for size segregation in the 3-D conical shaped spray. The smaller droplets are at the extremities of the spray while the larger droplets are at the centre of the spray (Tang *et al.*, 1994, Ganan-Calvo *et al.*, 1994 and Hartman *et al.*, 1999a) but the intensity of separation can depend on the geometry of the ground electrode. This

segregation of droplets is caused by droplet inertia and gives rise to a near monodisperse distribution of droplets within the spray.

1.2 Contents of this Thesis

Chapter 1 introduces the process of electrostatic atomization. The chapter briefly introduces the mode of atomization mainly used in this research, namely the cone-jet mode. The aims and objectives of this research are clearly set out. Furthermore this section of the thesis underlines the scope of this research.

Chapter 2 is dedicated to a critical literature review. Various modes of electrostatic atomization, jet break-up theory and the droplet production processes are discussed in this chapter. This chapter underlines the importance of cone-jet mode and its controlling parameters. It also reviews solid freeforming and processing methods of ceramics relevant to this thesis.

Chapter 3 gives an in depth description of the experimental details. Here the preparation and characterisation of the test liquids and suspensions used for the research carried out in chapters 4, 5, and 6 are discussed. The equipment used for electrospraying and characterisation of collected relics are described in this chapter. A description of the design of the printing equipment is also incorporated in this chapter.

Chapter 4 introduces the first investigation carried out to understand the role played by the liquid viscosity and its effect on electrostatic atomization and the droplet production process. This investigation was very important as my research

was addressing electrostatic atomization of viscous liquids and ceramic suspensions with a viscosity >100 mPa s, previously not attempted. Furthermore, this chapter investigates the effect of applied voltage on electrostatic atomization and the droplet production process of a viscous liquid.

Chapter 5 investigates electrostatic atomization of ceramic suspensions. Relics and droplets formed from a variety of ceramic suspensions are compared. Applied voltage – flow rate – atomization mode maps have been constructed for the first time for a ceramic suspension over a very wide range of flow rate down to 10^{-12} m^3s^{-1} (pico flow rates). The effect of changing the geometry of the ground electrode configuration is discussed. It was found that both the plate and ring ground electrodes produces a 3-D conical shaped spray, however a point like ground electrode was found to focus the spray onto the pointed head. The effect of applied voltage and flow rate on the jet diameter and relic size is quantified.

Chapter 6 describes how combining the ability of focussing the ceramic spray together with a 2-axis motion control system resulted in the pioneering of a novel technique of ceramic solid freeforming called ceramic electrostatic atomization printing (CEAP). The relics produced using this printing technique was an order of magnitude less than those produced by existing jet-based printers. In this novel process we use needles which are approximately ten times bigger than those used in jet-based printers, hence processing suspensions containing a high volume fraction of solids will no longer pose a problem of blockage within the needles. This chapter goes onto further explore the potential of this technique by using a multi-needle and multi-ground electrode configurations for printing multiple-

ceramic tracks. In addition a pre-designed polyurethane foam was used as the template and exposed to the ceramic electrospray produced by a ring-shaped ground electrode. The electrosprayed polyurethane template was then sintered to 900^{0}C. The sintered 3-D shape was found to be porous, hollow and self-supporting. The porosity of the ceramic foam was calculated and found to be >95%. Furthermore the struts were solid and did not contain voids in their central regions. This investigation paved the way to a novel technique for forming open cell 3-D complex shaped ceramic foams.

Chapter 7 makes conclusions based on the research carried out in chapters 4, 5 and 6 and gives a clearer picture of further exploitation of this novel forming technique. It also addresses the need for shielding the spray, as scatter becomes a significant problem with the production of finer droplets. The precision deposition of finer droplets is an issue which needs to be addressed for this technique to supersede jet printing.

1.3 Aims and Objectives of the Research

The primary aim was to understand the fundamentals of electrostatic atomization of viscous liquids and suspensions. Electrostatic atomization has many modes of evolution and understanding the controlling parameters was a crucial part of the first step. Literature, gave an understanding as to what parameters are of importance to the atomization process. The main parameters affecting the process are the liquid flow rate, applied voltage and liquid properties such as viscosity, conductivity, surface tension, density and electrical permittivity. The main interest in this process was that this technique of processing liquids was capable of

producing a near monodisperse distribution of droplets and finally relics, which is of primary importance to the material scientist.

There are many modes evolving from this process, namely microdripping, unstable, intermittent cone-jet mode, cone-jet, spindle and multi-jet modes are a few among others. The production of a near monodisperse distribution of droplets was of great interest and therefore investigations were carried out to understand the physics behind the droplet production process. It is simply understood that shortly after the mode of atomization has taken shape a jet is formed from which droplets emerge. However, the theory and the physics behind the mechanisms of jet break-up needed to be comprehended. Literature mentions that the applied voltage, liquid flow rate and the surrounding gas play a major role in the electrostatic atomization of a liquid in the stable cone-jet mode. The jet can break-up in the cone-jet mode of atomization in the asymmetric varicose, the lateral kink (whipping) and the ramified break-up modes. The transition from asymmetric to lateral kink jet break-up mode produces a wider distribution of droplets within the spray (Hartman *et al.*, 2000).

Cone-jet mode of atomization was the focus of this research as the generation of a near monodisperse distribution of relics on a substrate was of importance to the research objectives in this thesis. Thus, experiments were carried out to understand the formation and the stability of the cone-jet mode of atomization. A near monodisperse distribution of relics will only be generated in a state where stable cone-jet mode of atomization is achieved. Literature illustrating previous research carried out on cone-jet mode did not address generating a near

monodisperse distribution of relics from high viscosity liquids and ceramic suspensions (>200m Pa s). Furthermore the properties of a high viscosity liquid and ceramic suspensions are much different from those liquids previously used in electrostatic atomization (e.g. heptane). In addition such liquids have different electrical conductivities and together dc electrical conductivity and viscosity largely determine the formation and stability of the cone-jet mode.

It was also important to know whether electrospraying a viscous liquid can be modulated to produce sets of near monodispersed droplets and relics. This led to the research of various combinations of applied voltage and flow rate at which it was possible to achieve the stable cone jet mode and generate smaller and smaller sets of near monodisperse distribution of relics.

A viscous ceramic suspension was electrosprayed in the stable cone-jet mode at which the smallest ceramic relics would be generated and deposited onto a preshaped 3-D polyurethane template. The thought was to spray the polyurethane template and sinter to burn out the polyurethane, creating a 3-D ceramic foam structure.

According to the literature, the use of a ring or plate shaped ground electrode configuration produced a 3-D conical shaped spray. However, literature did not address the effect of varying the geometry of the ground electrode to that of a point like shape. This idea of changing the geometry of the ground electrode and focussing the spray led to the innovation of ceramic electrostatic atomization printing which is a new genus of solid freeforming materials.

1.4 Scope of Research

The beneficiary of this research points towards the rapid prototyping and the microfabrication industries, which are interested in solid freeforming. This prototype proved that suspension-jet technology could be superseded by ceramic electrostatic atomization technology. The current solid freeforming industry is tending towards taking suspension-jet printing to industrial mass production. It is seen from this research that the droplet sizes generated using ceramic electrostatic atomization printing are approximately an order of magnitude lesser than that achieved by enhanced versions of suspension-jet printers.

This prototype can be further enhanced to accommodate some form of shielding which may reduce scatter by which the deposition of regular, very fine (a few micrometers in size) relics would be expected after allowing for spreading on a substrate. Once this issue is addressed and resolved the technology can be used by companies such as IBM for semiconductor manufacture, Hewlett-Packard for commercial and domestic based printers, INTEL and AMD for manufacturing microprocessors. Therefore a bright future is forecast for ceramic electrostatic atomization printing.

CHAPTER 2

Literature Review

2.1 Electrostatic atomization and its various spray modes

Electrostatic atomization is a process where a liquid jet breaks up into droplets under the influence of an electrical force. If this electrical force is greater than the surface tension force of the liquid being atomized the liquid at the exit of the needle changes from that of a growing droplet to one that is of a conical shape with a jet attached to its apex. The jet emerges as a result of the charged accelerating ions within the liquid. The balance of forces acting on the growing droplet manifests in different spray modes (Bailey 1988, Cloupeau *et al.*, 1994 and Grace *et al.*, 1994).

Due to the lack of standard nomenclature in the literature there exists a great deal of confusion in the identification of spray modes. There are a number of parameters affecting this process, e.g. liquid properties, liquid flow rate, the applied voltage, ground electrode configuration, and this gives rise to the evolution of a variety of modes of spray (Cloupeau *et al.*, 1990 and Jaworek *et al.*, 1999).

2.1.1 Micro-dripping, Spindle and Multi-spindle mode

A liquid passed through a needle at a constant flow rate, without exposure to an electric field produces liquid droplets at a very low frequency. The application of voltage gives rise to an electric field and an increasing applied voltage increases

the droplet production frequency. The applied voltage and the liquid flow rate dictate the first three different spray modes, namely micro-dripping, spindle and multi-spindle (Jaworek *et al.*, 1999 and Grace *et al.*, 1994).

Micro-dripping occurs at the lowest liquid flow rates and produces a narrow size distribution of droplets with a low droplet production frequency. This comes about when the electrical forces acting on the hanging droplet overcomes the surface tension forces of that liquid droplet. When the surface tension forces are overcome a small droplet is ejected (see **Figure 2.1a**). Once this droplet is ejected the liquid at the exit of the needle relaxes and this process is repeated with the growth of another drop (Cloupeau *et al.*, 1990).

The spindle and multi-spindle modes occur at higher flow rates accompanied by higher electrical forces. These two modes produce broader size distributions of droplets. In these modes a cone is formed at the exit of the needle with a jet emerging from its apex. The jet breaks up in to small droplets with high surface charge. Due to the formation of small droplets the electric field overcomes surface tension and this results in the pulsated formation of a cone and a jet in periodic fashion. Once the cone and jet are formed and the jet goes on to breaking into droplets the cone and jet relax, with the jet fragmenting into droplets and the cone moving to its relaxation mode at which time the process is repeated once again (see **Figure 2.1b**).

In the case of the multi-spindle mode this same procedure takes place but once the cone and jet are formed and the droplets are produced, the cone relaxes but

another cone and jet emerge from the opposite side of the first formed cone and jet (Jaworek *et al.*, 1999) (see **Figure 2.1c**).

2.1.2 Intermittent Cone-Jet and Stable Cone-Jet

Intermittent cone-jet mode, which generally lies between the spindle/multi-spindle and the cone-jet mode is similar to the cone-jet mode but what differentiates it from the cone-jet is its stability (see **Figure 2.2a**). Also, the intermittent cone-jet mode and the spindle mode can appear similar but the main difference between the two modes is that in the spindle mode the liquid jet skews and it is later ejected and fragmentates into droplets. The intermittent cone-jet mode is not skewed and the jet is not ejected (Cloupeau *et al.*, 1989).

When interested in producing a near monodisperse droplet distribution the stable cone-jet mode is most important. This mode of atomization is brought about when an exact balance is achieved between the electric field strength and the surface tension of the liquid being atomized and therefore this mode is stable and its characteristics described in section 2.6 depends on liquid properties, flow rate and applied voltage (see **Figure 2.2b**).

2.1.3 Multi-Jet and Rim Emission mode

Increasing the applied voltage increases the electric field strength and subsequently the electric field strength around the liquid cone increases to a point where the cone does not relax anymore. Hence droplet production stabilises with time (stable cone-jet mode) but further increase of the applied voltage results in it

transforming into the multi-jet mode and then to the rim emission mode (Luttgens *et al.*, 1992).

With increasing applied voltage the liquid cone of the stable cone-jet mode becomes increasingly shallower. At a critical applied voltage the cone becomes too small for the needle. When this occurs the cone moves from the centre of the needle towards the edge of the needle. Hence, the jet skews (Tang and Gomez, 1996). When the applied voltage is further increased a second cone is formed. With further increase in applied voltage more cones appear and the spraying mode becomes multi-jet (Cloupeau *et al.*, 1994). The base of these cones are still attached to one another (see **Figure 2.3a**). This is sometimes considered to be a multiple number of jets evolving from a single drop or it could be said that a single droplet having multiple spraying points has emerged (Grace *et al.*, 1994). If the applied voltage were increased further a large number of very small cones would appear from the rim of the needle (see **Figure 2.3b**). It has been suggested that these large numbers of small jets are formed from a thin layer of liquid and this is referred to as the rim emission mode (Grace *et al.*, 1994).

2.1.4 Simple-Jet and Ramified

If the liquid flow rate is relatively high, the liquid has a larger kinetic energy which can be too large to be compensated for with the surface tension. When this occurs a jet is formed, which later breaks into droplets. This is the simple-jet mode (Bailey 1988). Here the purpose of the electrical forces are to mainly break the jet into droplets (see **Figure 2.4a**). If the electric field is increased around the simple jet, this can cause a radial electrical stress which overcomes the surface tension.

When this takes place smaller jets begin to emerge from the main jet which appear to have a shape similar to that of a fir tree (see **Figure 2.4b**). These small jets produce or break up into droplets with a polydisperse droplet distribution and this is called ramified spray (Jaworek *et al.*, 1999).

2.2 Jet Break-up theory

During cone-jet mode electrostatic atomization the electric field acting on the liquid cone tangentially accelerates the charge on the surface of the liquid toward the cone apex. This acceleration of the surface charge gives rise to a jet which emerges at the apex of the cone. At this stage the jet contains a relatively large charge. This charged jet later breaks up into primary, secondary and satellite droplets (Cloupeau *et al.*, 1989, Jaworek *et al.*, 1999, Hartman *et al.*, 1999b, 2000).

The theory behind jet break-up during cone jet mode electrostatic atomization have been studied by many workers. Rayleigh (1878) presented a theory which incorporated small varicose like instabilities on the liquid jet. His theory and calculations assume that electrical stresses are zero and the jet velocity is constant. Hence Rayleigh's theory was able to predict the growing varicose instability within the liquid jet. Later Weber (1931) modified Rayleigh's theory to incorporate liquid viscosity. His modified theory illustrates that the increase in viscosity gave a longer dominant wavelength. As the jet breaks up due to instabilities the wavelength of the jet is very much the fastest growing wavelength which is sometimes referred to as the dominant wavelength. This theory underwent further modification in 1968 by Yuen. Yuen incorporated non-linear aspects to the jet break up theory. Yuen's theory illustrated that the longer the

fastest growing wave length, the volume of the secondary and satellite droplets emerging from jet during break up becomes larger. Jameson (1970) used this theory to evaluate the droplet size distribution as a function of wavelength.

As the electrical stresses play a major role in the electrostatic atomization process charge is a foremost influence and can have a significant effect on the jet break up process. Melcher (1963), Parkin (1973) and Turnbull (1992) contributed to the understanding of the jet break up due to the charge on the jet induced by electrical stresses. Turnbull and Melcher assumed the liquid to be an insulator and perfect conductor, respectively. However, Parkin measured the growth rate of perturbations on a liquid jet, which he assumed to be a perfect conductor. The results presented by Parkin showed that Melcher's assumption was realistic and valid when compared with experimental results.

Cloupeau *et al.*, (1989) and Gomez *et al.*, (1991) both postulated that a liquid jet breaking up into droplets during the electrostatic atomization in the cone-jet mode was not in anyway influenced by the surface charge. Later this was validated with theory presented by Schneider *et al.*, (1976) and Neukermans (1973).

Hartman *et al.*, (1999a, 2000) presented a sound foundation to the understanding of jet break up. They investigated the jet break up mechanisms in the cone-jet mode as a function of liquid flow rate. Thus, jet break up mechanisms can be categorized into many flow rate regimes, as illustrated in **Figure 2.5**. The first regime does not involve formation of secondary and satellite droplets. The liquid

necks and produces a filament which later breaks into the first primary droplet. The area at the tip of the filament exhibits high pressure. This increase in pressure in the air surrounding the high jet velocity and/or the acceleration caused by the electric field causes the liquid in the filament to flow back into another primary droplet. The second regime is where the filament breaks near the second primary droplet before the liquid can flow back and form the primary droplet. In this regime it was seen that between every two primary droplets a secondary smaller droplet is formed. The third regime is where the filament between the main and secondary droplet breaks into a third droplet which is smaller than the main and secondary droplets. The fourth regime occurs when lateral or kink instabilities start to take effect. The liquid filament and the secondary droplets formed leave the jet in a non-linear manner. Hartman and co-workers refer to this regime as the filament whipping regime. In the fifth regime the entire jet starts to whip and is referred to as gentle whipping by Tang and Gomez (1996).

The jet break up regimes are clearly seen to be influenced by both varicose and kink instabilities. Hartman and co-workers report that in the forth and fifth regimes the width of the size distribution of the primary droplets start to widen significantly. Also, the wave number at the point of jet break up increases slightly with the increase in flow rate but for uncharged jets, fewer secondary droplets and satellites are produced with the increase in wave number. It is interesting that in the cone-jet mode of electrostatic atomization the opposite occurs. This is explained by the surface charge which is in the jet (Hartman *et al.*, 2000). Hartman and co-workers also show that with increase in the flow rate, the current through the liquid cone is greater and this results in the increase in the normal

electrical stress to surface tension ratio. This gives rise to short waves which can break up faster and therefore the liquid filament breaks a second time before it has time to flow back causing the formation of secondary and satellite droplets.

At higher flow rates the surface charge induces the whipping motion of the liquid jet to take shape. Hartman and co-workers also mention that jet break up regimes depend on the applied voltage and the diameter of the needle used in the atomization process. For a large needle diameter the current is almost independent of the applied voltage. Since the current determines the surface charge, the jet break up regime is not altered. However, for a finer diameter needle the current depends of the applied voltage. This implies that the jet break up regime depends on the applied voltage during the electrostatic atomization process. Hartman and co-workers conclude that to reduce the number of secondary and satellite droplets the current through the liquid cone should be low as possible, and should also have a flow rate which is approximately to the minimum flow rate possible for the liquid under test.

2.3 Importance of the Cone-Jet Mode

The cone-jet mode has been briefly described earlier. However, as the production of near mono-disperse droplets is of utmost importance to this research, formation and stability of this mode is discussed here in greater detail. In contrast, most other modes, e.g. spindle, multi-spindle, multi-jet, ramified produce a polydisperse distribution of droplets and relics. Microdripping produces a near monodisperse spray, but is know to have a low production frequency. The droplet size produced by the simple jet mode is determined by the inner diameter of the

needle. Therefore, if the droplets desired from a viscous liquid or a ceramic suspension were a few micrometers in size, the needle would have to have a similar inner diameter with an increased risk of blocking in the fine needle.

Theory states that the multi-jet and rim-emission modes can produce near-monodisperse droplets as the liquid flow rate per spraying point is the same as for a cone-jet and the number of spraying points per needle is much higher than that in the cone-jet mode but this requires practical verification.

Electrostatic atomization or electrospraying in the cone-jet mode was first mentioned in the De Magnete by Gilbert in 1600. Gilbert presented his observations based on a piece of amber, which attracted liquid droplets from a dry surface changing their shape to that of a cone. However, Zeleny (1914, 1915 and 1917) was the first to describe this process in a scientific paper.

Electrostatic atomization in the cone-jet mode can be described as at least three different processes mainly based on the work of Jaworek *et al.*, 1989, Cloupeau *et al.*, 1990, Fernandez De la Mora *et al.*, (1994) and Ganan-Calvo *et al.*, (1997). The first processes can be described as follows. The electric field induces a surface charge on the cone. As the charge within a liquid is mainly carried by ions, this charge is carried on the surface of the cone by these liquid ions. Due to the surface charge on the liquid cone, the normal electric field acting inside the liquid cone is smaller when compared to the normal electric field outside it. The tangential electric field accelerates the ions on the surface of the liquid towards the cone apex. The acceleration and the shape of the liquid cone are a result of the

balance of several forces - surface tension, gravity, those resulting from electrical stresses, inertia and viscosity as shown in **Figure 2.6**.

Taylor (1964) was the first to describe the balance between surface tension and normal electrical stress. However, Taylor's mathematical explanation is only validated in instances where there is no jet and no tangential electrical stress. This is too simplistic for as the real process does include jetting. There are two main charge transport mechanisms in the liquid. Firstly, due to the electric field within a charged liquid, transport occurs through conduction. Secondly, due to the tangential electric field, the ions within the liquid are accelerated to the apex of the cone. The velocities of the liquid are mainly governed by the flow properties of the liquid. This mechanism is referred to as charged convection. The shape of the cone is primarily determined by the balance between surface tension, normal and tangential electrical stresses and gravity. The liquid cone can be considered to be a perfect conductor having a low electric field strength within the liquid cone. As transport of charge primarily occurs due to conduction, when moving from the cone base towards the cone apex, the electric fields, surface charge and axial liquid velocity of the liquid become dominant. This results in a higher charge transport due to charge convection and a significant contribution from kinetic energy to the cone shape. In the liquid jet charge transport occurs mainly through charge convection.

The second process is jet break into droplets. The jet emerging from the cone apex breaks into a near bimodal distribution of droplets. This size distribution occurs because the jet breaks up into primary droplets which are found to have a narrow

size distribution with a smaller number of secondary droplets. In some cases between forming of main and secondary droplets a third type of droplet, namely satellites, appear as shown schematically in **Figure 2.7** and experimentally verified by Hartman *et al.,* (2000) as shown in **Figure 2.5**. The number of secondary droplets can be similar to that of the primary droplets. However, the total volume of the primary droplets are much larger than that the secondary droplet volume.

The third process occurs after a spray evolves producing droplets from the cone-jet mode of atomization. The electrical interaction between adjacent droplets causes a size segregation, where large droplets are found at the centre of the spray while smaller ones are at the extremities of the spray (Ganan-Calvo *et al.,* 1994, Hartman *et al.,* 2000). If the highly charged droplets evaporate, the Rayleigh limit of droplet charge can be reached. If this takes place droplet fission can occur which can significantly change the size distribution. This generally takes place if due to the droplet charge, the electrical stress becomes larger than the surface tension. Then the droplets become exceedingly unstable and a number of smaller droplets will be expelled and this is known as "Coulomb Explosions".

Rayleigh showed that:

$$q_R = 8\pi(\gamma\varepsilon_0 r_d^{\,3})^{\frac{1}{2}} \qquad 2.1$$

where q_R is the Rayleigh charge limit (C), γ is the surface tension (Nm^{-1}), r_d is the droplet radius (m) and $\varepsilon_0$is the dielectric constant in a vacuum (Fm^{-1}). Schweizer

et al., (1971) verified this equation using their experimental results. Tang *et al.,* (1994) have claimed that droplet charge for electrostatic atomization in the cone-jet mode is lower than the Rayleigh charge limit. However, at higher flow rates the droplets are closer to the Rayleigh charge limit that at lower flow rates. Law (1989) showed that the evaporation rate of a liquid is not influenced by the charge of the droplets if they are >0.1mm. He also showed that charge is not dissipated by evaporation but solely by the impact of ions and electrons from the surrounding gas.

In some cases the surrounding gas can play a major role by electrically discharging the atomization process as shown by Hayati *et al.,* (1987) and Cloupean *et al.,* (1989). This discharging of the jet can significantly disturb droplet production. Hartman *et al.,* (1997, 1999a and 2000) calculated the current produced during electrical discharge and showed that it is of the same order of magnitude as the current without discharge and that the droplet production process is disturbed at this stage. If the discharge produces an irregular pulsating current, the droplet production process is completely disturbed and a significantly wider distribution of droplets are formed. If the current is steady, then the spray is sometimes found to contain a narrow size distribution of droplets. However, the droplets produced during any one of the above cases are significantly different to those droplets produced in the cone-jet mode without discharge.

Hartman *et al.,* (1999a, 2000) also mention that it is most likely for discharge to start from the cone apex from where the jet emerges. The discharge process can be reduced by applying a positive applied voltage to the needle, changing the gas

around the needle and cone, spraying in a vacuum, by increasing gas pressure and by controlling the surface tension of the liquid. The lowest probability of discharge is generally found at the minimum flow rate of the liquid. A needle with a small diameter is susceptible to a smaller probability of discharge when compared to that with a larger diameter. Although the electric field strength at the liquid surface is determined by the needle diameter, the divergence of the electric field around the cone is larger for a smaller needle.

2.3.1 Parameters influencing the droplet production

The work of Kim *et al.,* (1976), Gomez *et al.,* (1990), Fernandez De la Mora *et al.,* (1990, 1994), Ganan-Calvo *et al.,* (1997), Chen *et al.,* (1997), and Hartman *et al.,* 1997, 1999a, 1999b and 2000) show that liquid properties such as the dc electrical conductivity, viscosity, surface tension, relative permittivity and density, and major process control parameters such as applied voltage and flow rate play an important role in the electrostatic atomization process in the cone-jet mode. Other factors that influence this process are the ground electrode configuration, the shape of the capillary, wettability of the material and gravity.

2.3.1.1 DC electrical conductivity

This is one of the main parameters influencing electrostatic atomization. If the conductivity is too low, the liquid cannot be sprayed in the cone-jet mode except, when extra charge is produced in the liquid drop at the exit of needle. Kelly (1990, 1994) developed a technique where he added extra charge into the liquid by electrical discharge within the liquid. The charge will ultimately move towards the liquid surface. Due to this charge a tangential electric stress will occur at the

liquid surface. For liquids with a high conductivity, creating extra charge is not necessary as conductivity of the liquid will be sufficient to pass a current from the needle to the liquid surface. Electrostatic atomization of a liquid with a high conductivity depends on the liquid flow rate and requires electrical discharge of the jet not to take place due to the surrounding gas (Hartman *et al.*, 2000).

2.3.1.2 Applied voltage

The applied voltage is another critical parameter contributing to the stability of cone-jet mode. Firstly, electrostatic atomization is an electric field driven process. The electric field strength depends not only on the applied voltage but also on the electrode configuration and on the shape of the liquid cone. The shape of the liquid cone depends on the electric field strength. This makes it difficult to include the applied voltage and more so the electric field strength into analytical equations. If the applied voltage is too low, then the spraying process is microdripping, spindle or the intermittent cone-jet. If the applied voltage is too high, then spraying is in rim-emission or multiple-jet mode (Luttgens *et al.*, 1992, Ganan-Calvo *et al.*, 1997).

If the applied voltage across the electrodes increases and the supply of liquid to the cone remains the same, then the liquid flow rate into the jet will increase and the liquid cone will become smaller. As a result, the increased electric field strength will be reduced and the flow rate towards the jet will decrease again until a stable jet with the appropriate flow rate into the jet is formed. This adjustment of the cone size reduces the effect of the increase in applied voltage. Consequently the influence of the applied voltage on the current and the droplet size is small.

2.3.1.3 Viscosity

Viscosity influences the jet break-up process and as a result has a significant effect on the droplet production. Weber (1931) showed that an increase in viscosity will lead to a lower dominant wave number. A lower dominant wave number results in a small increase in the primary droplet size and a significant increase in the size of secondary droplets. However, in most cases, the influence of viscosity on the droplet size is not considered. The results and discussion chapters of this thesis contain an extensive description of the effect of viscosity.

2.3.1.4 Flow rate

The liquid flow rate also has a significant influence on the spraying process. If the flow rate is low, the spraying process is not stable because the liquid cone relaxes to a droplet shape periodically. Above a minimum flow rate, the droplet production process becomes stable and the size distribution of the primary droplets become narrow. However, if the flow rate is increased above a critical value, then the droplet size distribution becomes more polydisperse. The polydispersity increases with the increase in flow rate and the process becomes more unstable with increasing flow rate. Equations presented by Ganan-Calvo *et al.*, (1997) and Rosell-Llombart *et al.*, (1994), show that the minimum flow rate is dependent on the liquid properties such as electrical conductivity and surface tension.

2.3.1.5 Surface tension

For the formation of stable cone-jet, the surface tension must be overcome by the electric stresses. The higher the surface tension, the larger the required electric field strength and this results in a greater probability of electrical discharge

occurring due to the surrounding air. A larger electric field will result in a higher surface charge on the cone. This results in a higher electric current through the cone and jet. A higher current results in a higher droplet charge. The droplet size is considered to be independent of the surface tension. Ganan-Calvo *et al.*, (1997) considered the droplet size to be independent of the surface tension for liquids which are highly conductive.

2.3.1.6 Relative permittivity

The relative permittivity of a liquid determines the polarization of it in an electric field. Polarization reduces the electric field within a liquid. The time taken for the charge to reach the liquid cone is determined by the liquid conductivity and the induced electric field. Fernandez de la Mora *et al.*, (1994) used a time constant presented by Velenga *et al.*, (1965) (see **eq. 2.2**) to derive equations to determine current I and the jet diameter d_j (see **eqs. 2.3 and 2.4**).

$$\tau = \frac{\varepsilon_0 \varepsilon_r}{K} \qquad 2.2$$

$$I = f(\varepsilon_r)\left(\frac{\gamma Q K}{\varepsilon_r}\right)^{\frac{1}{2}} \qquad 2.3$$

$$d_j = 0.4\left(\frac{Q \varepsilon_0 \varepsilon_r}{K}\right)^{\frac{1}{3}} \qquad 2.4$$

where K is the conductivity in $Sm^{-1}$and ε_r is the relative permittivity. I is the current in A and d_j is the jet diameter in m. Q is the liquid flow rate in m^3s^{-1}, ρ is

the density in kgm^{-3}, ε_0 is relative permittivity of free space in Fm^{-1} and γ is the surface tension in Nm^{-1}.

2.3.1.7 Density

Increase in liquid density decreases the minimum flow rate required for cone-jet mode electrostatic atomization. The scaling laws presented by Ganan-Calvo *et al.*, (1997) neglect density but Hartman *et al.*, (2000) show that the increase in density influences the droplets production process in the varicose jet break-up regime. In the jet break-up theory presented by Hartman *et al.*, (2000) density is linked with the acceleration and diameter of the liquid jet which in turn determines the droplet production process.

2.3.1.8 Ground electrode configuration

The needle is usually used as one of the electrodes. The geometry of the ground electrode determines the trajectory of the droplets. A ring shaped ground electrode not only segregates larger droplets within a spray in the central regions, but also produces very fine droplets which are found to recirculate about the ring. A plate-shaped ground electrode has a similar effect but does not accompany recirculation of droplets. The use of a point-like ground electrode is addressed in this thesis.

2.3.1.9 Capillary Shape and Material Wettability

The shape and the wettability of the needle material can significantly influence the shape of the cone formed, the stability of the jet and the mode of atomization. Cloupeau and Prunet-Foch (1994) state that very small changes in capillary shape or wettability can cause a difference in the spraying mode. Cloupeau and Prunet-

Foch (1989) also state that a change in wettability of the capillary causes liquid to accumulate at the exit of the needle, forming a meniscus over all or part of the perimeter of the needle. The liquid accumulated in this way periodically emits a jet which can contain fine droplets and then finally detaches as a large droplet. This cycle is repetitive. At the base of the cone, near the needle, the shape of the cone strongly depends on the shape of the needle, so an unstable behaviour at the liquid-capillary interface will give rise to an unstable jet.

2.4 Manufacturing Processes

The 21st century is demanding, mankind is constantly evolving and has done so in leaps and bounds, which has had an enormous effect on various industries. The manufacturing industry is constantly undergoing changes to stay in tune with the demand for novel manufacturing techniques.

The manufacturing process backdates to the 5th millennium BC (Bourriau, 1981) where man used clay to create shapes. This historical manufacturing process is the antecedent of the solid freeforming process, which is referred to as the fused deposition modelling, where the material, for e.g. clay, can be extruded linearly and combining this process with a computer control positioning system builds the shape required (Agarwala *et al.,* 1996a). The best description of solid freeforming is, the building of a house with bricks, which are placed on top of each other, creating the 3-D structure as opposed to subtracting space from a solid block. Hence SFF does not require moulds/walls to shape or hold the incrementally created structure.

Many scholars tend to classify the manufacturing process in to four principal categories namely casting, deformation, machining and joining (Lindberg 1990, Amstead *et al.,* 1969, Mair, 1993 and Ghosh *et al.,* 1986). The casting category can include sand, die, solvent and slip based processes and microcasting methods such as LIGA (Lithografie Galvanoformuing Abformung) and even injection moulding. Casting is where the material undergoes a change in state against the confining boundaries that define the shape. These changes in state involve phase changes, solvent evaporation and phase separation. In the second category dies, rolls and formers are used for compaction, drawing, forging, rolling and spinning. And in most cases these processes have undergone computerisation. Machining includes carving, turning, milling, electro-discharge machining, laser machining, and etching, while joining methods such as welding, soldering, brazing, adhesive bonding and the use of fasteners allow for manufacturing prefabricated components to be assembled in order to achieve a higher level of complexity.

Solid freeform fabrication is a genus of manufacturing. And as we demand precision in this day and age this method has become computer controlled. This has come about with the technological advancements in the expansion of the computer data handling capacity currently available on personal computers. The SFF method not only demonstrates its potential in the rapid prototyping industry but it shows its importance in the mass production line (Kruth, 1991). This method has further been enhanced to vary the composition of materials throughout the production of a complex component. This makes SFF a unique manufacturing technique as it has the capabilities of creating a 3-D functional

gradient in multi-phase ordered composition. Solid freeforming embraces the concept of design while keeping to a very high integrity.

The earliest form of solid freeforming which used a personal computer to create and form a 3-D shape was stereolithography. This process paved the way for rapid prototyping. In stereolithography a 3-D shape is formed with the precision movements of a personal computer synchronised with a laser. This process merges computing with manufacturing. This manufacturing technique meant that the human intervention was at a minimum (Pham *et al.*, 1998), product development cost and lead times were significantly reduced.

2.5 Ceramic solid freeforming

Solid freeforming has been demonstrated successfully for rapid prototyping of plastic components (Pham *et al.*, 1998). With the advancement in engineering ceramics SFF has been used to process ceramics (Cawley, 1996). Although ceramics have desirable properties, tooling required for engineering such a material is costly and does not always perform as expected from feasibility studies. Many processing techniques for powders are not necessarily practical for creating complex geometries. The introduction of SFF to ceramic processing has enabled the use of new ceramic materials under a variety of operational conditions.

The many SFF methods used for freeforming advanced ceramics are stereolithography (Agarwala *et al.*, 1996a), fused deposition (Agarwala *et al.*, 1996b), selective laser sintering (Subramanian *et al.*, 1995), laminated object

manufacturing (Griffin *et al.,* 1996), laser chemical vapour deposition, three dimensional printing (Cima *et al.,* 1995) and direct ceramic suspension-jet printing (Edirisinghe, 1997).

2.5.1 Stereolithography

This is a method of giving a computer the capabilities of building via a focused laser beam. Stereolithography is better denoted by multilayer photopolymerization and is based on the layered construction of a polymer or particle-filled polymer in a tank of photocurable monomer or oligomer (Leach *et al.,* 1993). Photocurable resins generally contain 2-5% photo-initiator that generates free radicals in the presence of UV light. The monomer or oligomer is polymerised when attacked by free radicals but the reaction stops in the absence of light because free radicals react with oxygen (see **Figure 2.8**).

The first stereolithography machine used for SFF entered commercial service in 1988 and was supplied by 3D systems (Kruth, 1991). This method of manufacture is one of the most widely used SFF techniques in the world (Kodama, 1981). This techniques is also used for creating ceramic components by polymerising a UV-curable binder filled with ceramic powder followed by exposure to UV radiation (Griffith *et al.,* 1996). Most of the enhanced versions of this system employ this forming strategy. Recent advancements in lasers and improvements in beam delivery mechanisms have further improved this process (Kruth 1991, Glardon *et al.,* 2001).

In order to make ceramic parts photo-polymerised monomer is charged with powder (Griffith *et al.,* 1996) and to achieve a high density, the freeforming body should be highly filled with typically 50-65 vol.% of solids. The suspension on the other hand must have a relatively low viscosity. A similar approach (Beaman *et al.,* 1997, Chartier *et al.,* 2002) is taken for producing ceramics using laser polymerisation of a ceramic suspension of upto 60 vol.% powder based on a UV photo-curable monomer. Thin layers (25μm) could be achieved and the dimensional resolution was 200μm. Flexural strength of the alumina components made in this way are similar to that of conventionally made ceramic (Doreau *et al.,* 2000). Alumino-silicate components with 50 vol.% powder have been produced in a similar way (Licciulli *et al.,* 2000 and Greco *et al.,* 2001)

A three dimensional part is fabricated by successive curing of layers of suspension as the focused laser beam scans the liquid surface to reproduce the information in a slice of a 3D computer image. The resulting solid ceramic-polymer composite is built up on an elevator platform, which lowers incrementally into a vat containing the liquid by a distance of 50-500μm, which is the effective layer thickness. As the elevator is lowered into the vat, liquid resin covers the last solidified layer.

The re-coating and levelling of a new layer of resin then ensures that the liquid level corresponds to the focal plane and excess resin beyond the desired layer thickness is removed (Pham *et al.,* 1998). The use of a laser is not the only way to photo-cure the pattern in each layer. Conventional photographic masking can be used by a mask being placed on a liquid crystal display on which the pattern of non-curing regions is updated layer by layer (Young *et al.,* 1999). Scanning with

conventional UV light transmitted thought an optical fibre with focussing lens and shutter has also been introduced (Wu *et al.*, 2001).

Once a planar resin surface is established the laser draws the part border followed by the hatching, filling in the area within the borders. The process is repeated several times until the component is built. The platform is raised and the solid polymer emerges from the vat. The cured resin serves only as a binder for ceramic particles and is removed by slowly heating to 250-500^{0}C, followed by high temperature sintering.

Resin re-coating is a time consuming process (Kruth, 1998) and may create trapped volume in the part where excess resin cannot be drained through the base (Pham *et al.*, 1998). The presence of trapped volume causes a build up of unwanted polymerised resin at the surface which may effect accuracy and surface finish. Although many re-coating mechanisms have been invented to eliminate this problem, e.g. scraper blade, inverted "U", viscous retention, positive displacement pump (Kruth, 1998), the contact between the re-coating mechanism and the liquid surface remains a problem. This problem is even more significant in highly viscous ceramic suspensions where a high shear stress transmitted during coating can damage the part under construction. A process in which a ceramic suspension is pre-laminated into semi-solid foils and pressed into the previous cured layers has been developed to overcome re-coating problems encountered with a scraper blade (Kruth, 1998).

Stereolithography, like other SFF methods can be used to make complex ceramic parts indirectly by making a polymeric mould which can be filled with ceramic suspension by low pressure injection moulding (Risthaus *et al.*, 2002, Knitter *et al.*, 2001a, Knitter *et al.*, 2001b). Wang *et al.*, (2000) have devised an indirect method in which a concentrated ceramic suspension is vacuum cast into a polymeric mould made by stereolithography which can have complex geometry and finer surface definition.

Another disadvantage associated with high viscosity ceramic suspensions is that it requires a longer time to drain the excess resin from the completed component. Stereolithography also requires supporting structures to hold the various connecting parts of the product at weak and overhanging sections during the formation of layers (Kruth, 1998) and these require additional material and time. The optimisation model presented by Pham *et al.*, 1999 assists decisions on part orientation on the platform and various slicing and hatching strategies have been devised to reduce time and distortion (Ma *et al.*, 1999). A model that predicts the depth of cure as a function of photo-initiator concentration and intensity can be applied to stereolithography apparatus as well as to coatings and to dental materials (Lee *et al.*, 2001). Furthermore, errors are taken into account in the model presented by Pham *et al.*, 2000.

2.5.2 Fused deposition of ceramics

The creation of an artefact from a cylindrical strand of deformable ceramic has its origin in the Egyptian Naqada 1 period (4500-4000BC) (Bourriau, 1981) where coiled clay pots were produced. The application of computer control to a movable

extrusion head has spawned a range of construction methods based on this ancient idea. In Fused Deposition Modelling (FDM) (Crump, 1991) a thermoplastic polymer is extruded through a 0.5-1mm diameter nozzle using the solid polymer strand as the extrusion ram (see **Figure 2.9**).

Temperature control is to ±5°C and dimensional accuracy relies on the use of shrinkage compensation factors (Dao *et al.*, 1999) and optimised deposition (Ziemian *et al.*, 2001, Kulkarni *et al.*, 1999). This process is also described as melted extrusion modelling (Yan 2000). In multiphase jet solidification (MJS) (Greul *et al.*, 1995, Greul *et al.*, 2000, Geiger *et al.*, 1994), a ceramic or metal powder suspension in a wax or polymer vehicle is extruded onto the building platform. In a similar approach, fused deposition of ceramics (FDC), structural (Agarwala *et al.*, 1996a) or piezoelectric ceramics are prepared either directly (Lous *et al.*, 2000) or by first making a disposable mould (Bandyopadhyay *et al.*, 1997). Piezoelectric ceramics and polymer-ceramic composites with functional gradients have been prepared in this way for sensors and actuators (Safari *et al.*, 1998, Safari 1999 and Safari *et al.*, 1999). The filament diameter is typically 1.8mm (Rangarajan *et al.*, 2000) and the method can be extended to multiphase materials (FDMM) (Chen *et al.*, 2001 and Allahverdi *et al.*, 2001).

Photonic band gap structures for GHz frequencies and piezoelectric actuators with spiral or bellows geometry can be made in this way. The method can also be used to make fugitive moulds consisting of latticework that can subsequently be infiltrated with ceramic slurry. When the ceramic is fired a controlled ordered architecture of porosity remains (Bose *et al.*, 1999).

Extrusion freeforming is a term that best embraces all these techniques but it is presently used specifically for extrusion of monomer to produce, typically nylon 6 on a heated platform by extrusion through a 250μm diameter nozzle. This method too can be used for ceramic prototyping.

Ideally, in these processes a range of nozzle diameters is preferred (Tyberg, 1999) so that large nozzles can be used to fill bulk while fine nozzles are introduced for fine detail. Tseng and Tanaka (2001), have approached this problem with a variable nozzle that can provide extrudate diameter from a single adjustable nozzle. They also describe a planar adjustable nozzle that deposits layers of different width from a pressurised chamber. The extrudate can be drawn off by a roller, which also helps weld it to the previous layer. Bonding to the previous layer has a strong influence on the final component strength and can be related to the forming parameters (Yan *et al.*, 2000).

Fused deposition of ceramics was developed for the fabrication of functional ceramic parts. The technique is based on FDM technology, which was developed and commercialised by Stratasys Inc. (USA) for processing polymer and wax parts (Agarwala *et al.*, 1996a).

The starting materials for FDC are filaments of ceramic powder mixed with thermoplastic polymer or wax binder. The filaments are manufactured in ways similar to that used by the ceramic injection moulding industry. The starting materials are mixed, granulated and extruded to produce continuous lengths of flexible filament. Sufficiently low viscosity is required of the filament which is

typically 0.5-2mm nominal diameter (Agarwala *et al.,* 1996a), for it to be fed into a movable head with a heated nozzle where it softens to just above its melting point at the exit. The filament is then deposited by raster motion according to the patterns defined by the CAD model. Layer building starts by defining the boundaries followed by raster motion of the nozzle head depositing material inside these boundaries as a series of adjacent streams. Each stream is deposited on top of or next to its predecessors and bonds by contact fusion. The molten filament solidifies rapidly upon deposition by natural cooling. The filament is laid layer upon layer, and a 3-D object resembling the model is built and then subjected to binder removal and sintering to produce a dense ceramic component.

A significant advantage of FDC is that it is not demanding upon equipment; it uses a low viscosity feedstock that can be readily dispensed using low pressures (< 0.7 MPa) (Beaman *et al.,* 1997). Material is delivered on demand and the process does not require a large reservoir of expensive feedstock at the start. There is very little material waste during or after production of the model (Pham *et al.,* 1998). There are generally no concerns about operator exposure to toxic materials or lasers. Little cleaning is needed and the materials can be changed quickly. Because the material solidifies quite rapidly after it leaves the nozzle, it is possible to form short overhanging features without the need for supports although, in general, they are used. A dual tip mechanism dispenses two materials - a primary material for modelling and a secondary material for producing a support structure.

Internal defects are a concern when this technology is used to fabricate structural ceramic components (Agarwala, 1996a). These defects usually arise from

debonding or poor bonding between adjacent streams or adjacent layers, or incomplete filling in the part (Agarwala *et al.,* 1996a). Their causes are inconsistent material flow due to variation in filament diameter, filament slippage between rollers or excessive cooling of previously deposited adjacent streams. Incomplete filling occurs as the nozzle turns around. The filament traces a curved tool path instead of the sharp turn defined in the CAD model. Consequently, voids can be found within the part. The use of a more intelligent tool path, software, build strategies and machine control software have helped to improve part quality and accuracy (Kruth, 1991). As the resolution of the process is dictated by the filament thickness, another drawback of FDC is its inferior surface finish compared with parts produced using other SFF techniques (e.g. stereolithography) (Agarwala *et al.,* 1996a). Subsequent finishing operations are needed for improvement of the surface (Hilmas, 1996). One approach to the amelioration of surface ripples is to incorporate a blade that trowels the freshly deposited extrudate and is described as contour crafting (Khoshnevis *et al.,* 2001).

The prototyping of investment casting positives is a major application (Agarwala *et al.,* 1996b). Extrusion freeforming, which uses two extruders to dispense dissimilar materials into a small mixing head, has been employed to prototype functionally graded material (Hilmas *et al.,* 1996). A Multiphase Jet Solidification (MIS) process, very similar to FDC, has been developed by the German Fraunhofer Institutes IFAM and IPA for the fabrication of both metal and ceramic near-net shape parts for functional applications (Greul, 1996).

Direct writing with a positive displacement pumped suspension and plotter system (Yan *et al.,* 2000 and Yang *et al.,* 1999) has also been used for ceramic

processing and bears a formal similarity to FDC in that a suspension of ceramic particles is extruded through a nozzle to produce a pattern on the substrate. It has been used to create resistors, microwave components and thermal print heads. It allows multiple layers with a constant cross sectional area to be deposited on uneven surfaces. It can be used for a range of ceramic pastes for ZnO varistors and capacitor dielectrics (Tohver, 2002 and Morissette, 2001).

2.5.3 Selective laser sintering

Selective Laser Sintering (SLS) originated at the University of Texas in Austin in 1986 and was commercialised in 1992 and is shown in **Figure 2.10** (Glardon *et al.,* 2001). A wide choice of laser sintering machines have been developed subsequently (Kruth, 1991). It has been used for metals, ceramics (Bourell *et al.,* 1992) and polymers (Atwood *et al.,* 1996). A thin layer of powder is spread out and levelled over the top surface of the building platform. A laser then selectively scans this layer to fuse the forming areas as defined by the geometry of the cross-section of a CAD model. Although the process is described as sintering complete fusion occurs in many polymer and metal selective laser sintering processes and the expression selective laser melting is more appropriate.

The laser energy also fuses consecutive layers together. The building chamber is purged with inert gas and is often heated to raise the temperature of the uppermost layers of powder. This reduces the additional laser energy required to heat the powder to its fusion temperature during fabrication and may help to reduce residual stress development. A titanium alloy nozzle increases the quality

of detail and surface finish that can be achieved in selective laser sintering (Dao *et al.*, 1999).

Powder can be delivered into the moving laser target by dry powder flow, which may be gas-assisted, selectively by suspension-jet printing or by metering and dispensing of dry powder. A method of dry powder dispensing that has its origins in the sand painting of the Najavo North American Indians has been suggested (Pegna, 1997) and could provide a route to functionally graded materials. The quest now is for combined shape and compositional control that will pave the way for the selective laser sintering of three dimensional functional gradients. After each layer is deposited, an elevator platform lowers the part and the next layer of powder is deposited. When the shape is completely built, the finished part, buried within a cake of loose powder, is separated from the loose particles which may sometimes be recycled. The build time can be predicted and there are strategies to minimise it (Pham, 2000a). Parts processed by SLS are often porous and post-processing is necessary when strength is required in ceramic parts (Beaman, 1997). Conventional sintering and hot isostatic pressing are two common methods used to increase part density.

In SLS, no support structure is needed as the unfused powder remains in place to act as a support itself. Changing from one material to another is simpler than many of the liquid-based SFF techniques, given the dry solid nature of the starting material.

Selective laser sintering can process powders directly without the use of a sacrificial binder (McALEA *et al.*, 1997) unlike SFF methods which demand specific materials such as photo-polymers in stereolithography. In some variations of SLS, low temperature fusion of a binder is used to assemble the powder and subsequent pyrolysis and sintering steps are needed. The reason for this approach is that laser sintering of high melting point ceramics requires a high level of laser energy and can create large thermal gradients, thermal shock and hence difficulty in forming a contiguous shape (Subramanian *et al.*, 1995). This is partially overcome by incorporating a second phase binder of lower melting point into the ceramic powder. Volpato *et al.*, (2001) use the term indirect selective laser sintering to describe the low temperature joining of particles with a binder to form parts with overhangs. The term direct metal laser sintering is reserved for the selective melting of powder using high laser intensity (Simchi *et al.*, 2001).

The extent of conversion and hence the strength of the part is dependent upon the laser energy (Subramanian *et al.*, 1995). Each material requires different heating and laser parameters (Pham *et al.*, 1998). Process maps have been devised to predict thermal gradients and residual stresses (Beuth *et al.*, 2001). Temperature cycles and thermal gradients in a laser-melted thin wall enclosure have been measured with embedded thermocouples and high speed imaging with a digital infrared camera (Griffith *et al.*, 1999). The corresponding residual stresses were estimated by a hole-drilling method using laser interferometry to measure strain. Maximum local residual stresses in the region of 300 MPa were reported. Parts require slow cooling in the machine before they can be removed for post

processing. Recycled powders must be sieved to remove agglomerates, which interfere with the smooth application of the next level of powder.

Numerous methods have been employed to increase the powder bed density in order to increase the ceramic or metallic part density without sacrificing freeforming capability. Conventional means of improving the powder bed density include the use of spherical particles, bimodal size distributions of powder, agglomeration of fine powder and optimising the volume fraction of combustible binder (Beaman *et al.*, 1997). Another approach is to increase the effectiveness of the powder distribution process in SLS by the use of electrostatic (Melvin *et al.*, 1996) and magnetic fields (Melvin *et al.*, 1992) or mechanical agitation of the powder and/or powder bed (Bunnel *et al.*, 1995). On the other hand, in some applications, e.g. ceramic moulds for metal casting, porosity in the part is an important function and SLS processing of these parts allows direct fabrication. Laser sintering of zircon sand and silica sand has been used in industry while research with graphite and other types of ceramics continues (Kruth, 1991).

2.5.4 Laminated object manufacturing

Laminated Objected Manufacturing (LOM), was developed in 1985 and commercialised by Helisys Corporation in the USA to build components with layers of paper or plastic (Kruth, 1991). The sheets are laser-cut according to the pattern defined by CAD and laminated with adhesive to the previous layer. The laser also dices the excess material to help with extraction of the finished component. The waste material is left in place during part building to serve as a

support. The process is repeated until the component is formed. **Figure 2.11** illustrates the process.

Laminated object manufacture has been modified to fabricate ceramic components (Cawley *et al.,* 1997). Instead of paper, thin (≈100μm) ceramic tape, which is pre-processed by mixing ceramic powder with an appropriate binder by tape casting, roll compaction or extrusion, is used. After the sheets have been stacked to assemble a physical 3-D model of the original CAD description, the part is removed from the platform and the waste material is separated manually. The part is then subjected to binder removal followed by sintering. As lamination occurs under applied pressure, one concern is the relaxation of residual stresses causing delamination and bloating during binder burnout. Pressure can be applied during pyrolysis to counteract this (Klosterman *et al.,* 1997). Zhang *et al.,* (2001) describes the roll forming of 700μm alumina tape followed by lamination, binder removal and pressureless sintering. The difficulties with ceramic LOM are also debated by Kochan *et al.,* (1999).

In one sense, in contrast to most SFF processes, LOM is a subtractive method because it traces the outlines of the parts and discards waste during layer fabrication (Cawley *et al.,* 1996). This makes it potentially the fastest technology for building parts with a high ratio of volume to surface area (Pham *et al.,* 1998). Because the processing of the sheet can be completely separated from component building, microstructural defects within each layer can be minimised (Cawley *et al.,* 1996). The interfaces between layers however, provide a unique set of defects. Furthermore, shrinkage or thickness variation during part fabrication can be

compensated as the thickness of the sheet materials is known beforehand (Cawley *et al.,* 1997) and thus LOM has the potential of yielding a highly accurate part.

Another advantage of LOM is that tapes of two or more types of material with different properties can be added to different regions, paving the way for fabricating functionally graded materials or multilayered composites with alternating compositions (Griffin *et al.,* 1996).

In LOM, the part remains embedded within a block of supporting material that is diced and broken into chunks before removal. Because the surfaces adhere to one another, cleaning is a manual process (Klostermann *et al.,* 1997) and much care is needed, as the scrap is as strong as the part. The amount of scrap generated is large and is not directly recyclable. It is also hard to make hollow parts due to the difficulty in removing the core (Pham *et al.,* 1998). This difficulty also extends to narrow passages, internal cavities with restricted access, blind holes etc. Another issue is that waste chunks must be tiny enough to be manipulated through small openings. The shear strength of the part is affected adversely by poor adhesion between layers during lamination (Crump *et al.,* 1991a and b).

CerLOM, a modification developed by Lone Peak Engineering Inc., USA has been used to combine tapes of different ceramic materials to fabricate multilayered composites with alternating composition (Griffin *et al.,* 1996). Another LOM modification, the CAM-LEM process, was developed at Case Western Reserve University, USA (Cawley *et al.,* 1996). This technology adopts a 'cut-then-stack' approach where the layer is cut to shape prior to placement onto

the stack to be laminated. Therefore, it is possible to cut arbitrary angles by inclining the laser relative to the sheet to produce bevelled edges at the contour. This avoids 'staircasing' in the stack direction. Furthermore, layers of unfired and fugitive tapes can be added to the partially complete stack instead of being built onto it. The fugitive tapes are organic materials that can be removed by thermolysis later. There is thus no need to remove waste material manually after assembly and hollow components can be constructed. In both of these modifications, the green part must be subjected to binder removal and then sintered.

Research on the use of a non-planar LOM process has also been carried out to build curved-layer parts instead of only having flat layers (Klosterman *et al.*, 1997). This concept has been implemented with ceramic tapes to fabricate ceramic matrix composites for aircraft engine components.

2.5.5 Laser chemical vapour deposition

Coatings are deposited from vapour phase reactants on heated substrates by chemical vapour deposition and this provides a method of making ceramic coatings or thin free standing layers. If laser heating is used and the beam moved parallel to the substrate, some control of coating geometry accrues but if the beam is moved perpendicular to the substrate then a thin rod can be drawn out into free space and, if the substrate, orientation with respect to the beam is adjusted, complex network structures can be produced (Lehmann *et al.*, 1995a, Lehmann *et al.*, 1995b and Wanke *et al.*, 1997).

The method is successful if the reaction product is strongly absorbing. The laser powder can be automatically modulated in response to the growth rate to produce a range of geometrical shapes of carbon, iron, nickel and nickel-iron alloys (Maxwell *et al.,* 1998). Laser chemical vapour deposition (LCVD) offers high purity, solid freeformed products with gowth rates of 1 mms^{-1} (Wallenberger, 1995). Fibres of diameter 20μm can be produced in the form of micro-springs using high strength fibres such as boron.

The method is well-suited to the production of high temperature thermocouples in the form of built-in sensors in ceramics or ceramic composites (Sun *et al.,* 1999a). The target temperature is about 700°C. A similar method can be used to infiltrate layers of powder from the vapour phase (Sun *et al.,* 1999b).

Gas precursor methods have become known as SALD, Selective Area Laser Deposition (Birminghan *et al.,* 1996) and SALDVI, Selective Area Layer Deposition Vapour Infiltration (Maxwell *et al.,* 1998). In SALD, shapes are built from the solid decomposition products of the gas precursor, either pyrolitically or photolytically according to the pattern defined by the scanning laser. In SALDVI the parts are formed by selectively infiltrating the powder by vapour. Although still in their early stages, approaches using gas precursors look promising because of their capability of producing high temperature structural materials, which are beyond current SFF processes and difficult to process by traditional methods (Conley *et al.,* 1997).

2.5.6 Three dimensional printing

Three Dimensional Printing (3DP) was developed at Massachusetts Institute of Technology, USA in 1992 as a method to form preforms for powdered metals and ceramics (Sachs *et al.,* 1992 and 1993). It has been used to produce ceramic cores and shells for casting applications under the name Direct Shell Production Casting (DSPC) invented by Soligen Corporation (Uziel, 1997).

The three dimensional printing process is illustrated in **Figure 2.12**. A powder is levelled by a roller to provide a thin layer, typically 170μm thickness. As an alternative to the roller, mechanical, acoustic or ultrasonic vibration can be used to consolidate the powder bed (Sachs, 2000). A printhead then moves across the powder in raster motion and prints a layer of binder selectively onto the loose powder as defined by the CAD model. In early work on metal powders (316 stainless steel 15-30μm dia.) the spraying of binder cut a trench through the powder bed and redistributed the powder. This was solved by pre-treating the metal powder with 0.05 wt.% salt and moistening the powder bed to increase its cohesive strength (Melican *et al.,* 1992). As the binder diffuses through the powder by capillary action, neighbouring particles are pulled together by surface tension effects (Sachs *et al.,* 1993). The layer printing process is repeated and parts are built in a container which is fitted with a piston to lower the part incrementally into it. On completion it is oven cured and excess powder is removed by immersion in a water bath before sintering.

As in SLS, overhanging features are supported by the free powder. 3DP does not require high energy, does not involve lasers or any toxic materials and is relatively

cheap and fast (Carrion, 1997). The process can be adapted to suit a variety of powders and to generate the desired pore size and shape. By using multiple printheads, additives may be deposited in a prescribed fashion to create gradients in composition, e.g. in the fabrication of compositionally graded zirconia-toughened alumina (ZTA) ceramic multilayers. Compositional control at a resolution of 100μm is possible (Jackson *et al.*, 1999).

The technology was developed initially to produce ceramic moulds for metal castings directly and although the final parts may be porous, they are sufficiently strong for the intended applications. With proper placement of droplets, printed parts with controlled surface texture and internal microstructure may be created. This method has been used to make casting moulds with tailored surface texture for orthopaedic implants that encourage bone in-growth (Curodeau *et al.*, 2000). However, fabrication of structural ceramic parts using this process is more challenging. Although the use of fine powder improved sintering of the 3DP parts, its high surface area decreased the powder flowability and therefore it became difficult to obtain layers of defect-free powder. Several methods have been implemented to produce dense ceramic parts with fine powder by intermediate isopressing or by modifying the binder or powders (Cima *et al.*, 1995).

The process has been considerably refined by direct suspension-jet printing of the powder bed onto a porous support (Uhland *et al.*, 1999). This overcomes the microstructural inhomogeneities known to characterise compacted powder

(Lange, 1984). Direct printing means the powder is well-dispersed in a liquid and is then suspension-jet printed.

Dimensional control of the part is determined both by the accuracy of drop placement within the plane of printing and by the vertical position of the powder layer (Sachs *et al.,* 1992). Due to the compressibility of the powder, loads applied from above cause the thin layer of powder to displace downward from its original position and therefore a loss of vertical dimensional control can occur. Layer displacements are most severe in the middle regions of powder beds. Using a higher packing density in the powder bed reduces compressibility and therefore helps to minimise layer displacement, but then additional pre-processing work is necessary (Lee *et al.,* 1995).

Surface finish due to the raster scanned by the printhead on the layers can lead to a stair-stepping effect in the XY plane as well as in the build direction (Conley *et al.,* 1997). Surface finish is also determined by the interaction of the binder with the powder. This technique has also been applied to metal powders for the manufacture of metal tooling (Allen *et al.,* 2000).

It is often difficult to see the formal or topological similarities between diverse manufacturing processes which have been given a distinct proprietary identity. This matter has been discussed in relation to the difficulty that students have in apprehending the taxonomy of manufacturing processes (Zhao *et al.,* 2002). For example, 'direct writing' processes using pressured suspension reservoirs (Yang *et al.,* 1999, King *et al.,* 1999 and Morissette *et al.,* 2001) are related to FDC. They

are also three dimensional, or multilayer printing processes. Likewise, offset lithography, along with most other printing processes can be adapted to solid freeforming (Leyland *et al.*, 2002) and used to make multiple layer ceramics based on the well-established lithographic printing of circuits (Ramsey *et al.*, 1997, Walton *et al.*, 2000 and Shepherd *et al.*, 1997).

2.5.7 Direct ceramic suspension-jet printing

Direct Ceramic Suspension-Jet Printing, (Blazdell *et al.*, 1995), makes use of jet printers to create components by multi-layer printing of ceramic powder that has been well dispersed in a liquid carrier. Unlike 3DP, the ceramic powder is dispensed directly through the nozzle instead of just the binder. This process has the potential to produce a wide range of fine ceramic contours with high resolution enabling the manufacture of miniature components (Edirisinghe, 1997). It allows functional gradients (Mott *et al.*, 1999) that are effectively stepless in the direction perpendicular to the printing plane to be produced by suspension blending and dilution. Gradients can potentially be made in three dimensions so that both shape and composition of an object can be downloaded from a computer. This method relies on suspension preparation by colloidal processing so that particles are well dispersed. Thus agglomerates, often identified as the source of critical defects in ceramics (Lange, 1984) are either removed by filtration or cause the nozzle to block rather than being deposited into the work piece, thereby providing fail-safe operation.

Suspension-jet printing belongs to the family of non-contact printing methods (Heinzl *et al.*, 1985 and Lloyd *et al.*, 1988). Suspension from a reservoir is

converted into droplets, and propelled through air to the substrate. A wide range of substrates can be printed on to, they do not have to be smooth or flat. It is a computer-controlled process which enables variable data to be printed continuously at high speed (Keeling, 1981). Among the main attributes of an suspension-jet printer, which differentiates it from other printing techniques are high speed printing, silent non-impact operation, electrically controlled by computers, no post-printing treatment, uneven or delicate surfaces are acceptable, there is a multi-suspension capability and the capacity for rapid change of image(Keeling, 1981 and Le 1989).

Aside from the well-established reprographic applications of home and office printing, suspension-jet printing technologies have also penetrated the emerging markets of rapid prototyping and medical imaging (Le 1998 and Carrion *et al.*, 1997), of high speed titration (Litborn *et al.*, 1998), mass spectrometry sampling (Onnerfjord *et al.*, 1998), combinatorial chemistry (Lemmo *et al.*, 1998 and Oldenburg *et al.*, 1998) and tissue engineering (Klebe, 1988). Other applications of suspension-jet printing include printing of hybrid microcircuits (Teng *et al.*, 1987), metallisation of the grid patterns of solar cells (Teng *et al.*, 1988) and deposition of patterned luminescent doped-polymer films (Hebner *et al.*, 1998).

One of the early practical continuous suspension-jet printers was demonstrated by R. G. Sweet of Stanford University in the 1960s (Heinzl *et al.*, 1985). Since then, several suspension-jet printing techniques have been implemented in a wide variety of ways. A brief account of the recent development of suspension-jet printing has been presented by Le (1998). There are two main types of printer:

continuous and drop-on-demand (DOD) and their features have been compared by Edirisinghe *et al.*, (1998).

As shown in **Figure 2.13**, a continuous suspension-jet printer forms a stream of droplets even when there is no print demand. Droplets are charged and deflected to their destination in an electric field and those not required are collected or recirculated. It is often used for high-speed printing of bar codes and for date labelling. In the DOD suspension-jet printer, suspension droplets are formed only when required. The forces used to create and transport them may originate from mechanical, electrostatic, magnetic or thermal transduction.

In the continuous suspension-jet printer using the Sweet method an electrically conducting suspension is delivered from a pressurised reservoir through a 30-200μm diameter nozzle. Just before the nozzle, a piezoelectric actuator superimposes a modulated pressure and on leaving the nozzle the stream breaks up into a continuous series of droplets at a matching frequency which are equi-distant and of equal size. The break-up reduces the liquid surface area (Rayleigh, 1882) and droplet radius would be variable without the superimposed pressure wave. By perturbing the jet at a fixed frequency close to the spontaneous droplet formation rate, the droplet formation process is synchronised with the forced vibration and suspension droplets of uniform mass are ejected.

2.5.8 Scope of solid freeforming

The scope of SFF is enormous in the rapid prototyping, manufacturing and medical industries. One of the areas where solid freeforming methods have much

to offer is in medicine (Ashley, 1993). Its particular value lies in the ability to use data generated from computed X-ray tomography, sometimes edited for shrinkage, for the creation of individual prostheses (Webb, 2000 and Vander Sloten *et al.*, 2000). Selective laser sintering has been used to make models of human temporal bone (Levy *et al.*, 1994). Stereolithography has been successfully used for polymeric implants in cranioplasty (Levy *et al.*, 1994) but the authors point to the problem of warpage and the long processing time. Ceramic implants for orbital floor prostheses have been made stereolithographically by photo-curing a resin-hydroxyapatite suspension (Levy *et al.*, 1994).

Models generated from computerised tomography (CT) data can be used for surgical planning and teaching (Petzold *et al.*, 1999). Accurate physical replicas of the patient's individual topography can be made. The complex architecture of trabecular bone modified by osteoporosis can be reproduced on a macroscopic scale from high resolution CT or magnetic resonance micro-imaging for visual or biomechanical analysis (Bibb *et al.*, 2000). Models of the structure of the ear allow a surgeon to become familiar with the individual anatomy of each patient. SFF models also assist in maxillofacial surgery (Stoker *et al.*, 1992 and Ono *et al.*, 2000). The accuracy of a model of a child's skull made from nylon by selective laser sintering was < 1 mm in each direction. In tooth transplantation, a duplicate of the donor tooth created from CT data assists pre-contouring of the alveolar bone and hence reduces the extra-oral time of the donor tooth to about 8 minutes (Lee *et al.*, 2001).

MedLAM, a proprietary laminated object manufacturing process, has been used to prototype bioceramic implants with tailored porosity and these can serve as

sites for bone formation and tissue regeneration (Griffin *et al.*, 1997). A suspension of calcium polyphosphate in a photo-curable resin and dispersant was used to make porous implants by stereolithography followed by thermolysis to remove the resin and then by sintering (Porter *et al.*, 2001). Calcium phosphate powder coated with a methylmethacrylate-butyl methacrylate copolymer has been assembled by indirect selective laser sintering into a porous implant. After infiltration with phosphate, sintering at 800°C and implantation was repleted with mature bone growth after 4 months (Vail *et al.*, 1998). An indirect sterolithography method using epoxy resin moulds have been used to make porous hydroxyapatite bone graft material from CT data (Chu *et al.*, 2001).

Superb latticework structures have been produced by FDM (Hutmacher *et al.*, 2000 and Zein *et al.*, 2002) for bone substitute scaffolds. These are composed of polycaprolactone with 7 vol.% hydroxyapatite. Filament diameters in the range 260-370 μm were extruded. In this application, the staircase defect in FDM does not appear. In vitro studies showed that the scaffold architecture was completely filled by cellular tissue in 3-4 weeks (Hutmacher *et al.*, 2001). Similar structures have been made in other biodegradable polymers for bone scaffold by extrusion freeforming used a constant gas pressure extruder (Xiong *et al.*, 2001). Sintered ceramic latticework scaffolds can be prepared and ceramic filaments of 60μm diameter after sintering can be made by this process (Grida, private communication) but for filaments below about 100μm the cooling is so rapid that strong welds are not formed. Solid freeforming methods can be used indirectly to good effect. Thus three dimensional printing has been used to make ceramic

moulds in which to cast cobalt chromium bone prostheses with a graded porous surface to promote bone attachment and growth (Melican *et al.*, 1992).

2.6 Ceramic foams

Ceramic foams are a class of porous materials with large voids usually in the range 10 μm – 5 mm. The voids, usually referred to as cells, can be surrounded by ceramic walls (closed cell foam) or contain solid material at only cell edges (struts) thus creating an interconnected structure (open cell foam). Therefore, ceramic foams can be formed with low density, thermal conductivity, dielectric loss and thermal mass. These materials can also be made to possess high porosity, specific strength, permeability and tortuosity to flow, thermal shock resistance, specific surface area, hardness and resistance to wear and resistance to environmental degradation. Open cell ceramic foam have many uses: Fluid filters, catalyst supports, burners, gas diffusers, flame barriers, liquid aerators and as a biomaterial for bone replacement and as a carrier for cells, enzymes and bacteria (Colombo, 2002).

Ceramic foams already available commercially or being researched are made of various materials, such as cordierite (Inui *et al.*, 1985), mullite (Montanaro 1998 and Ashby 1983), silicon carbide (Otzuka *et al.*, 1995), alumina (Hagiwara *et al.*, 1987 and 1988, Tantry *et al.*, 1993, Brown *et al.*, 1994, Peng *et al.*, 2000), silicon oxycarbide (Colombo *et al*, 1998) and some composite foams, e.g. alumina-zirconia (Lange *et al.*, 1987, Brezny *et al.*, 1992,1993a and b, Vedula *et al.*, 1998 and 1999, Salvini *et al.*, 2000), alumina-mullite (Brezny *et al.*, 1992) and silicon

carbide-alumina (Lannguth, 1995 and 2000). Silicon carbide foams have both high thermal and electrical conductivity and are used as heating elements. In addition to the fact that it is hard, highly abrasive and resistant to most acids and bases, its low cost and thermal shock resistance make it the preferred material for molten iron filtration and as a heat-exchange medium in regenerative incinerators (Brockmeyer *et al.*, 1982, 1986, 1988 and 1989).

The unique properties of each variety of ceramic foam starts to evolve during the manufacturing process. For instance, if a template was used to prepare foam (see section 2.6.1.1) its pore size determines the pore size of the finished ceramic product.

2.6.1 Forming routes

The development of ceramic foams has opened a new era for a variety of industries because they are durable in severe environments and their surface characteristics permit them to satisfy specific functional purposes. With the growing demands of ceramic foam for industrial applications, a number of technologies have been developed to form them. To date ceramic foams with uniform pore structures and pore sizes ranging from a few hundred micrometers to a few nanometers can be achieved for diverse purposes by either physical or chemical processing. Open-cell ceramic foam and closed-cell ceramic foams are produced by different processes. However, the most common method used is the polyurethane sponge process and therefore this is distinctive compared to the other routes described below.

2.6.1.1 Polymeric route

In this method, a sponge impregnated with a ceramic slurry, is burned leaving a ceramic foam. The polymeric sponge method typically produces open-cell ceramic foam (Schwartzwalder *et al.*, 1963 and Saggio-Woyansky *et al.*, 1992).

Organic foam used in ceramic foam manufacture is made to a high tolerance so that there is controlled consistency in the ceramic product. The organic material must be resilient enough to spring back without excessive deformation after the ceramic slurry is applied. Additionally, the manufacturer must be able to control the burnout of the organic material so that the same product characteristics can be reproduced repeatedly (Brockmeyer *et al.*,1988). Some of the polymeric-sponge materials which can satisfy these requirements are polyurethane, cellulose and polystyrene. The low softening temperature of polyurethane makes it particularly attractive as a template material. When the impregnated foam is heated, the polyurethane burns very easily (Holland, 1963).

The slurry is made up of finely divided ceramic particles, water, and additives. The ceramic particles chosen depend on the particular application and desired properties of the final product. For example, for a molten-metal filter, the ceramic chosen must be able to withstand chemical attack and have high temperature strength. Generally, any oxide, borides, nitrides, carbides, silicides or minerals can be used as the ceramic component in the slurry (Holland 1963). Typically, the ceramic particles are less than 45μm diameter. Water is most often used as the carrier in the slurry. The amount of water can range from 10 to 40% by weight of the total slurry (Yarwood, 1976, 1978 and Brockmeyer, 1982).

Once the polymeric template has been selected and the ceramic slurry prepared, the next step is to impregnate it with slurry. Typically, the sponge like template is compressed to remove air, immersed in the slurry, then allowed to expand. The slurry infiltrates the open cells of the sponge.

After the sponge has been infiltrated, the next step is to remove excess slurry from the sponge. The techniques used to achieve this goal range from a simple process of compressing the sponge between wooden boards (Holland, 1963) or passing through preset rollers (Yarwood, 1978 and Pryor, 1977). At this stage the impregnated foam can be further shaped since it is still flexible. Any shape formed at this point must be sustained until the ceramic is sintered.

.

The infiltrated sponge is dried to deposit the ceramic particles on the sponge after the excess slurry is removed. Drying can be done in air, in an oven, or by microwave heating. Air drying will typically take between 28800-86400s. Oven drying can be used in the temperature range between 100°C and 700°C from 15 minutes to 21600s.

.

The open-cell structure is heated in air to between 350°C and 800°C for 900s to 21600s to remove the organics from the slurry and to volatilize the polymeric sponge. The heating ramp chosen for this step depends on the temperature at which the chosen sponge material decomposes. Slow, controlled heating to the desired temperature is critical in this step which can be combined with the final step of sintering the ceramic, but in most cases separate drying, pyrolysis and sintering steps are important for precise control of the final open-cell structure.

An air-setting agent may be added to the ceramic slurry to aid in setting or bonding of the ceramic slurry prior to firing. The most commonly used setting agent is aluminium orthophosphate; a quantity of 25wt.% is added (Brockmeyer, 1982).

Antifoaming agents are added to prevent foaming of the slurry. Ravault (1974 and 1975) has described the use of antifoaming agents for reducing the tendency of the slurry to form bridges or windows in the porous structure. This closed structure results in reduced permeability of the final product. Ravault described the advantage of using a 1wt.% of silicone or a low-molecular-weight alcohol to prevent bridge or window formation within the foam.

The final step is densification of the ceramic network by sintering. In this step, controlled heating is important to prevent collapse of the ceramic framework. The exact heating ramp and atmosphere used depend on the ceramic material and the desired final properties of the foam.

Ceramic foams produced by the slurry method have low strength because (i) they usually contain a central hole (Tulliani *et al.*, 1999) as shown in **Figure 2.14** and (ii) the struts are likely to contain cracks (Vedula *et al.*, 1999) as shown in **Figure 2.15**. Both these defects are caused by incomplete and/or non-uniform coating of the polymeric foam by the ceramic slurry. Edirisinghe *et al.*, (1999) have eliminated this defect by using a polymeric ceramic precursor solution instead of a slurry. However, precursor methods are expensive and the ceramic produced by pyrolysis of the precursor usually contains a high level of carbon, which lowers

the strength of the foam and its resistance to degradation at elevated temperatures.

2.6.1.2 Other routes

Several other methods of producing ceramic foams are described in the literature.

In the direct foaming method reactants including the desired ceramic constituents can be combined to produce a foam. The mixture contains a polymer carrier which is burned out, leaving a foam ceramic. This direct foaming method produces both open cell and closed cell foam. Saggio-Woyansky *et al.*, (1992), produced foamed ceramics by combining two components A and B. Component A comprised of a pre-polymer and acetone and component B comprised of distilled water, alumina, HCl and a surfactant. Component B was added to the pre-polymer mixture and stirred vigorously until a creamy consistency was achieved. The mixture was allowed to rise (as a result of the CO_2 produced), cure and dry. Mixing was typically 15s; rise time was 120-180s, cure time was 600s and drying time was 86400s.

The gel-casting technique has been adopted for the production of ceramic foams using foamed suspensions (Sepulveda 1997 and 1999). In this process a ceramic slurry containing organic monomers is cast in a mould. The monomer mixture is polymerised *in-situ* to form gelled parts. At an intermediate stage foam generation is introduced before *in-situ* polymerization. With the association of gel-casting and foaming, the structure of the foam can be well retained and strong "green" structures are produced prior to sintering. Sepulveda (1997) demonstrated that

this process can be applied successfully to most ceramic powders including hydroxyapatite.

In the hot isostatic pressing method powder compacts or partially pre-sintered bodies are sintered directly under high gas pressure. The densification rate under high pressure gas is slower than that under ordinary ambient pressure. The samples have lower density and higher open porosity. This type of foam has good wettability for water due to higher liquid suction rates (lshizaki, 1995).

A sol-gel system can develop porosity during phase transformations or chemical reactions. This principle has been used in producing porous alumina (Bagwell *et al.,* 1996) and meso and micro-porous silica (Sakka *et al.,* 1993 and Klein *et al.,* 1996).

Fitzgerald 1995, has produced SiC foams by using a replication technique in which the polymer was first infiltrated into the pores left between partially sintered salt performs. The salt is then leached away with water and the polycarbosilane foam is converted to SiC foam after pyrolysis.

Colombo *et al.,* (1998), have produced open cell ceramic foams from preceramic polymer (silicone resin) and blown polyurethanes. In this approach the preceramic polymer was dissolved in dichloromethane and added to a liquid polyol containing the amine and catalyst. Isocyanate was then added to the mixture. The materials obtained were pyrolyzed in nitrogen. The ceramic foams produced consisted of an amorphous silicon oxycarbide ceramic.

Ultramet Corporation in the USA has developed chemical vapour deposition for producing open cell ceramic materials (Sherman *et al.,* 1991). The process begins with the pyrolysis of a resin-impregnated thermosetting foam to obtain an open cell carbon skeleton. The individual ligaments can then be coated with a variety of materials (metals, oxides, nitrides, carbides, borides, silicides) by a variation of the chemical vapour deposition (CVD) process and referred to in the literature as chemical vapour infiltration (CVI). In this process 10-100μm of the desired metal or ceramic is deposited onto the surface of the carbonaceous skeleton. The process uses high rates of deposition available through CVD (100 to 400μms^{-1}) while actually depositing material through the carbon skeleton via CVI. The carbon skeleton is first heated to the temperature necessary for the deposition reaction; the gas being used to deposit the material is then drawn through the skeleton and the gaseous precursor compound is reduced or decomposed at the surface of the skeleton. A principle application of these foams is in the fabrication of thermal insulators. Preliminary trials at the Ultramet Corporation with zirconia open cell refractory ceramics have found that thermal insulation equivalent to that of the NASA space shuttle protective system has been achieved at 550°C or even higher operating temperatures.

Sunderman (1973), describes an unusual technique for producing open-cell ceramic foams. In this approach, pre-swelled ball shaped granules of clay are placed in a mould which has the shape of the final product. The mould is then passed through a furnace at 900°C to 1000^{0}C in an oxidizing environment. The heat and high pressure air first causes the clay balls to bind to one another.

Subsequently, when sufficient heat is transferred through the clay particles, growth occurs and the mould is filled. The resulting ceramic foam is then cooled.

Motoki *et al.*, (1978), describes a porous ceramic produced by mixing four components. The first component comprises of one of a variety of acids (e.g. HCl, H_2SO_4 and HNO_3) and phosphates (e.g. acidic aluminium orthophosphates and acidic zinc orthophosphates). The second component contains a cement material, e.g. any oxides of an alkaline earth metal with a particle size of <150μm. The third component, a "metal" blowing agent, produces hydrogen gas by reaction with acids. Examples of metal blowing agents are magnesium, chromium, manganese, iron, and cobalt. The fourth component is a foaming stabilizer and gives uniform foaming.

The four components are mixed together to form a pasty mass. Typically the amounts used are 80wt.% of the cement and alkali-metal silicate, 15wt.% of the acid or acidic phosphate, 1wt.% of metal blowing agent, and 5wt.% of foaming stabilizer. In this process, the formation of a pasty mass is critical; otherwise the mixture will not foam properly. Once the components are mixed, the acidic solution reacts with the metal blowing agent in the presence of the cement material. Hydrogen gas is evolved and the mixture forms a foam and hardens simultaneously. The result of this concurrent foaming and hardening is a closed cell ceramic foam with a predominantly closed cellular structure, imparting very low permeability (Motoki, 1978).

Jackson (1985), describes a process for making a high strength ceramic foam by careful control of the cell size. The density of the wet foam controls the cell size of the resulting ceramic foam. The aeration process may be repeated several times to produce optimal density for achieving the 60μm mean cell size. The amount of layer-silicate material, e.g china clay, varies from 15-60wt.%. Additives, such as binders, foaming agents and filters may be added to the silicate suspension. The wet foam is heated to approximately 1000^0C to sinter (Jackson *et al.*, 1985).

Helferich *et al.*, (1989), describes a technique for producing a ceramic foam whereby particulate metal reacts with alkali to produce hydrogen gas which results in foaming. This process utilizes an alumino-silicate hydrogel, a refractory ceramic material, a particulate metal, a surfactant and a gel strengthening agent. The hydrogen has many functions. It reacts with the particulate metal to cause foaming. The metal is typically aluminium, present in amounts of 1-2wt.% with a 6-9μm particle size. The refractory ceramic material can be any suitable refractory oxide, carbide, nitride, boride or silicide.

The surfactant helps to control the pore size by breaking up the hydrogen bubbles that evolve during foaming. The presence of the surfactant also helps to produce an open cell ceramic foam. The preferred class of surfactants are the silicone glycols, present in amounts of 4-8wt.% An important component in this process is the gel-strengthening agent, which is typically silica fume used in amounts of 1-4wt.%. In this process, the silicate slurry is added to the aluminate slurry which contains all the additives. Some setting of the mixture starts immediately and at this point the desired shape is moulded. Soon after the components have been

mixed, the particulate metal reacts with the alkali in the hydrogel to evolve hydrogen gas, generating the porous structure. The body is now washed in water to leach out the alkali constituents. The open-cell ceramic is then fired to burn out the organic components and to sinter the ceramic network (Helferich *et al.*, 1989).

Yoshino *et al.*, (1980) have developed a closed-cell ceramic foam using a process where the ratio of the number of metal atoms from a carbonate to those from a phosphate must be between 1/3 and 3/2. If the ratio is less than 1/3, the balance between foaming and setting is disturbed. As a result, uniform, fine cells cannot be attained and the product is a poor water and heat resistant closed cell ceramic foam. If the ratio is above 3/2, the solution made before foaming is extremely unstable and the result is a foamed structure with very little expansion.

The polymetal carbonate used in this method has two functions. Firstly, it evolves CO_2 to foam the solution. Secondly, it acts as a hardening agent. Carbonate and phosphates of alkaline-earth metals are commonly used. The process generally consists of mixing together 60wt.% of metal phosphate, 15wt.% of metal carbonate and 25wt.% of water. The addition of water is important to control the viscosity of the solution. If the viscosity is too low, shrinkage will occur before the closed cell ceramic foam sets. If the viscosity is too high, the other components are difficult to mix. Typically the carbonate is added to the phosphate solution as it is being mixed at high speed. Once the carbonate is added, the mixture is cast in a mould. Foaming of the mixture at room temperature occurs within 600s after adding the carbonate. The foam sets within 600-3600s. The onset of foaming, the time for setting and the volume expansion of the foam can be controlled by the

amounts of carbonate and phosphate used and the stirring speed during mixing. Foamed volumes can be from 5 to 40 times the original volume (Yoshino *et al.*, 1980).

Meek *et al.*, (1985), fabricated ceramic foams by microwave heating of glass and metal micro-balloons. The micro-balloons range between 30 and 130μm in diameter for glass balloons and 400 to 600μm for metal. In this process about 25wt.%. of glass balloons and 73wt.% of potassium silicate binder were used. A microwave coupling agent was also added to the mixture to improve energy absorption at room temperature. Examples of coupling agents are glycerol, nitrates and potassium silicate. This mixture was then placed inside a microwave oven and heated for 300-1800s (5-30 minutes) in air. Meek *et al.*, (1985) suggested that fibres can be added to improve the strength of the closed cell ceramic foam.

Nakajima *et al.*, (1990), have produced porous alumina structures by partially reacting coarse alumina particles with ultrafine silica particles. Mullite formed on the surface of the alumina particles during sintering binds the alumina particles together and leaves pores between them. This porous body must be produced at < 1700°C. This is proper temperature range for the formation of mullite. This process was developed in response to the undesirable low porosity and high production costs of alumina foams made by conventional methods. In the conventional process alumina powder is combined with a binder and heated to > 2000°C. The high sintering temperature results in both low porosity and high costs.

2.6.2 Porosity

The fraction of the bulk volume of the porous sample that is occupied by pore or void space is defined as porosity. Porosity is also called voidage (Dullien, 1979).

2.6.2.1 Types of pore

Types of void can be classified as below (Dullien, 1979):

- Pore or void space which forms a continuous phase within the porous medium is called interconnected or effective pore space.
- Pore or void space which consists of isolated pores in a medium is called non-interconnected pore space.
- Pore or voids interconnected only from one side is called dead end or blind pores.

Descriptions of porous materials are based on the dimensions of the pores. Materials are microporous when pores are <2nm diameter, mesoporous when the pore diameter is in the range of 2-50nm and macroporous when the pore diameter is > 50nm (Nettleship, 1996).

2.6.2.2 Porosity evaluation

Porosity evaluation has been largely researched as a part of filter characterization. There are various experimental methods used to determine porosity but it is important that methods used must be time efficient, cost effective and allow usage

after testing. Two most common porosity evaluation methods (Shapiro,1992) are briefly described below:

The density method depends on determining the bulk density of the sample and density of the solids in the sample. Since the mass of a porous medium resides entirely in the solid matrix:

$$\frac{V_s}{V_a} = \frac{\rho_a}{\rho_s} \qquad 2.5$$

where ρ_s is the density of the solids in the sample, ρ_a is the bulk density of the sample, V_s sand V_a are volume of solid and bulk body, respectively. The porosity (P) can be calculated as (Gibson *et al.*, 1988, Philipse *et al.*, 1991, Chao *et al.*, 1996 and Salvini *et al.*, 2000):

$$P = 1 - \left(\frac{V_s}{V_a}\right) \qquad 2.6$$

$$P = 1 - \left(\frac{\rho_a}{\rho_s}\right) \qquad 2.7$$

Porosity can also be estimated by both optical and scanning electron microscopy (SEM). These microscopical techniques can be used in conjunction with image analysis tools to estimate porosity across a wide area of the sample. However, image analysis values can be underestimates of the actual volume of porosity (Nangrejo *et al.*, 2001).

The literature review leads to the conclusion that a new solid freeforming process with the capabilities of producing fine ceramic relics (<100μm) is worthy of investigation. Therefore, electrostatic atomization of viscous liquids and ceramic suspensions were studied extensively as described in Chapters 3-6. Ceramic electrostatic atomization printing and the production of ceramic foam are novel and significant outcomes of this work.

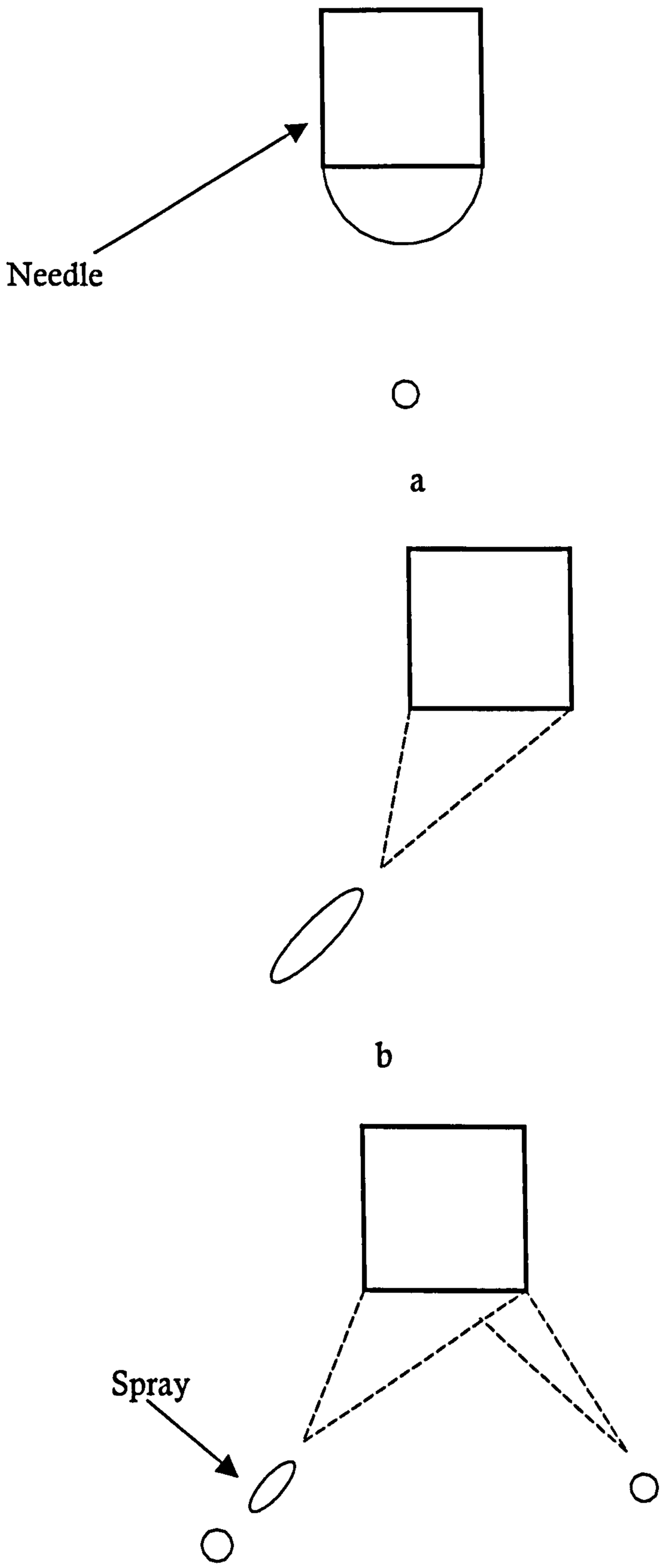

Figure 2.1 Schematic representation of a) Micro-dripping, b) Spindle and c) Multi-spindle. Dotted lines illustrate instability

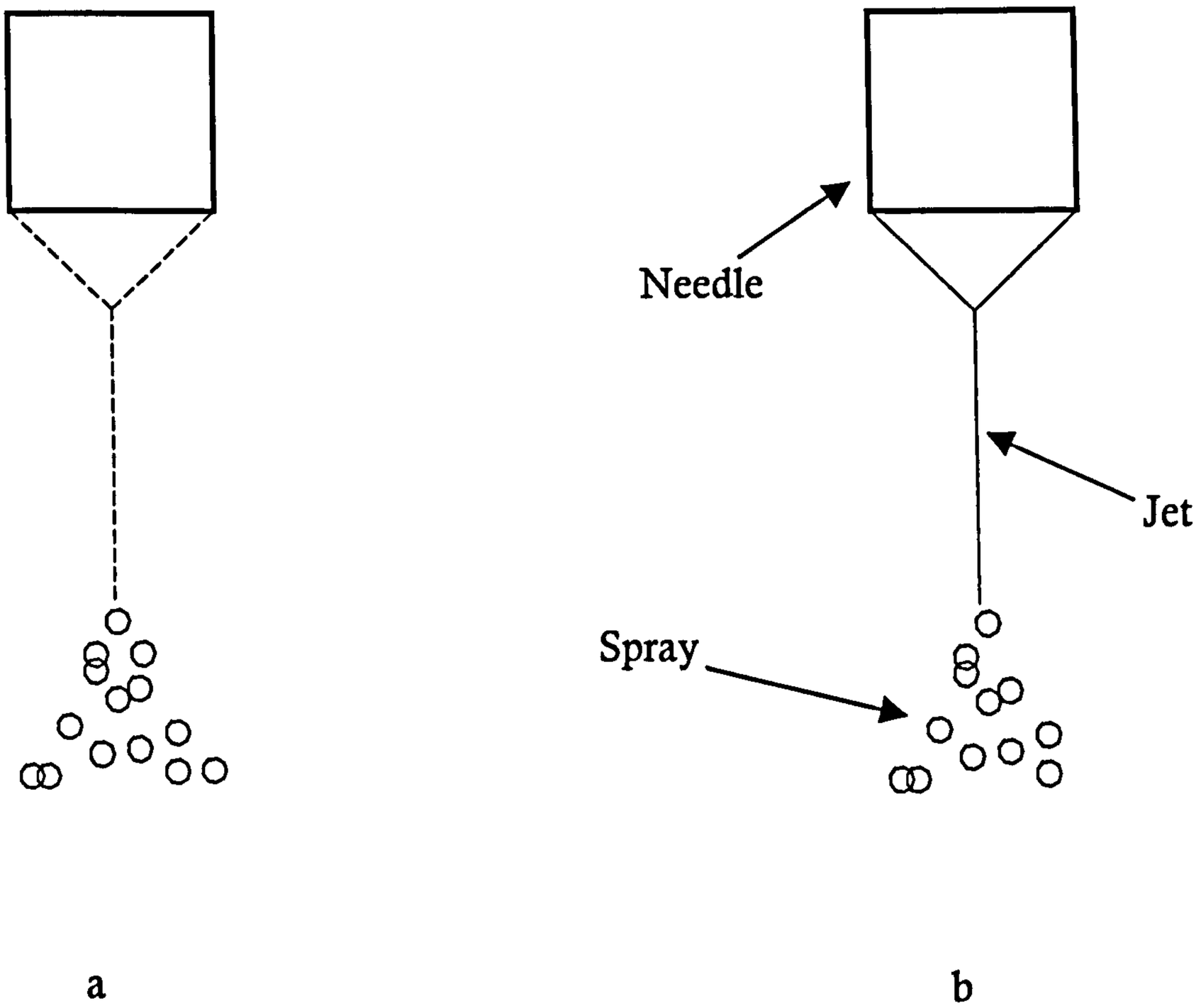

Figure 2.2 Schematic representation of a) Intermittent Cone-Jet and b) Stable Cone-Jet. Dotted lines illustrate instability

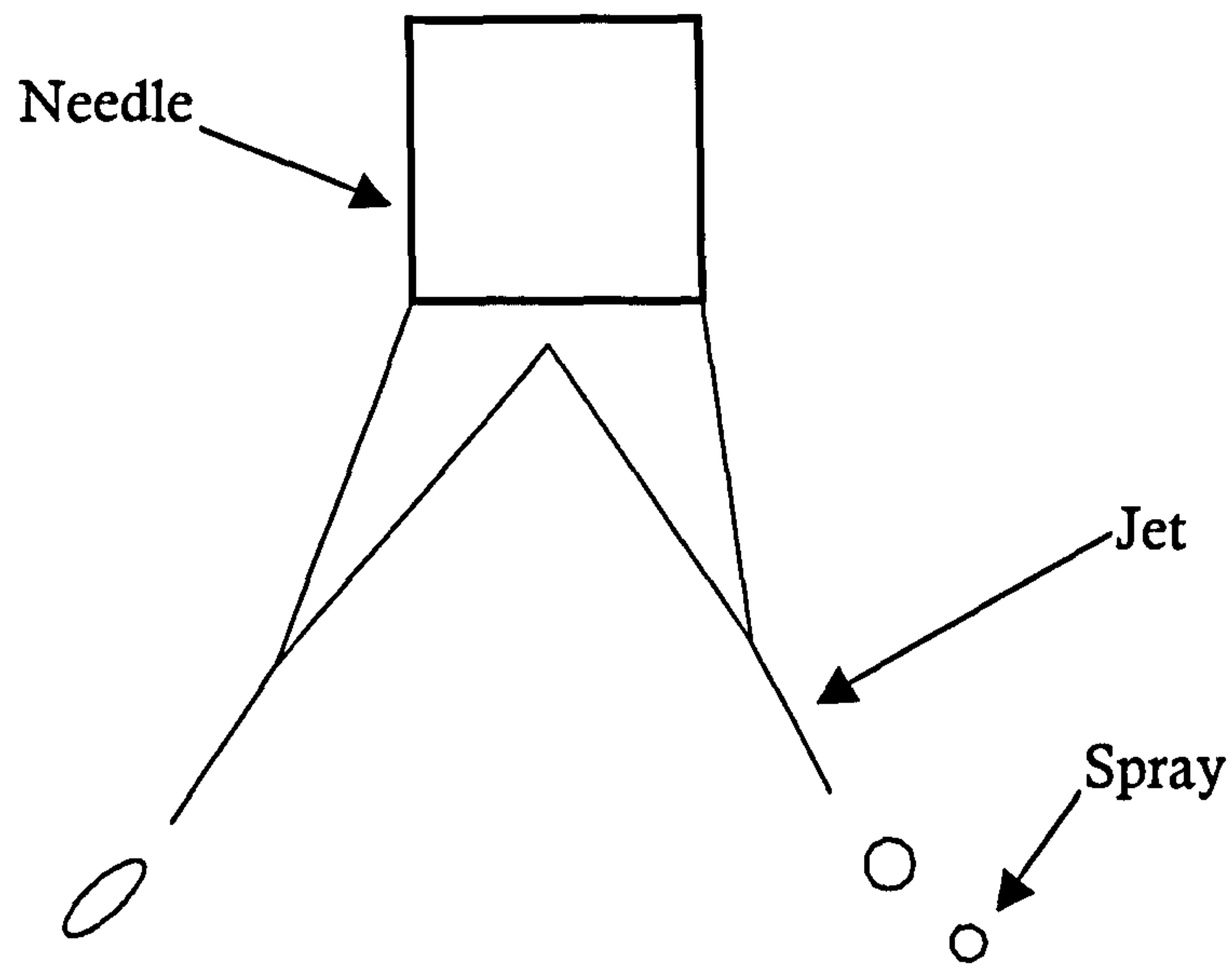

a

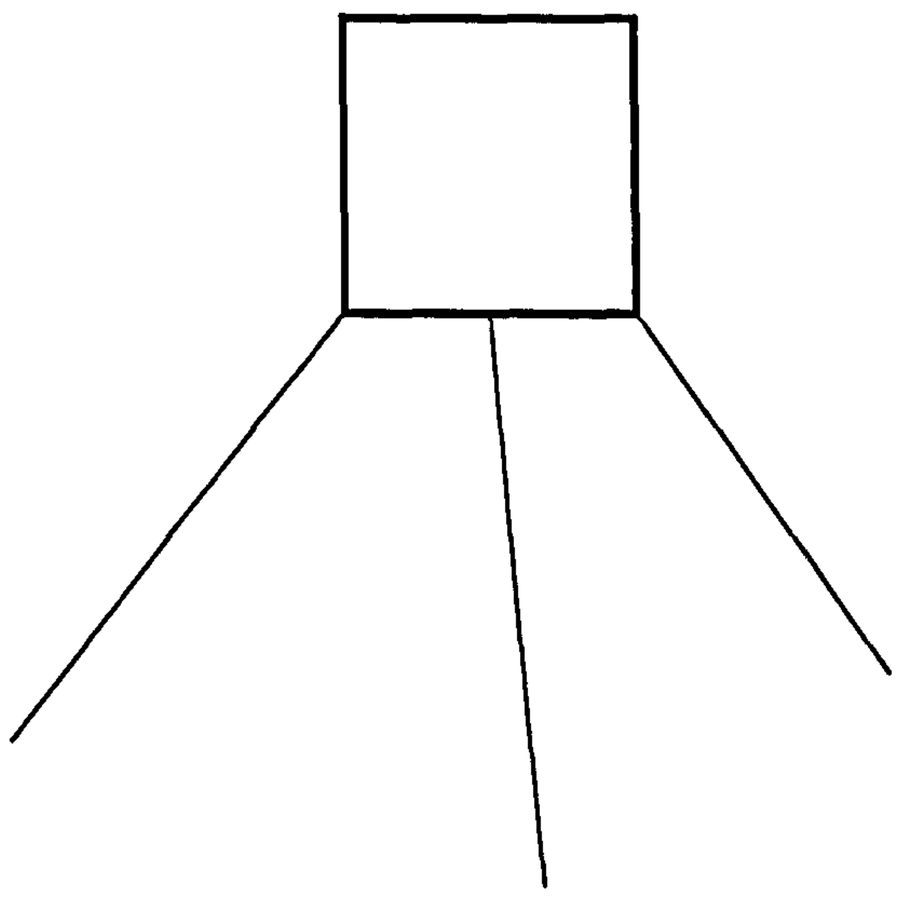

b

Figure 2.3 Schematic representation of a) Multi-Jet and b) Rim Emission

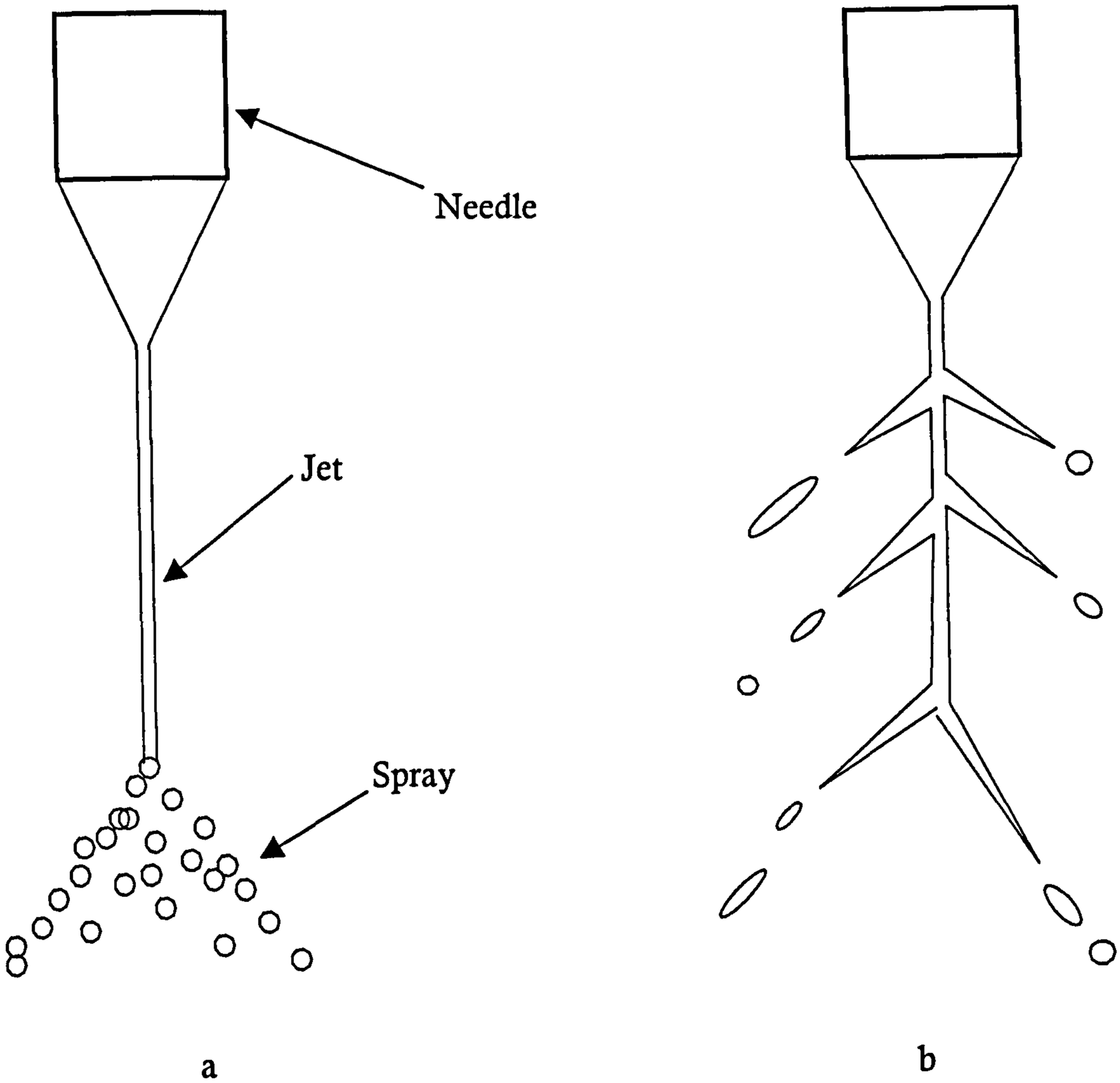

Figure 2.4 Schematic representation of a) Simple-Jet and b) Ramified

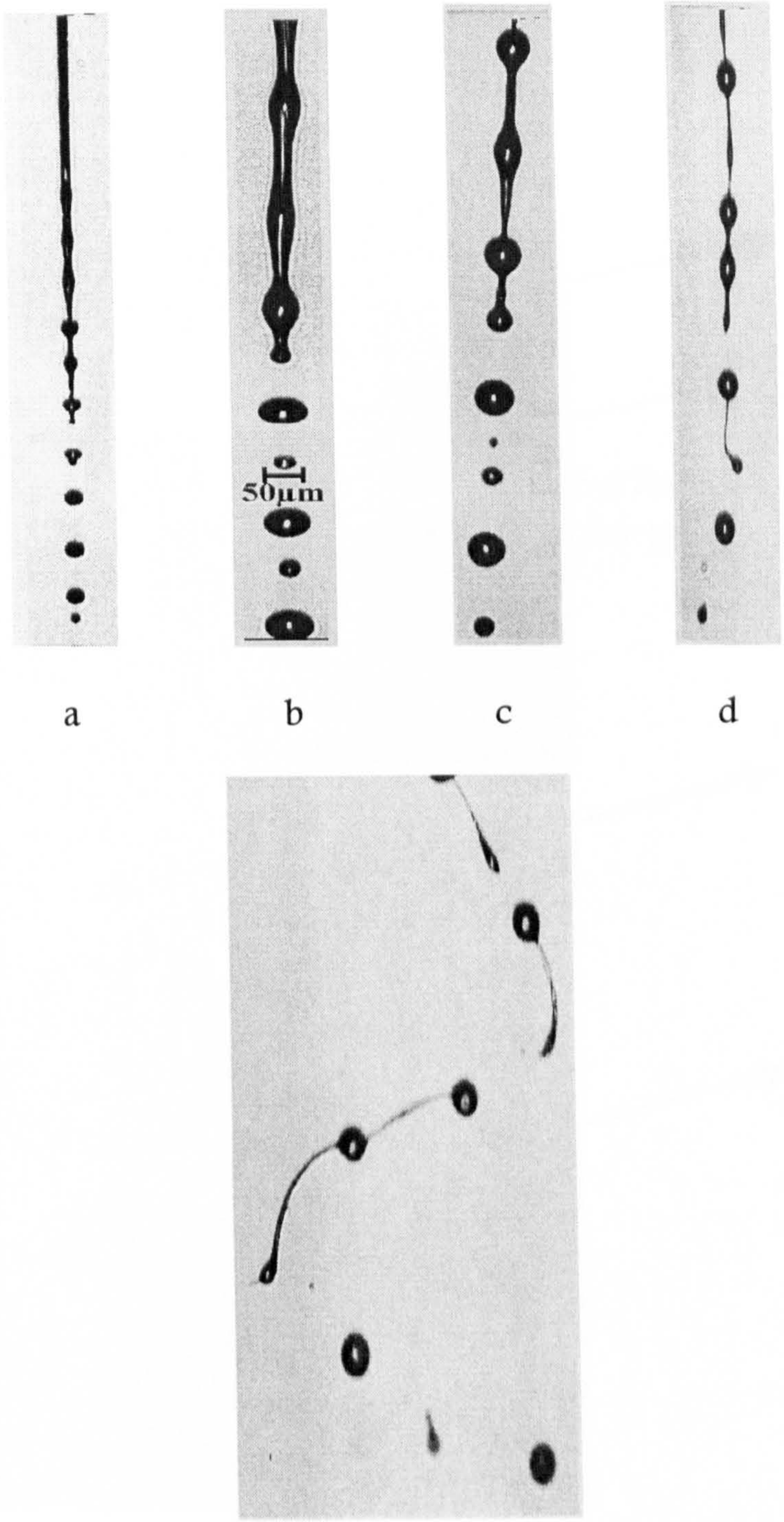

a b c d e

Figure 2.5 Jet break-up regimes as described by Hartman *et al.,* (2000): **a**) first, where only primary droplets are formed, **b**) the formation of primary and secondary droplets in the second regime, **c**) the formation of smaller sattelite droplets in the third regime, **d**) the fourth, where the jet exhibits the ejection of droplets in a non-linear fashion and **e**) the entire jet whips in the final phase

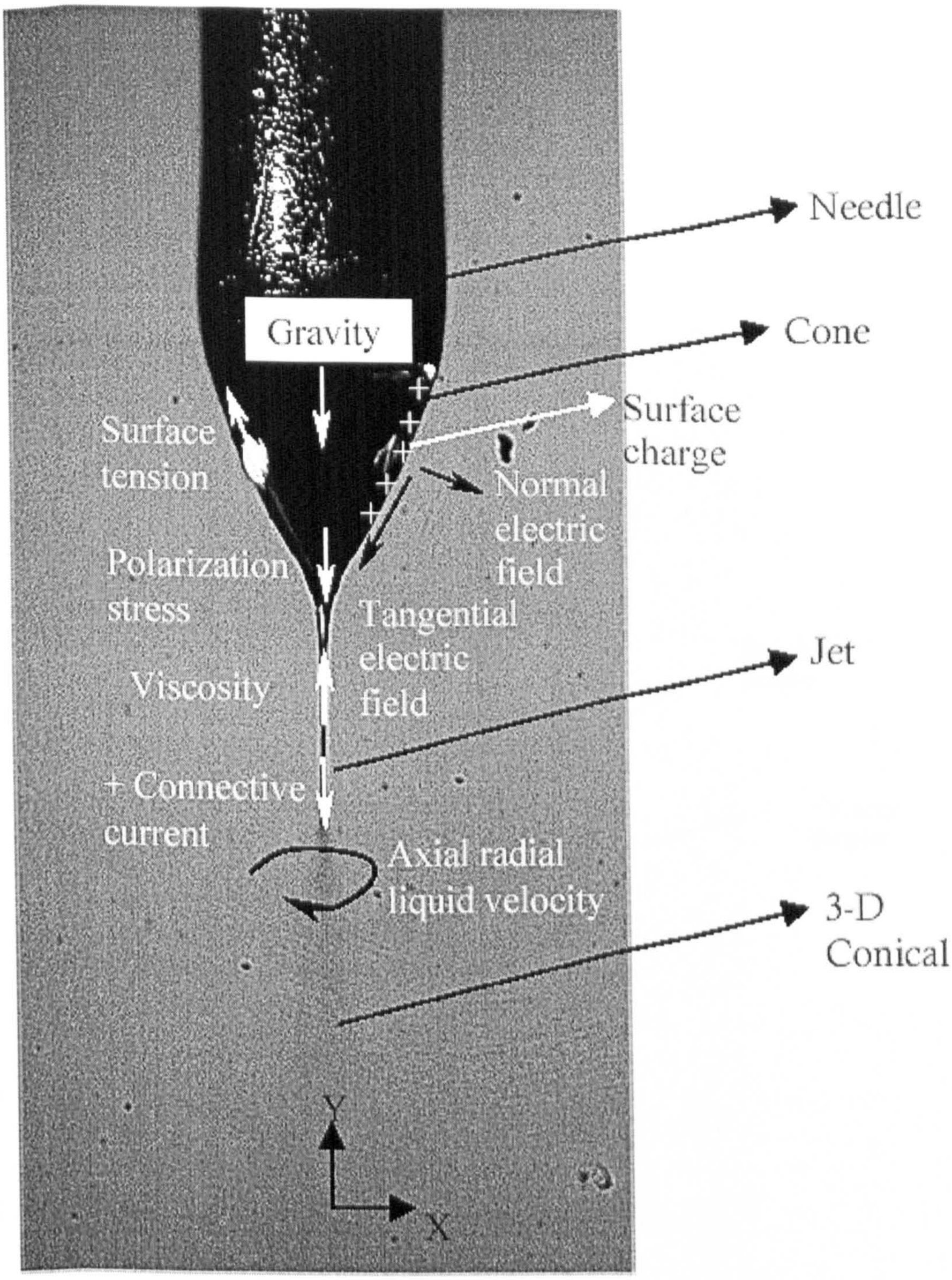

Figure 2.6 Forces acting on a liquid subjected to cone-jet mode electrostatic atomization

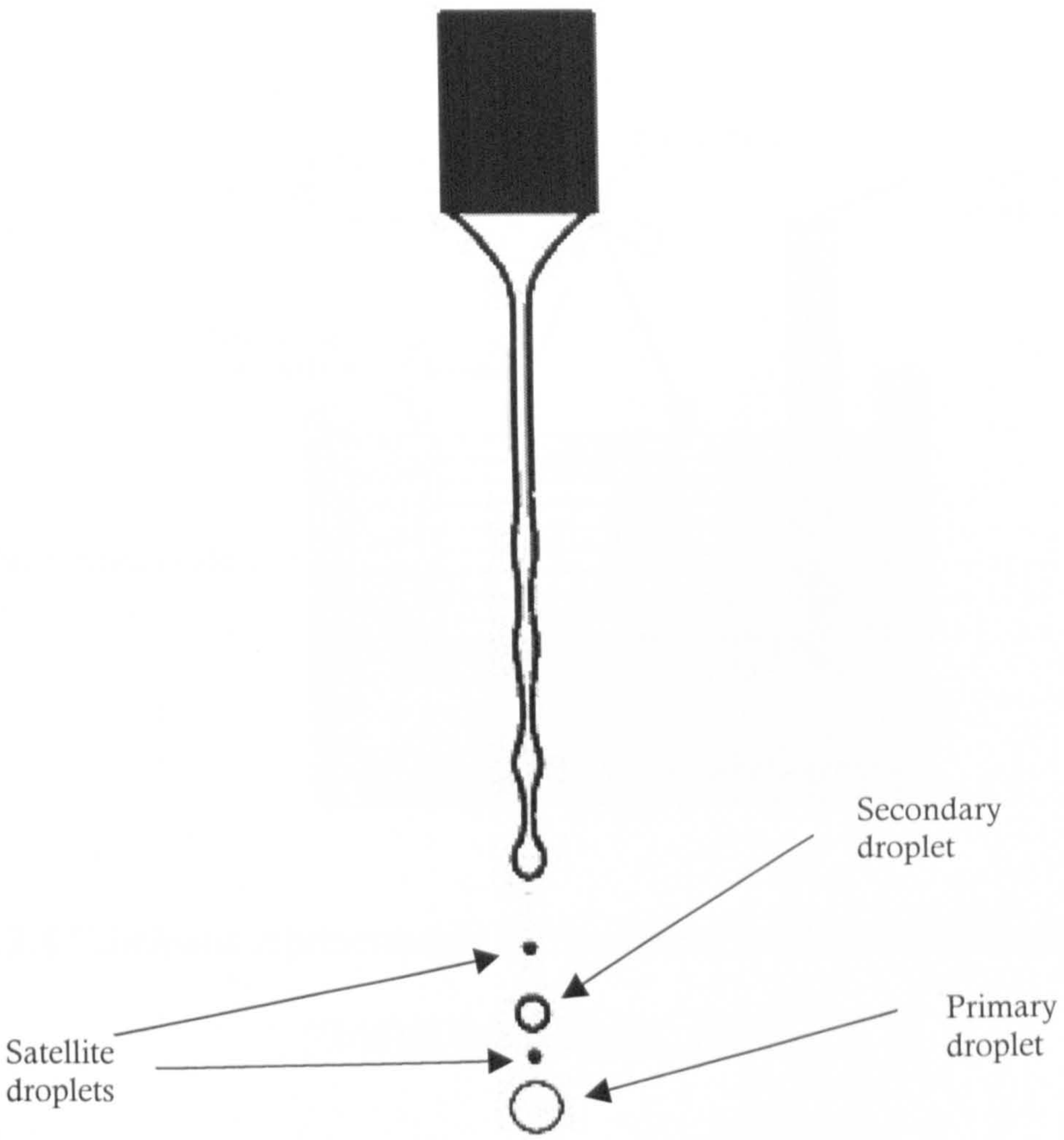

Figure 2.7 Jet break up illustrating the formation of sattelite droplets between primary and secondary droplets

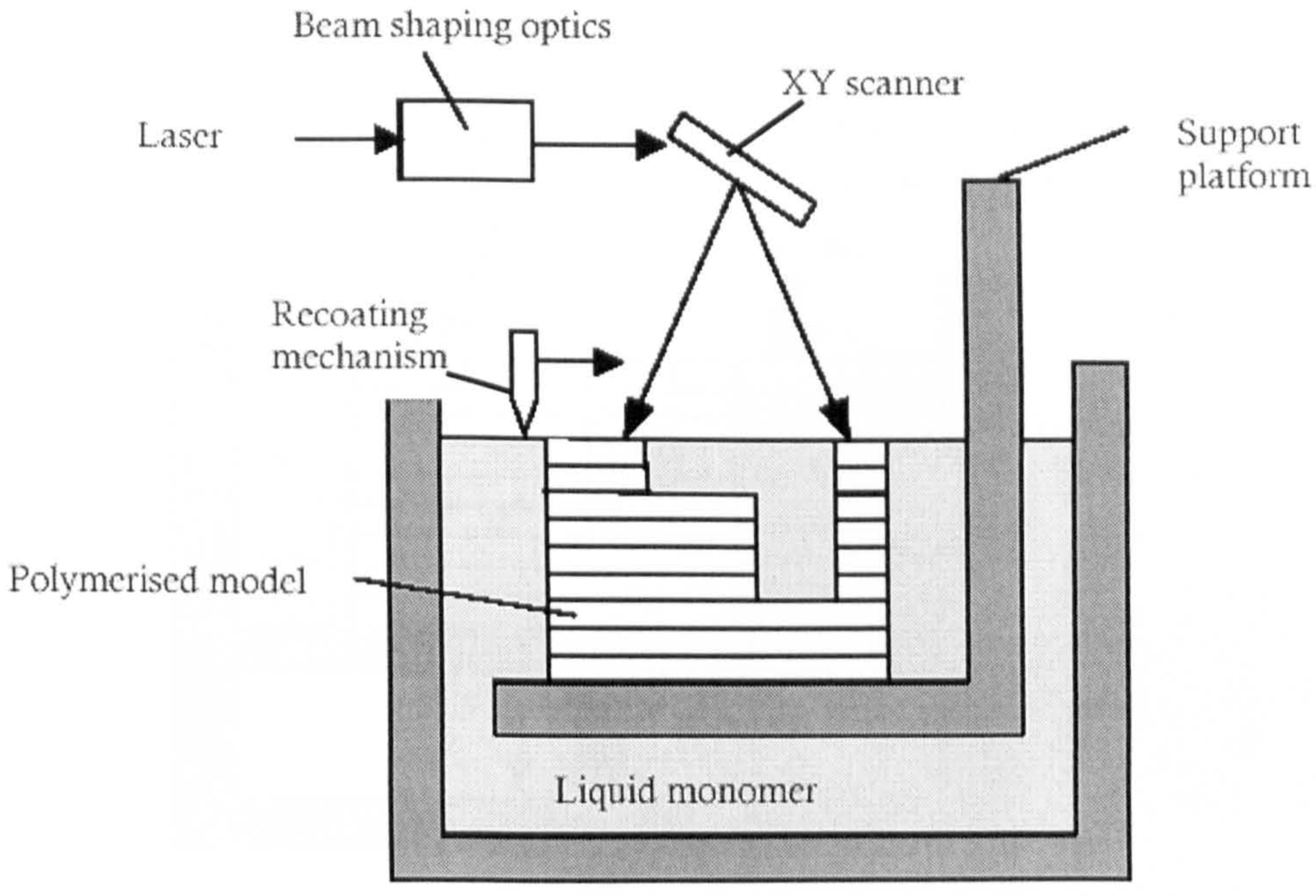

Figure 2.8 Schematic representation of 3D systems stereolithography apparatus

(Griffith and Halloran, 1996)

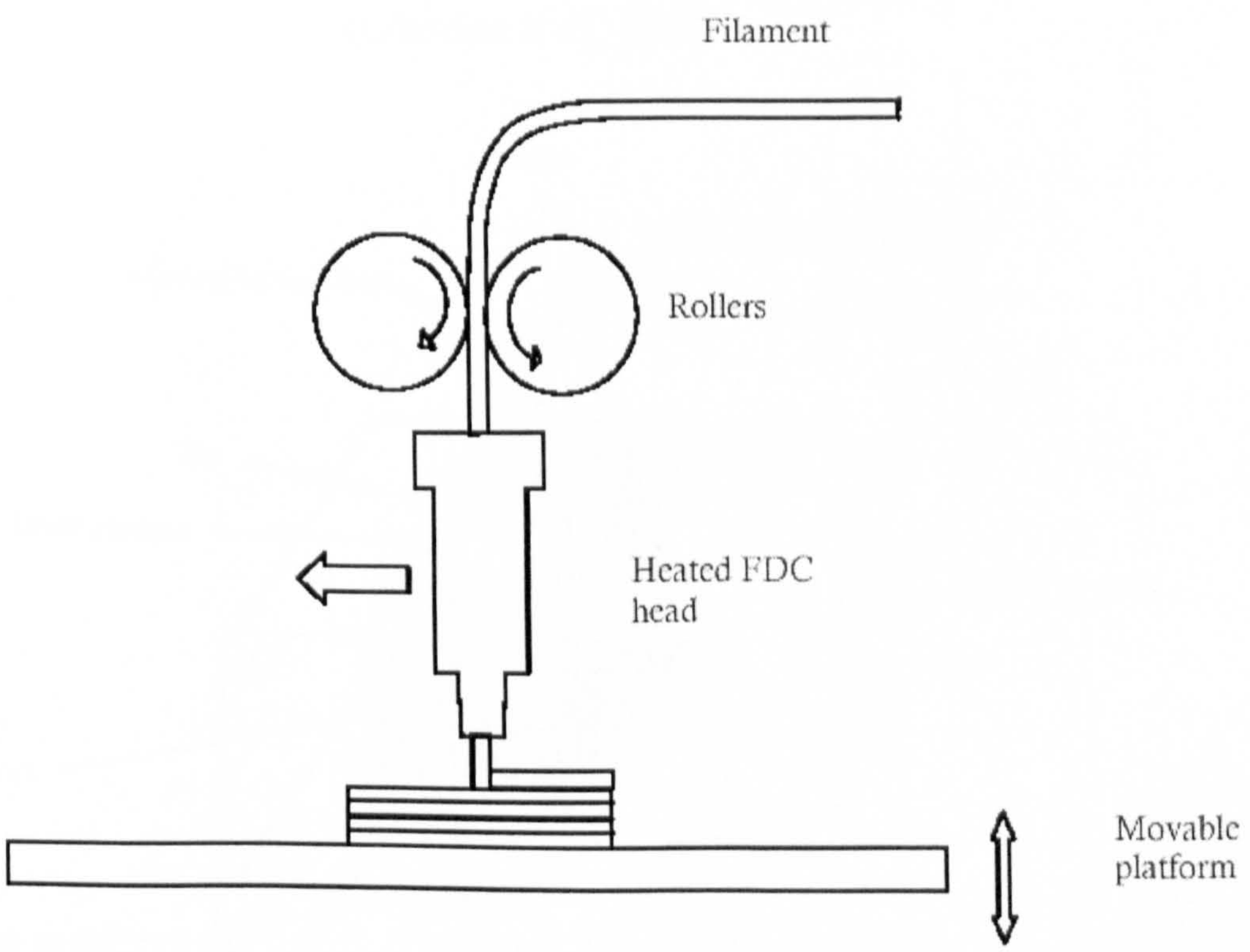

Figure 2.9 Schematic representation of apparatus used for fused deposition of ceramics (Conley and Marcus, 1997)

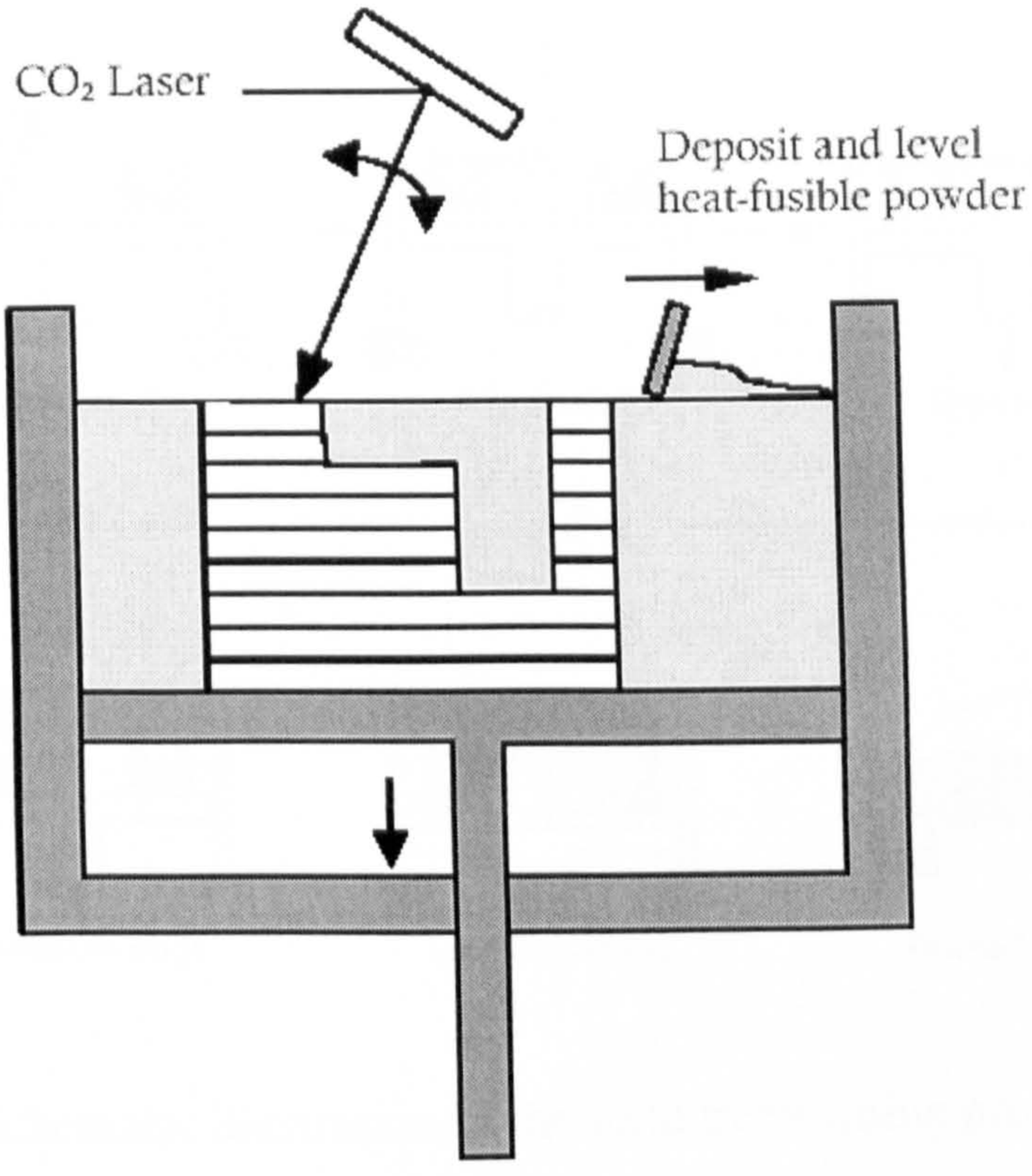

Figure 2.10 A schematic diagram illustrating the selective laser sintering process (Glardon *et al.*, 2001)

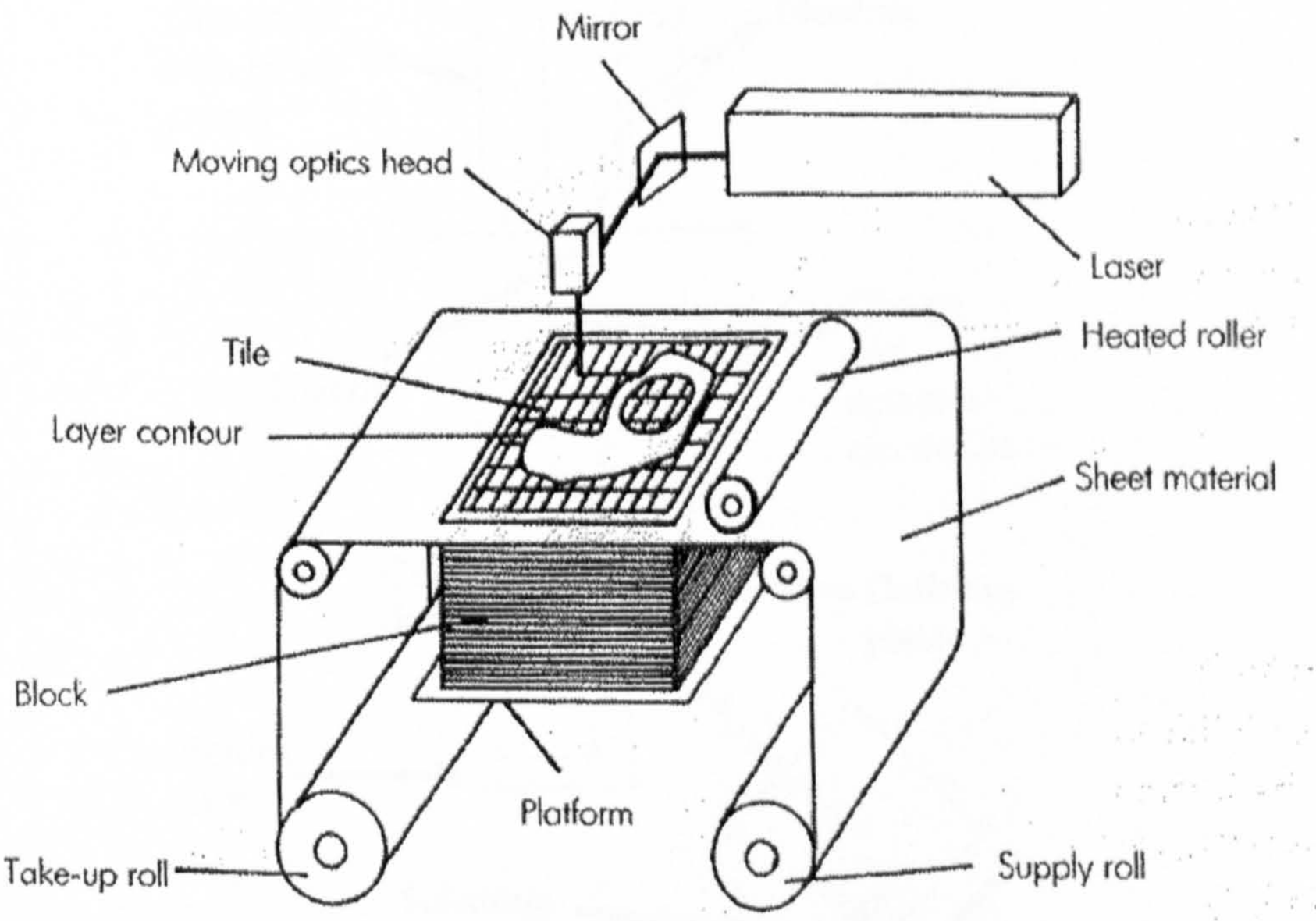

Figure 2.11 Schematic representation of laminated object manufacturing (Conley and Marcus, 1997)

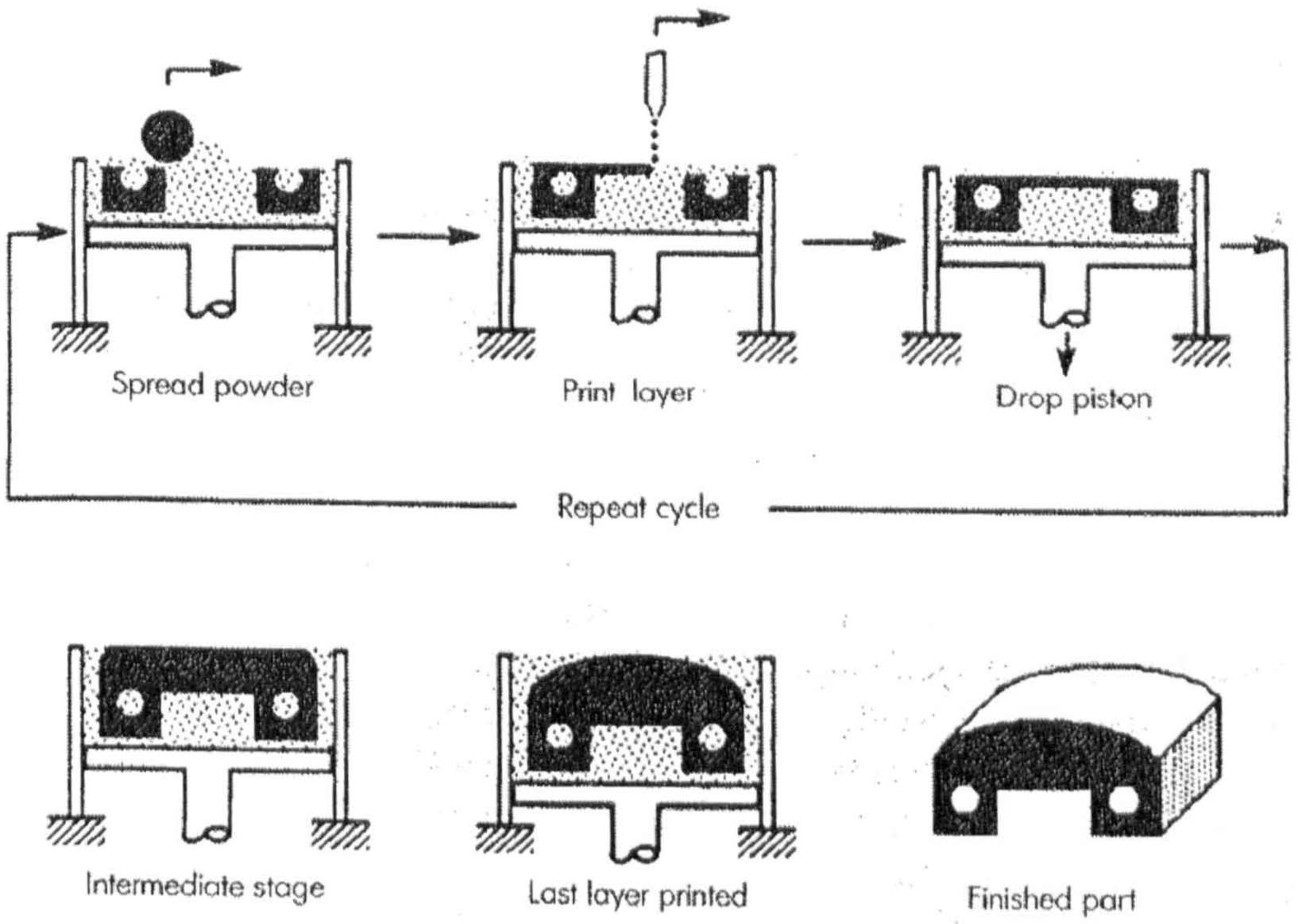

Figure 2.12 Schematic illustration of the solid freeforming process 3-D printing (Sachs *et al.*, 1992)

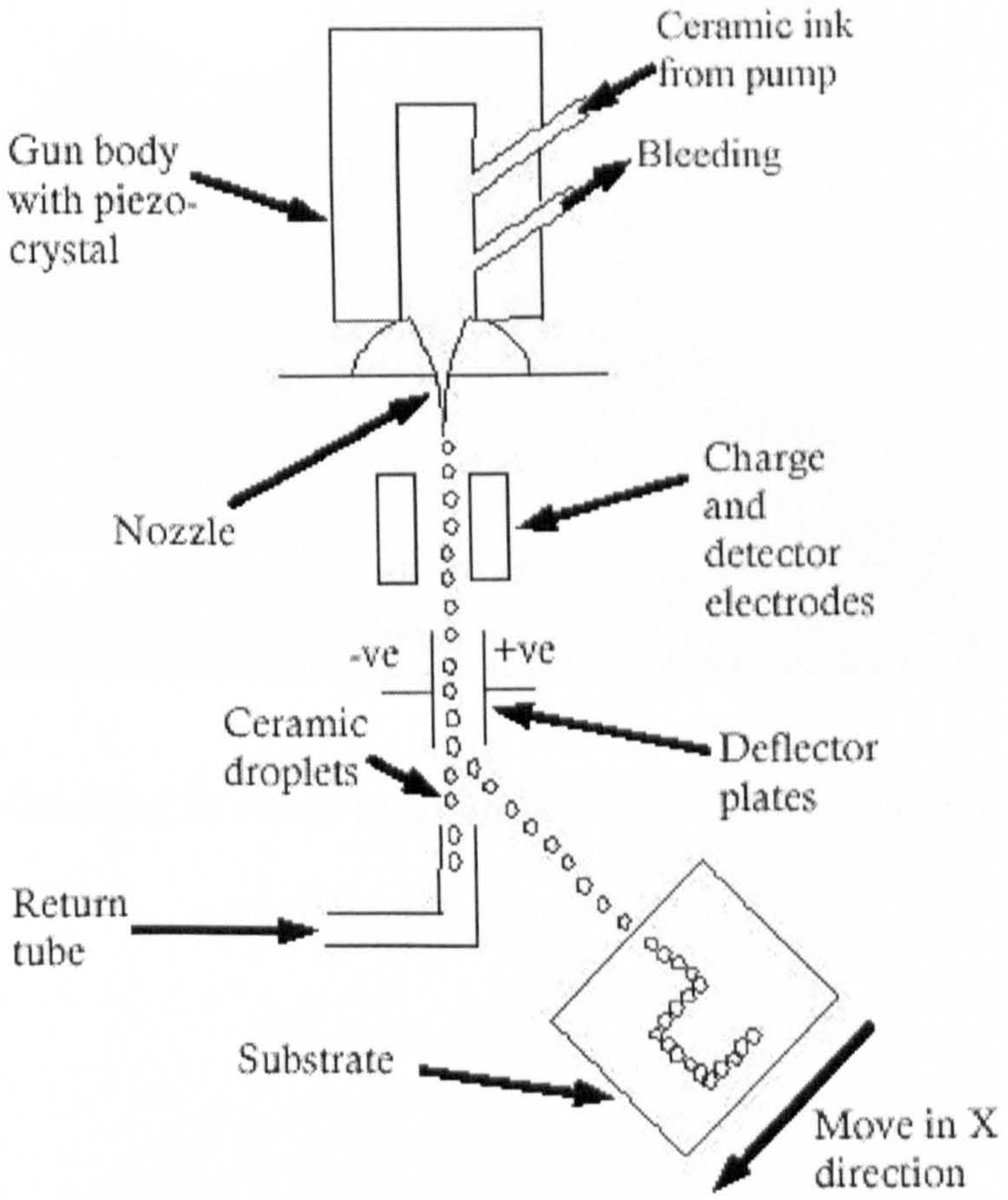

Figure 2.13 Schematic diagram showing the principle of operation of a continuous suspension jet-printer (Teng and Edirisinghe, 1998)

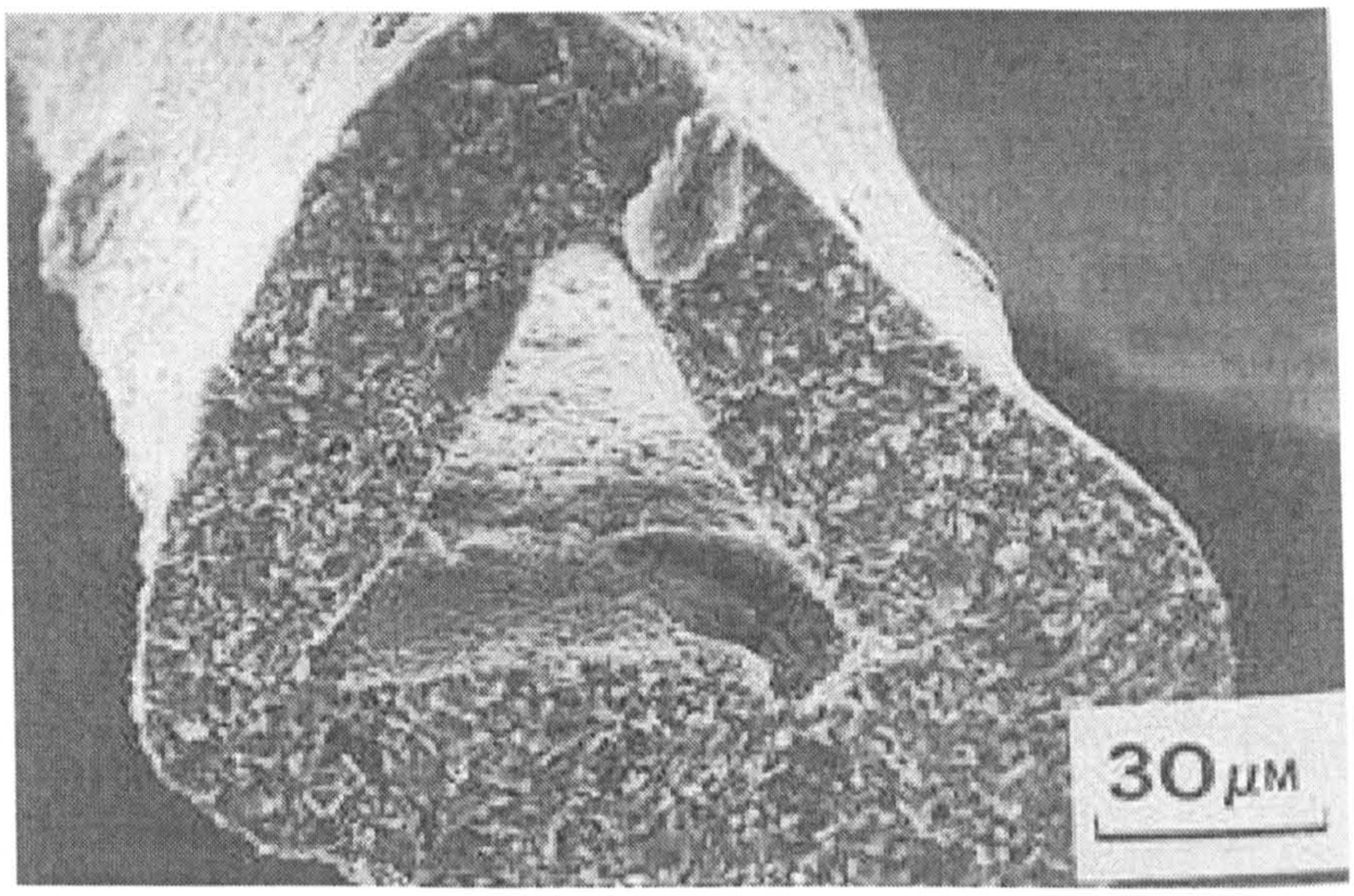

Figure 2.14 Strut cross-section of a ceramic foam processed using a slurry and a porous template. A central void is clearly seen (Hagiwara and Green, 1987)

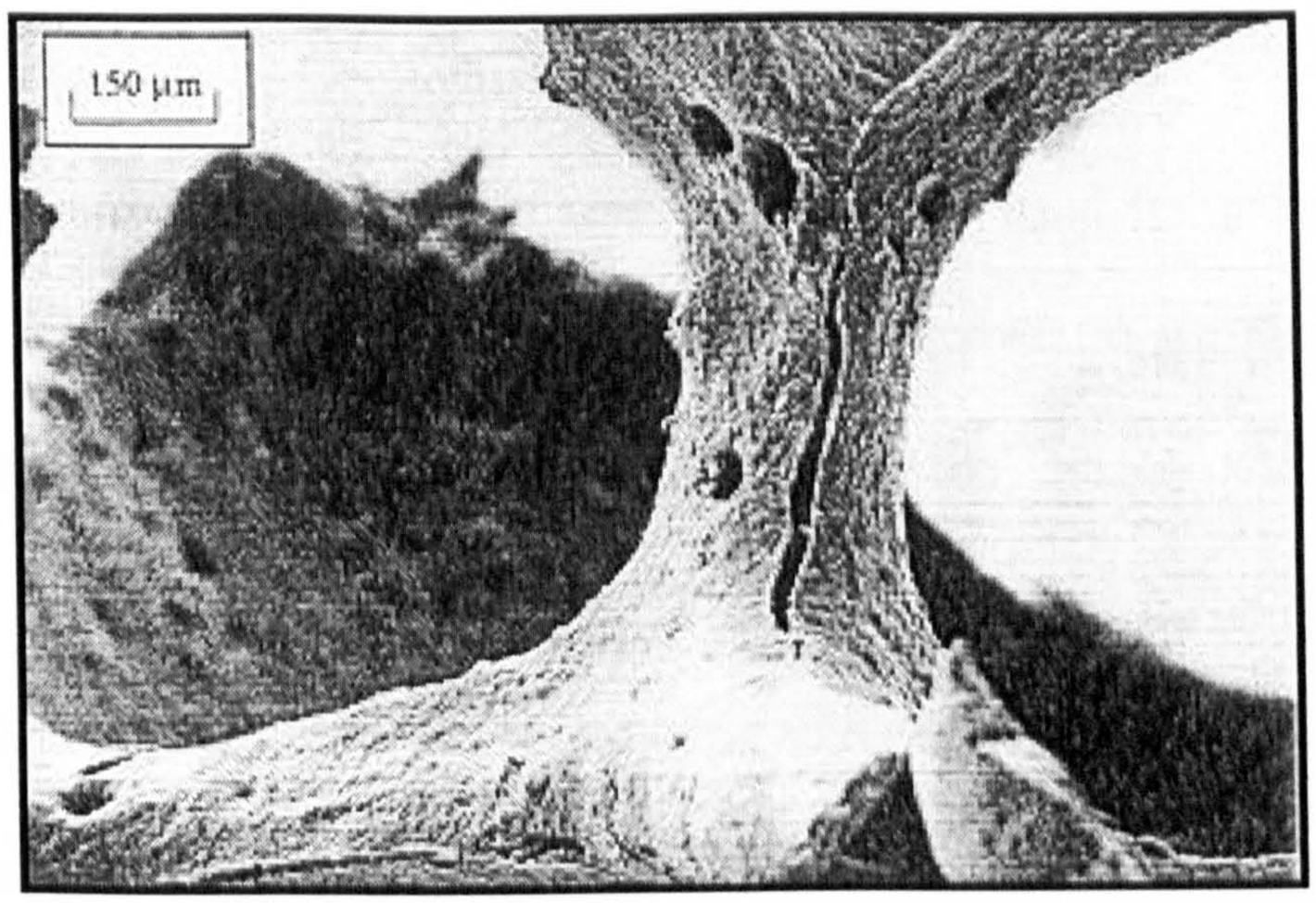

Figure 2.15 Cracking in struts in a ceramic foam processed using the slurry method (Vedula, 1999)

CHAPTER 3

Experimental Details

The materials and the techniques used for preparing, processing and characterizing the liquid mixtures and ceramic suspensions are described in detail in this chapter. Experiments described in this thesis were repeated at least three times to check reproducibility. Measurements were calibrated against a known value in the literature and is identified at each section of work described below. In all instances the error was <1%.

3.1 Materials

3.1.1 Liquid mixtures

Glycerol, distilled water and citric acid crystals were used for preparing liquid mixtures to investigate the effect of viscosity on electrostatic atomization. **Table 3.1** gives full details of the constituents.

Table 3.1 Details of glycerol, water and citric acid used to make liquid mixtures.

Material	Grade	Density kgm^{-3}	Supplier
Glycerol	GPR	1310	BDH Chemicals Ltd., Lutterworth, UK
Distilled water	Single distilled	1000	Queen Mary, University of London, UK
Citric acid	GPR	1540	BDH Chemicals Ltd., Lutterworth, UK

3.1.2 Ceramic suspensions

Five alumina suspensions were formulated using a near-monodisperse powder containing particles of size ~0.5μm. The composition of the suspensions were selected based on prior work in the Department of Materials, Queen Mary,

University of London, where suspension development research has taken place over fifteen years. The first four were used to understand the effect of increasing the powder content within a suspension. This was carried out using the constituents given in **Table 3.2**. Thus, four suspensions (CS1-CS4) were made with each containing a different weight percentage of alumina powder (1, 3, 5 and 20wt.%). These four suspensions had the same weight percentage of dispersant added to them.

Table 3.2 Details of constituents used in ceramic suspensions CS1-CS4.

Material	Grade	Density kgm^{-3}	Supplier
Alumina	ALCOA A16.SG	3987	ALCOA, Ludwigshafen, Germany
Ethanol	GPR	790	BDH Chemicals Ltd., Lutterworth, UK
Zephrym	PD3315	1100	Uniqema, Cleveland, UK

The second suspension (CS5), details of which are given in **Table 3.3**, was designed to contain 57 wt.% (20 vol.%) of alumina.

Table 3.3 Details of constituents used in ceramic suspension CS5.

Material	Grade	Density kgm^{-3}	Supplier
Alumina	ALCOA A16.SG	3987	ALCOA, Ludwigshafen, Germany
Ethanol	GPR	790	BDH Chemicals Ltd., Lutterworth, UK
Efka	401	950	Efka Chemicals, Heerenveen, Holland

3.2 Preparation of liquid mixtures

The glycerol used was fresh and single distilled water was obtained just prior to mixing. Citric acid crystals were used to control the conductivity of the liquid mixtures so as to maintain a dc electrical conductivity of $25mSm^{-1}$.

3.2.1 Roller mixing

Carefully measured weight percentages of distilled water and glycerol (25, 50 and 75 wt.%) and 1-7 wt.% of citric acid crystal were added together. Samples of distilled water and citric acid, and samples of glycerol and citric acid were also prepared. These were left to stand for 3600s to ensure that phase separation and precipitation of the citric acid did not take place. Later the samples were left agitating on a roller mixer till required for electrostatic atomization which was carried out within 21600s. Before each sample was electrosprayed the homogeneity of the mixtures were checked by careful observation.

3.3 Preparation of ceramic suspensions

Suspensions CS1-CS4 were mixed by ultrasonic disruption. Suspension CS5 had a much higher powder content and was mixed using a high energy bead mill.

3.3.1 Ultrasonic disruption

Initially 5wt.% Zephrym PD3315 was dissolved in ethanol. Subsequently the respective weight percentages of alumina (1, 3, 5 and 20wt.%) were added and mixed by ultrasonic disruption.

A Sonifer 250 (Branston Ultrosonics, Danbury, CT USA) ultrasonic probe was used and mixing was carried out in a beaker inputting 75W over 600s with constant stirring. The alumina suspensions were kept in well sealed bottles and agitated on rollers until required for electrospraying.

3.3.2 High energy bead milling

Carefully measured quantities of ethanol and Efka 401 dispersant were mixed into a beaker and stirred manually. Later alumina powder was added to the ethanol-Efka mixture and stirring was continued. Subsequently, the suspension was put through a high-energy bead mill (Glen Creston Dyno-mill, Type KDL A, Stanmore, UK) for mixing. The operating details of the mill are shown in **Table 3.4**. The suspension was passed through the mill five times and on each occasion the output was collected in a fresh container. Throughout the milling process the temperature was monitored so as to not exceed 40^0C.

Table 3.4. Bead mill operating conditions

Variable	Details
Tip Speed	$14ms^{-1}$
Type of beads	0.5 mm diameter yttria stabilized zirconia
Volume of beads in chamber	216 ml (80% of capacity)
Pump flow rate	$0.5ml\ s^{-1}$
Milling temperature	40^0C (Maximum)
Stirrer motor current	0.2 A

The milled alumina suspension was kept on rollers and agitated until required for electrostatic atomization.

3.4 Characterisation

The investigations carried out in chapters 4, 5 and 6 rely on the accuracy of each measurement made using in-house instrumentation. Each instrument was calibrated before use on each day and thoroughly cleaned between samples.

3.4.1 Loss-on-ignition

Samples of suspensions were heated to 600^0C to check the alumina content after mixing.

3.4.2 Density

The density was measured using the well-established density bottle method. Calibration was carried out by measuring the densities of known liquids (e.g. distilled water and glycerol) for the work described in chapter 4. For the research described in chapters 5 and 6, ethanol was used for calibrating the density bottle.

3.4.3 Viscosity

The viscosity of the water-glycerol mixtures were measured using a Haake 150 Rheostress rotational meter (Haake GmbH, Karlsruhe, Germany). This is a controlled stress rotational rheometer. In this case glycerol was used to calibrate the rheometer. A U-tube viscometer was used to measure the viscosity of the ceramic suspensions. The viscometer was immersed in a thermostat water bath maintained at 25^0C. Single distilled water and ethanol were used respectively, to calibrate the U-tube viscometer to calculate the nominal factor C (see equation 2 below). This estimated value was then used in comparison with the C value quoted by the manufacturer. The viscosity of the suspensions were calculated as follows:

$$\eta = \upsilon\rho \tag{3.1}$$

$$\upsilon = Ct \tag{3.2}$$

Where η is the dynamic viscosity of the suspension in mPa s, υ is the kinematic viscosity of the suspension in mm^2s^{-1}, ρ is the density of the suspension in gcm^{-3}, C is the nominal factor in mm^2s^{-2} and t is the mean flow time in seconds.

3.4.4 DC Conductivity

The conductivities of all the liquid samples were measured using a cell which had a cell constant (A/L) of $7.27x10^{-3}m$.

$$K = \frac{L}{AR} \tag{3.3}$$

Here K is the conductivity of the liquid in Sm^{-1}, L is the internal length of the cell in m, A is the internal area of the cell in m^2 and R is the measured resistance of the liquid across the plates in Ohm. The conductivity cell was calibrated using KCl and ethanol.

3.4.5 Surface Tension

The surface tension of all the liquid samples were measured using the Du Nouy ring method. Samples were placed in a dish and the ring was immersed into the sample. The dial on the balance was slowly and carefully turned until the ring rose to the surface of the liquid and pulled on the liquid surface without detaching itself and rising above the liquid surface. At this stage the value was read off the dial of the instrument. The instrument was calibrated with distilled water, glycerol and ethanol.

3.4.6 Relative permittivity

As in the case of the conductivity cell, a special glass cell was made to much smaller dimensions and was calibrated in similar fashion to the conductivity cell. The relative permittivity was calculated by first measuring the capacitance across the cell with the liquid inserted in it. The relative permittivity of the sample was calculated using $\frac{Cd}{\varepsilon_0 A}$, where C is the capacitance, d is the distance between the plates and ε_0 is the permittivity of free space. A, which is the area of the plates was $4.7 \times 10^{-5} m^2$ and d was 3.85mm.

3.4.7 Sedimentation behaviour

The sedimentation behaviour of the liquid mixtures (S1-S5) was not carried out as the mixtures were left on the roller mixer till it was required for atomization and no phase separation was apparent. The ceramic suspensions were subjected to a sedimentation test. A standard pyrex test tube was calibrated for volume against height. The suspensions (CS1-CS5) were poured into the tubes, sealed and left undisturbed. Sedimentation in the first 10800s (3 hours) was negligible for all five suspensions. However, over 36×10^3s (10 hours), sedimentation in CS1-CS4 increased but was much less in CS5. Therefore, all the suspensions were mixed continuously on rollers until required for electrostatic atomization.

3.5 Equipment used for Spraying

3.5.1 Capillary and ground electrode configuration

The equipment used for electrospraying consists of a stainless steel needle having a straight edged exit (0.2 mm and 0.48 mm inner and outer diameter,

respectively) held in epoxy resin, 8 or 6 mm below which a circular ring (diameter 15mm)/square shaped plate (each side of length 15mm) or a point like (with a tip diameter of ~0.13mm) ground electrode was placed, respectively. In the case of the ring and the plate shaped ground electrodes the needle was held axi-symetrical (see **Figure 3.1**).

3.5.2 Multi-needle configuration

The multi-needle and multi-ground electrode electrospraying apparatus consists of three stainless steel needles (each having 0.2 mm and 0.48 mm inner and outer diameters, respectively) held in epoxy resin, 6 mm below which three point like ground electrodes were placed in-line (see **Figure 3.2**).

3.5.3 Syringe pump

Each needle inlet was connected to a syringe mounted on a Semat A99FMZ syringe pump (Semat International Ltd., St.Albans, UK) using silicone rubber tubing. The flow rates were adjusted accordingly by either changing the cross-sectional area of the syringe or by varying the number on the rate selector switch. The flow rate is calculated as follows:

$$FR = 0.23446 \times RS \times SCA \qquad (3.4)$$

Where FR is the flow rate in $mlhr^{-1}$, 0.23446 $cmhr^{-1}$ is the factor given by the manufacturer of the syringe pump, RS is the number selected on the rate selector switch and SCA is the syringe cross sectional area in cm^2. For each study the flow rate was calibrated over long (60, 180, 300 and 600s) and short (1, 3, 5 and 10s)

periods of time, as flow rate consistency is an important factor in electrostatic atomization. The flow rate was then converted to m^3s^{-1}.

3.5.4 Power source

Each needle and ground electrode were connected to a Glassman FC30 high voltage power supply (Glassman Europe Ltd., Tadley, UK) which was capable of applying upto 30 kV.

3.5.5 Data Recording in Real Time

A microscope was used in conjunction with a CCTV camera (WAT-502A Watec Co. Ltd., Kanagawa, Japan), a monitor, a computer and a video recorder (VCR) in order to record the electrostatic atomization process, in particular at the needle and at the ground electrode. A high-speed camera (Kodak EktaPro, EM motion Analyser/Model 1012) on loan from the EPSRC Engineering Instrument Pool at Rutherford Appleton Laboratories, Oxford, UK was used for capturing droplet trajectories as they emerge from the jet. This camera was capable of capturing 12000 frames s^{-1}.

3.6 Printing

3.6.1 Materials and Equipment

Suspension CS5 was used. The substrates on which the relics could be collected in or deposited on were carefully chosen as spreading after deposition needed to be kept to a minimum. Furthermore, the substrates needed to be free of all impurities and opaque to allow for relic analysis to be carried out by optical microscopy. Three types of substrates were used (**Table 3.5**).

Table 3.5 Details of substrates used

Identification	Trade name and type	Supplier
SUB-1	Silicone release paper	Sterling-Lohja, Glossop, UK
SUB-2	Acetate transparency for photocopying	Nice Day Office Supplies, London, UK
SUB-3	Coated polyester substrate	Autotype International Ltd, Wantage, UK

3.6.1.1 Synchronised 2-axis motion control system

This section describes the careful design considerations taken into account during the building of the 2-axis computer controlled printing system. The electrical hazards of this part of the work were considerable and therefore all the materials except the two carriages were made of insulators (see **Figure 3.3**). Perspex and PET were the two main insulating materials used.

The printing system is 2-axis (X-Y), stepper motor driven and controlled using a programmable motion-controller which communicates directly with a PC.

3.6.1.2 Stepper motor

Each stepper motor was capable of dividing an entire 360^0 rotation to 4000 equal steps. The X and Y tables are mounted directly on one another keeping the 2-axis profile very low. The stepper drives used incorporate mini-stepping technology (electrical sub-division of position) and this together with a ball screw pitch of 5mm, gives a theoretical resolution of 2.5 μm.

3.6.1.3 Limit sensors

A datum and an end of travel limit sensor were fitted on each of the tables to trigger the controller when a respective carriage reached a limit.

3.6.1.4 Motion synchronising software

Motion Planner software, was used to create a character, a word or a geometry using X and Y co-ordinates and this was downloaded to the 2-axis controller. This allowed the system to follow the path of the co-ordinates given.

3.6.1.5 Table and Frame

Perspex was used for the table base and the frame which was used for holding the substrate. PET stilts were used for connecting the perspex base to the perspex frame.

3.6.2 Printing

Once the suspension was made to flow through the nozzle, a voltage was applied between the needle and the point-like ground electrode. The flow rate and applied voltage were adjusted to obtain the stable cone-jet mode of electrostatic atomization. Printing was carried out to investigate the main capabilities of the device. Thus, single needle printing and multi-needle printing was performed, the former over a range of applied voltages and flow rates.

3.7 Electrospraying ceramic foams

3.7.1 Materials

Ceramic suspension CS5 was used. General purpose polyurethane foam used in commercial packaging was cut to shape and/or prefabricated as required.

3.7.2 Electrospraying

The ring electrode configuration and the set-up shown in **Figure 3.1** was used for this study. Spraying was carried out in the stable cone-jet mode obtained at an applied voltage of 10kV and a flow rate of 1.67×10^{-9} $m^3 s^{-1}$. Spraying was carried out for 3600s and, in some instances for 18000 while the template was rotated manually to suite.

3.7.3 Pyrolysis and Sintering

The template was heated to 900^0C at $0.083 Ks^{-1}$and left to soak in a muffle furnace for 3600s before cooling in the furnace to the ambient temperature. Some pyrolyzed foams were sintered at 1200^0C with heating at $0.083 Ks^{-1}$ and soaking at this temperature for 3600s before cooling in the furnace to the ambient temperature in order to develop more strength for handling.

3.8 Measuring relic sizes

3.8.1 Optical microscopy

The relics resulting from droplets were studied straight after deposition in each investigation. Relic sizes were measured by optical microscopy using Image-Pro Plus software (Media Cybernetics, L.P. Del Mar, California, U.S.A). The entire substrate was traversed under the microscope both length-wise and width-wise, taking care not to miss any relics. In some cases fine fibres were used as guides so as to not miss relics, this was only used for when counting individual relics within prints containing thousands of relics. In instances where relics were counted in printed tracks, a representative area was clearly defined and this will be discussed in Chapter 6.

The contact angles of the relics (spherical cap of liquid) were measured using a special eyepiece, attached to the optical microscope. It contains a set of cross-wires, one fixed while the other can be rotated. The fixed wire was used to represent the base of the relic and the other was moved to the tangential edge of the spherical cap in contact with the substrate. Thus both left and right-hand side contact angles were measured and an average value was obtained.

3.8.2 3-D AutoMontage

This is a special software suite used in conjunction with a microscope to generate a 3-D image from a collection of slices from a 2-D image. The relics were studied using a Nikon M600M optical microscope which was fitted with a stepper motor driven stage which allowed z-plane movement with a resolution of 0.1μm. Using this software, it was possible to slice relics from their base to the top and generate a 3-D image of all the relics. This part of the work was carried out at the analytical laboratories of Autotype International Ltd, Grove Road, Wantage Oxon OX12 7BZ, United Kingdom.

3.8.3 Estimating droplet sizes

Using the average contact angle value and the diameter of the relic the droplet size can be estimated using volume equivalence as shown below. Volume of a relic sitting (V_R) on the substrate is given by:

$$V_R = \frac{\pi}{4} d^3{}_r \left(\frac{1}{4Sin\theta} - \frac{1}{24Sin^3\theta} \right) \qquad (3.5)$$

where d_r and θ are the relic size and average contact angle, respectively.

Assuming that the effect of evaporation during atomization is negligible, the corresponding droplet diameter (D_D) is given by:

$$D_D \approx 0.91 d_r \left(\frac{1}{4 \sin \theta} - \frac{1}{24 \sin^3 \theta} \right)^{\frac{1}{3}}. \qquad (3.6)$$

3.9 Measuring droplet sizes

The Malvern Spraytec system on loan from Malvern Instruments Ltd, Malvern, United Kingdom was used. This instrument works on the well-established laser diffraction technique. This system was set-up with the laser beam just under the ring electrode (see **Figures 3.4** and **3.5**). Suspensions CS1-CS4 were made to flow at various controlled flow rates and applied voltages to obtain electrostatic atomization. During the electrospraying process the system constantly analysed the droplets produced.

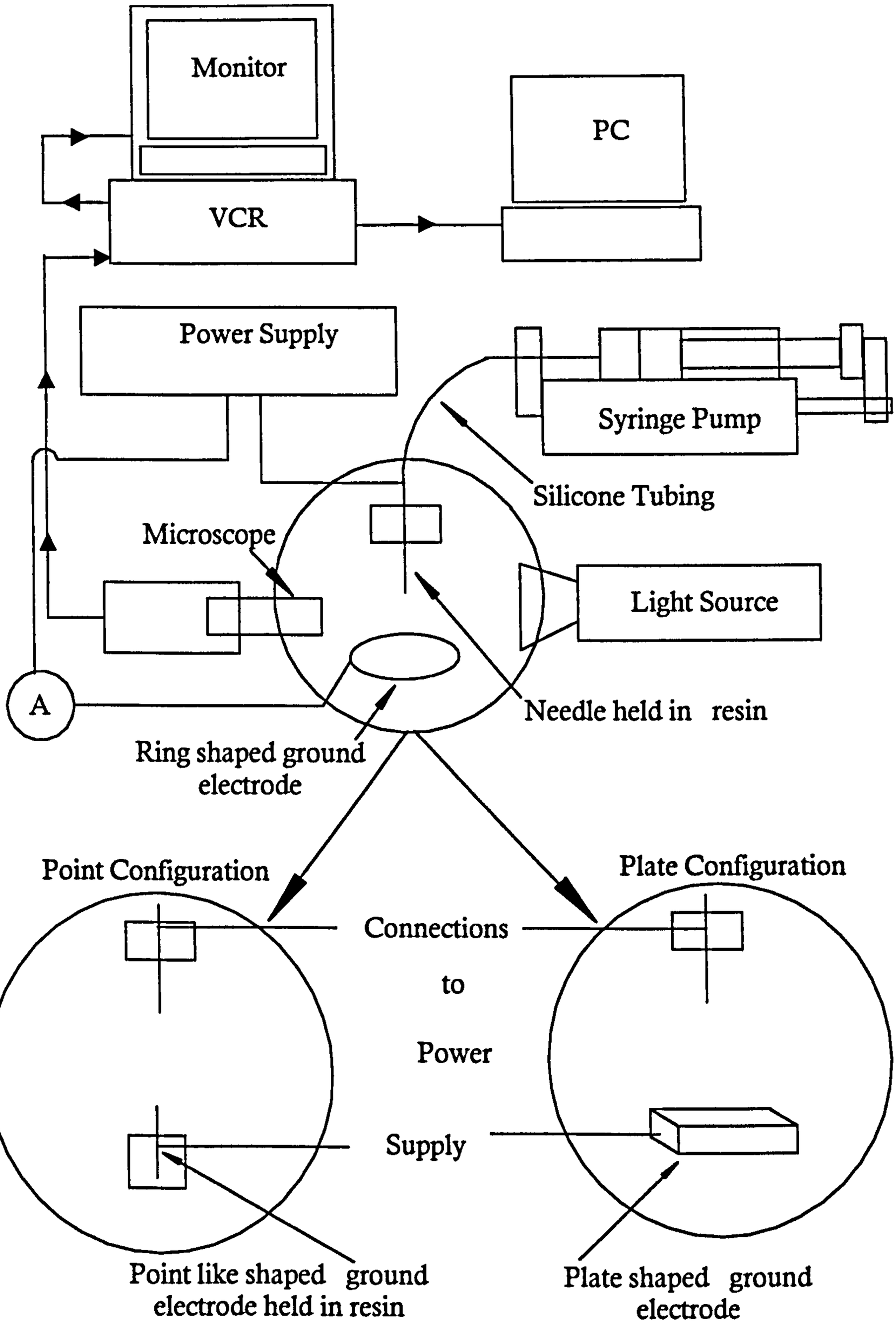

Figure 3.1 Schematic diagram of electrostatic atomization apparatus indicating the three electrode configurations used in the experiments

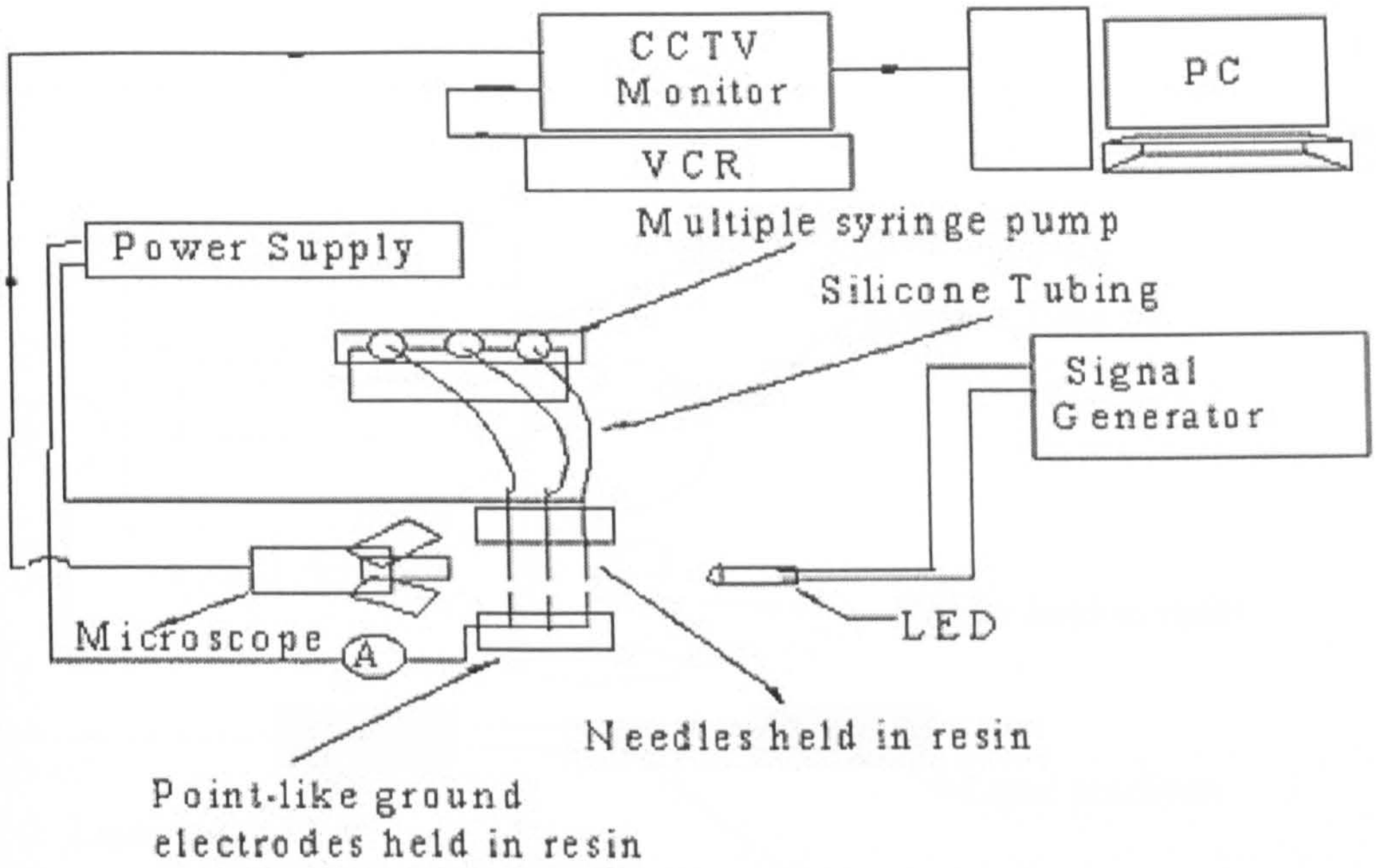

Figure 3.2 Schematic diagram of electrostatic atomization apparatus with multiple needle and multiple point-like ground electrode configuration

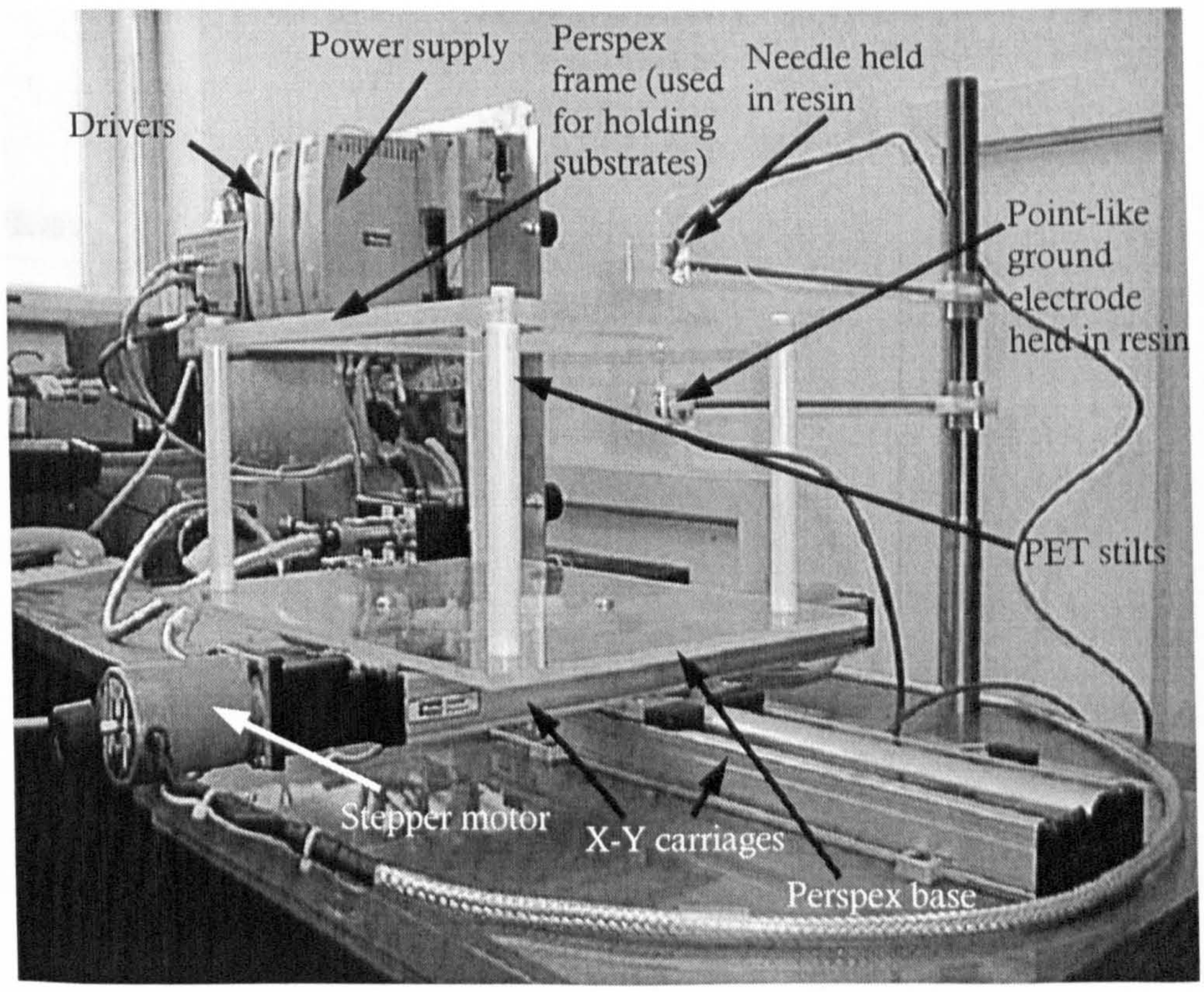

Figure 3.3 Schematic representation of the 2-axis printing device

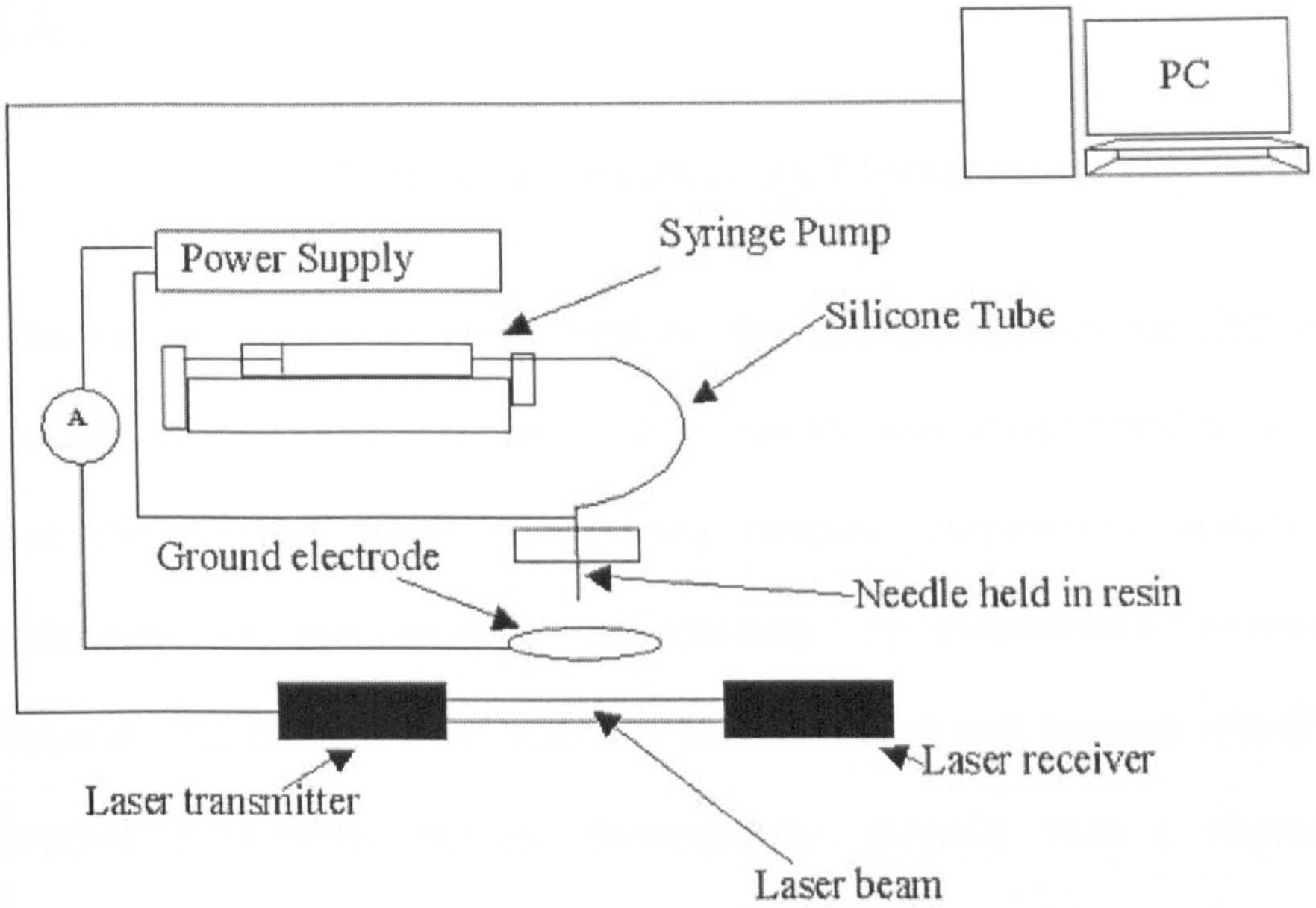

Figure 3.4 Schematic diagram illustrating the incorporation of the Malvern Spraytec system in the electrostatic atomization rig

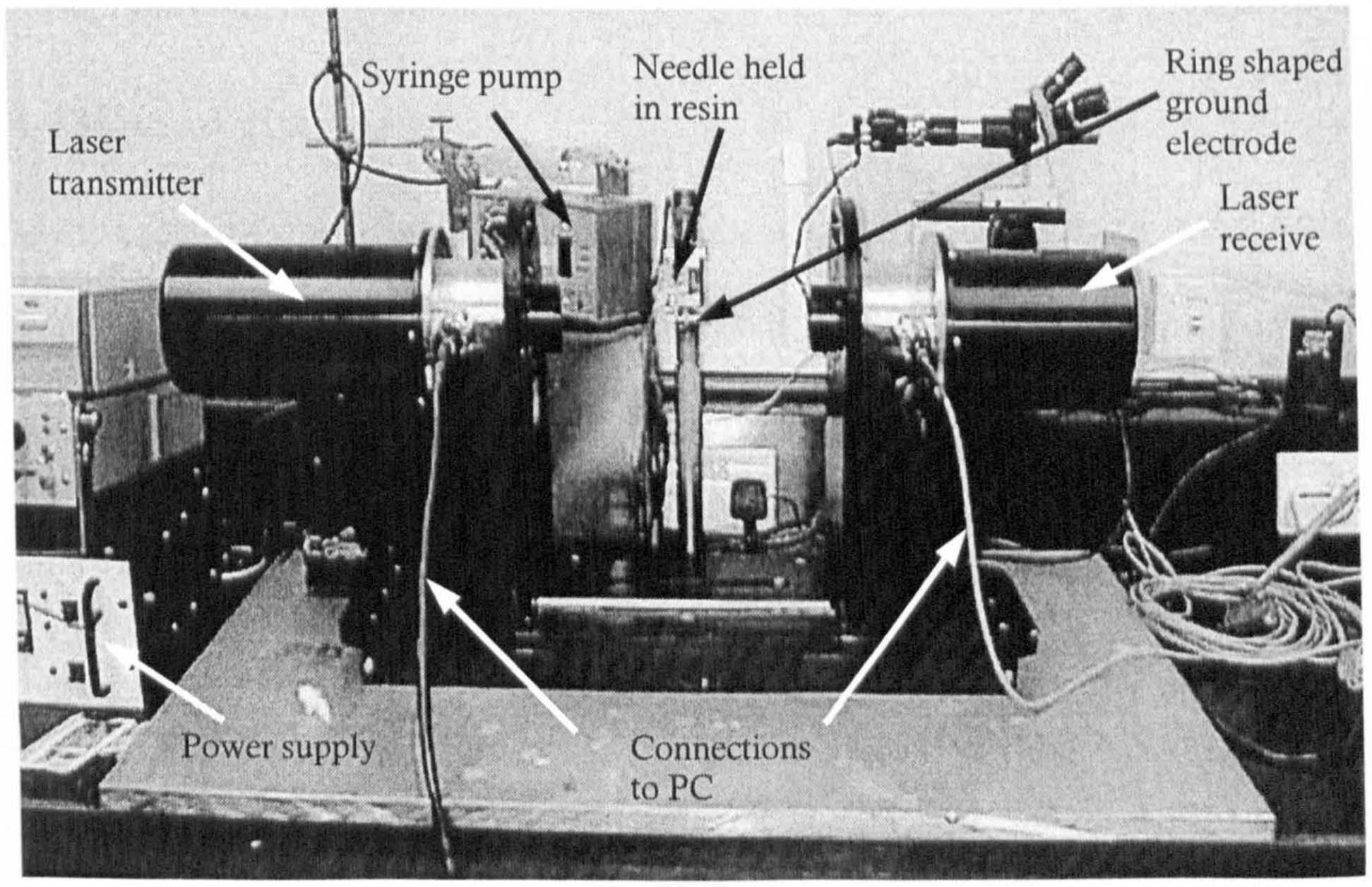

Figure 3.5 The Malvern Spraytec system incorporated in the electrostatic atomization apparatus

CHAPTER 4

Effect of Viscosity on Electrostatic Atomization

This chapter describes work which explores the effect of viscosity on electrostatic atomization in the stable cone jet mode. Viscosity was investigated in this way because the ultimate goal of studying ceramic suspensions requires the understanding of the increase of viscosity in electrostatic atomization experiments. For the first time, viscosity was increased well beyond 100mPa s in electrostatic atomization studies. Subsequently, glycerol with a viscosity of 1338mPa s was subjected to electrostatic atomization at various applied voltages to investigate the size of relics obtained. This investigation forms the backbone of the research carried out in chapters 5 and 6.

4.1 Effect of citric acid

The dc conductivity of glycerol was increased by the addition of citric acid as shown from **Figure 4.1**. A conductivity of 25 mSm^{-1} was set and appropriate amounts of citric acid were added to water, glycerol and water-glycerol mixtures to keep their conductivity constant.

4.2 Water-Glycerol mixtures

4.2.1 Properties

The challenge is selecting test liquids which give a systematic variation in viscosity while other properties such as conductivity, surface tension and, to a lesser extent, density and relative permittivity which also affect electrostatic

atomization, are kept approximately constant. In the samples investigated (**Table 4.1**) the conductivity was kept constant at 25 mSm^{-1} by the addition of citric acid. A wide range of conductivities have been investigated in electrostatic atomization studies. Most investigations used liquid with a conductivity <<25 mSm^{-1}, however, samples with relatively high conductivities have also been studied previously by Chen et al., (1995, upto 800 mSm^{-1}), Gomez et al., (1998, 13-16 mSm^{-1}) and Sato et al., (1999, 4000 mSm^{-1}). As given in **Table 4.1**, the surface tension values of the samples are between 62-70 Nm^{-1}. The density and relative permittivity has varied more, between 1000-1310 kgm^{-3} and 45-78, respectively but does not affect the results significantly as shown in the discussion in section 4.2.3. In contrast, viscosity was varied over two orders of magnitude.

Table 4.1 Composition and properties of samples S1-S5

Sample	Water *wt.%*	Glycerol *wt.%*	Citric Acid *wt.%*	Density *kgm^{-3}*	Viscosity *mPa s*	Surface tension *mNm^{-1}*	Relative permittivity
S1	98.35	0	1.65	1000	1	70	78
S2	72.67	24.22	3.11	1050	94	69	72
S3	48.09	48.09	3.83	1090	298	66	59
S4	23.74	71.21	5.05	1220	603	63	53
S5	0	93.27	6.73	1310	1338	62	45

4.2.2 Electrostatic atomization

Using the equipment described in section 3.5.1 electrospraying of samples S1-S5 was carried out at approximately the same flow rate and applied voltage. During electrostatic atomization the flow rate varied between 5.8×10^{-11} – 6.2×10^{-11} m^3s^{-1}. The applied voltage was kept in the range 7-7.2 kV. The current was measured as indicated in **Figure 3.2** and was 73 nA. Exploratory experiments showed that this flow rate and applied voltage was most appropriate for water-glycerol mixtures if

the intention is to obtain stable cone-jet mode of electrostatic atomization. In addition, the low flow rate regime used in this work helps to prevent the formation of secondary droplets (Hartman *et al.*, 1999a, 2000).

4.2.3 Characteristics of cone/jet

In the case of samples S1-S3, stable cone-jet mode atomization was not obtained (see **Figures 4.2a-c**) under the conditions used. However, it was observed that as the amount of glycerol increased from S1 to S3, the instability decreased and the electrostatic atomization of S3 showed gentle whipping as described by Tang and Gomez (1996). Mixtures S1, S2 and S3 contained a high proportion of water with higher surface tension and higher relative permittivity (**Table 4.1**). These properties together with a relatively high conductivity of 25 mSm^{-1} prevents electrostatic atomization in the stable cone-jet mode at the flow rate and applied voltage selected for this study.

Liquids containing a high proportion of water are indeed difficult to electrostatically atomize in the cone-jet mode (Smith 1986, Tang and Gomez 1995, Borra *et al.*, 1999) unless specified conditions (e.g. flow rate, applied voltage, surrounding atmosphere and conductivity) are met (Borra *et al.*, 1999, Jaworek and Krupa 1999).

High viscosity samples S4 and S5 both gave a stable cone-jet over a long period of time (>30 minutes) as shown in **Figures 4.3a and b**. Although the shape and size of the cones of S4 and S5 and their ensuing jets are different in appearance, these

are various manifestations of stable (steady) cone-jet mode electrostatic atomization (Gavan-Calvo *et al.*, 1999).

To estimate the jet diameter in S4 and S5, the viscous dimensionless parameter (δ_m) defined by Gavan-Calvo *et al.*, (1997) was calculated using

$$\delta_m = \sqrt[3]{\frac{\rho\varepsilon_0\gamma^2}{K\eta^3}} \qquad (4.1)$$

where ρ is the density, γ is the surface tension, K is the conductivity and η is the viscosity. Using the values in **Table 4.1**, for samples S1-S5, $\delta_m \leq 1$. The δ_m value of S5 is the lowest followed by S4. As $\delta_m \leq 1$, the jet diameter (d_j) for S4 and S5 is given by (Gavan-Calvo *et al.*, 1997):

$$d_j \approx \sqrt[3]{\frac{(\beta-1)^{\frac{1}{2}} Q\varepsilon_0}{K}} \qquad (4.2)$$

where β is the relative permittivity. Equation 4.2 is only applicable if the stable cone-jet mode prevailed.

Using values in **Table 4.1**, at a flow rate (Q) of 6×10^{-11} m^3s^{-1} equation (4.2) gives d_j = 0.5μm for mixtures S4 and S5. This is expected as the values of Q, ε_0 and K in equation (4.2) do not change for these mixtures and although β varies from 45-53, as d_j depends on $(\beta)^{1/6}$, its effect is negligible. Measured jet diameters of S4 and S5 at a distance of 5mm from the end of the nozzle are 22 μm and 16 μm, respectively, >>0.5μm. However, equation (4.2) does not take into account

viscosity. Also in practice, the jet diameter is a strong function of the axial distance. Therefore, it is important to make comparisons at a fixed point (relative to the nozzle) below which there is negligible change in jet diameter.

4.3 Relics and Droplets

The relics analysed soon after deposition on silicone release paper illustrated that a variation in liquid viscosity has a significant effect on the relics characteristics. **Figure 4.4a-e** shows optical micrographs of the relics generated during electrostatic atomization of liquid mixtures S1-S5. It is clear that as viscosity increases from 1mPa s in S1 to 1338mPa s in S5 the relics get coarser.

4.3.1 Relic size distributions

Liquid mixture samples S1-S3 did not atomize in the stable cone jet mode. As shown in the **Table 4.2**, the relics size distribution was found to be wide in S1,S2 and S3. Samples S4 and S5 was found to atomize in the stable cone jet mode and the relics were found to be increasing in size with the increase in liquid viscosity. Overall, relics of all the liquid mixture samples illustrate that with the increase in viscosity the relics increase in size but reduce in number (see **Table 4.2**). A significant change was detected in relic size range, mean and standard deviation in the samples studied, with higher viscosities increasing all these values (see **Table 4.2**). Furthermore, the contact angles of relics increases with increase in viscosity because spreading on the silicone release paper is more difficult.

Table 4.2. Relic size data and the average contact angle of droplets of each sample on silicone release paper

Sample	Relics					Average contact angle/degree
	Number	Minimum size/μm	Maximum size/μm	Mean size/μm	Standard deviation/μm	
S1	190	29	70	50	15	26
S2	152	67	180	125	41	30
S3	125	125	235	167	43	31
S4	86	210	320	270	50	33
S5	26	450	620	548	78	49

4.3.2 Droplet sizes and contact angles

Using equations 3.5 and 3.6 in chapter 3 the droplet size was estimated as described in section 3.8 and is shown in **Table 4.3**. The estimates are less accurate for S1-S3 which gave the unstable cone-jet mode (Jaworek *et al.,* 1999). Thus, for S4 and S5 which gave stable cone-jet mode, droplet diameters ranged from 112 to 171 μm and 253 to 337 μm, respectively.

Table 4.3. Droplet sizes deduced from relic sizes of each sample

Sample	Droplet Size/mm	
	Min	Max
S1	17	23
S2	45	60
S3	77	121
S4	112	171
S5	253	337

Jaworek *et al.,* (1999) concluded that the increase of viscosity caused a decrease in the size of droplets. However, in their study the spindle mode was used and there was no attempt to keep the conductivity constant as in our investigation. According to Rosell-Llompart and de la Mora (1994), in the cone-jet mode the

effect of viscosity on droplet size is dependent on the dimensionless parameter π_η given by:

$$\pi_\eta = \frac{\sqrt[3]{\gamma^2 \rho \beta \varepsilon_0}}{\eta} \qquad (4.3)$$

They suggest that if π_η is >>1 viscosity has no effect but if << 1, the droplet size increases with increasing viscosity and moreover, a broader size distribution of droplets occur. In equation 4.3, η dominates the value of π_η compared with the other variables (γ, ρ and β). Using data in **Table 4.1**, for samples S4 and S5, clearly π_η<< 1 and this is the reason for the significant increase in droplet size on increasing the viscosity by more than twice from S4 to S5 (**Table 4.1**). Hartman *et al.,* (2000) have also found that in the cone-jet mode primary droplet size is directly proportional to viscosity. Rosell-Llompart and de la Mora (1994) investigated viscosities of upto 140 mPa s while in the case of Hartman *et al.,* it was below <100 mPa s. In this work, we have investigated viscosities of >1000 mPa s and report a significant increase of both droplet and relic size, the latter is very important in the context of materials processing.

4.4 Effect of Applied Voltage

As the applied voltage plays a major role in electrostatic atomization (Jaworek *et al.,* 1999, Cloupeau *et at.,* 1990, 1994) it was necessary to understand the effect of increasing the applied voltage on a viscous liquid. Sample S5 was used and the flow rate was kept constant at 8.3×10^{-10} m^3s^{-1}.

4.4.1 Mode and cone shape

Initially stable cone jet mode was achieved at a flow rate of ~$8x10^{-10}m^3s^{-1}$ and applied voltage of 4kV. In the stable cone-jet mode, the shape of the cone changed appreciably with increasing voltage (see **Figures 4.5a-d**). The cone was found to get shallower (distance from exit of the needle to the apex of the cone) with the increasing voltage. On exceeding 4.75kV it was observed that multi-jets were formed at the exit of the needle (see **Figure 4.6**).

4.4.2 Jet diameter

With increasing applied voltage the cone becomes more asymmetrical as its height decreased. This reduction in the cone height caused the jet diameter to reduce from 35μm to 8μm (**Figure 4.7**). The cone became more asymmetric with increasing applied voltage making the jet to skew. With the reduction in jet diameter and skewing, the jet was found to gently whip (Tang and Gomez 1996).

4.4.3 Relic and droplet size

The relics (see **Figure 4.8a-d**) varied from 25 to 160μm. The silicone release paper on which these relics were deposited on has a much lower surface free energy (20mN m^{-1}) than the surface tension of the glycerol and this helps to minimise the spreading on deposition (Tay and Edirisinghe 2002).

The minimum and maximum droplet sizes generated by electrostatic atomization of the viscous liquid are given in **Table 4.4**. These were estimated from the relic sizes and equations 3.5 and 3.6 described in Chapter 3.

Table 4.4 Relic and droplet size distribution for each applied voltage

Voltage/kV	Relic size/μm		Droplet size/μm		Contact angles/degree
	Min	Max	Min	Max	
4.0	25	159	14	89	50
4.25	36	135	20	74	51
4.50	25	120	14	67	50
4.75	16	102	9	56	51

It is seen that by increasing the applied voltage during stable cone-jet mode electrostatic atomization of glycerol having a viscosity of 1338mPa s, the relic size was successfully reduced to between 25 and 120μm at 4.50kV. However, further increasing in applied voltage caused the formation of multi-jets and electrostatic atomization could not be controlled.

In summary, this work reveals that the increase in viscosity over three orders of magnitude upto 1338 mPa s with the electrical conductivity held constant had a significant effect on the electrostatic atomization of liquids and their mixtures. A higher viscosity helped to produce stable cone-jet mode electrostatic atomization with a smaller jet diameter. In the cone-jet mode, the size of relics and the droplets from which the relics originated increased significantly due to the increase in viscosity and, moreover, produced a wider size-distribution of relics and droplets.

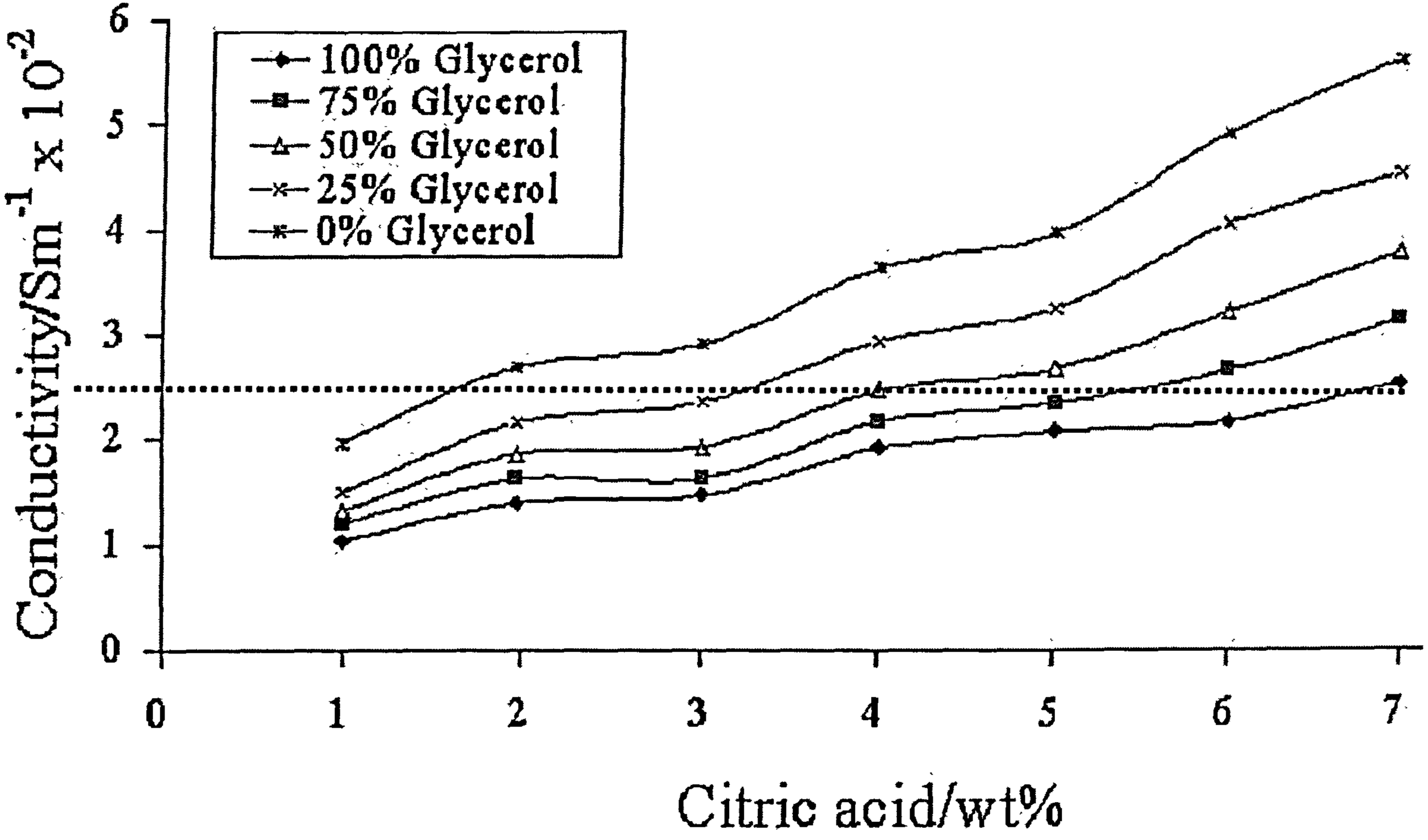

Figure 4.1 Variation of dc conductivity in samples S1-S5 with addition of citric acid

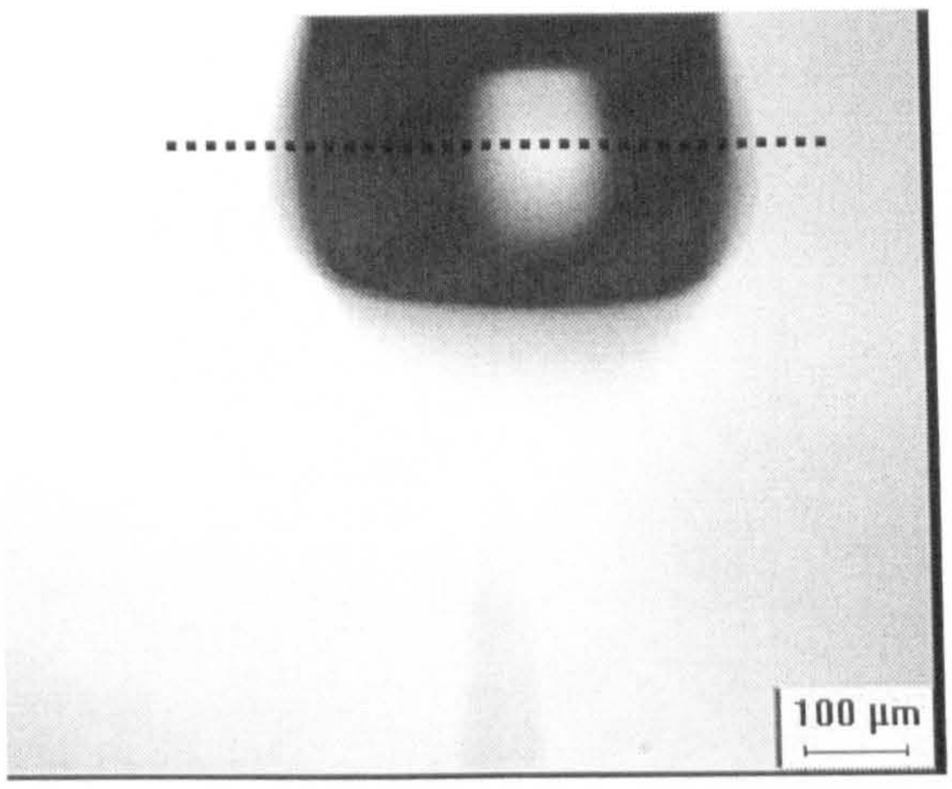

a

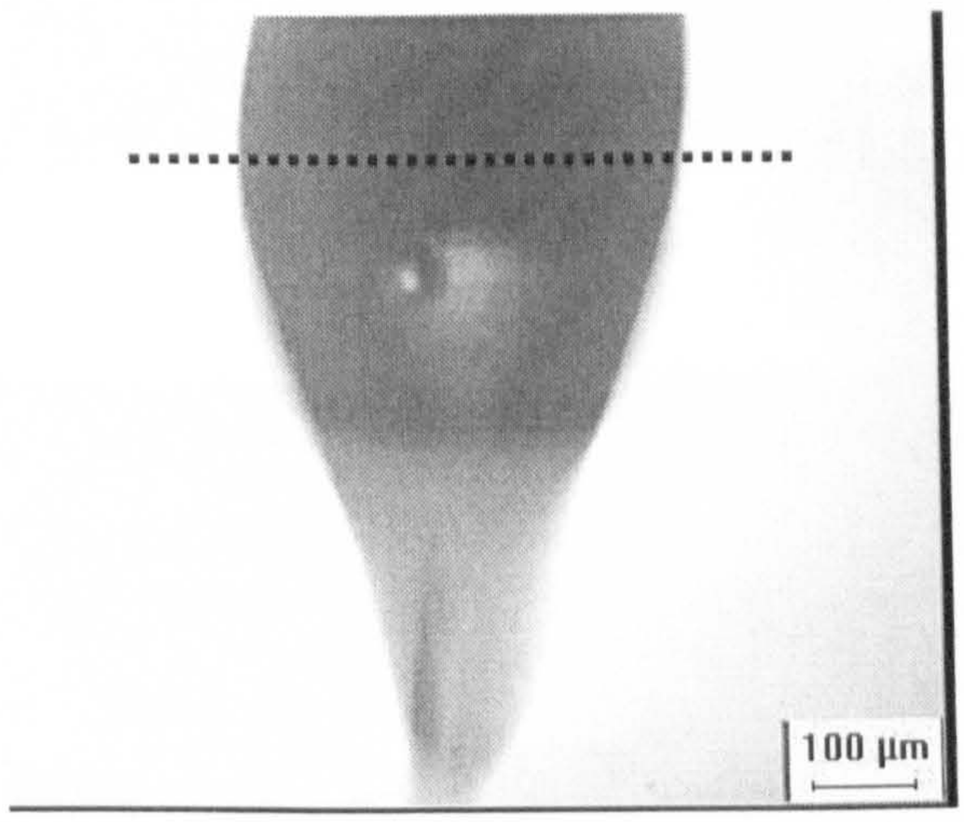

b

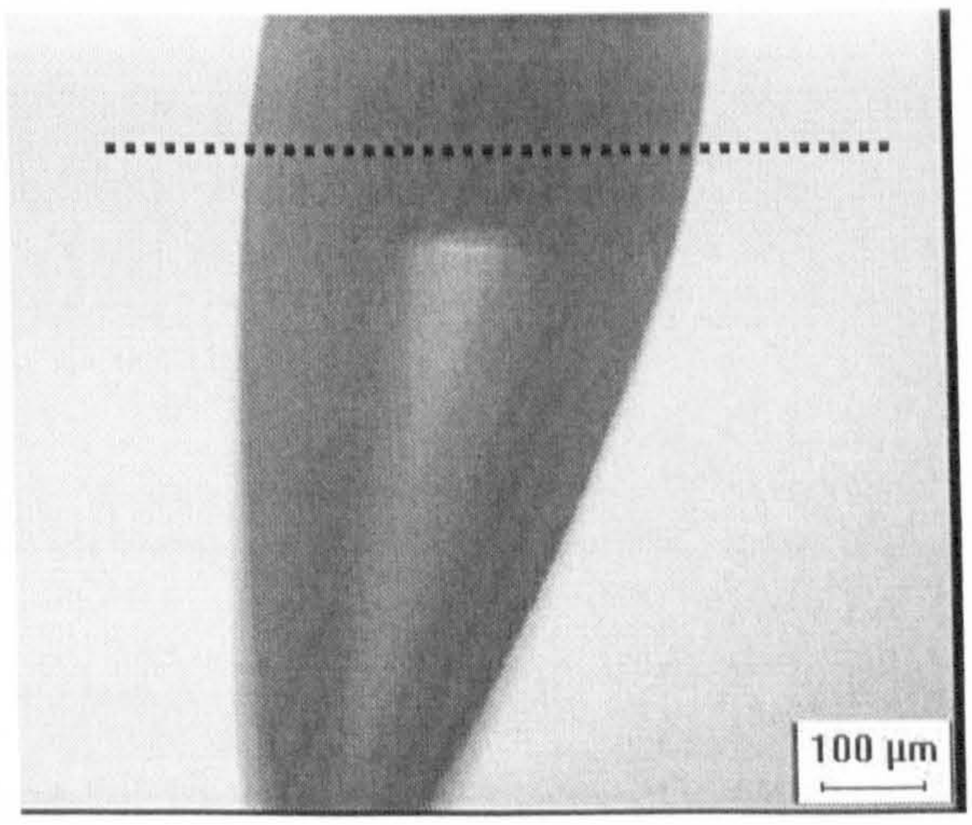

c

Figure 4.2 Unstable cone-jet mode atomization of liquid mixtures a)S1, b)S2 and c)S3 at an applied voltage of 7kV and flow rate of $6x10^{-11}m^3s^{-1}$. The dotted line indicates the exit of the needle.

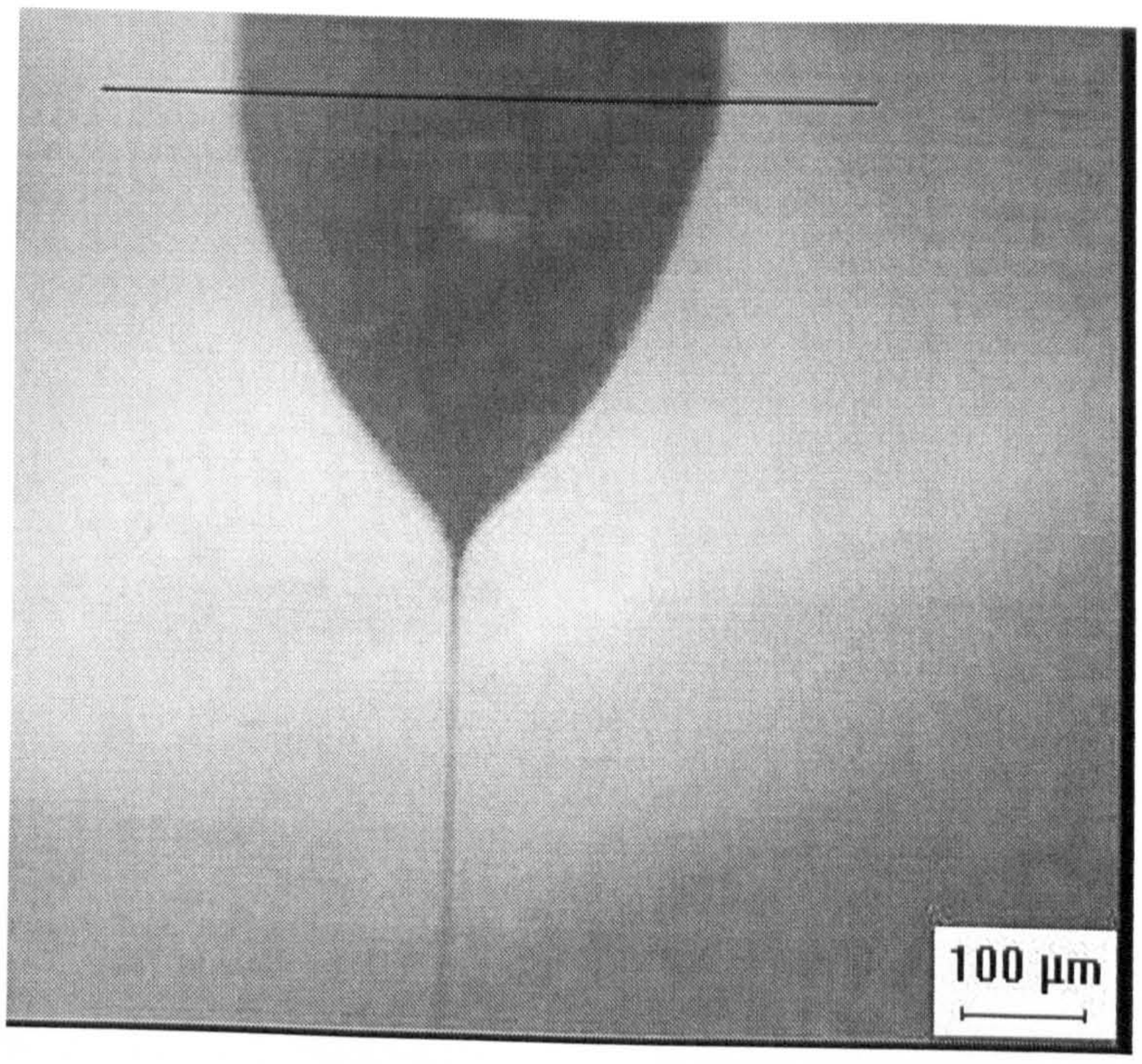

a

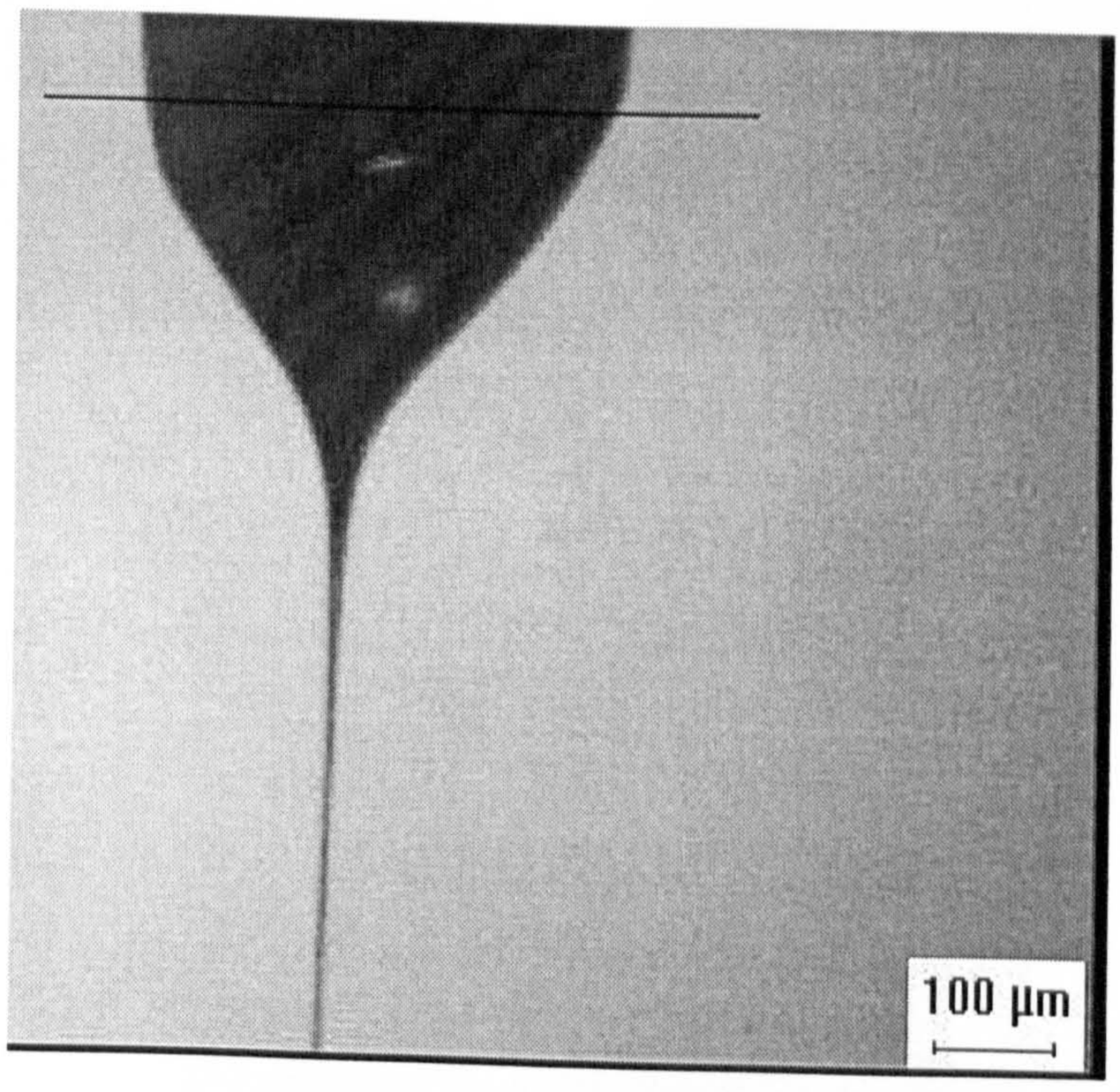

b

Figure 4.3 Stable cone-jet mode atomization of liquid mixture a)S4 and b)S5 at an applied voltage of 7kV and flow rate of $6x10^{-11}m^3s^{-1}$. The solid line indicates the exit of the needle.

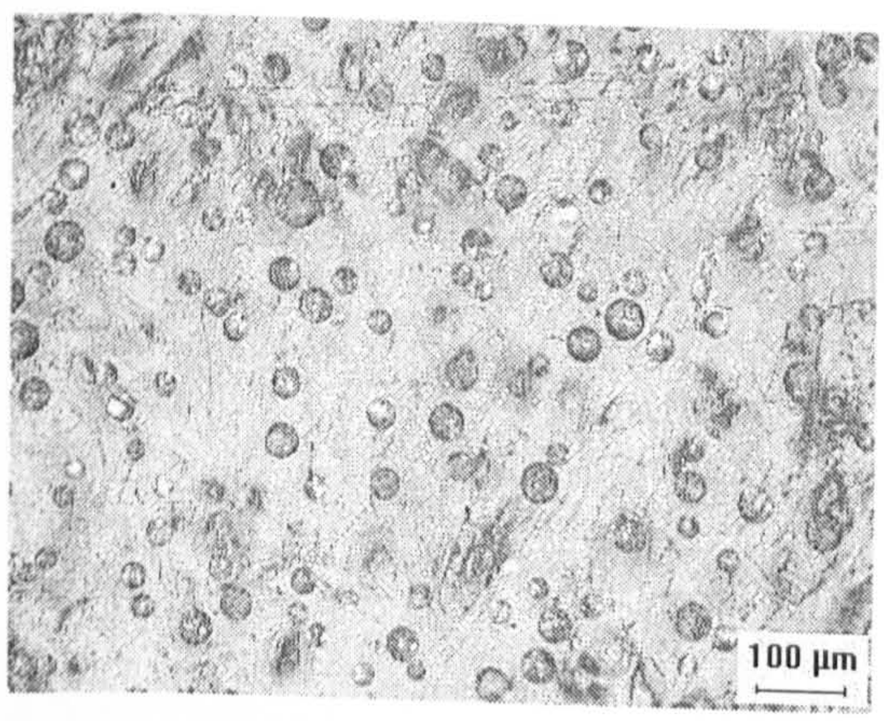

a

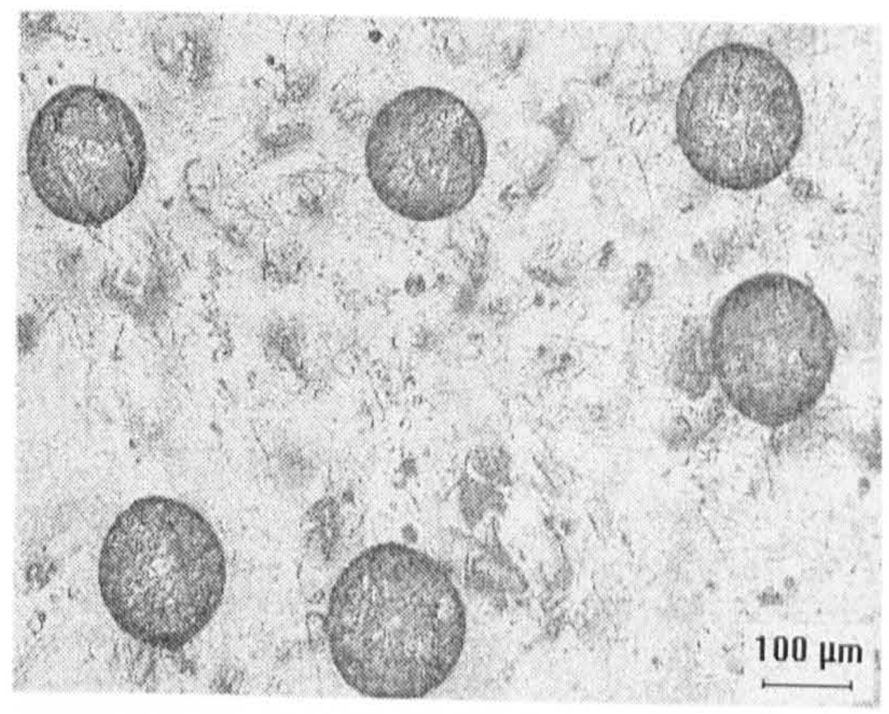

b

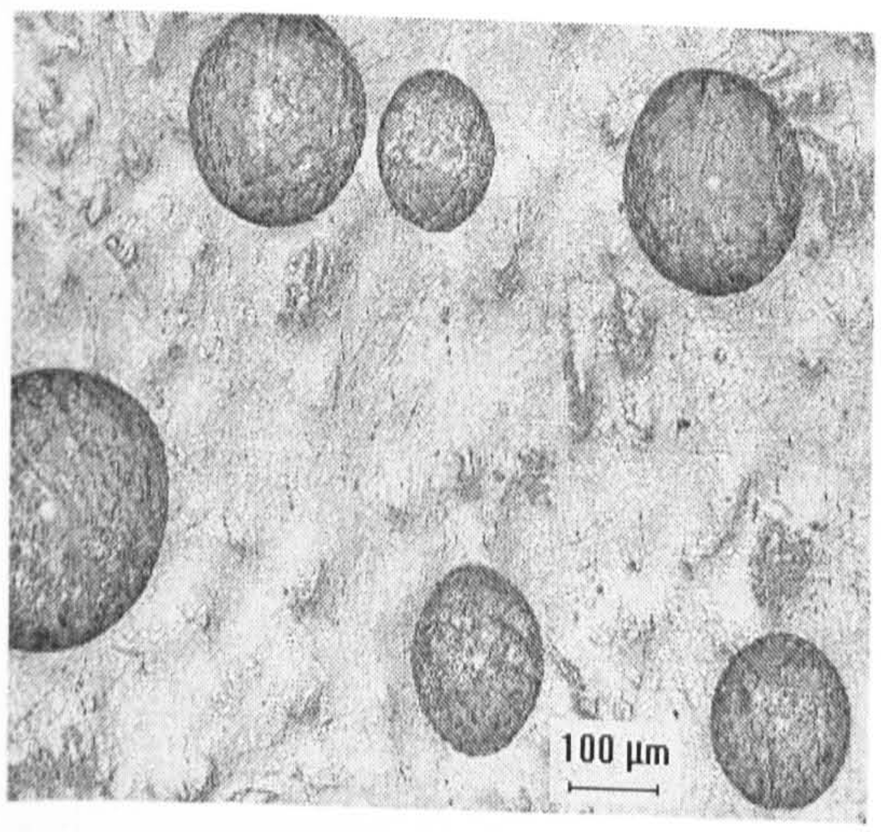

c

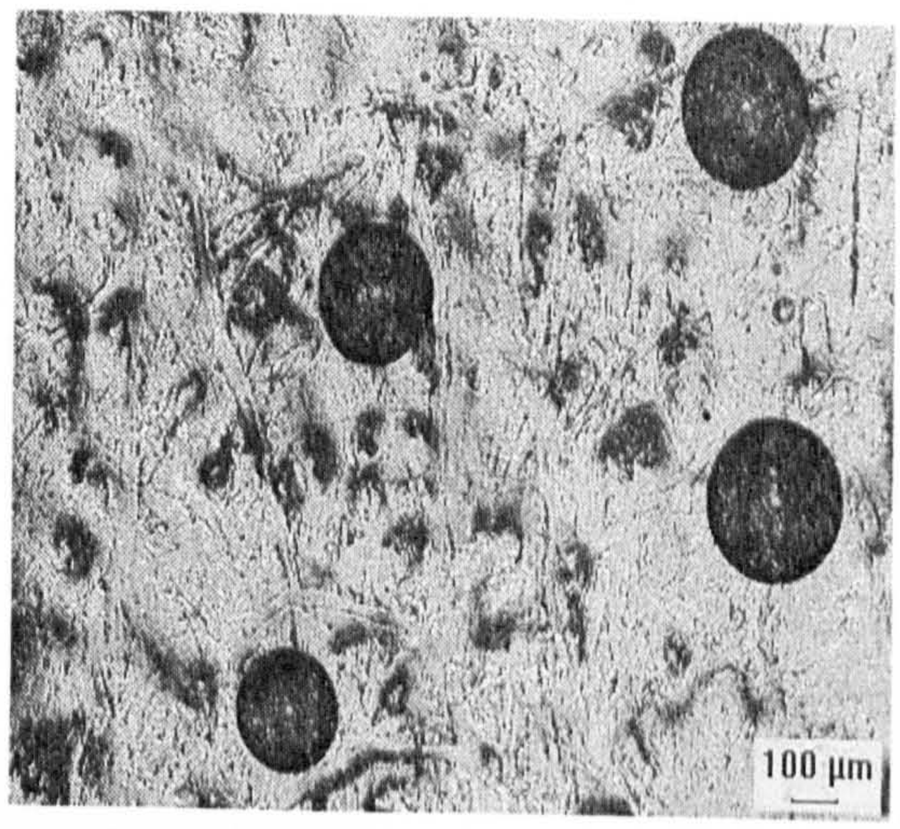

d

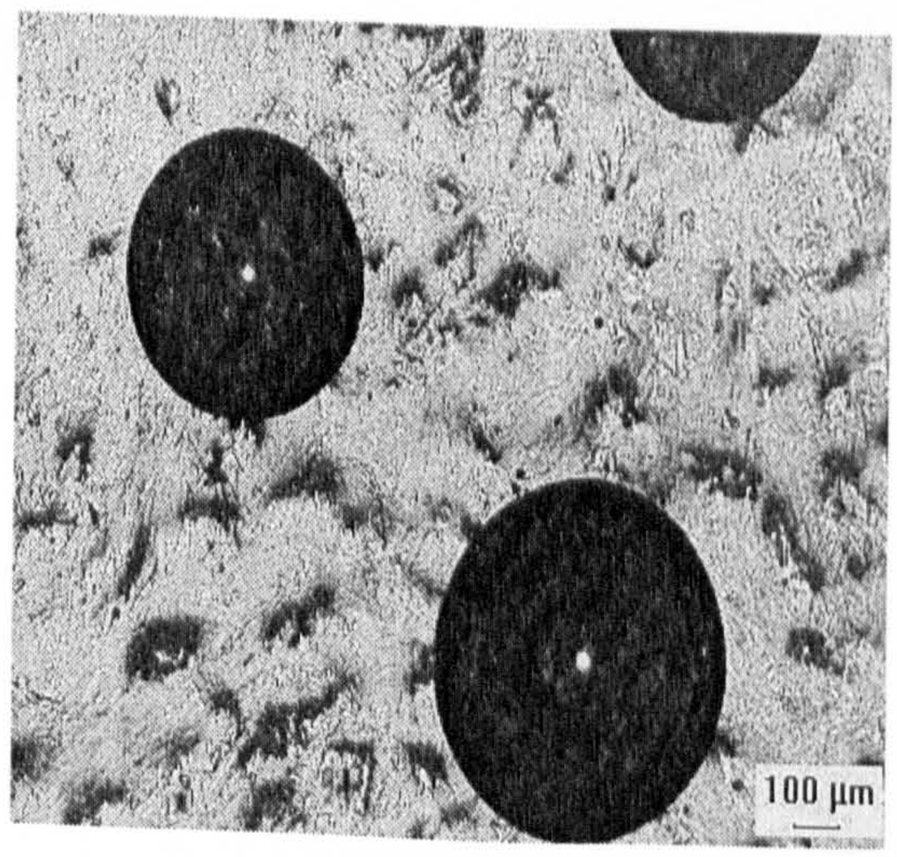

e

Figure 4.4 Optical micrographs of relics obtained from mixtures a)S1, b)S2, c)S3, d)S4 and e)S5

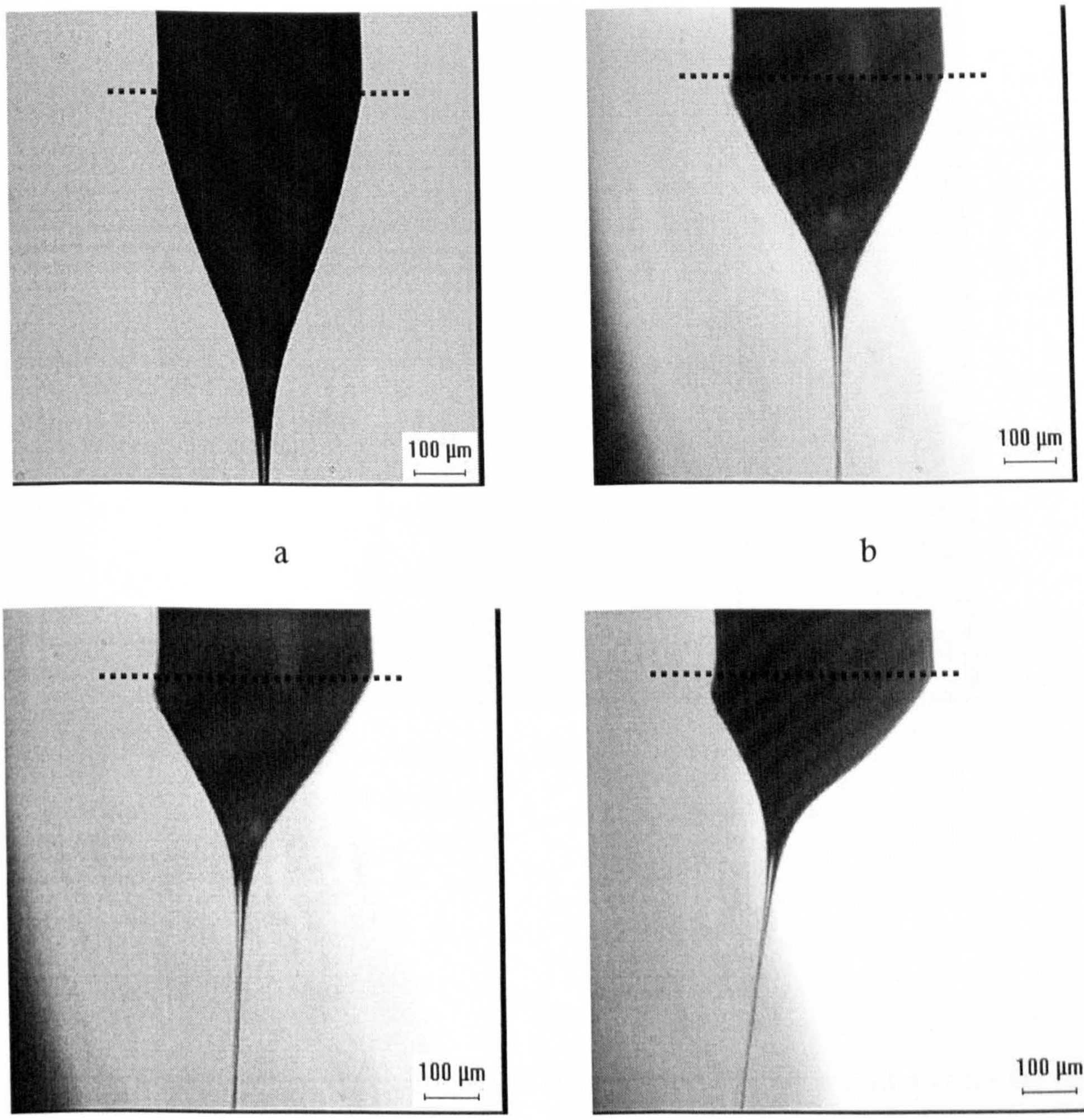

Figure 4.5 Stable cone-jet mode electrostatic atomization of glycerol at a constant flow rate of ~$8x10^{-10}m^3s^{-1}$ and applied voltages (kV) of a)4.0, b)4.25, c)4.50 and d)4.75. The dotted line indicates the exit of the needle.

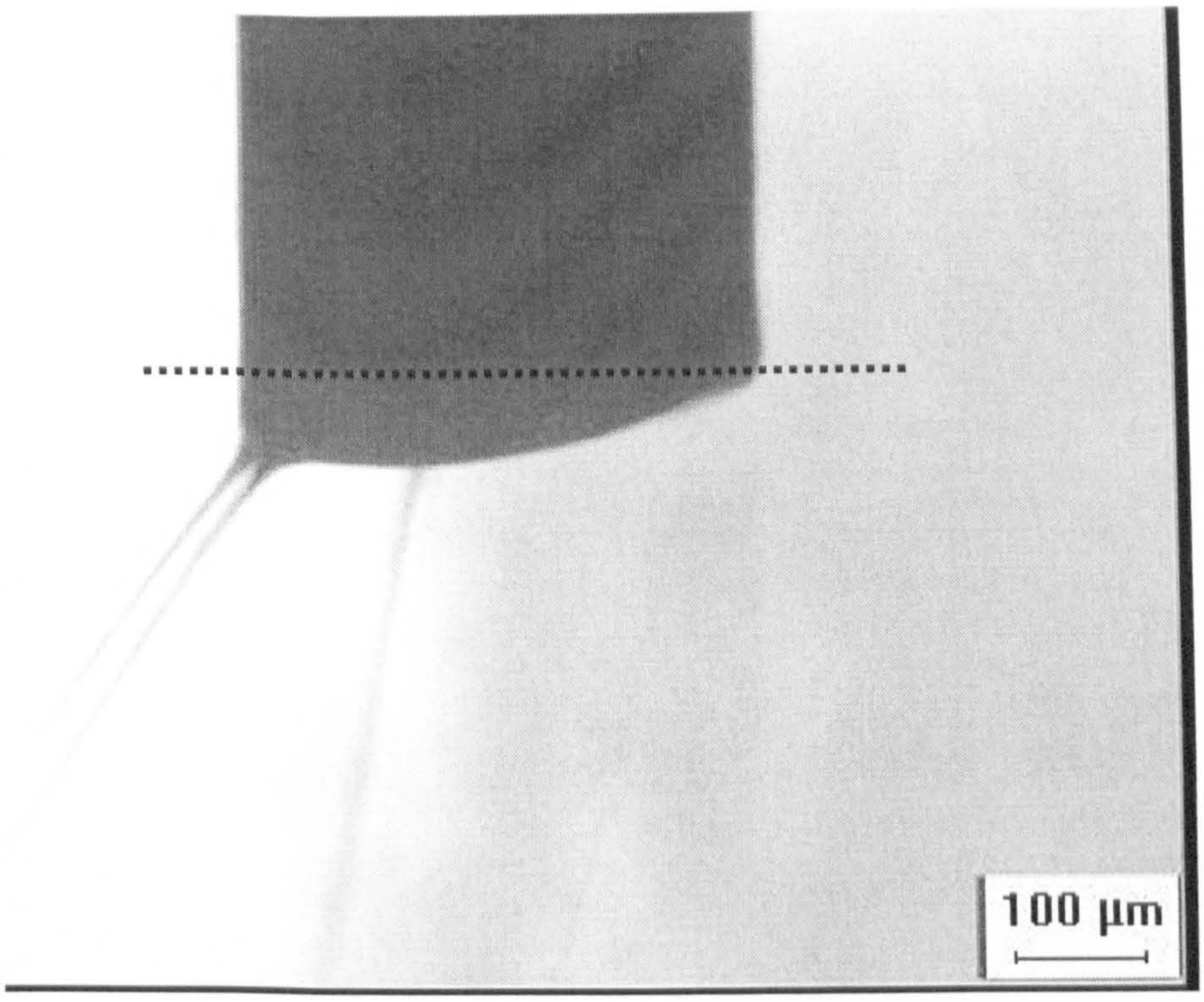

Figure 4.6 Multi-jet mode electrostatic atomization of glycerol at a constant flow rate of ~$8x10^{-10}m^3s^{-1}$ and at an applied voltage of 4.78. The dotted line indicates the exit of the needle.

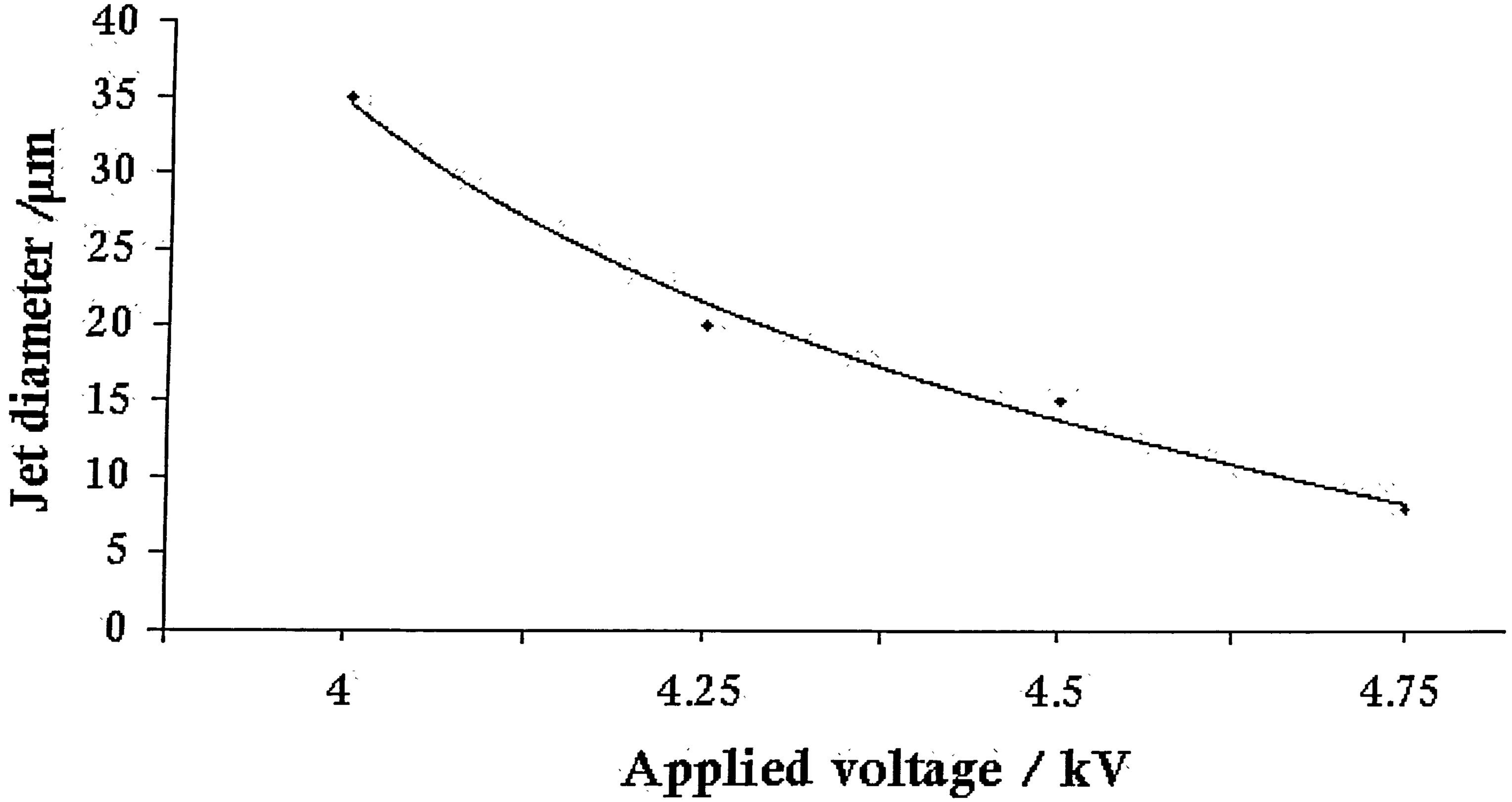

Figure 4.7 Variation in jet diameter with increasing applied voltage for glycerol at a fixed flow rate of $8x10^{-10}m^3s^{-1}$.

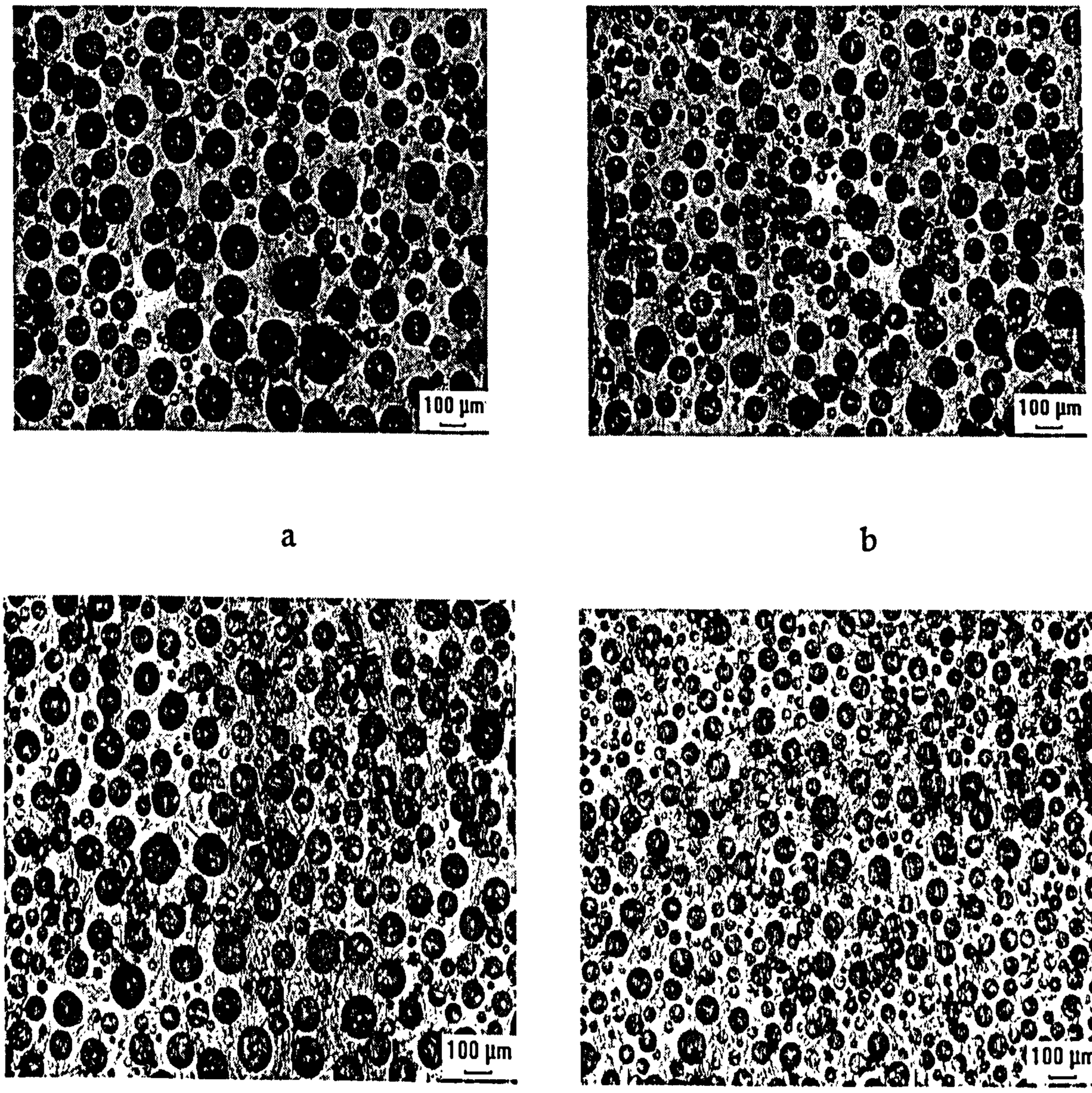

Figure 4.8 Optical micrographs of relics generated by electrostatic atomization of glycerol at applied voltages (kV) of a)4.0, b)4.25, c)4.50 and d)4.75. The flow rate in all instances was ~$8x10^{-10}m^3s^{-1}$

CHAPTER 5

Electrostatic atomization of ceramic suspensions

This chapter describes the investigations on electrostatic atomization of different ceramic suspensions under different conditions - flow rate, applied voltage and ground electrode configuration. The construction of applied voltage – flow rate – mode of atomization maps for ceramic suspensions is a new input to the aerosol science and engineering literature. Ceramic filler was selected as the intention was to develop novel high resolution microfabrication techniques for these materials. Alumina was used as a standard as it is easily available and commonly used in ceramic investigations (Dörre and Hübner 1927).

5.1 Suspensions

5.1.1 Types

As mentioned in chapter 3 two types of alumina suspensions were formulated. The first containing ethanol and Zephrym was prepared to understand three crucial points. Firstly, the effect of varying the powder content in the suspension was explored. Secondly, the effect of using ultrasonic disruption for mixing was tested and, thirdly, the possibilities of electrostatic atomization in the cone-jet mode was investigated. Based on this experience, the constituents of the second ceramic suspension was modified to contain ethanol and Efka 401 dispersant to incorporate a much higher volume loading of alumina (21 vol.%) and it was prepared using a high energy bead mill.

5.1.2 Properties

Table 5.1 shows the properties of the first series of suspensions (CS1-CS4). The alumina loading was checked by loss-on-ignition results. Compared with the literature on liquids used for electrostatic atomization (<100mPa s), it is striking that they have much higher viscosities.

Table 5.1 Composition and properties of suspensions CS1-CS4

Samples	Alumina		Ethanol	Zephrym	Density	Viscosity	Surface tension	Electrical conductivity	Relative permittivity
	wt.%	*vol.%*	*wt.%*	*wt.%*	*kgm^{-3}*	*mPa s*	*mNm^{-1}*	*Sm^{-1}*	
CS1	1	0.2	94	5	793	1131	24.2	2.56×10^{-4}	26
CS2	3	0.6	92	5	811	1172	25.1	2.13×10^{-4}	24
CS3	5	1.04	90	5	822	1197	25.8	1.97×10^{-4}	23
CS4	20	4.8	75	5	943	1243	27.3	1.29×10^{-4}	19

The composition and properties of the alumina suspension made using bead milling is given in **Table 5.2**. Compared with CS1-CS4, it has a much higher viscosity, relative permittivity and surface tension and much lower dc conductivity due to the higher alumina loading.

Table 5.2 Composition and properties of the second suspension (CS5)

Alumina		Ethanol	EFKA 401	Density	Viscosity	Surface tension	Electrical conductivity	Relative permittivity
wt.%	*vol.%*	*wt.%*	*wt.%*	*kgm^{-3}*	*mPa s*	*mNm^{-1}*	*mSm^{-1}*	
56.5	20.6	43.0	0.5	1413	1420	64	0.043	54

5.2 Electrostatic atomization

Both the suspensions were initially electrosprayed to observe the operating conditions for the stable cone-jet to prevail. This was carried out by varying the applied voltage and flow rate systematically.

5.2.1 Dilute suspensions

Although suspensions CS1-CS4 were subjected to electrostatic atomization under a number of combinations of flow rate to applied voltage, it was clear that the stable cone-jet mode was not achievable. Also, during electrostatic atomization some alumina sedimented probably due to the incompatibility of the constituents and/or the inadequacy of the mixing method.

Eventually electrostatic atomization was carried out at a flow rate of 8.37×10^{-11} m^3s^{-1} and an applied voltage of 5 kV with the ring shaped ground electrode. The measured current (see **Figure 3.1** in Chapter 3) was 59 nA. **Figures 5.1a-d** illustrate the change in modes of atomization. In the case of CS1 the multi-spindle mode was achieved but under the same flow rate and applied voltage CS2 gave the unstable cone-jet mode while both CS3 and CS4 gave the spindle mode.

Relics were collected on silicone release paper during electrostatic atomization on four separate occasions. **Table 5.3** presents the statistics of the relics and respective contact angle. **Figures 5.2a-d** show typical optical micrographs of the relics.

Table 5.3 Relic statistics for suspensions CS1-CS4

Suspension	Contact Angle /degree	Relic sizes/μm							
		Run-1		Run-2		Run-3		Run-4	
		Min	Max	Min	Max	Min	Max	Min	Max
CS1	25	66	712	41	839	26	724	55	760
CS2	27	61	376	32	514	24	436	91	427
CS3	29	39	545	32	524	15	503	50	434
CS4	30	54	365	33	450	14	414	74	429

The relic data was used to deduce the droplet sizes according to equation 3.5 and 3.6 (Chapter 3). These results are compared with the output of the Malvern Spraytec device and shown in **Table 5.4**.

Table 5.4 Statistical data of droplets calculated from relic data and measured using the Malvern device

Sample	Calculated Mean /μm				Calculated St.dev./μm				Malvern	
	Run-1	Run-2	Run-3	Run-4	Run-1	Run-2	Run-3	Run-4	Mean /μm	St.dev./μm
CS1	110	119	111	109	69	90	85	71	111	77
CS2	106	116	103	133	53	68	71	54	129	68
CS3	124	120	108	140	82	78	78	65	125	74
CS4	114	107	106	133	54	77	83	60	137	79

In order to elucidate comparisons, all data sets are plotted in **Figures 5.3a-d.**

These graphs show that although the suspension did not atomize in the stable cone-jet mode the estimated droplet sizes correlate remarkably well with that of the output obtained from the Malvern device.

5.2.2 Concentrated suspension

This suspension containing almost five times the volume loading of alumina compared with suspension CS1-CS4 was observed to atomize in the stable cone-jet mode over a wide range of flow rate and applied voltage combinations for all three ground electrode configurations (see **Figure 5.4a-c**). Operating maps were generated based on the observations made during electrostatic atomization of suspension CS5 with a point-like ground electrode configuration. This was done in two stages. Firstly, the flow rate regime 10^{-9} to 10^{-8} m^3s^{-1} was investigated. Secondly, the pico-flow rate regime (10^{-12} to 10^{-11} m^3s^{-1}) was studied. Hysteresis

effects were not observed in the construction of both maps. The substrate used for the collection of relics of CS5 was coated polyester substrate.

It was observed that at an applied voltage and flow rate of 7kV and $1.67x10^{-9}m^3s^{-1}$, respectively, the stable cone-jet mode of electrostatic atomization was achieved. However, as shown in **Figure 5.5** the stable cone-jet mode prevails almost over the entire flow rate regime of $10^{-9}m^3s^{-1}$ if the applied voltage is held between 7-10kV. The effect of varying either applied voltage or flow rate with the other held constant is shown by the data contained in **Tables 5.5** and **5.6**.

Table 5.5 Jet diameter and relic size distribution of CS5 with increasing applied voltage and at constant flow rate of $1.67x10^{-9}m^3s^{-1}$

Applied voltage/kV	Jet diameter/μm	Relic sizes/μm	
		Min	Max
8	17	350	400
9	13	100	280
10	6	30	60
11	3	10	27

Table 5.5 and **Figure 5.6** illustrates that with the flow rate kept constant, increasing applied voltage affects both the jet diameter and hence the relics generated. It is seen that as the applied voltage was increased from 8-11kV the jet diameter reduced from 17 μm to 3 μm and the relic sizes were found to decrease significantly. At the applied voltage of 7kV the relics could not be individually resolved. With the increase in applied voltage the suspension is further accelerated towards the cone apex. Thus, the cone shape changes as witnessed by its depth (distance from needle exit to the apex of the cone) as seen in **Figure 5.7.**

Consequently, a thinner jet emanates from the apex of the cone generating finer relics.

However, keeping the applied voltage fixed at 8kV and varying the flow rate gave the opposite effect on both the jet diameter and the size of relics generated during stable cone-jet mode of atomization as shown in **Table 5.6** and graphically illustrated in **Figure 5.8**.

Table 5.6 Jet diameter and relic size distribution of CS5 with increasing flow rate at a constant applied voltage of 8kV

Flow rate/$10^{-9}m^3s^{-1}$	Jet diameter/μm	Relic sizes/μm	
		Min	Max
2	18	335	425
4	21	367	489
6	25	429	537
8	27	512	631
10	36	500	713

As the flow rate is increased from 2 $x10^{-9}$ to $10x10^{-9}m^3s^{-1}$ the jet diameter doubles from 18μm to 36μm and the relic sizes increase dramatically. The cone depth increases significantly with flow rate as shown in **Figure 5.9**.

In the pico-flow rate regime the change in mode of atomization with flow rate and applied voltage is shown in **Figure 5.10**. The cone-jet mode prevails over a large span of flow rates and applied voltages. It was observed that when the flow rate was kept constant at just over $2x10^{-12}m^3s^{-1}$and the applied voltage was raised gradually to above 7kV the cone became shallower (**Figures 5.11a** and **b**) in the

first instance and subsequently the jet skews, and then gently whips (Tang and Gomez, 1996).

Compared with **Figure 5.5** (lower flow rate regime), at pico flow rates more atomization mode changes are seen. A larger increase in applied voltage beyond 7kV at a flow rate of $2.17 \times 10^{-12} m^3 s^{-1}$ changed the mode of atomization to spindle $\rightarrow$ multi-spindle $\rightarrow$ multi-jet and rim emission modes (**Figures 5.11c-f**). If the applied voltage was further increased after obtaining the rim emission mode the jet discharged. If the applied voltage was reduced from the point at which stable cone-jet mode was achieved (7kV), the jet becomes unstable at first and then the mode of atomization changes to microdripping (see **Figures 5.12a** and **b**).

In the pico flow regime the increase in applied voltage had the same effect on jet diameter and size of relics generated, as for the lower flow rate regime. **Table 5.7** and **Figures 5.13** show that as the applied voltage is increased from 7kV to 8.4kV the jet diameter decreases from 7μm to 4μm and the resulting relics vary from a minimum of 0.3μm to a maximum of 33.8μm.

Table 5.7 Jet diameters and relic size distributions of CS5 with increasing applied voltage at a flow rate of $2.17 \times 10^{-12} m^3 s^{-1}$

Applied voltage/kV	Jet diameter/μm	Relic sizes/μm	
		Min	Max
7	7	0.3	33.8
7.5	6	0.3	31.7
8	5	0.3	29.6
8.4	4	0.3	27.9

Also, the increase in flow rate at a constant applied voltage resulted in generating a larger jet diameter and subsequently larger relics. As the flow rate was increased from 2 $x10^{-12}$ to $10x10^{-12}m^3s^{-1}$ the jet diameter was seen to increase from 6μm to 33μm (see **Figure 5.14**) with a significant increase in size of relics from a minimum relic size of ~0.4μm to a maximum relic size of 78.6μm (see **Table 5.8**).

When the applied voltage was kept constant (just above7 kV) and the flow rate was increased by almost an order of magnitude, in the stable cone-jet mode, the cone became deeper (**Figures 5.15**).

Table 5.8 Jet diameters and relic size distributions of CS5 with the flow rate increasing in the $10^{-12}m^3s^{-1}$ range at an applied voltage of 7kV

Flow rate/$x10^{-12}m^3s^{-1}$	Jet diameter/μm	Relic sizes/μm	
		Min	Max
2	6	0.5	35.3
3	9	0.4	37.8
4	12	0.7	39.7
5	16	0.7	41.2
6	22	0.8	47.4
7	23	0.9	51.3
8	25	1.1	67.3
9	27	3.1	71.4
10	33	3.6	78.6

As mentioned in previous chapters the parameters applied voltage and flow rate affect the stability of the cone-jet mode and the droplet production process significantly. During the mapping of the suspension, data such as relic sizes, jet diameter and cone shape were all recorded only for stable cone-jet mode of electrostatic atomization.

No attempt was made to study the jet diameters and relics under different atomization modes as this study focussed on the cone-jet mode.

5.2.2.1 Electrospraying with ring ground electrode

The electrostatic atomization of suspension CS5 with a ring shaped ground electrode was studied as it was a key feature in the preparation of ceramic foams described in Chapter 6. In this configuration CS5 achieved the stable cone-jet mode at an applied voltage of 10kV and flow rate of $1.67x10^{-9}m^3s^{-1}$ but on exceeding this applied voltage the mode of atomization was found to change to the multi-jet mode. The aim was to obtain the finest relics for the foam processing research. Therefore, the variation in jet diameter and relic sizes for different applied voltages at a constant flow rate of $1.67x10^{-9}m^3s^{-1}$ in the cone-jet mode was investigated and results are presented in **Table 5.9** and **Figure 5.16**. Increasing applied voltage to 10kV reduced the jet diameter by 35% **(Figure 5.16)** and allowed the relic size to be reduced to <100μm **(Table 5.9)**

Table 5.9 Jet diameters and relic sizes of CS5 electrosprayed in the ring ground electrode configuration at different voltages with a flow rate of $1.67x10^{-9}m^3s^{-1}$

Applied voltage/kV	Jet diameter/μm	Relic sizes/μm	
		Min	Max
7	37	4.1	172.1
8	33	2.5	157.3
9	29	1.3	121.4
10	24	0.8	97.1

5.3 Focussing the electrospray

It is known that for a ring or plate shaped ground electrode the spray is of a 3-D conical shaped spray is produced with some recirculation at the edges (Hartman *et al.*, 2000, Tang *et al.*, 1996). The only difference between the ring and plate ground electrode configurations is that different jet break up modes can occur but this was not investigated in detail in the present work. The change to a point-like ground electrode helps to focus the 3-D spray.

In both ring and plate scenarios there is radial droplet segregation within the spray with larger droplets in the central regions of the spray while smaller droplets are at the extremities of the spray (Gañán-Calvo *et al.*, 1997 and Hartman *et al.*, 1999a). No one has previously had a need to focus the spray.

The point-like shaped ground electrode was found to focus the 3-D conical spray onto the pointed head of the ground electrode (see **Figure 5.17**). This figure illustrates the stable cone-jet mode, from which the droplets were focussed and attracted to the pointed head of the electrode.

Overall, electrostatic atomization of ceramic suspensions was capable of generating fine droplets from a coarse needle compared with jet based printers where the droplet size is directly proportional to the needle diameter. A significant drawback in the jet-printer is needle clogging with ceramic suspension. This was not observed in the present work with electrostatic atomization and the droplet size could be controlled by tailoring the applied voltage and the flow rate.

In summary this work has enabled the development of applied voltage – flow rate – mode of atomization maps for ceramic suspensions between the flow rates of $1x10^{-9}m^3s^{-1}$ to $1x10^{-12}m^3s^{-1}$. The affect of applied voltage and flow rate variation on jet diameter and ceramic relic diameters have been quantified. The affect of using a point-like ground electrode is illustrated.

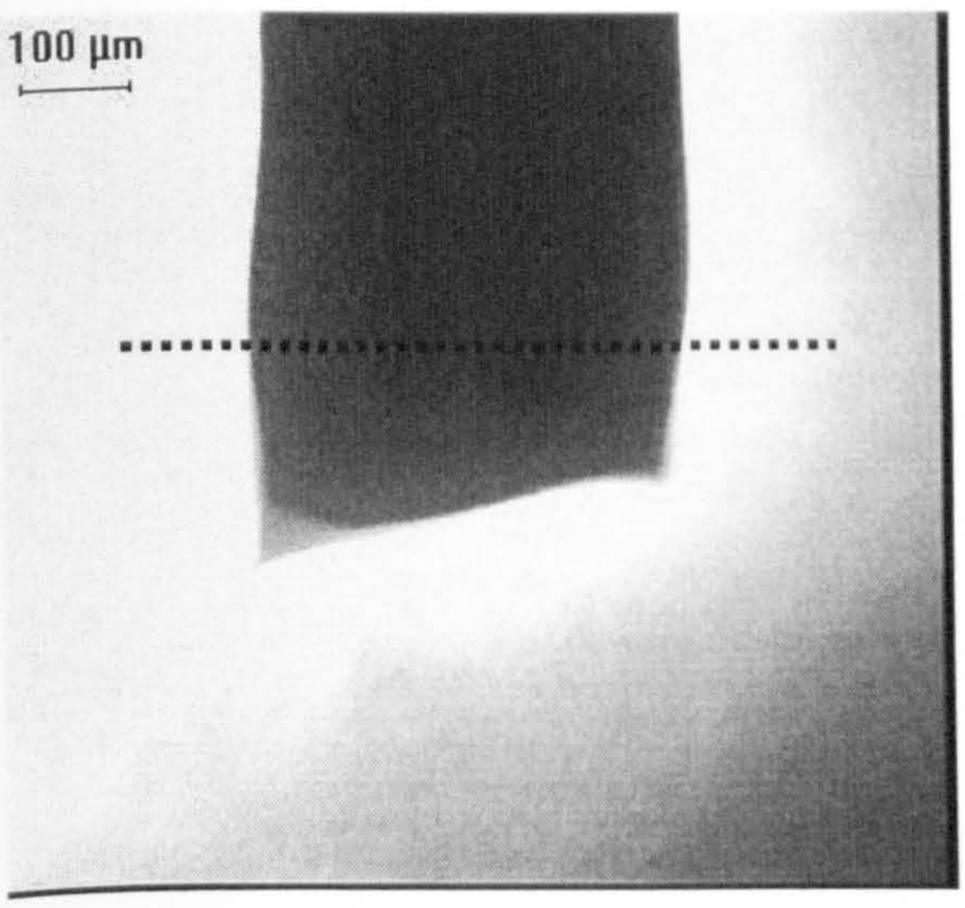

a

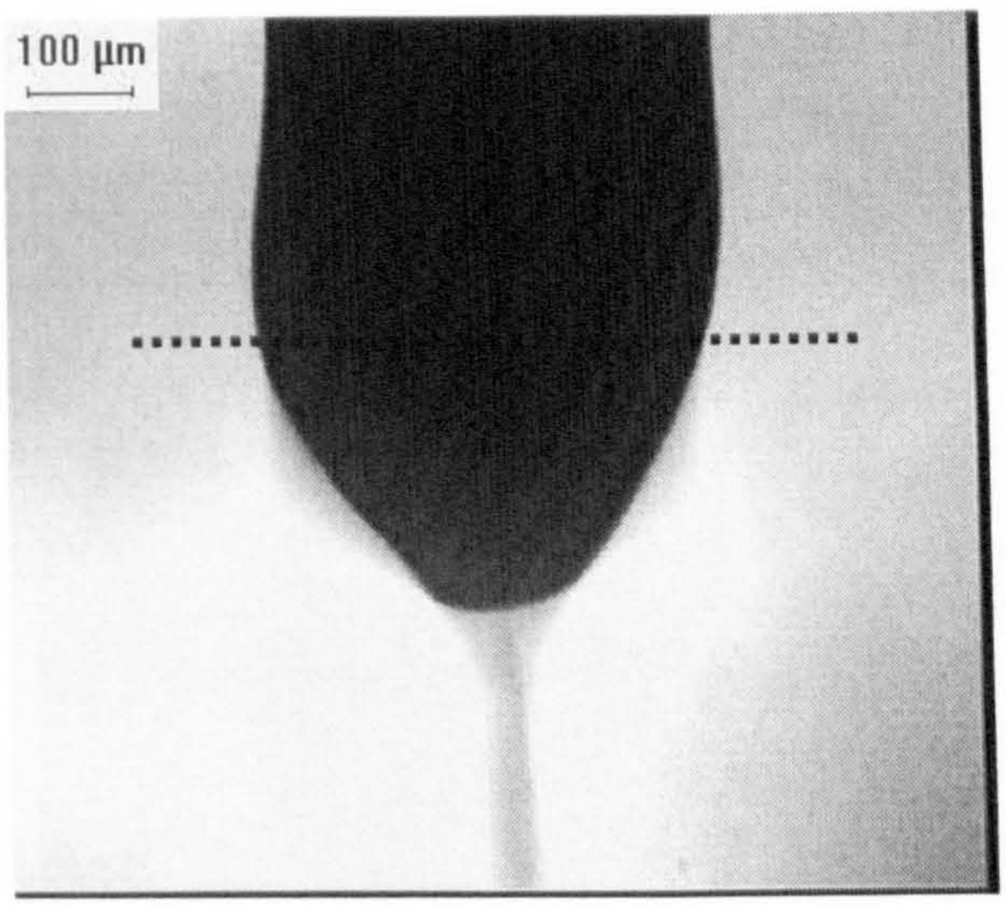

b

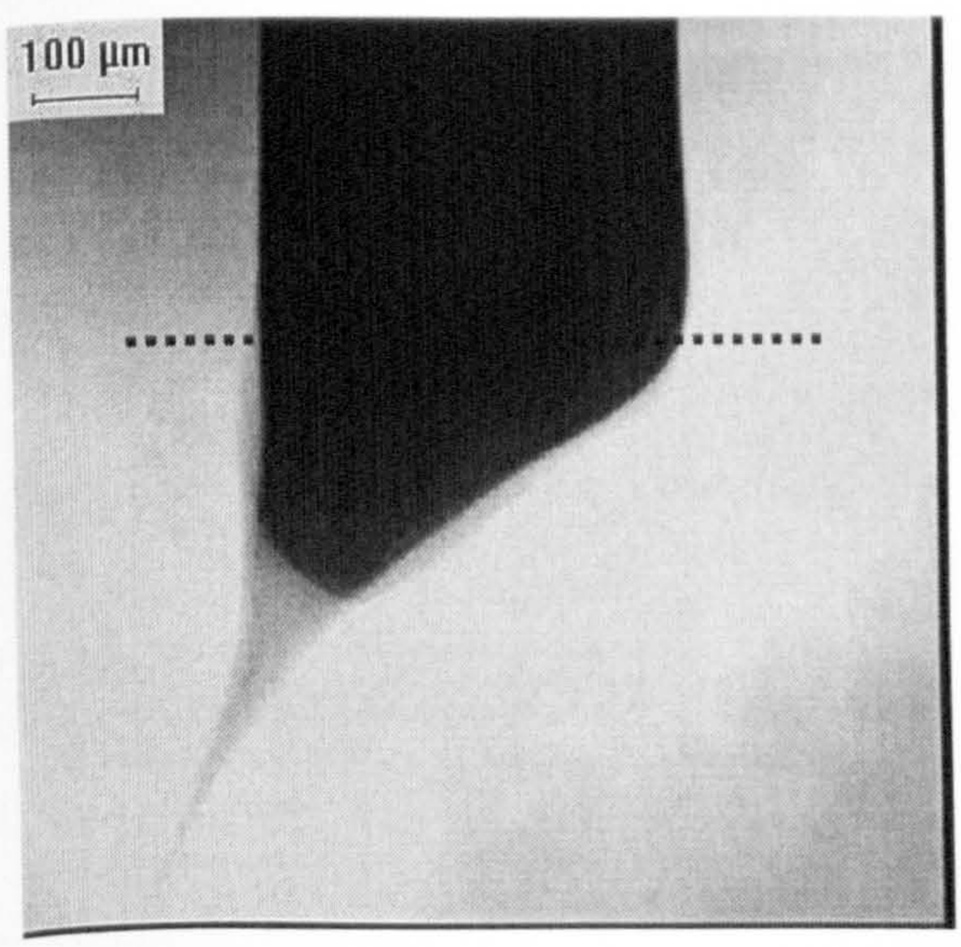

c

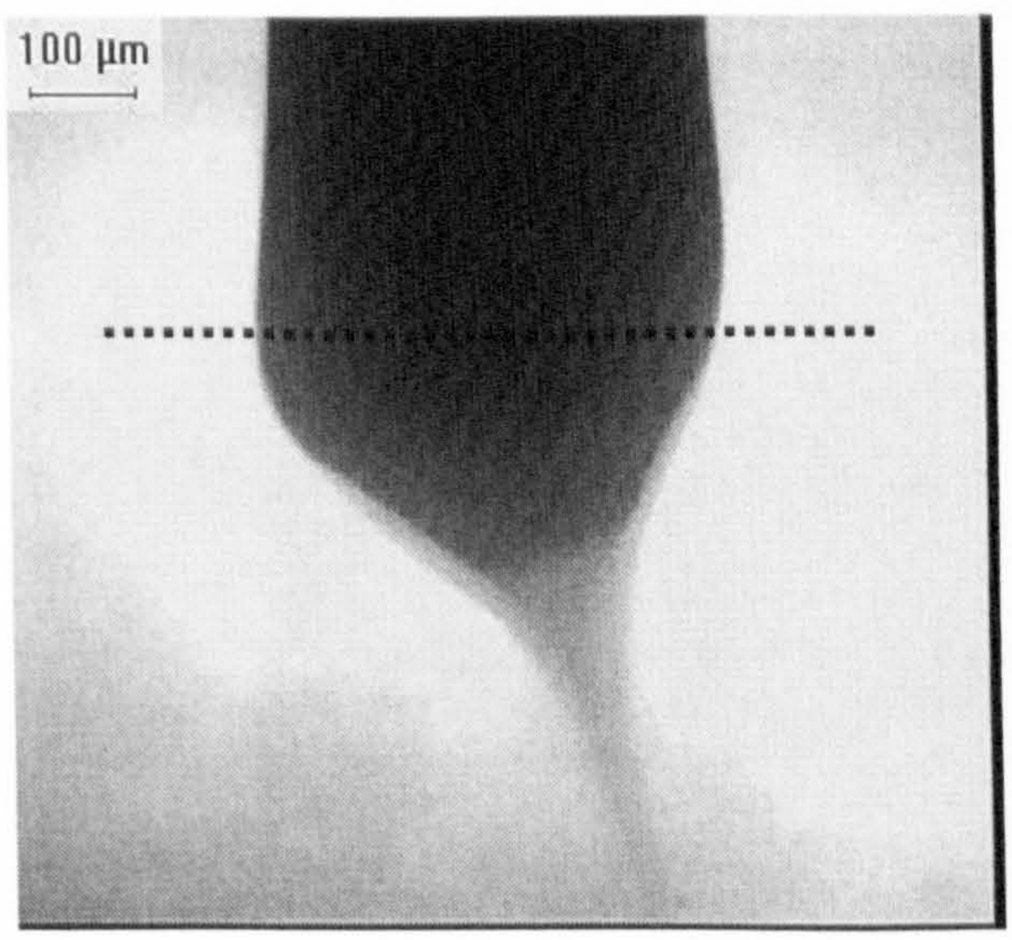

d

Figure 5.1 Electrostatic atomization of suspensions a)CS1, b)CS2, c)CS3 and d)CS4 at an applied voltage of 5kV and a flow rate of $8.37 \times 10^{-11} m^3 s^{-1}$. The dotted line represents the exit of the needle.

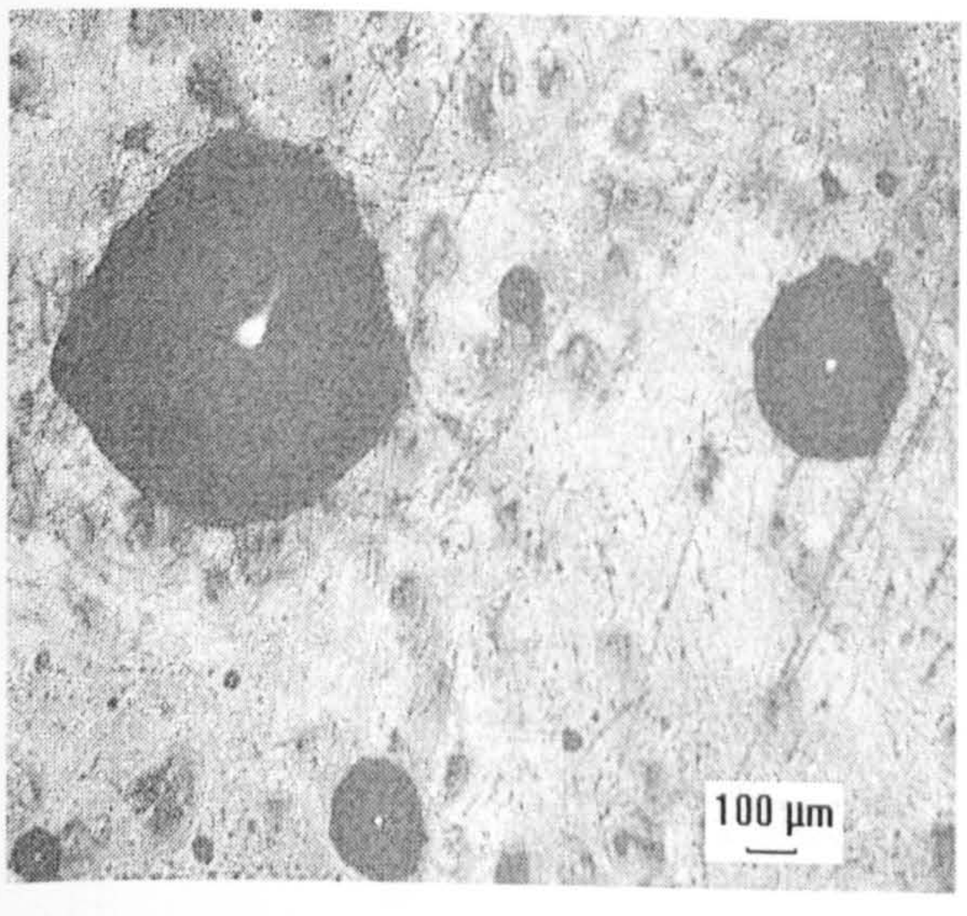

a

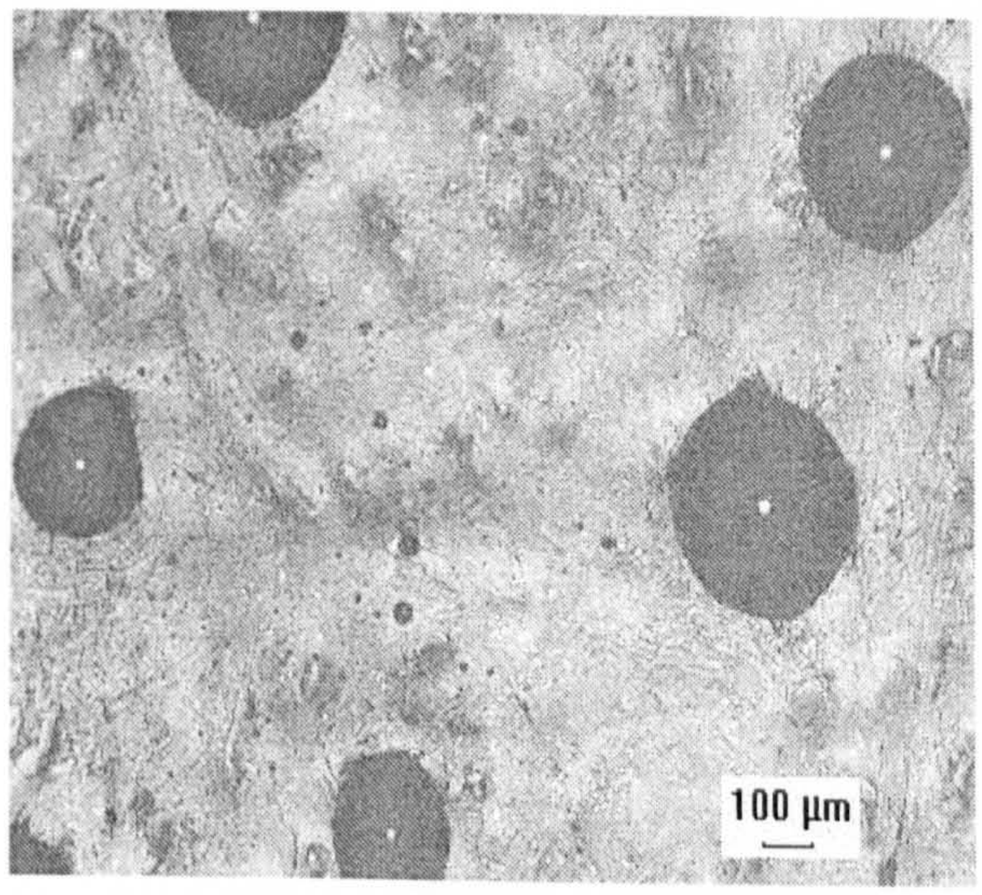

b

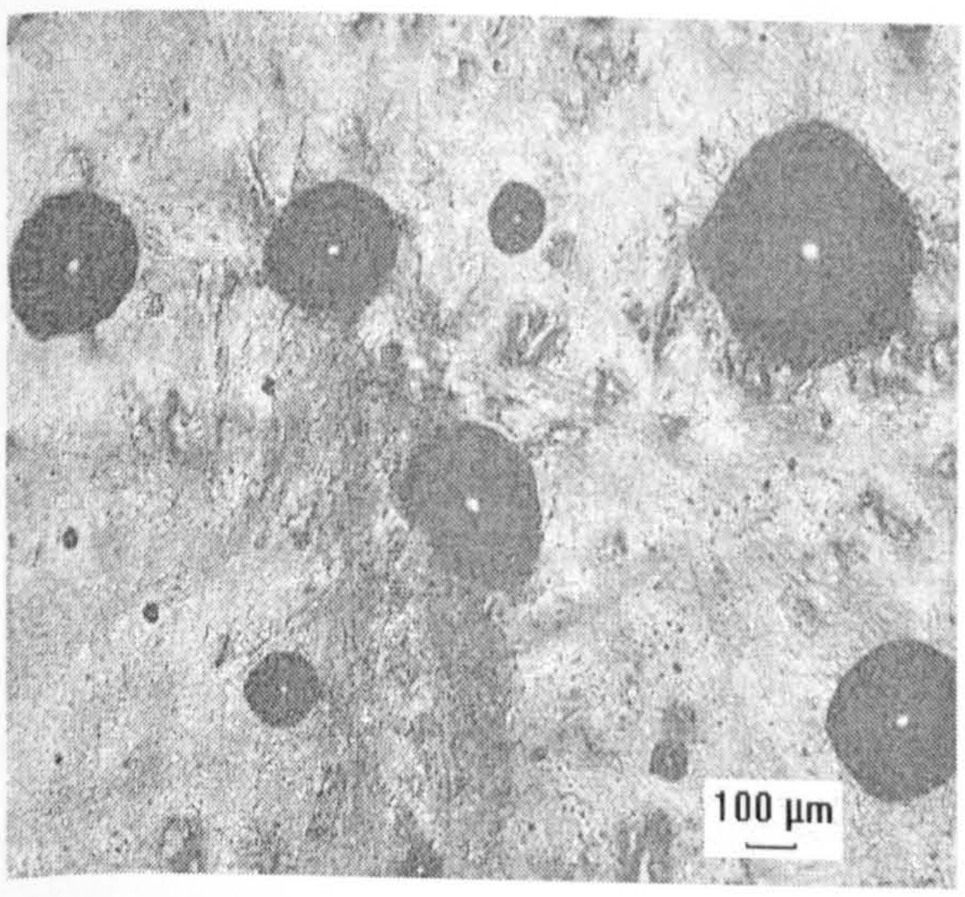

c

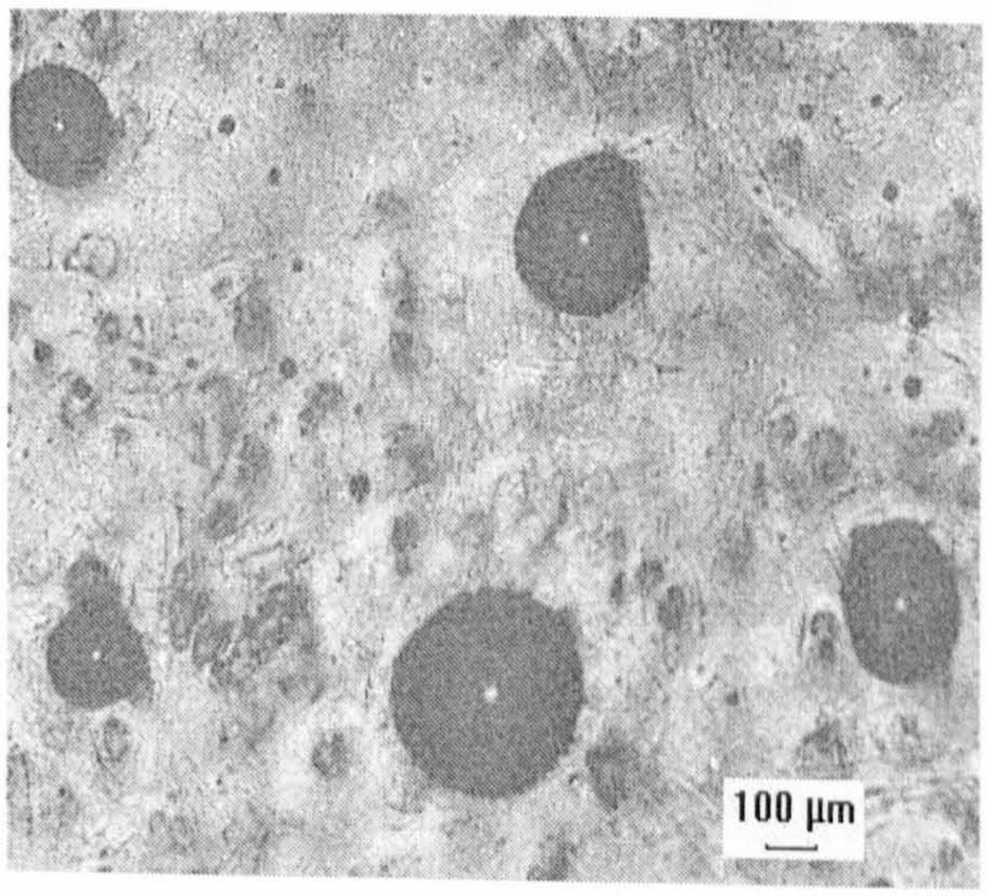

d

Figure 5.2 Typical relics of atomized samples a)CS1, b)CS2, c)CS3 and d)CS4

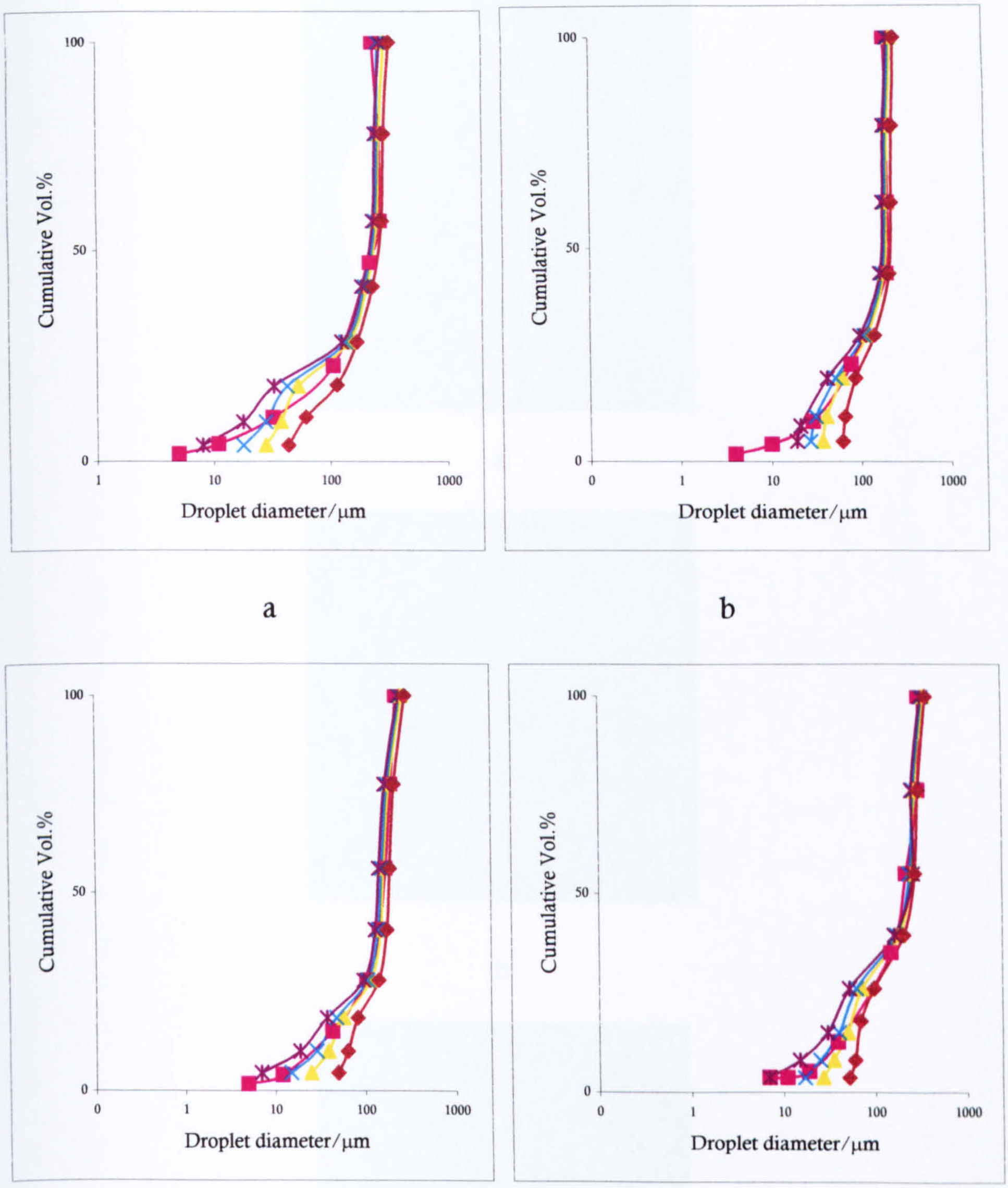

Figure 5.3 Comparisons of droplet sizes of a)CS1, b)CS2, c)CS3 and d)CS4 obtained from the Malvern instrument and estimated from relics

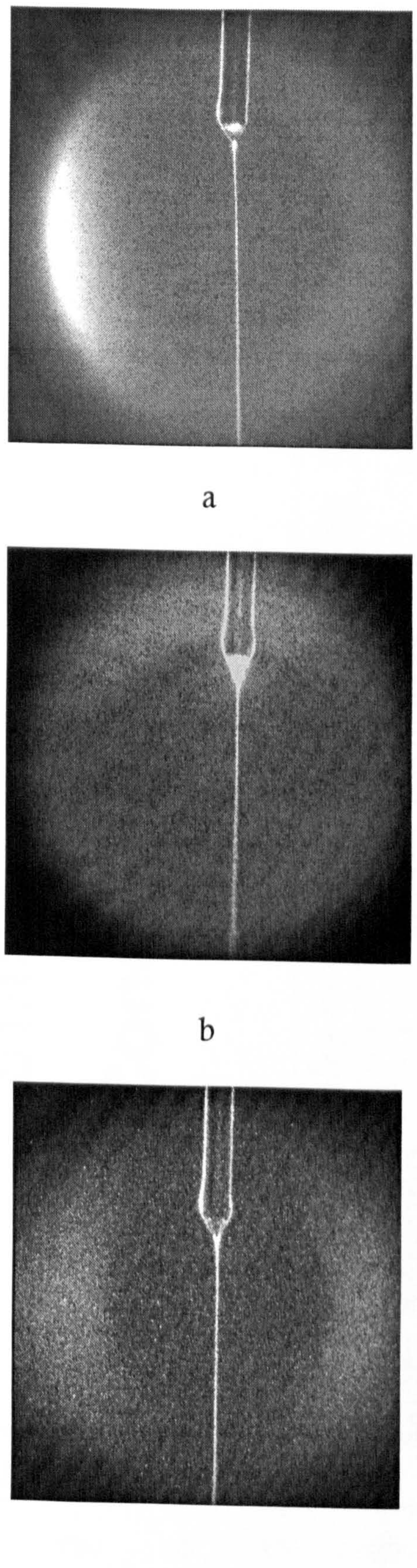

a

b

c

Figure 5.4 Stable cone-jet mode achieved during electrostatic atomization of CS5 with a) ring, b) plate and c) point-like ground electrode configurations at an applied voltage of 10kV and a flow rate of $1.67 \times 10^{-9} m^3 s^{-1}$

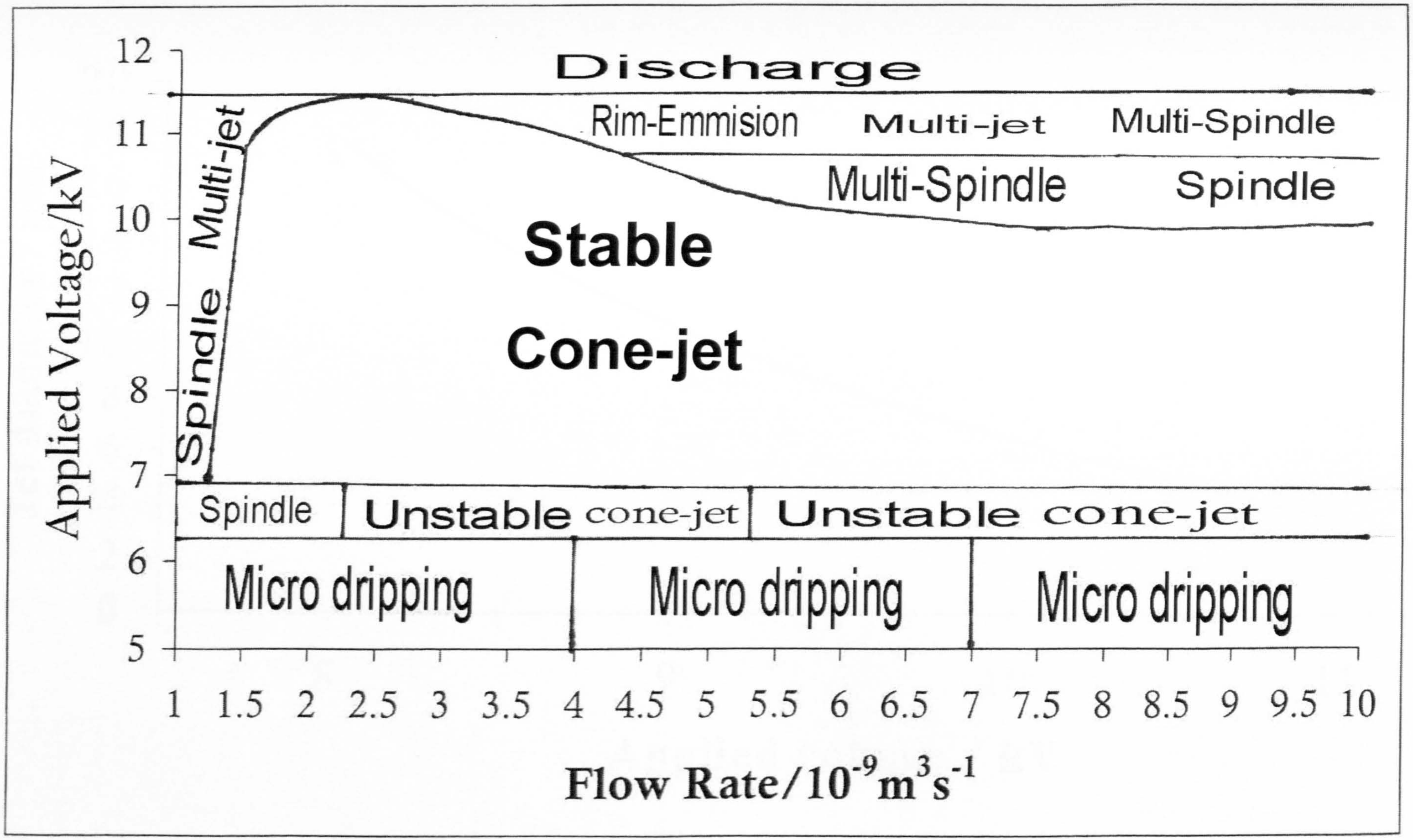

Figure 5.5 Operational map for suspension CS5 in the flow rate regime $10^{-9}m^3s^{-1}$

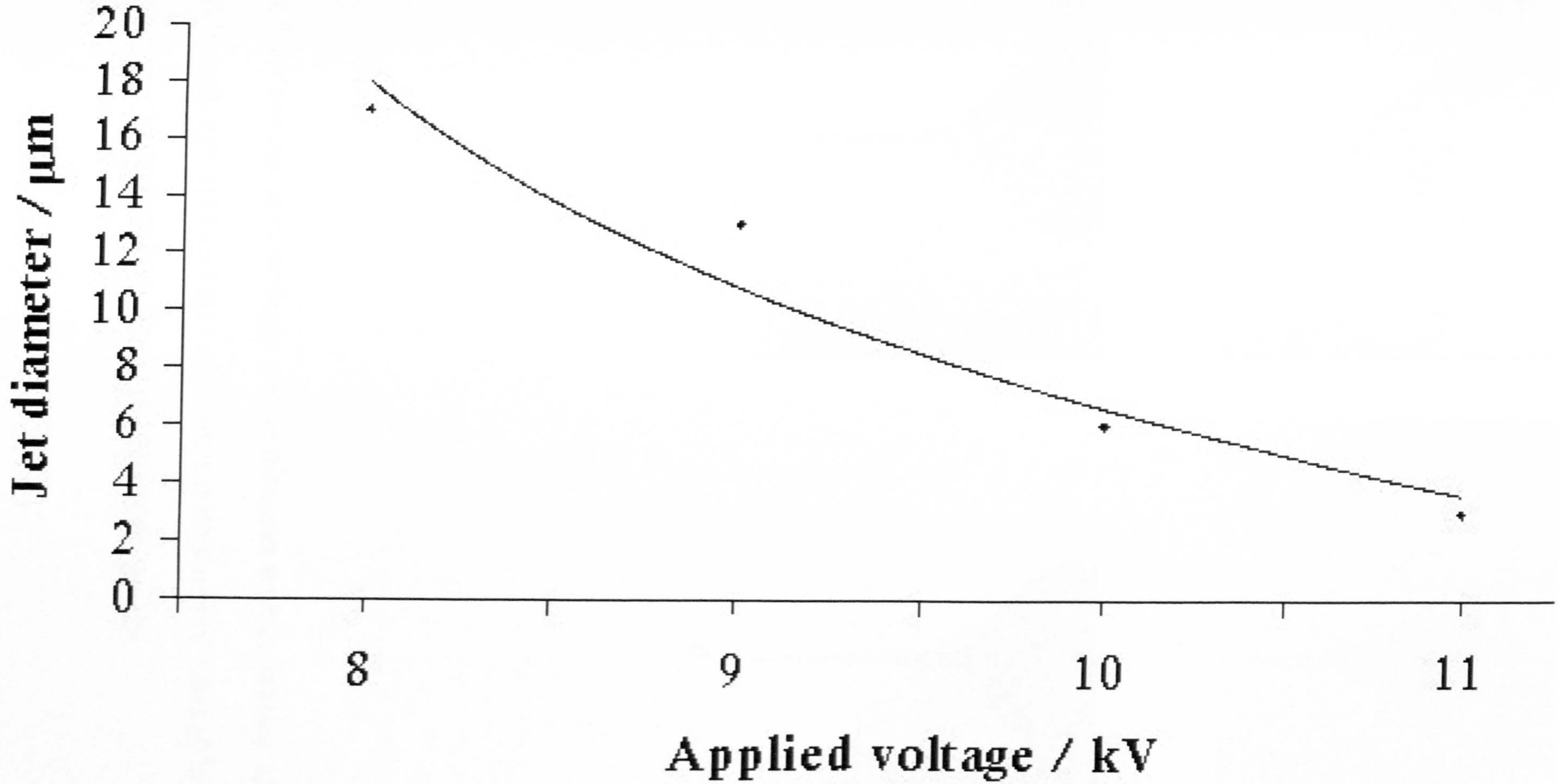

Figure 5.6 Variation of jet diameter with increasing applied voltage for suspension CS5 with the flow rate held control at ~$10^{-9}m^3s^{-1}$

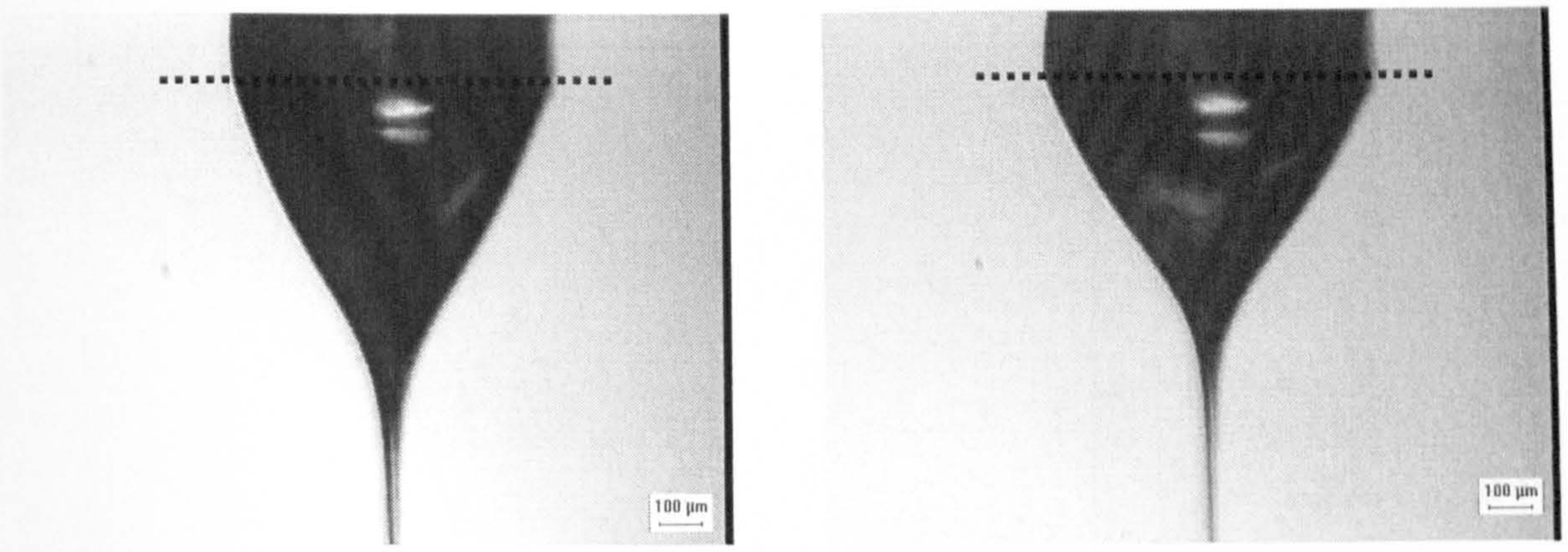

Figure 5.7 Variation in cone shape and jet diameter with increasing applied voltages (kV): a)8, b)9, c)10 and d)11 at a constant flow rate of $1.67 \times 10^{-9} m^3 s^{-1}$. The dotted line represents the exit of the needle.

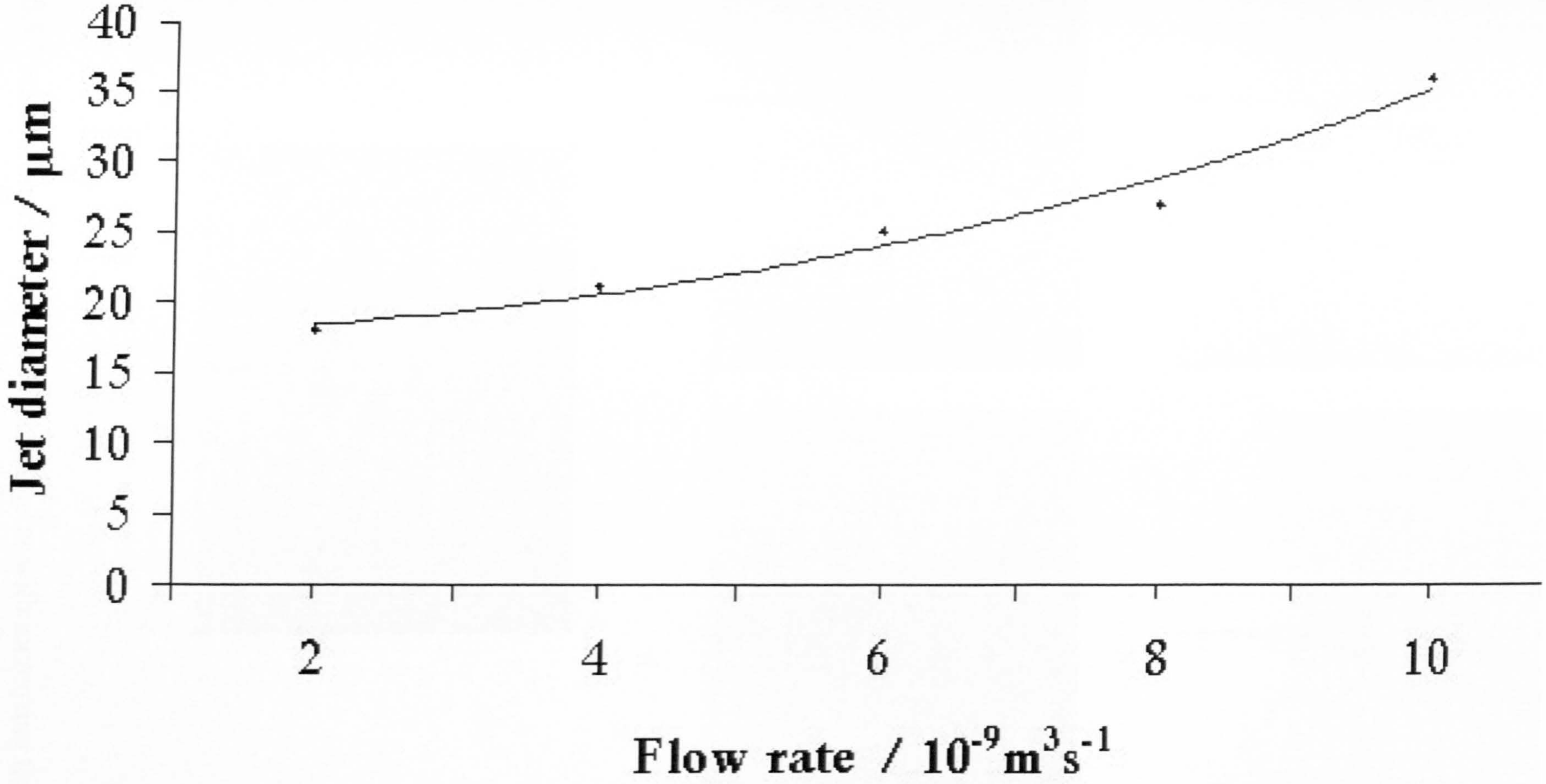

Figure 5.8 Variation of jet diameter with increasing flow rate for suspension CS5 at a constant applied voltage of 8kV

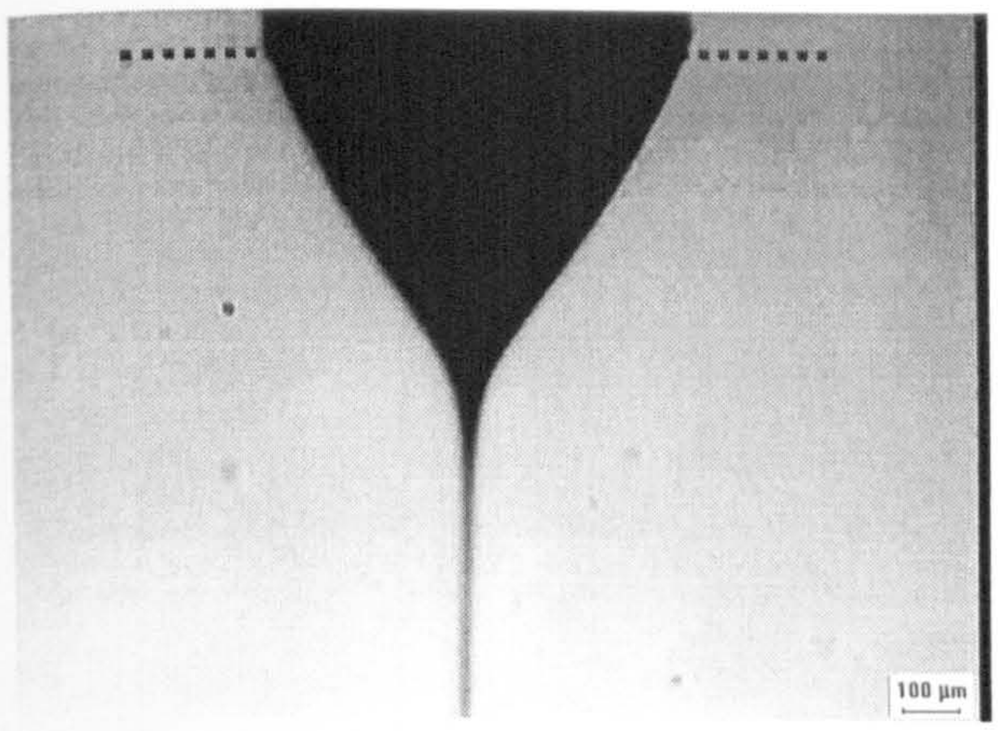

a

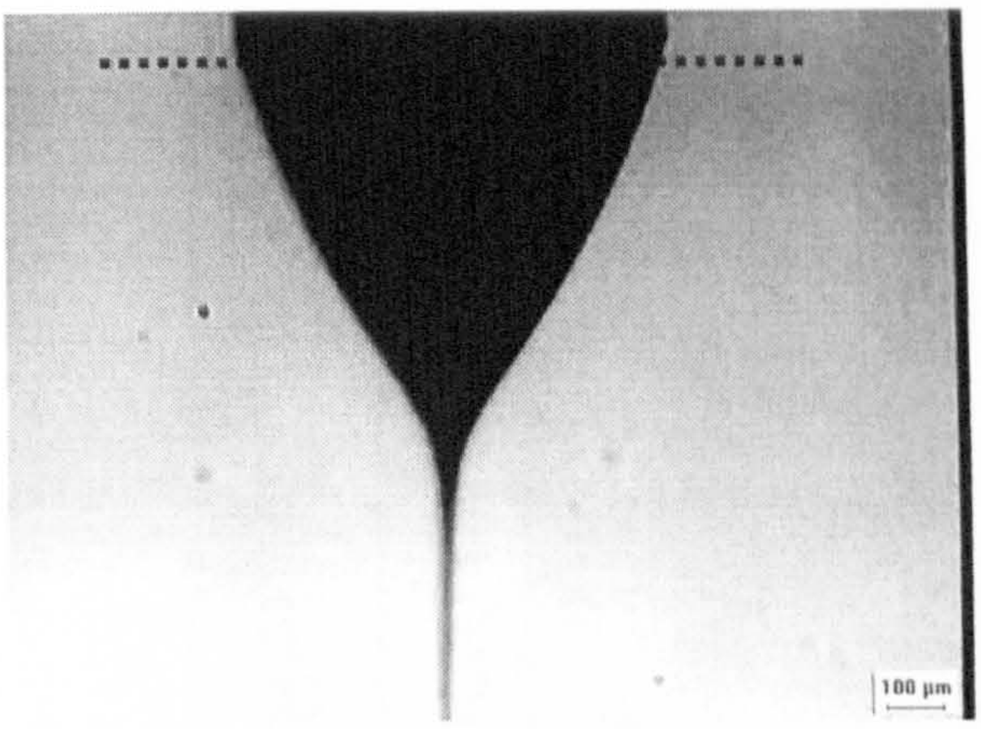

b

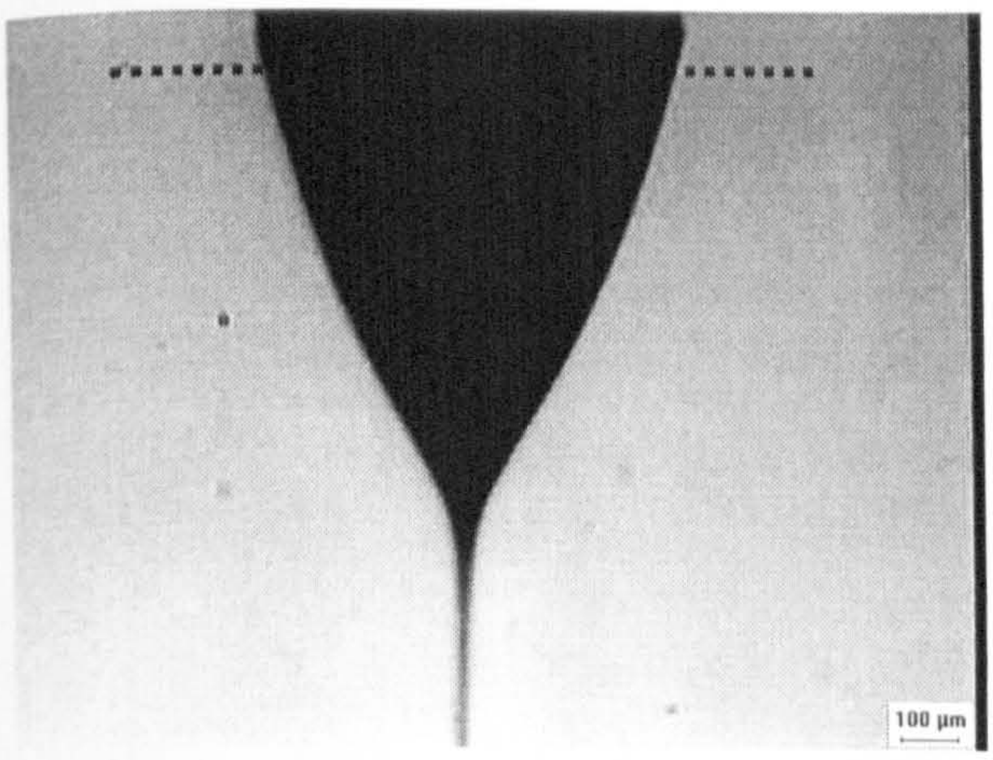

c

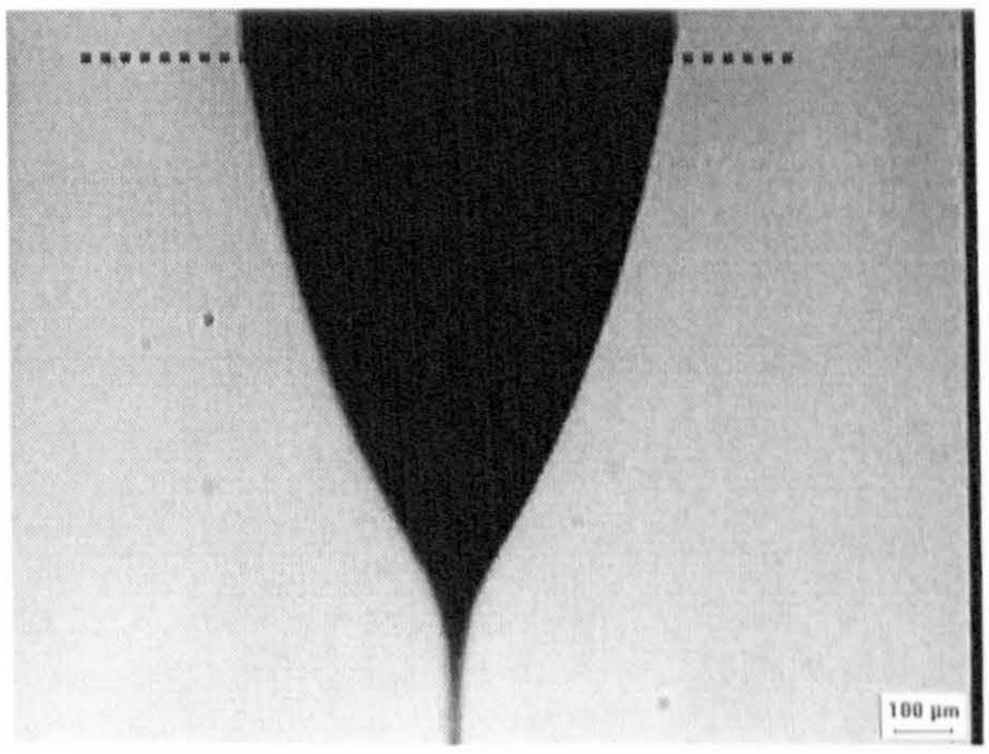

d

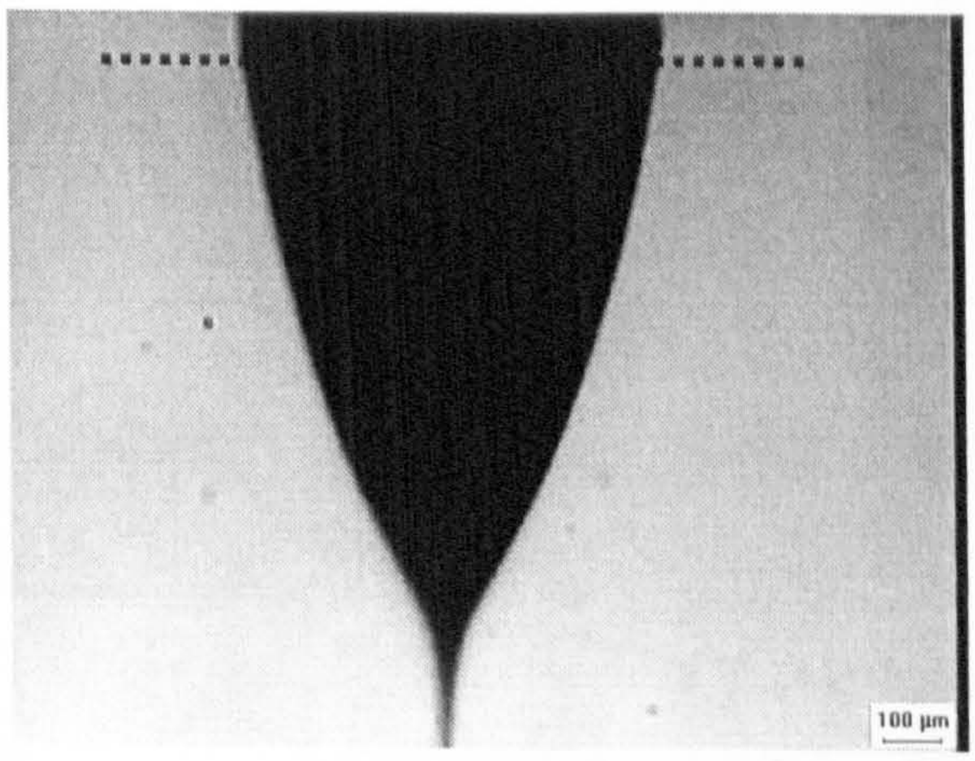

e

Figure 5.9 Variation in cone shape and jet diameter with increasing flow rates ($x10^{-9}m^3s^{-1}$): a)2, b)4, c)6, d)8 and e)10 at a constant applied voltage of 8kV. The dotted line represents the exit of the needle.

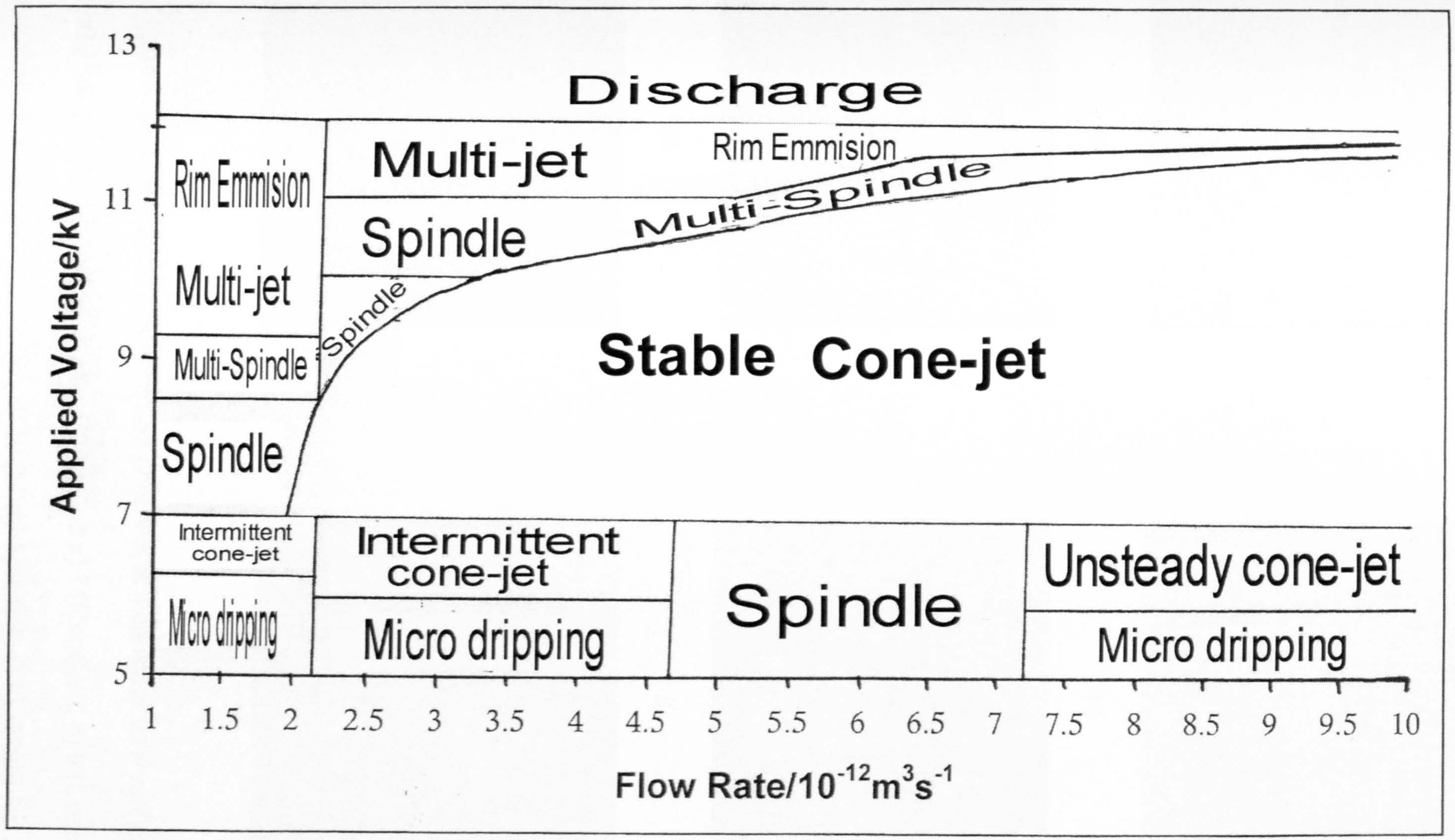

Figure 5.10 Operational map for CS5 in the flow rate regime $10^{-12}m^3s^{-1}$

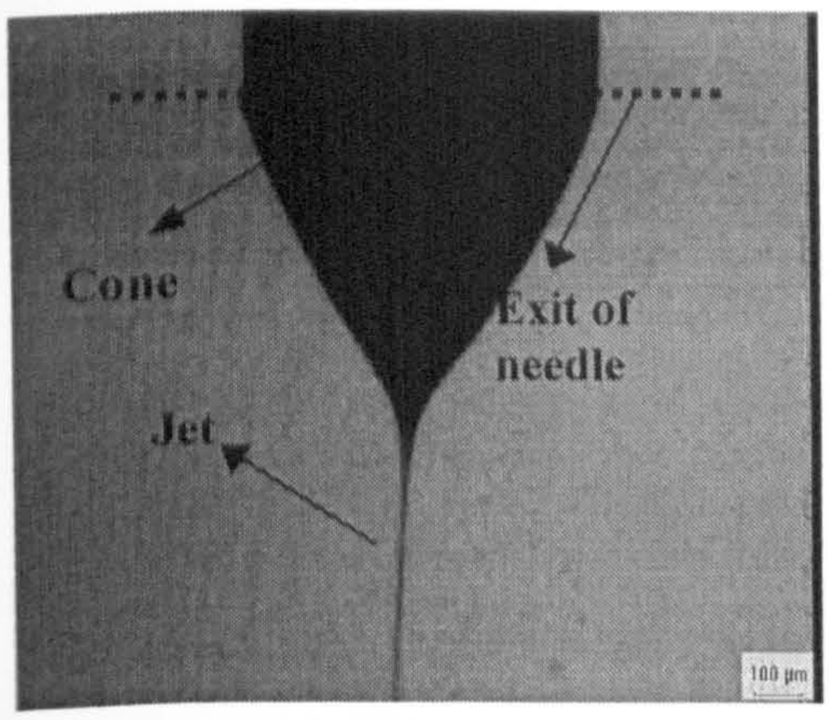

a)

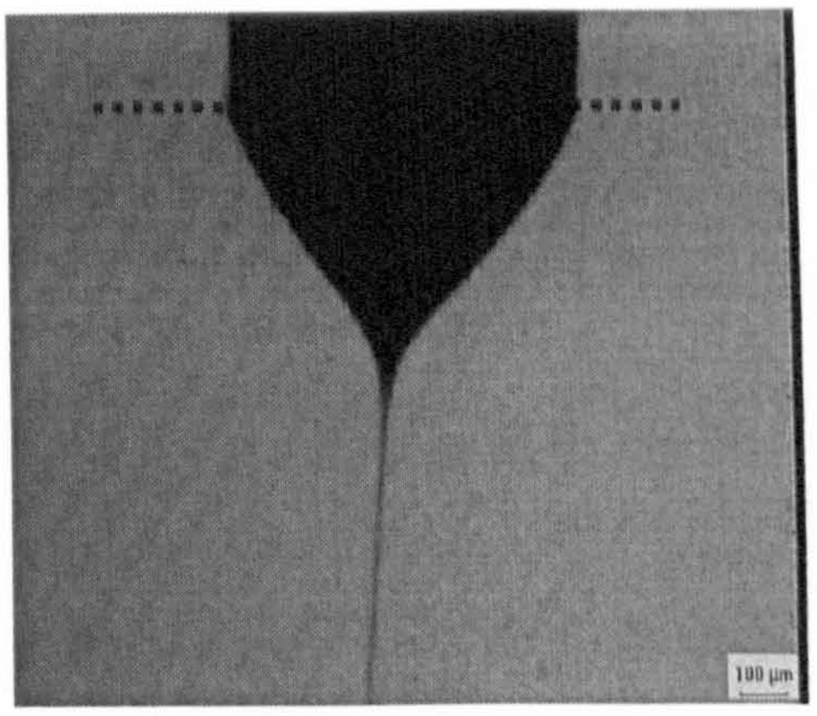

b)

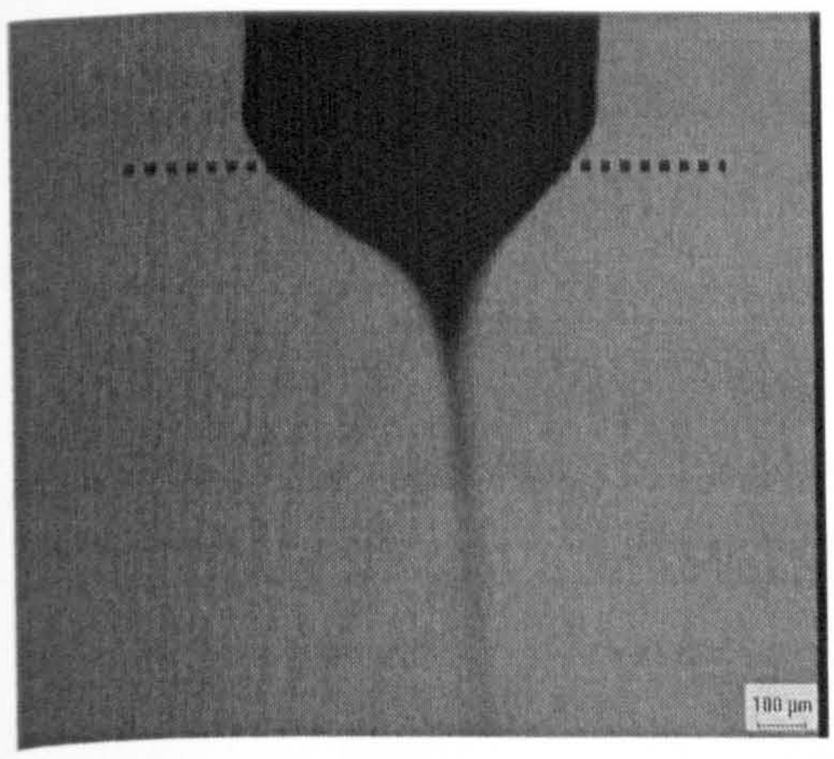

c)

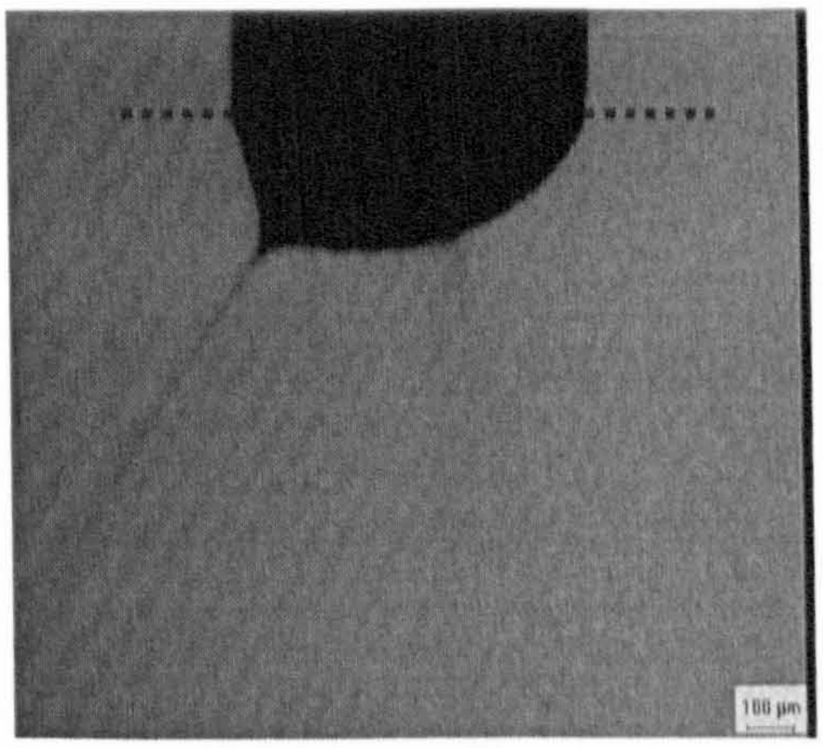

d)

e)

f)

Figure 5.11 Atomization modes of CS5 observed at a constant flow rate of $2.17x10^{-12}m^3s^{-1}$ with the applied voltage (kV) set at: a) 7 (Cone-jet), b) 8 (Cone-jet – with shallower cone), c) 9 (Spindle), d) 10 (Multi-Spindle), e) 11 (Multi-jet) and f) 12 (Rim emission). The dotted line represents the exit of the needle.

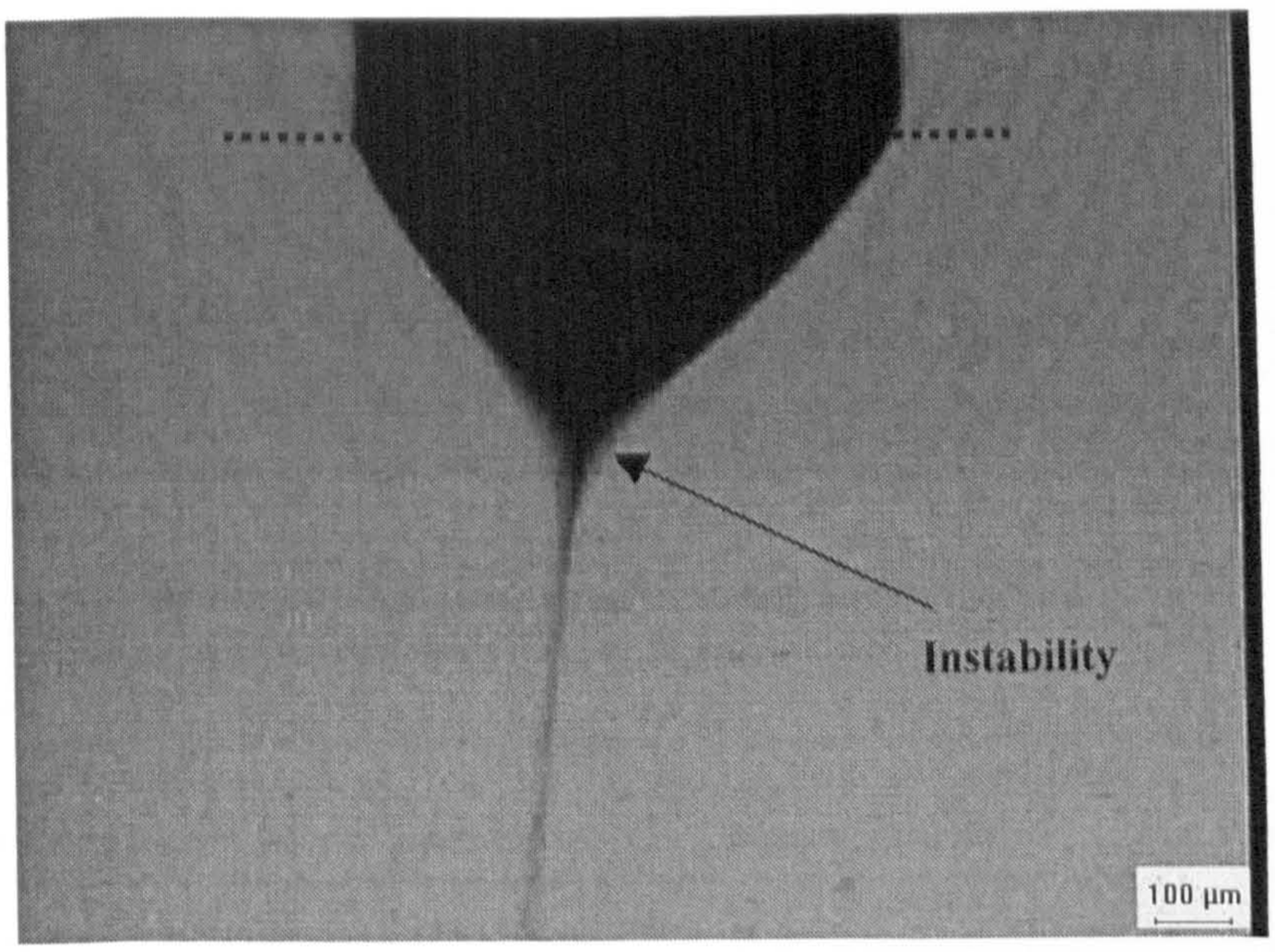

a)

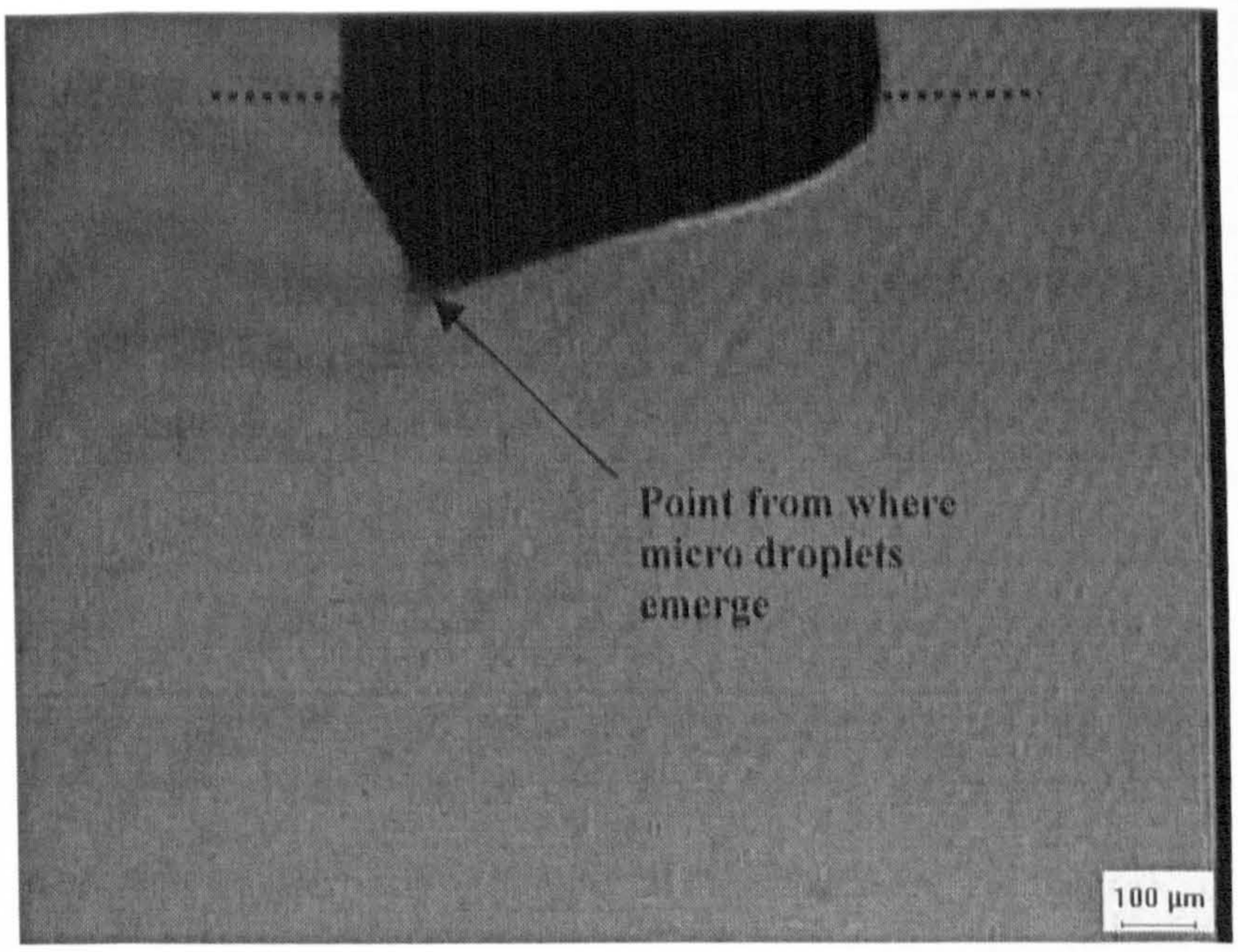

b)

Figure 5.12 Atomization modes of CS5 at a constant flow rate of $2.17 \times 10^{-12} m^3 s^{-1}$ with applied voltage (kV) set at a) 6(Unstable cone-jet) and b) 5(Micro-dripping). The dotted line represents the exit of the needle.

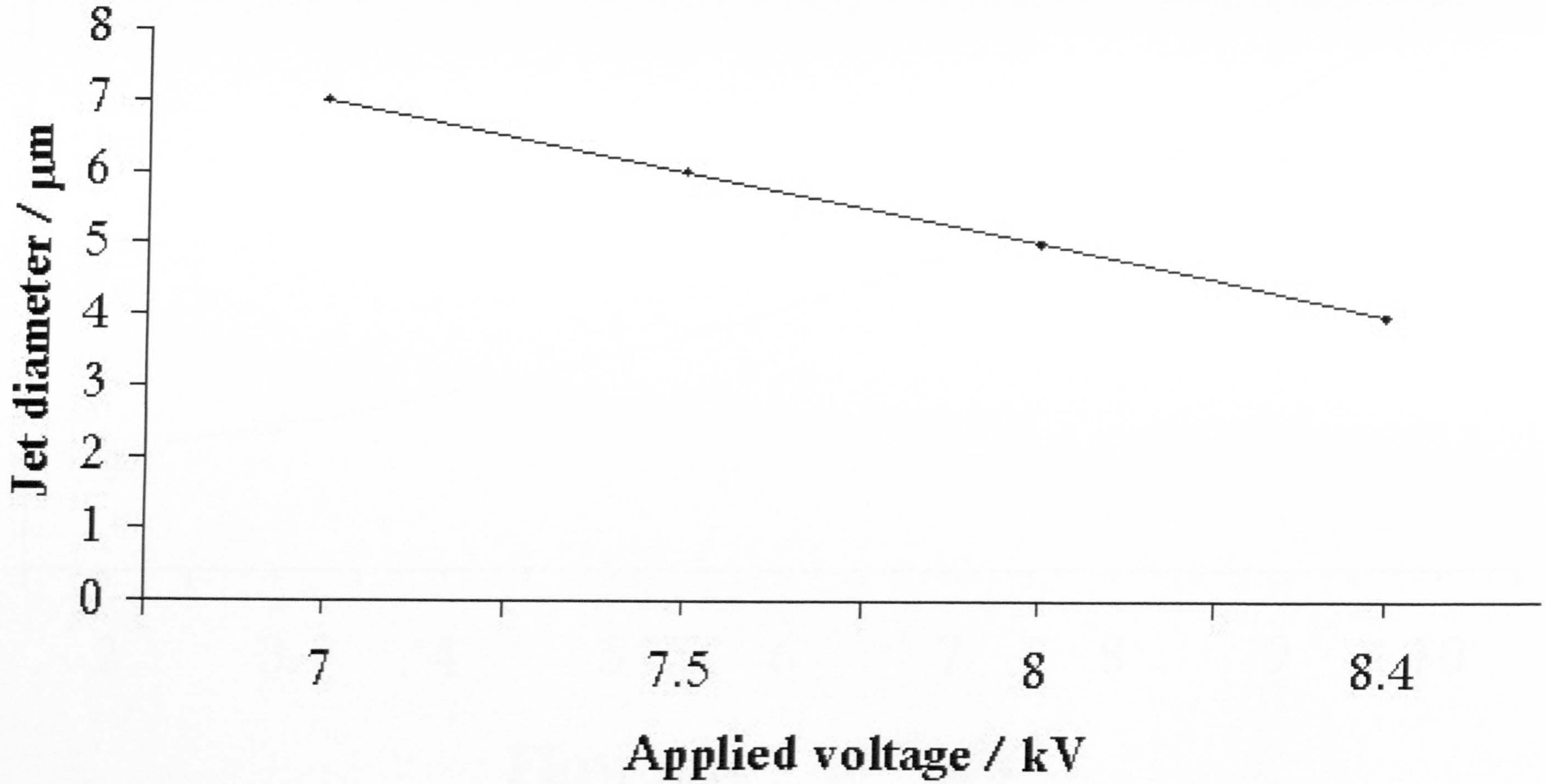

Figure 5.13 Variation in jet diameter with increasing applied voltage for CS5 with the flow rate kept constant at $2.17 \times 10^{-12} m^3 s^{-1}$

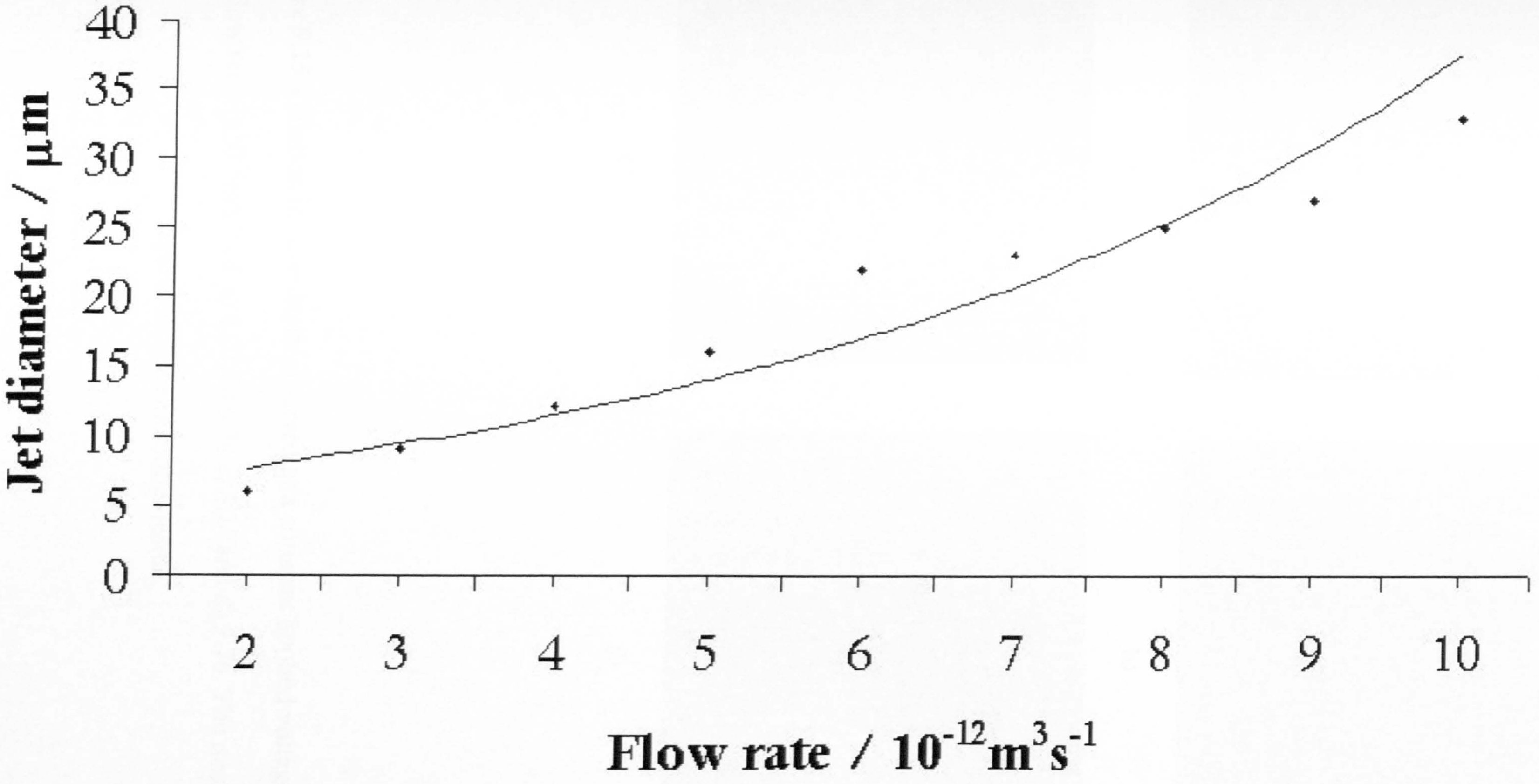

Figure 5.14 Variation in jet diameter of CS5 with increasing flow rate at a constant applied voltage of 7kV

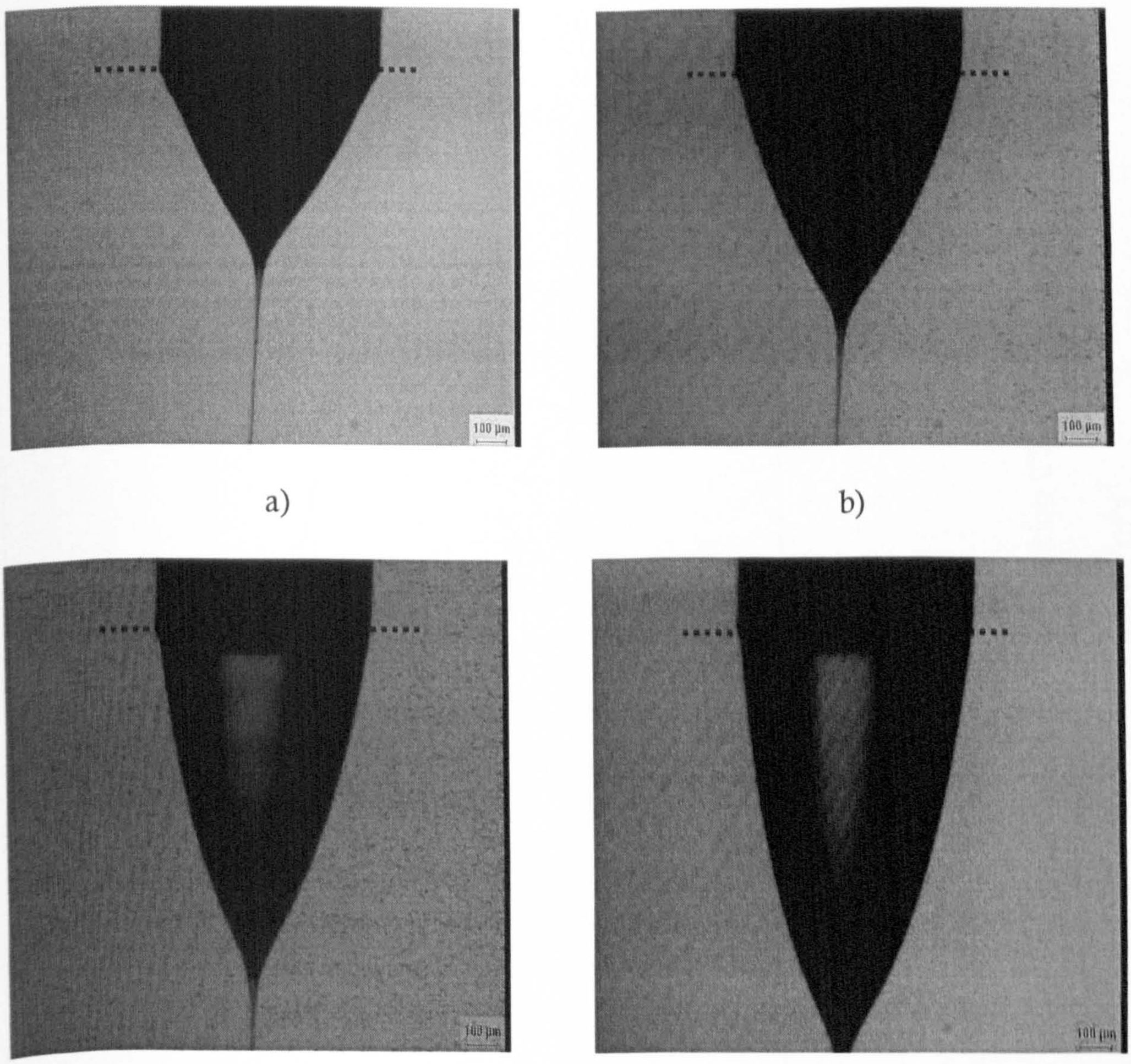

Figure 5.15 Variation in cone depth observed at a constant applied voltage of 7kV for flow rates ($x10^{-12}m^3s^{-1}$) of: a) 4.07, b) 6.24 c) 8.13 and d) 9.76. The dotted line represents the exit of the needle.

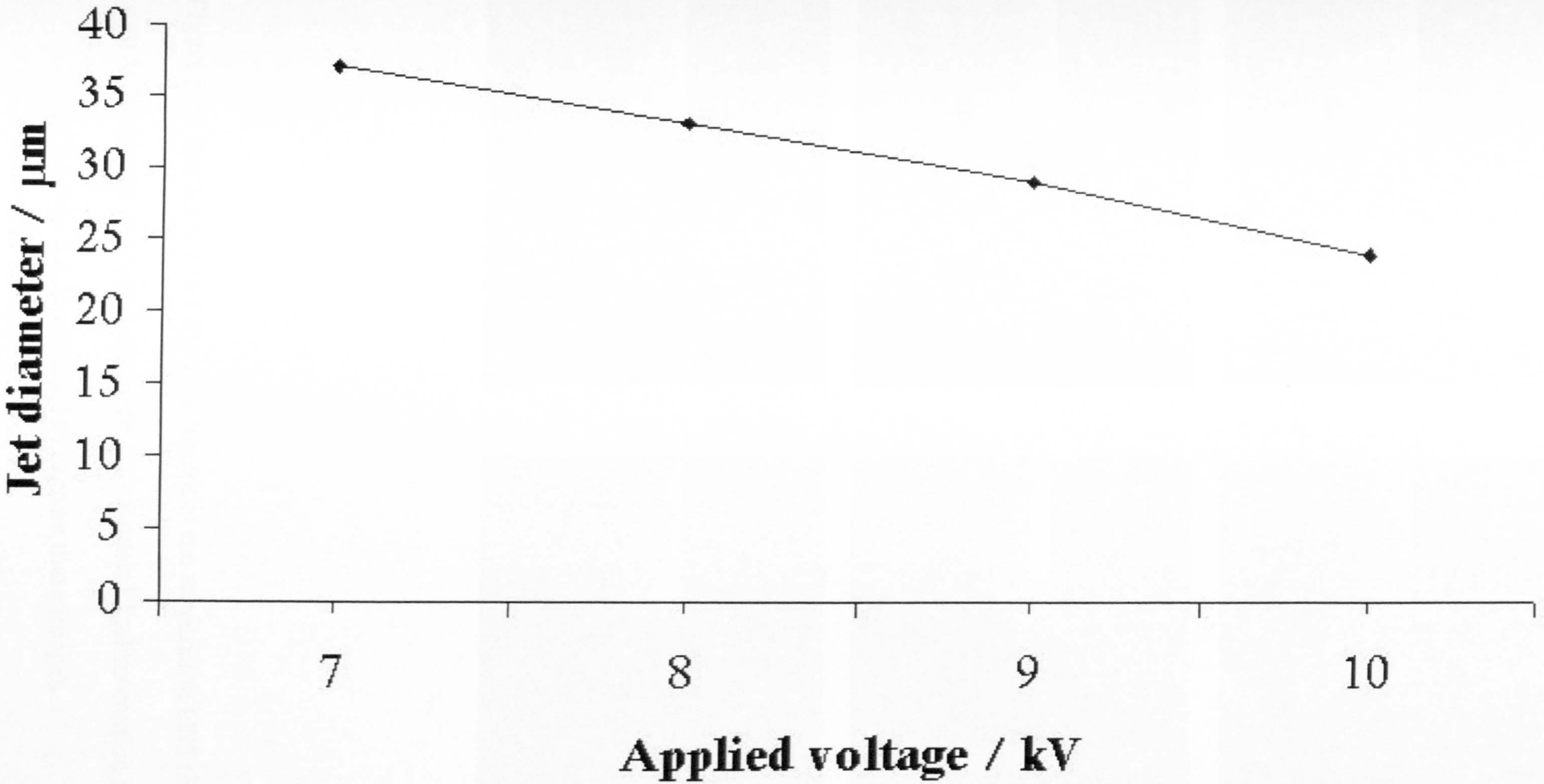

Figure 5.16 Variation of jet diameter with increasing applied voltage for suspension CS5 in the ring shaped ground electrode configuration at a flow rate of $1.67 \times 10^{-9} m^3 s^{-1}$

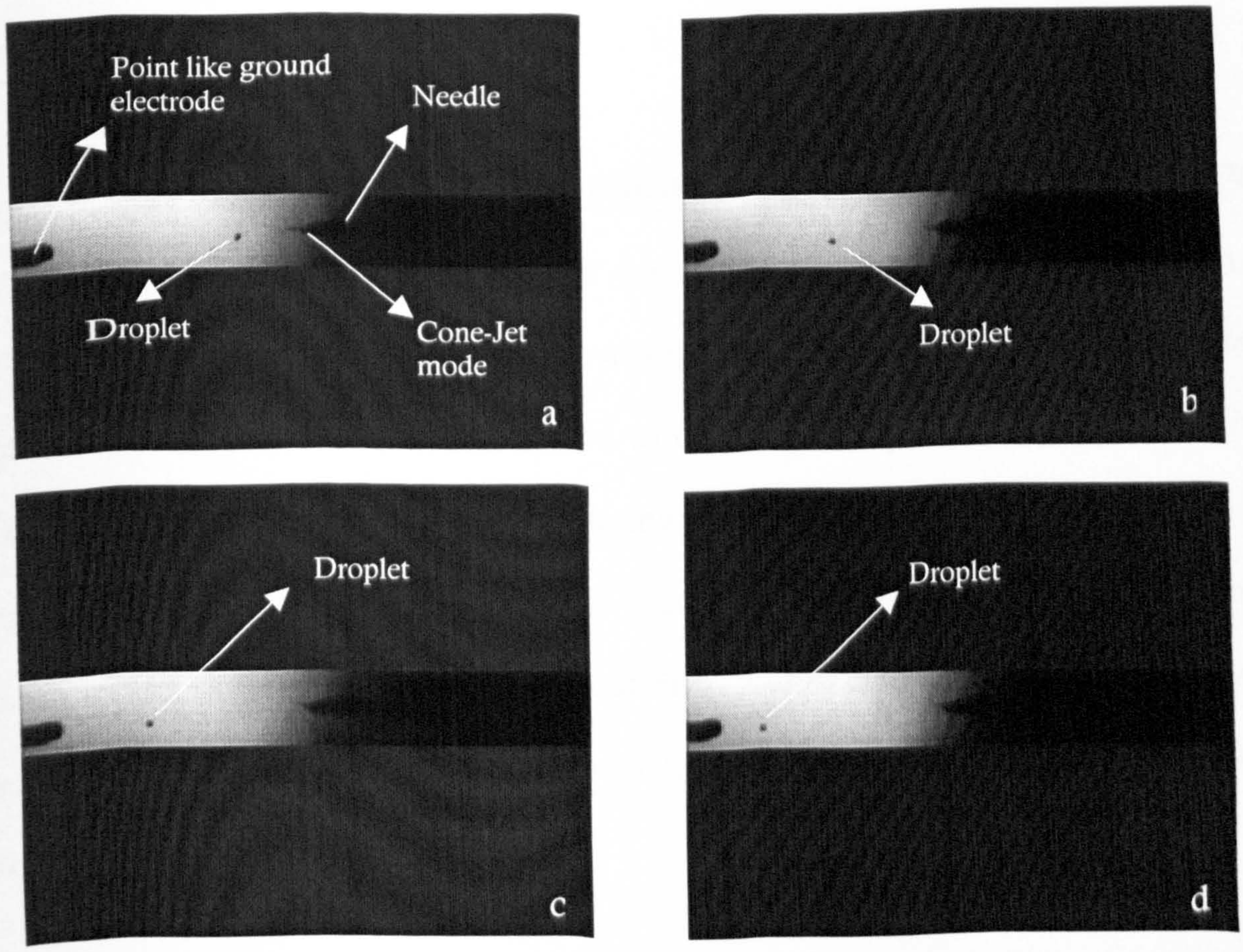

Figure 5.17 Sequence a to f shows a droplet of the suspension CS5 moving towards the point-like ground electrode. The Kodak EktaPro camera system (section 3.5.5) was used to capture these images.

CHAPTER 6

Ceramic electrostatic atomization printing and foam processing

This chapter describes the two major innovations resulting from this research. The first was ceramic electrostatic atomization printing (CEAP). Here the ceramic suspension CS5 was subjected to electrostatic atomization in the stable cone jet mode and printed after focussing the sprays using a point-like ground electrode. The second was where CS5 was electrosprayed in the cone-jet mode with a ring shaped ground electrode and the resulting droplets were deposited on a polyurethane template. Thus, a novel forming method for open-cell ceramic foams was uncovered.

6.1 Ceramic electrostatic atomization printing

6.1.1 Characters and words

As the applied voltage was increased focussing of the ceramic spray becomes increasingly difficult as the droplets become finer. **Figure 6.1** shows the print quality at each applied voltage and more scatter of relics is clearly observed with increasing voltage.

The relic sizes at an applied voltage does not vary within one character or between characters in the prints shown in **Figure 6.1**, unless overprinting has taken place. **Table 5.5** in Chapter 5 shows that a significant decrease in the relic size distribution was obtained on increasing the applied voltage to 10kV where the actual relic sizes obtained were between 30μm to 60μm. However, there was an appreciable amount of scatter of the relics accompanying size control. On

further increasing the applied voltage to 11kV the relic sizes reduced further to 10μm to 27μm but scatter was worse as seen from **Figure 6.1e**.

Optical microscopy showed that the contact angle of the alumina droplets on the acetate substrate was 30^0. Using the relic sizes in **Table 5.5** in Chapter 5 with equations 3.5 and 3.6 in Chapter 3, the minimum size of the droplets produced at 11kV is estimated to be ~5μm. Thus, droplets generated were extremely fine and scatter observed, despite the use of the point-like ground electrode, is not totally surprising. However, this is the very first design of this printing device. Improvements like further reducing the radius of the point-like ground electrode and shielding the spray can be effective in reducing scatter. The relics produced at 8kV gave the best compromise ~375μm in size, while retaining good print quality **(Figure 6.1b)**. At this voltage the relics produced are much bigger as shown in **Table 5.5** in Chapter 5 (170μm to 200μm). Spreading of the deposit is more prevalent at larger droplet sizes but this can be minimised by reducing the surface free energy of the substrate (Tay and Edirisinghe, 2002).

6.1.1.1Effect of applied voltage and flow rate on the print quality

Figure 6.1e illustrates that as the applied voltage is set to 11kV the print quality reduces as scatter is predominant. Further increasing the applied voltage from 11kV discharged the printing process.

The flow rate also has a significant effect on the relic sizes during CEAP. It is seen from **Figure 6.2** that increasing flow rates from 4 $x10^{-9}m^3s^{-1}$ to $10x10^{-9}m^3s^{-1}$ affects both the width of a character in the print and its quality. The width of a

printed character within the print is seen to increase with increasing flow rate. This is due to the fact that the jet diameter increases with increasing in flow rate as discussed in Chapter 5. A high flow rate with an incompatible applied voltage results in a significant reduction in the print quality as shown in **Figure 6.2d**.

6.1.2 Single tracks

The print on coater polyester substrate shown in **Figure 6.3** spanned a length of ~102mm and a width of ~70mm. The printing time involved was ~180s. Sections indicated in **Figure 6.3** are 10mm x 10mm. The relic size distribution, in the "straight" regions 1, 4, 8 and 10 of the print were slightly narrower in contrast to those of "corner" regions 2, 3, 5, 6, 7 and 9 (**Figure 6.3 and Table 6.1**). At corners there is an abrupt 90^0 change in printing direction and the variations in relic size distributions are caused simply by mechanical noise.

Table 6.1. Statistical analysis of relics present in each section

Section	Relic data				
	Number present	Minimum size/μm	Maximum size/μm	Mean size/μm	Standard deviation/μm
1	1296	1.1	21.9	5.8	6.0
2	1935	0.3	29.2	4.2	5.9
3	1894	0.6	28.9	4.8	6.6
4	1537	1.4	31.2	6.0	7.0
5	2145	0.3	30.5	4.4	6.1
6	1553	0.3	29.8	4.9	6.3
7	1657	0.4	33.8	3.9	5.8
8	1578	1.3	26.8	5.7	6.6
9	1809	0.4	31.4	4.2	6.2
10	956	1.9	29.7	7.8	7.6

Comparison of optical micrographs and 3-D images of the "straight" sections with the "corner" sections (see **Figures 6.4** and **6.5**) shows the variation of relic size in all three dimensions. The images of section 4 (**Figure 6.4**) show more

consistency while section 7 (**Figure 6.5**) contains more variation in relic size in all three dimensions. The relics at a corner section also appear "clumped" to some extent. This is caused by the change in direction during printing and accompanying deceleration and acceleration required by the 2-axis system to negotiate the corners.

6.1.2.1 Effect of applied voltage and flow rate

Increasing applied voltage at a constant flow rate gives rise to finer droplets, however control of deposition reduces, hence scatter increases as shown in **Figure 6.6**. Increasing the flow rate, at a constant applied voltage produces larger droplets but the effect on scatter is not as pronounced as shown in **Figure 6.7**. This is because the increase in flow rate produces coarser droplets and these are easier to focus using the point-like ground electrode.

6.1.3 Multiple tracks

The point-like ground electrodes helped to focus the fine droplets of the spray from each needle and this combined with the synchronised x-y table helped to freeform multiple tracks on a coated polyester substrate simultaneously. Stable cone-jet mode of atomization was achieved in all three needles (**Figure 6.8**) at an applied voltage of 10kV with a flow rate of 1.67×10^{-9} m^3s^{-1} and printing was carried out under these conditions.

As shown in **Figure 6.9,** three tracks were printed simultaneously. Relics in each track are in the size range 20μm to 50μm, are approximately 55μm apart and not exactly in line with each other and therefore the actual width of the ceramic track

increases to ~70μm. Overprinting was not attempted but overlapping of the relics and minimising the track width can be achieved by decreasing the pitch on the ball screws used for positioning the x-y table, a fixed value in the present device. However, even with the present device the track width is <<190μm, obtained using ink-jet printing (Nur *et al.*, 2002). On either side of each track finer relics in the size range 10μm to 20μm prevailed due to scatter caused by imperfect focussing.

The statistical analysis of the size of relics in the tracks in **Figure 6.9** are presented in **Table 6.2**. The relic size in the 3-track section (marked **A** in **Figure 6.9**) printed simultaneously was remarkably similar to a single track (marked **B** in **Figure 6.9**). Moreover, the data was consistent with the relic sizes in the tracks of the entire print (**Table 6.2**) which spans over ~156mm. The printing time involved was ~300s.

Table 6.2.Details of relic sizes in printed tracks

Parameter	Entire Print	3-Track Section	Single Track
Number counted	63020	7292	2227
Mean/μm	29.7	27.7	27.8
Standard deviation/μm	9.2	9.4	7.8

Further increasing the applied voltage produces much finer relics but made focussing of the droplets more difficult **(Figure 6.10)**. The obstacle this technique faces is the increasing amount of scatter with the decrease in droplet size. **Figure 6.10** also shows that at a higher applied voltage the droplets are attracted by the adjacent ground electrodes causing an overlap in the relics which could lead to short circuiting of the tracks.

Comparing **Figures 6.9** and **6.10** with our previous investigation carried out with a single needle (see **Figure 6.1**) the width of a printed line is greater in this investigation. This is because, in this study, there exists an interaction between adjacent electric fields due to the multiple electrode configuration and this affects the focusing of the sprays. This drawback can be improved by optimizing the distance between the needles and introducing appropriate shielding. The investigations carried out to understand the effect of applied voltage and flow rate on the print quality of individual characters and tracks illustrate the importance of a balance being achieved in both parameters. The idea of having a novel, cheap yet but superior ceramic processing technique in which the needles used are of a large diameter, yet capable of producing fine relics is appealing for manufactures in the printing industries. However, there exists a compromise - the finest relics bring with them a greater scatter which significantly reduce the print quality by distortion of the print.

Shielding the scatter needs to be addressed and resolved if this technique is to make a significant impact in industry. However, designing and incorporating some form of shielding in this process is seen to be a tall order as the process control is affected by the electric field which must not be disturbed so as to achieve stable cone-jet mode, in which the fine, near-monodisperse droplets and relics evolve.

6.2 Processing ceramic foams

6.2.1 Template

Scanning electron micrographs of the polyurethane template used is shown in **Figure 6.11** and shows that the mean cell size and the mean cell window size of the template are 751μm (standard deviation 27μm) and 552μm (standard deviation 34μm), respectively.

6.2.2 Electrospraying

With the applied voltage and flow rate set to 10kV and $1.67 \times 10^{-9} m^3 s^{-1}$, respectively, it was possible to spray the polyurethane template continuously in the stable cone-jet mode (see **Figure 6.12**). **Figure 6.13** shows a typical optical micrograph of the alumina relics produced in this way. Details of relic and droplet sizes, the former collected on a coated polyester substrate are given in **Table 6.3**, the latter being estimated using equations 3.5 and 3.6 in Chapter 3.

Table 6.3 Relic and droplet sizes from CS5 electrospraying to prepare ceramic foams

Relic sizes/μm	Number of relics	Droplet sizes/μm
0.8	131	0.5
1.0	119	0.6
1.8	95	1.0
2.4	87	1.3
3.2	76	1.8
4.9	81	2.7
7.1	79	3.9
10.5	78	5.8
15.6	61	8.6
18.1	56	10.0
21.9	61	12.0
35.5	43	19.5
40.9	38	22.5
43.5	33	23.9
47.5	30	26.1
50.2	28	27.6
63.5	21	34.9
97.1	9	53.4

6.2.2.1 Foam produced

By comparing the cell size of the polyurethane template and the size of droplets (**Table 6.3**) it is clear that the fine droplets generated had completely been absorbed/penetrated by individual struts as a central void is not observed in the sintered fractured struts (see **Figures 6.15** and **6.16**). The alumina foams produced had a volume porosity of 96% calculated using equations 2.6 and 2.7 in Chapter 2 (**Figure 6.14**). The apparent density of the alumina foam (ρ_a) was 174 kgm^{-3} and the theoretical density of alumina (ρ_s) was taken as 3987 kgm^{-3}. The production of fine droplets resulted in the replication of even the finest detail (as shown in **Figure 6.15**) of the template, and the struts did not contain a central hole or cracks (see **Figures 6.14 - 6.16**). It must be noted that these results required a spraying time of 3600s. Reduction of spraying time resulted in incomplete penetration of the struts of the polyurethane foam therefore causing voids in them. If the spraying time is increased >>3600s, the porosity of the foam reduces dramatically and it also hampers the replication of fine detail of the foam.

Electrosprayed templates were both assembled and subjected to deformation prior to pyrolysis, to produce twisted structures and artefacts, as illustrated in **Figures 6.17a** and **b**.

6.2.3 Soaking in slurry

In order to compare with foams prepared by electrospraying, the polyurethane template was soaked in suspension CS5 for 3600s and then heated to 900^{0}C. In addition to the presence of inherent defects generated by this method as discussed

in Chapter 2 (section 2.6), the foam also contained a large number of closed cell windows due to excess suspension in the template (see **Figure 6.18**).

In summary, the work described in this chapter has lead to two novel and specified innovations, namely ceramic electrostatic atomization printing and a processing of ceramic foams. The affect of applied voltage and flow rate on ceramic electrostatic atomization printing has been elucidated, however, scatter remains a significant problem. Ceramic foam without voids or cracks in the struts have been processed using a concentrated (21 vol.% solids) suspension.

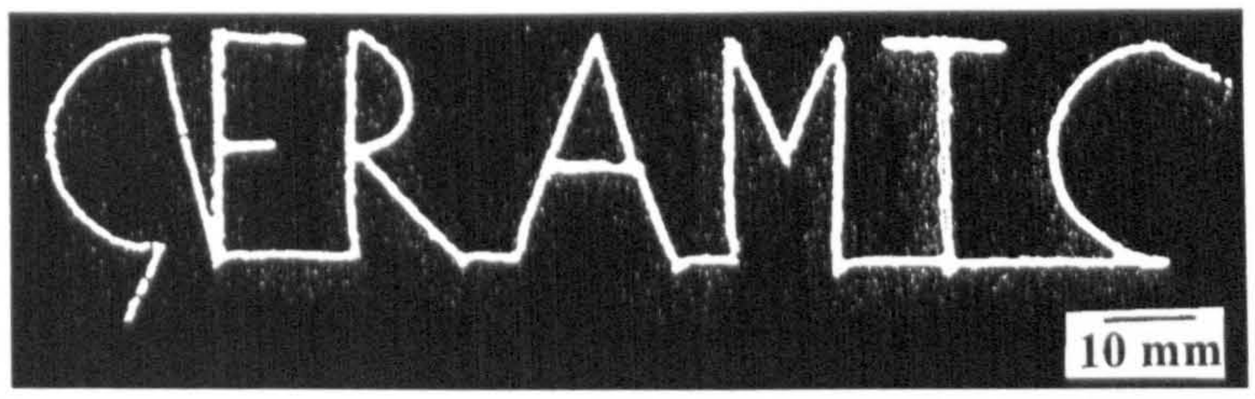

a

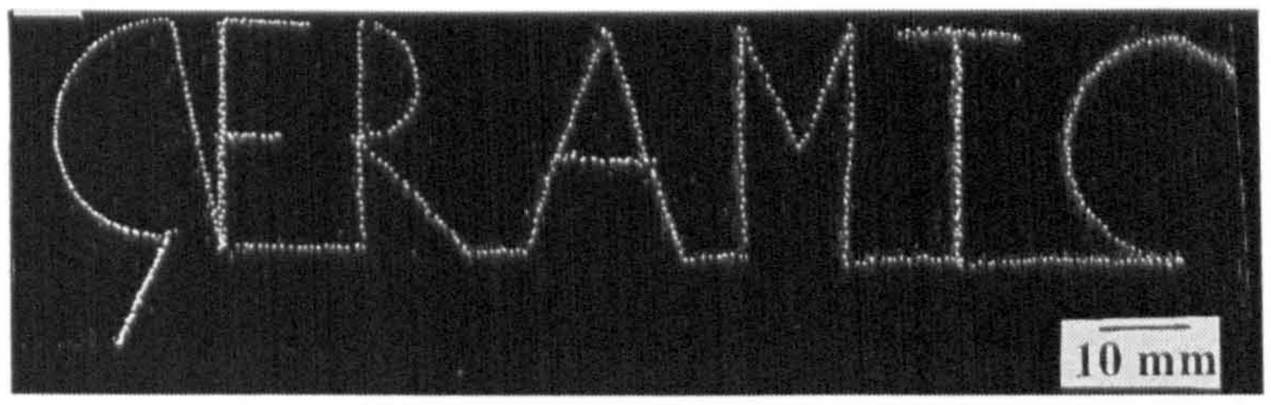

b

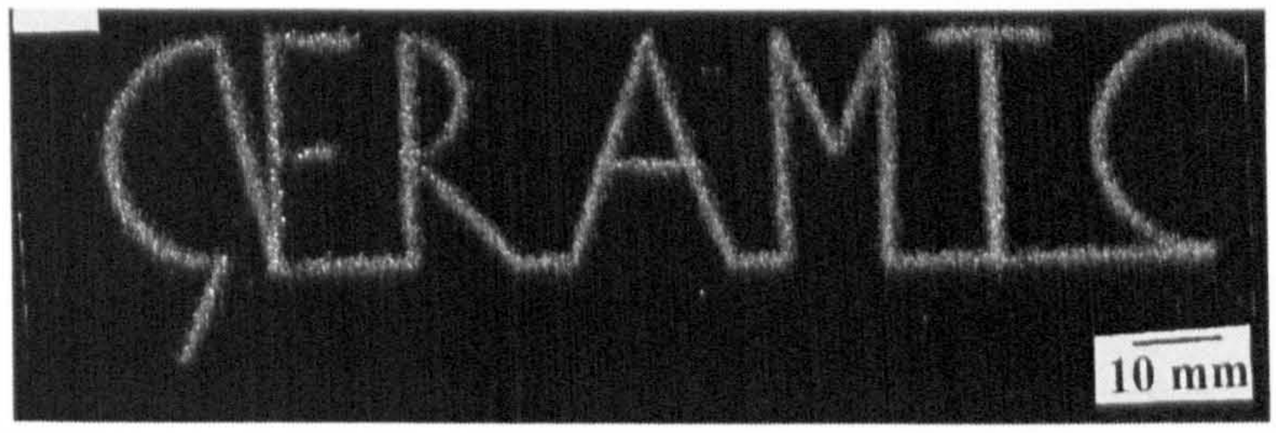

c

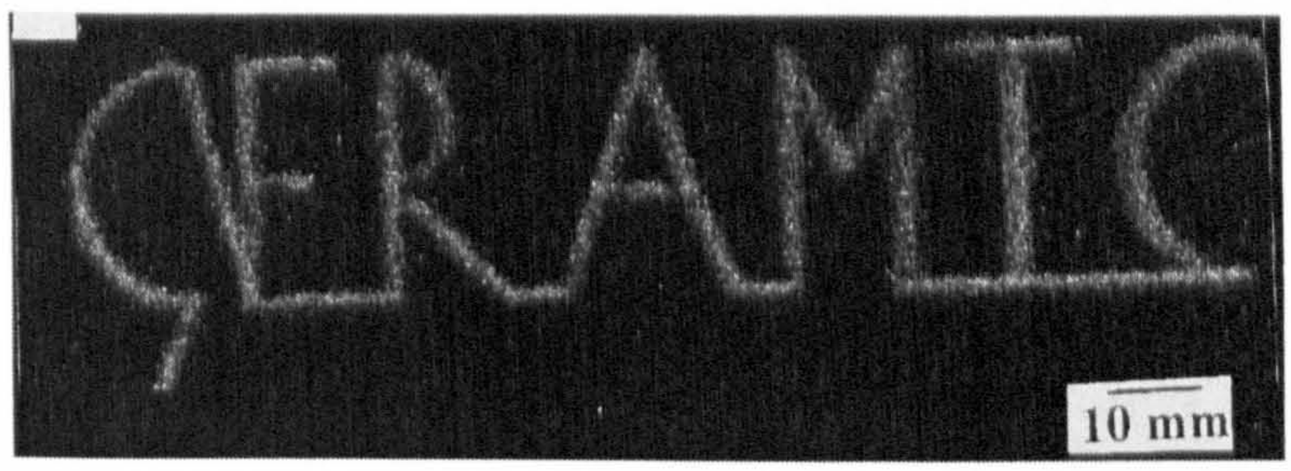

d

e

Figure 6.1 Printing performed at a constant flow rate of $1.67 \times 10^{-9} m^3 s^{-1}$ with increasing applied voltages (kV) of a)7, b)8, c)9 d)10 and e)11

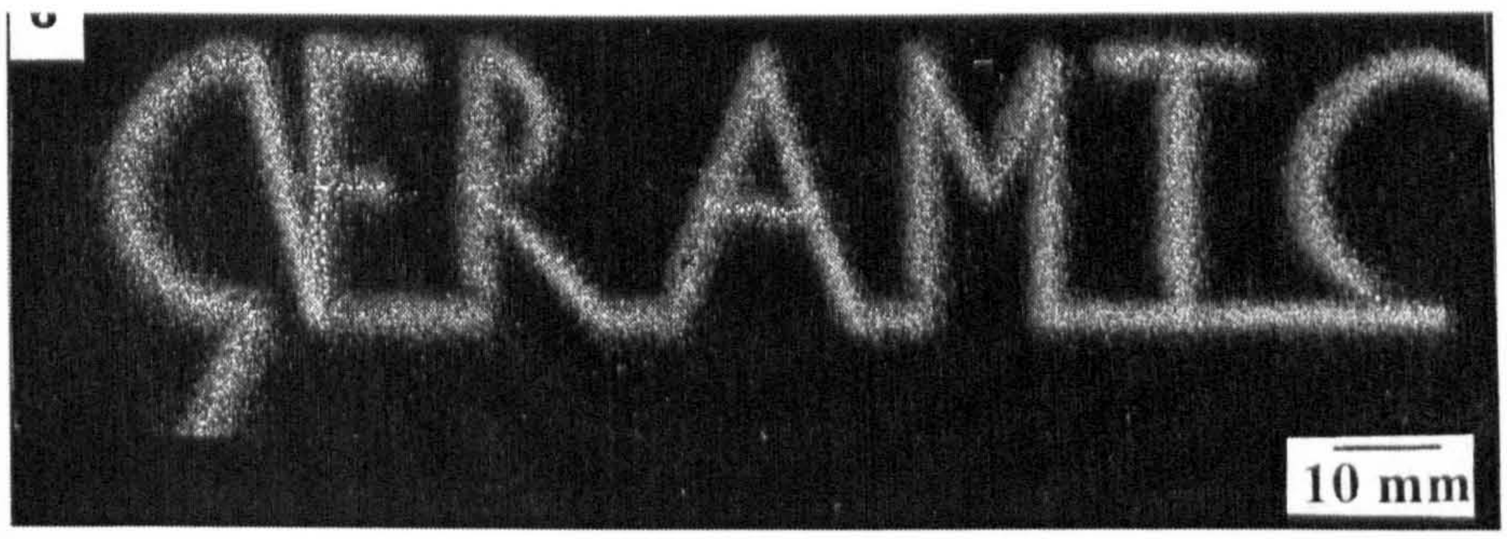

a

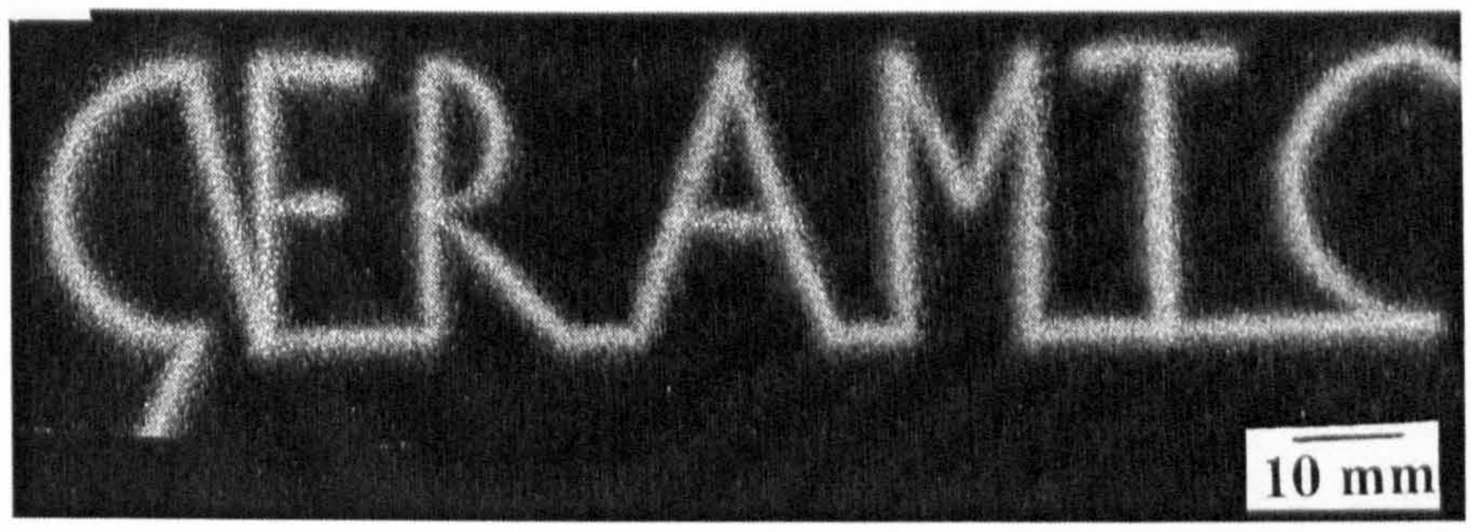

b

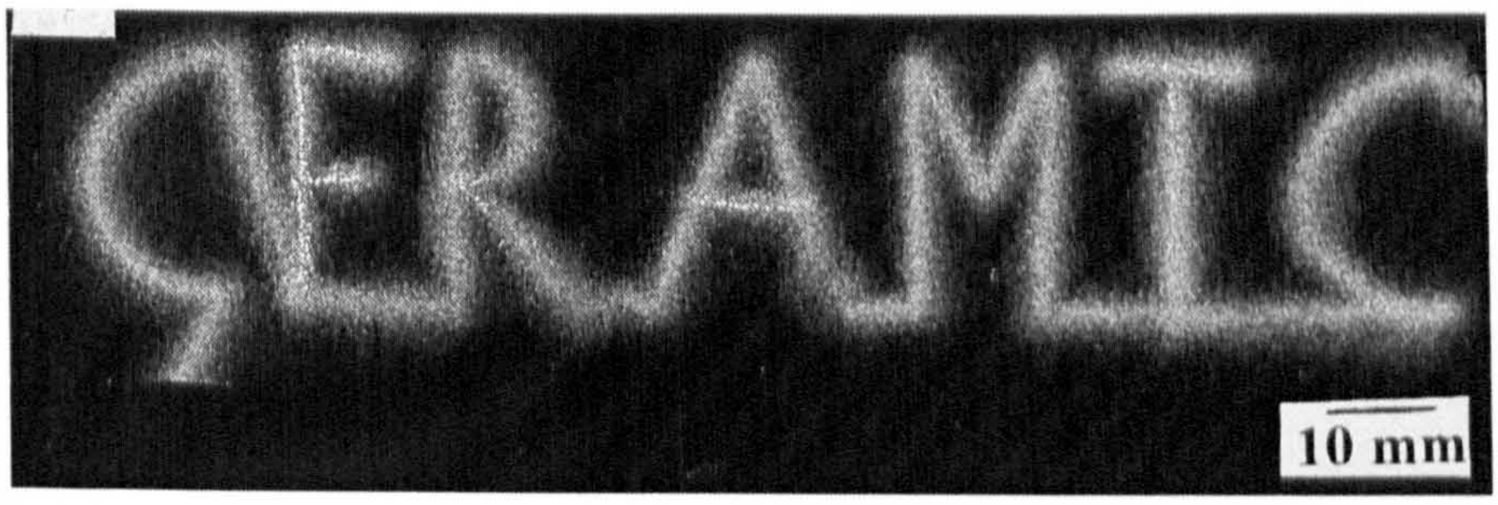

c

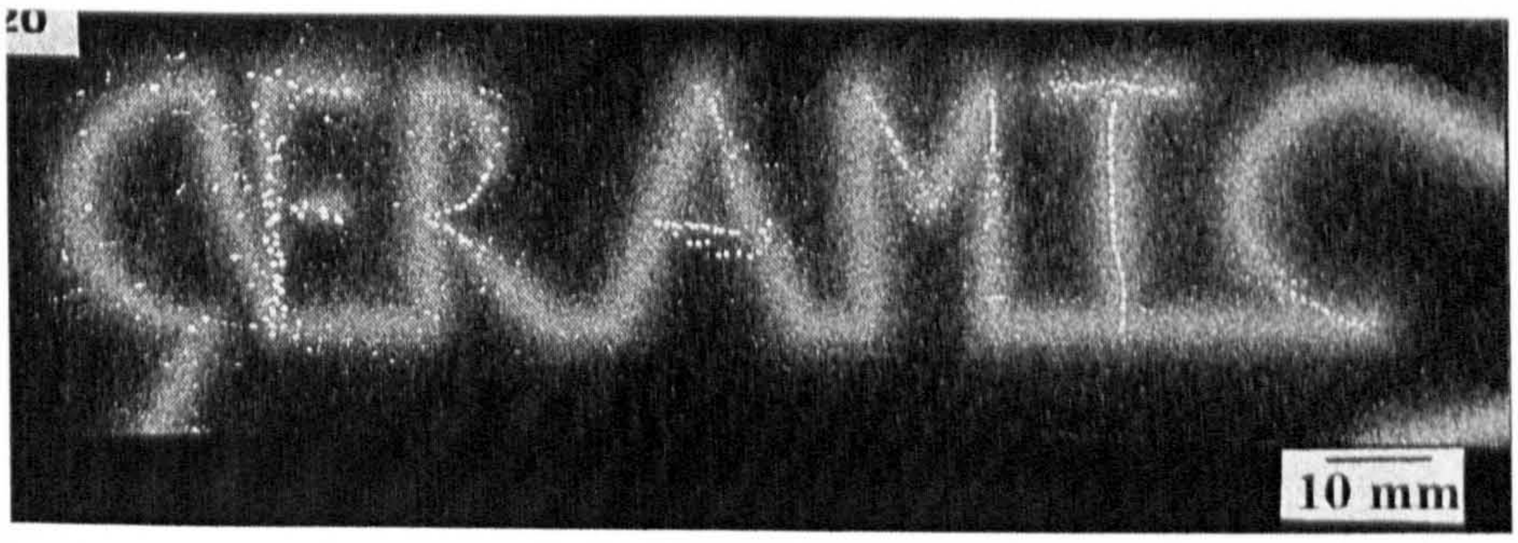

d

Figure 6.2 Printing performed at a constant applied voltage of 8kV and varying flow rates ($x10^{-9}m^3s^{-1}$) of a)4, b)6, c)8, and d)10

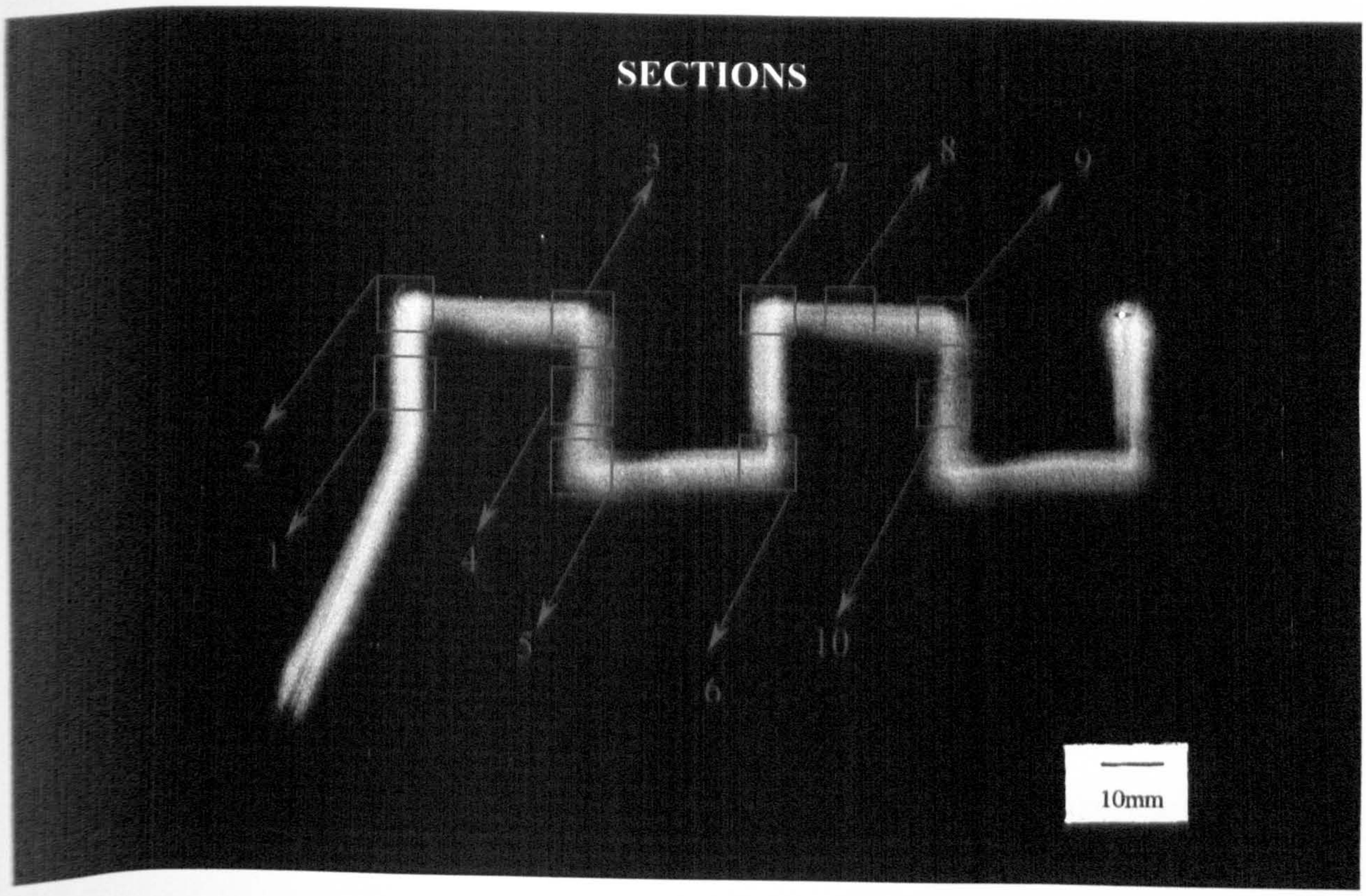

Figure 6.3 Printing tracks with CS5 at 7kV and $2.17 \times 10^{-12} m^3 s^{-1}$

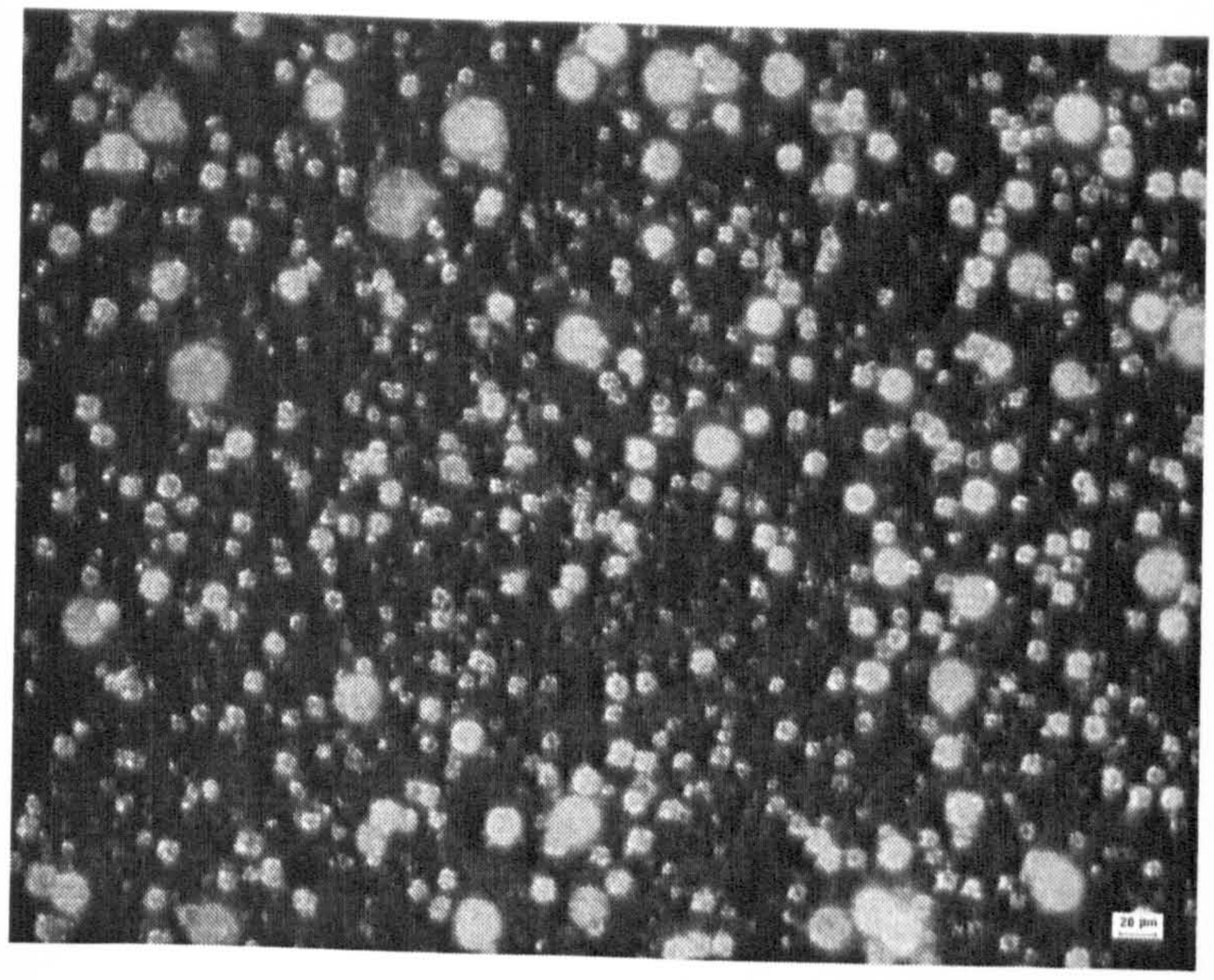

a

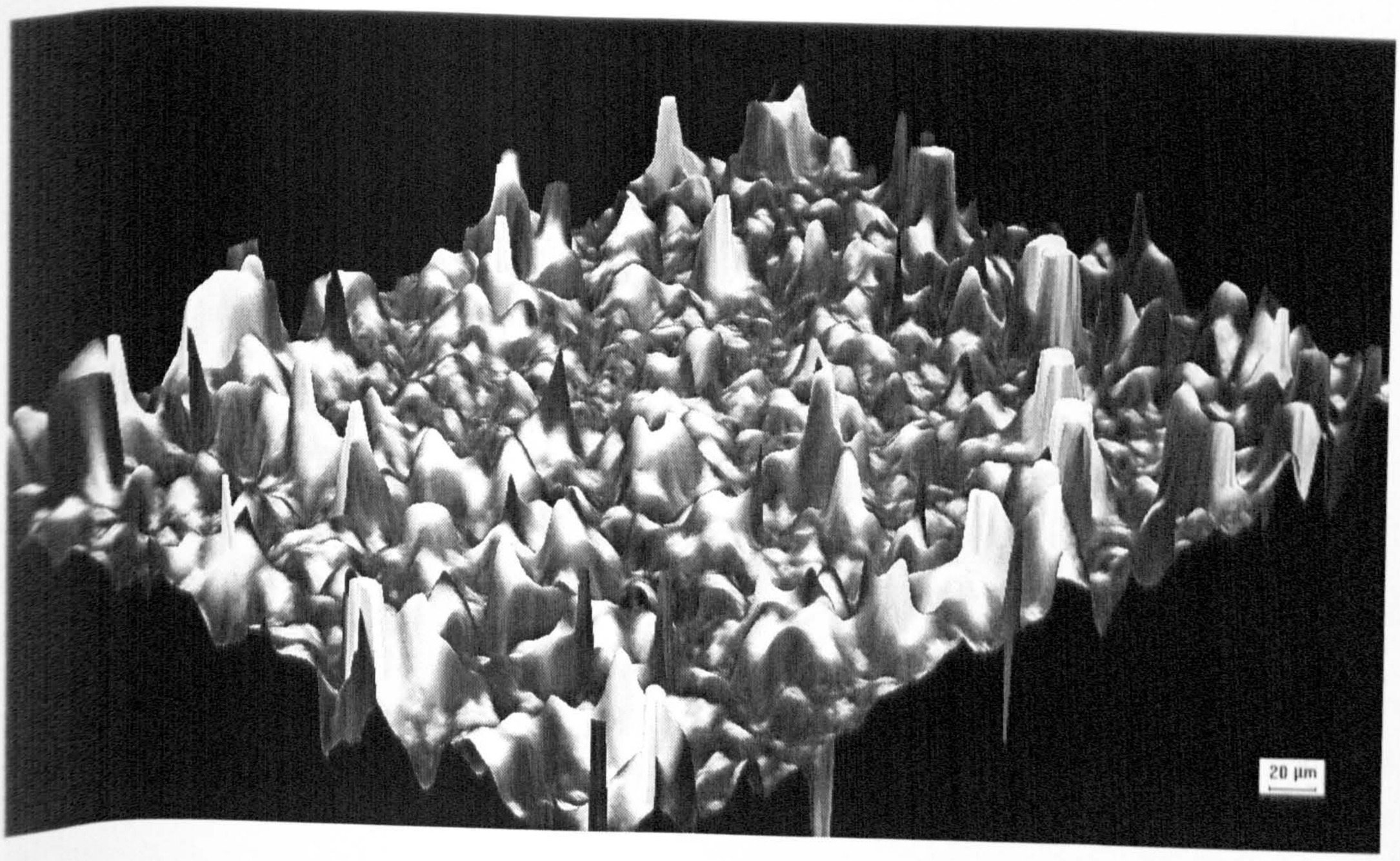

b

Figure 6.4 a) Optical micrograph and b) 3-D image of alumina relics present in "straight section" 4 in **Figure 6.3**

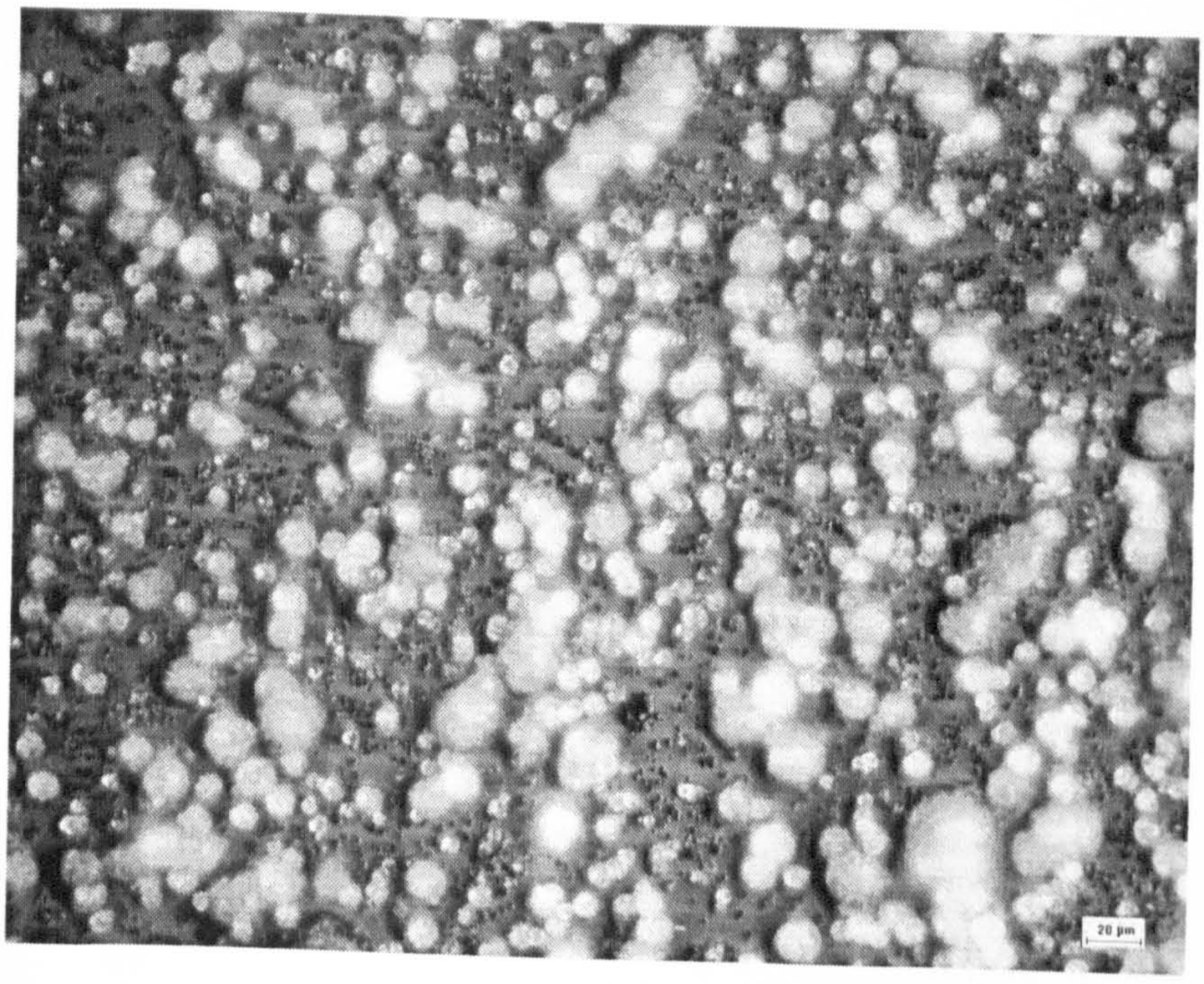

a

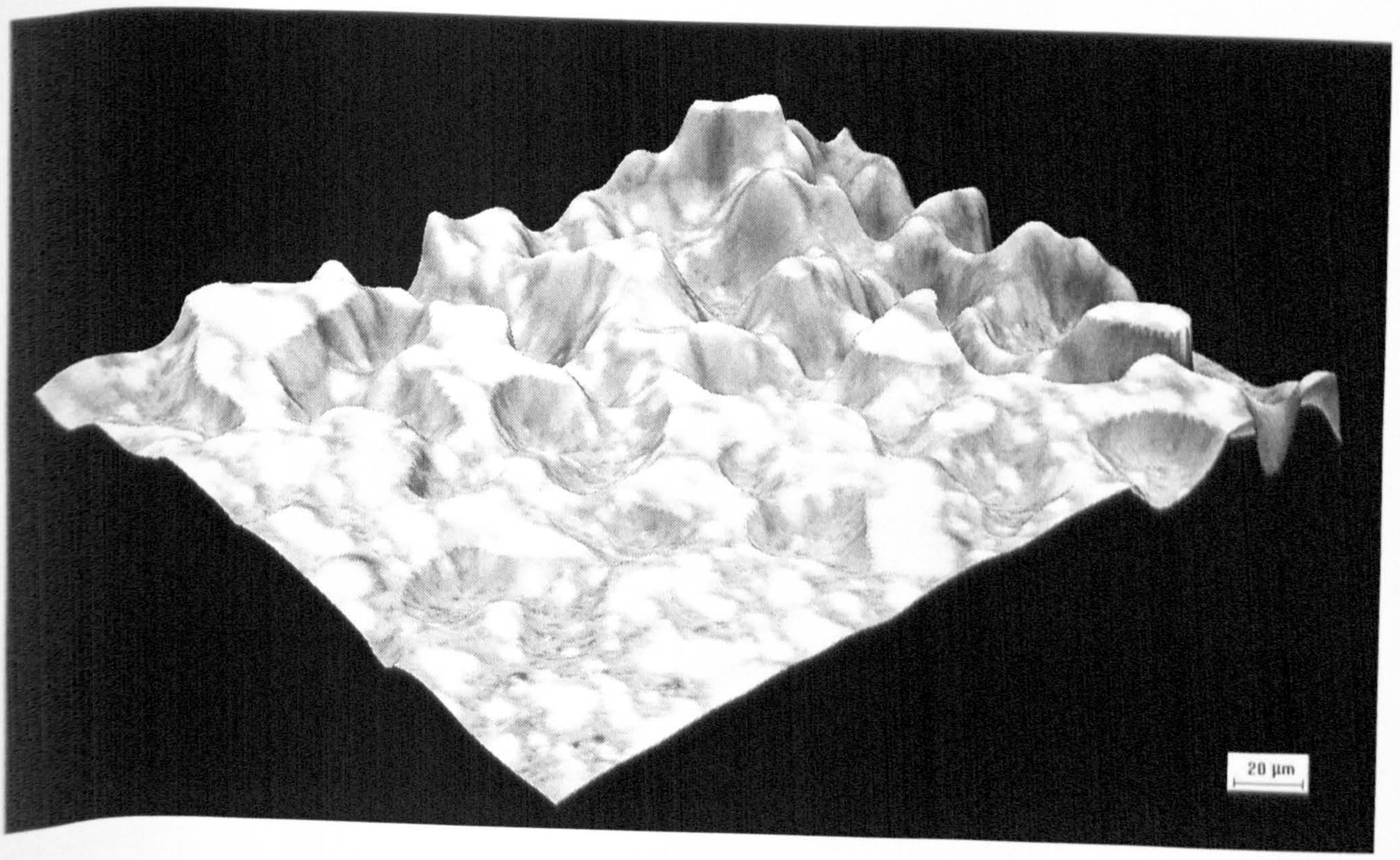

b

Figure 6.5 a) Optical micrograph and b) 3-D image of alumina relics present in "corner section" 7 in **Figure 6.3**

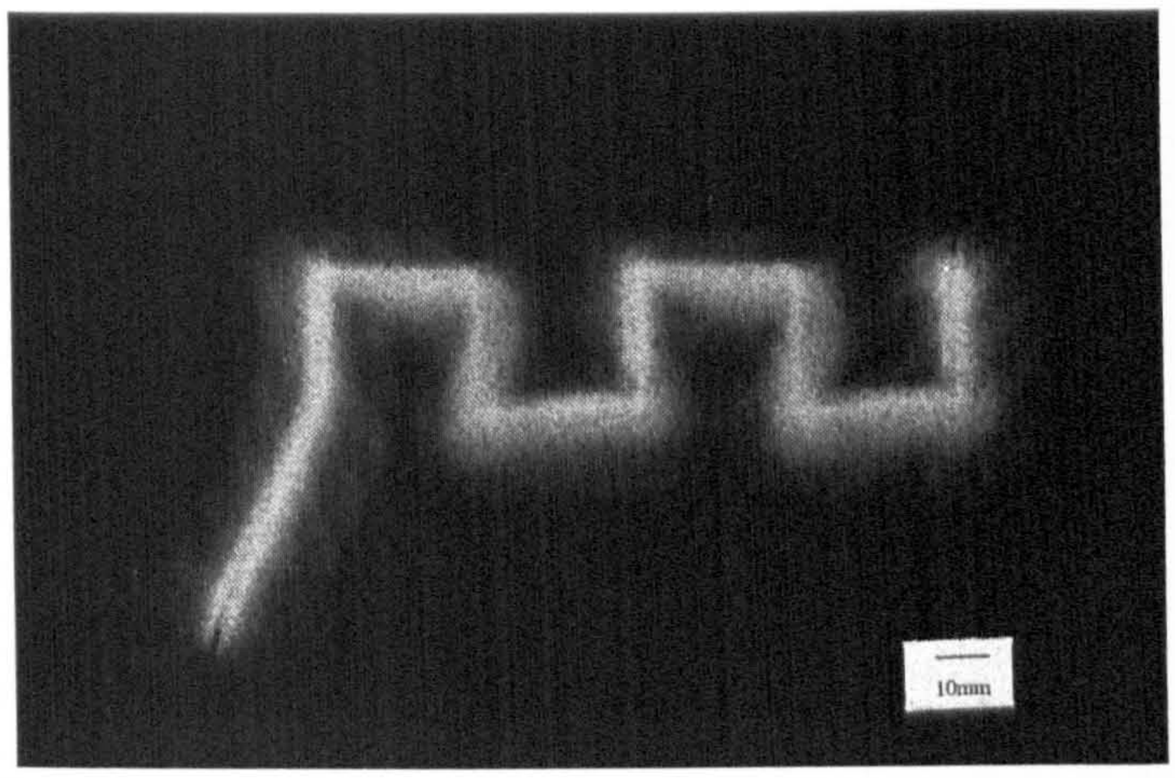

a

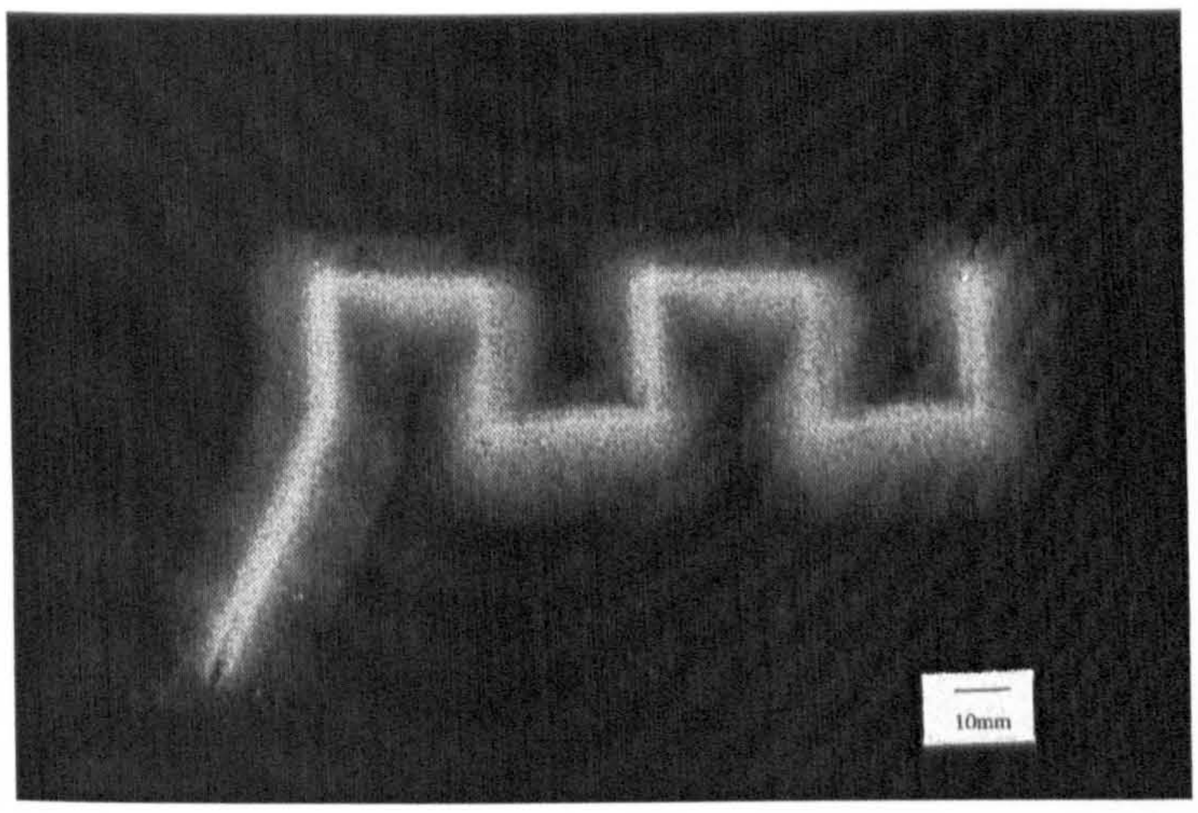

b

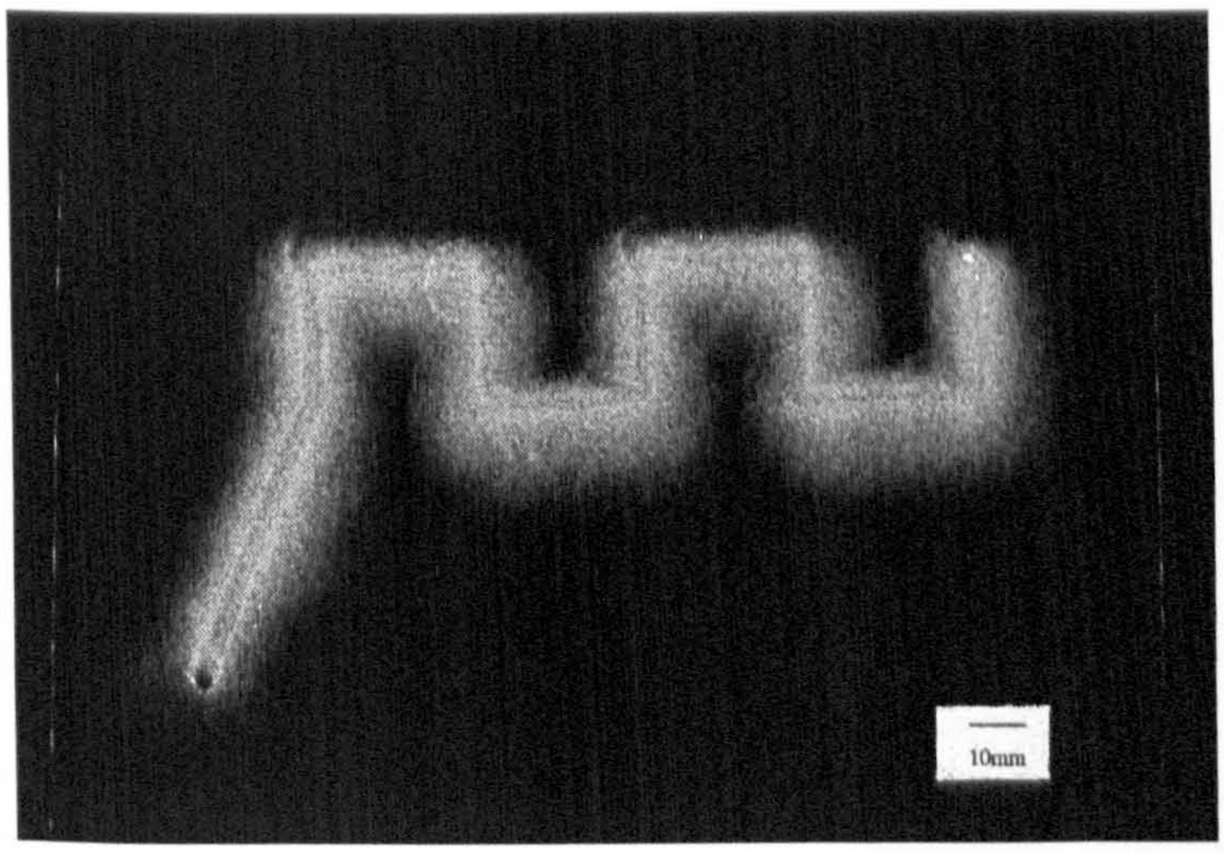

c

Figure 6.6 Tracks printed at a constant flow rate of $2.17 \times 10^{-12} m^3 s^{-1}$ with increasing applied voltage (kV) a)7.5, b)8 and c)8.4

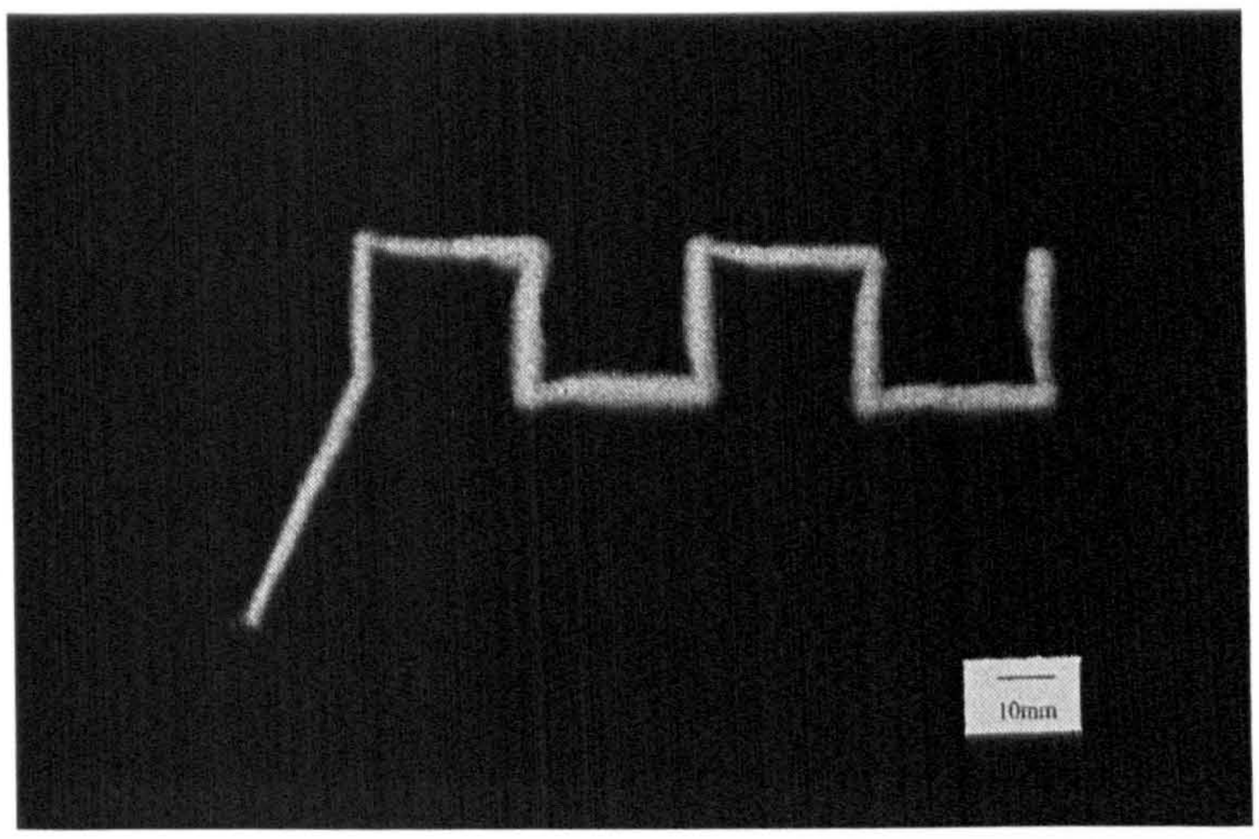

a

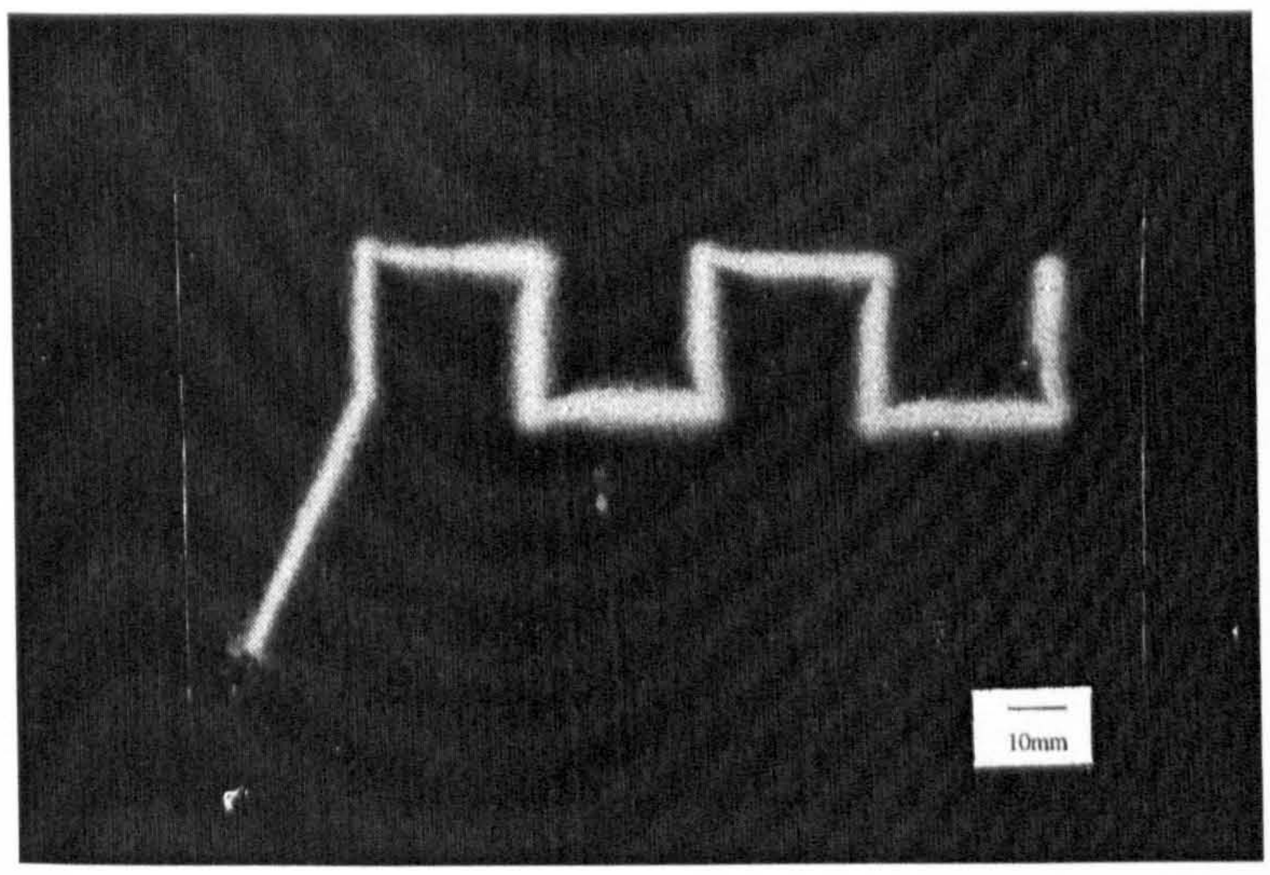

b

c

Figure 6.7 Printing of tracks at a constant applied voltage of 7kV with increasing flow rates ($x10^{-12}m^3s^{-1}$) of a)4, b)7 and c)10

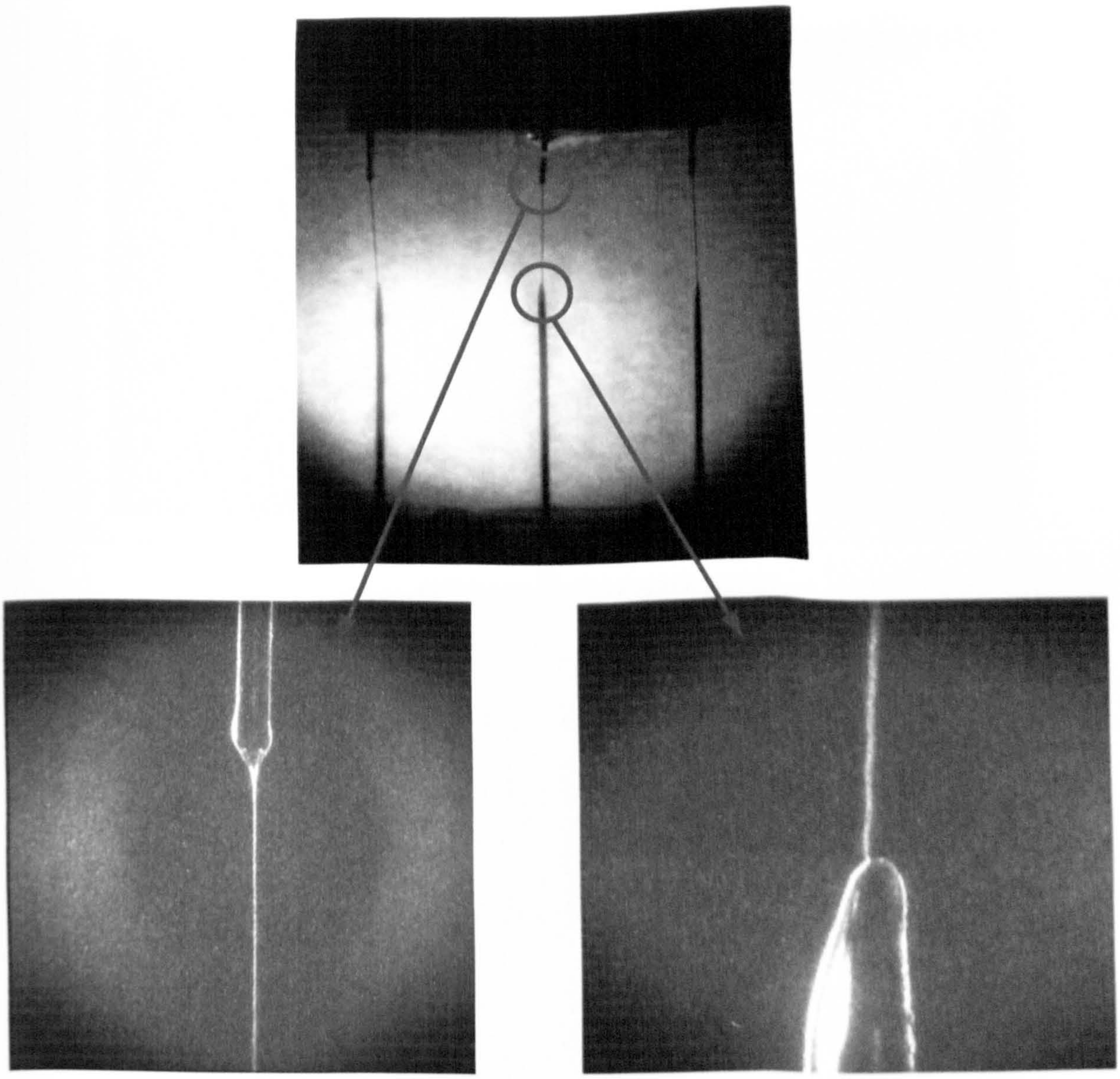

Figure 6.8 The 3-needle system used with cone-jet mode electrostatic atomization at the needles, and focussing of the jet from each needle to the ground electrode at an applied voltage of 10kV and flow rate of $1.67 \times 10^{-9} m^3 s^{-1}$

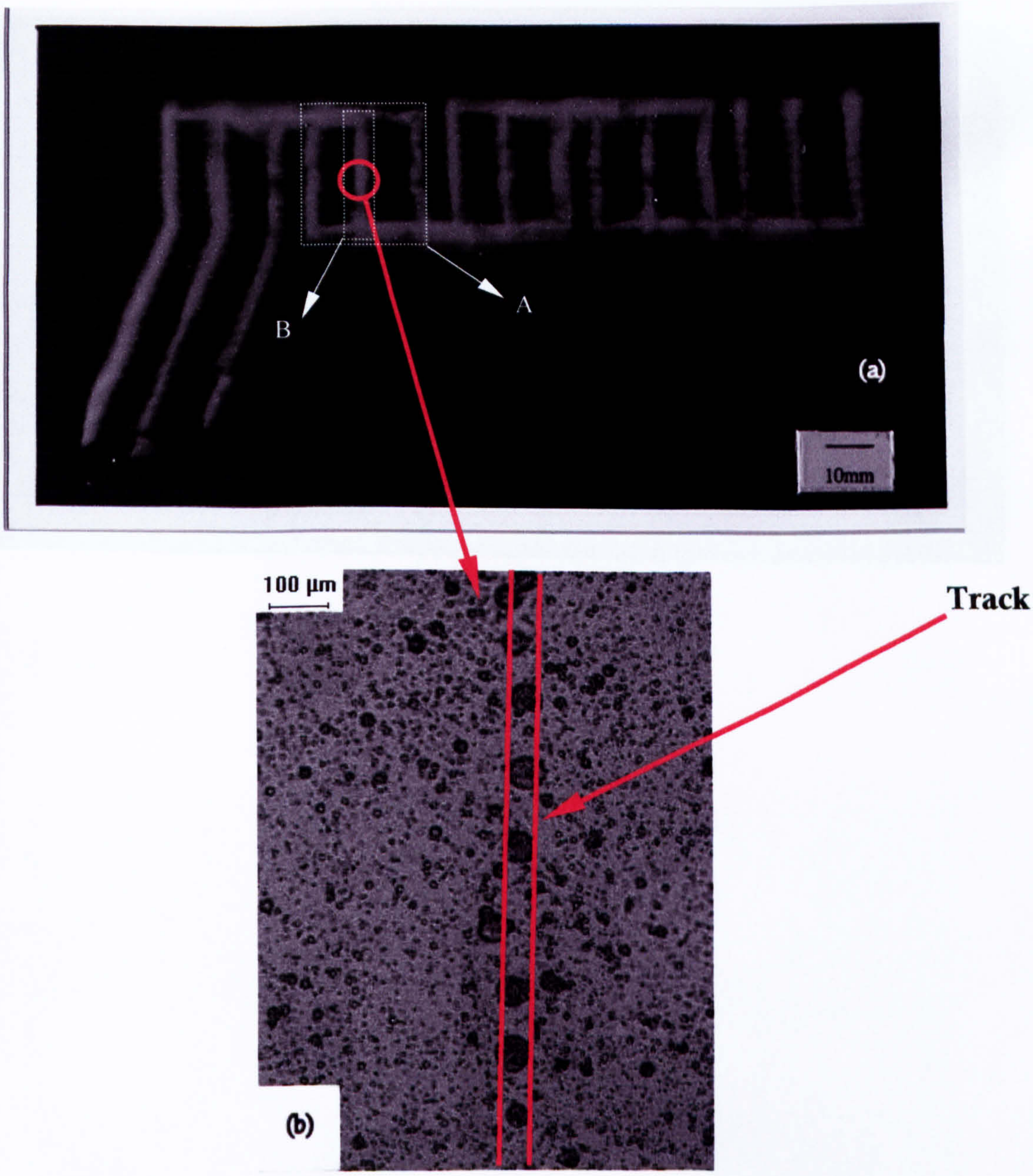

Figure 6.9 a) Track printed at an applied voltage of 10kV and flow rate of $1.67 \times 10^{-9} m^3 s^{-1}$ and b) optical micrograph of relics at position indicated in a)

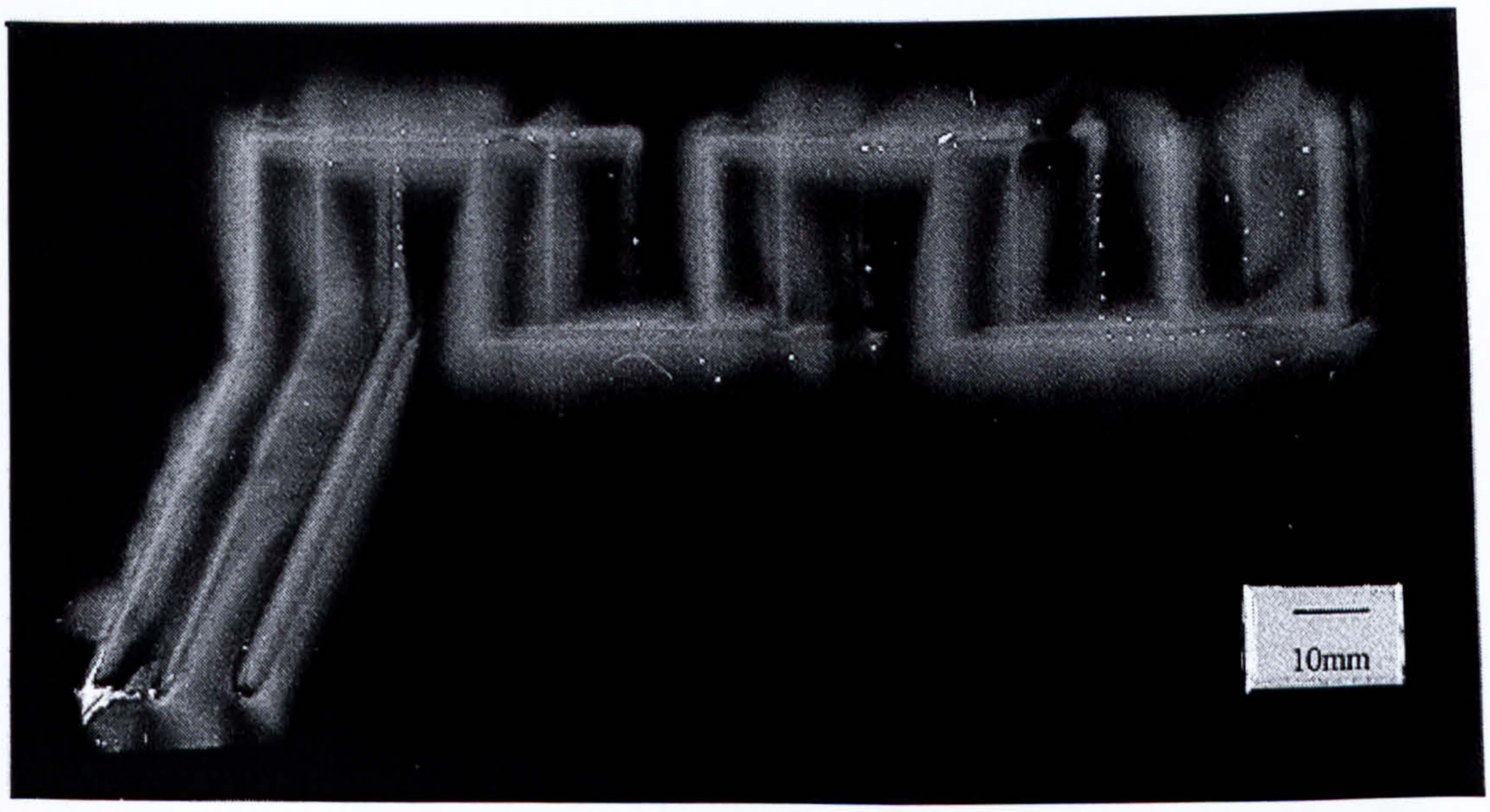

Figure 6.10 Multi-track printed at an increased voltage of 12kV with flow rate set at $1.67 \times 10^{-9} m^3 s^{-1}$

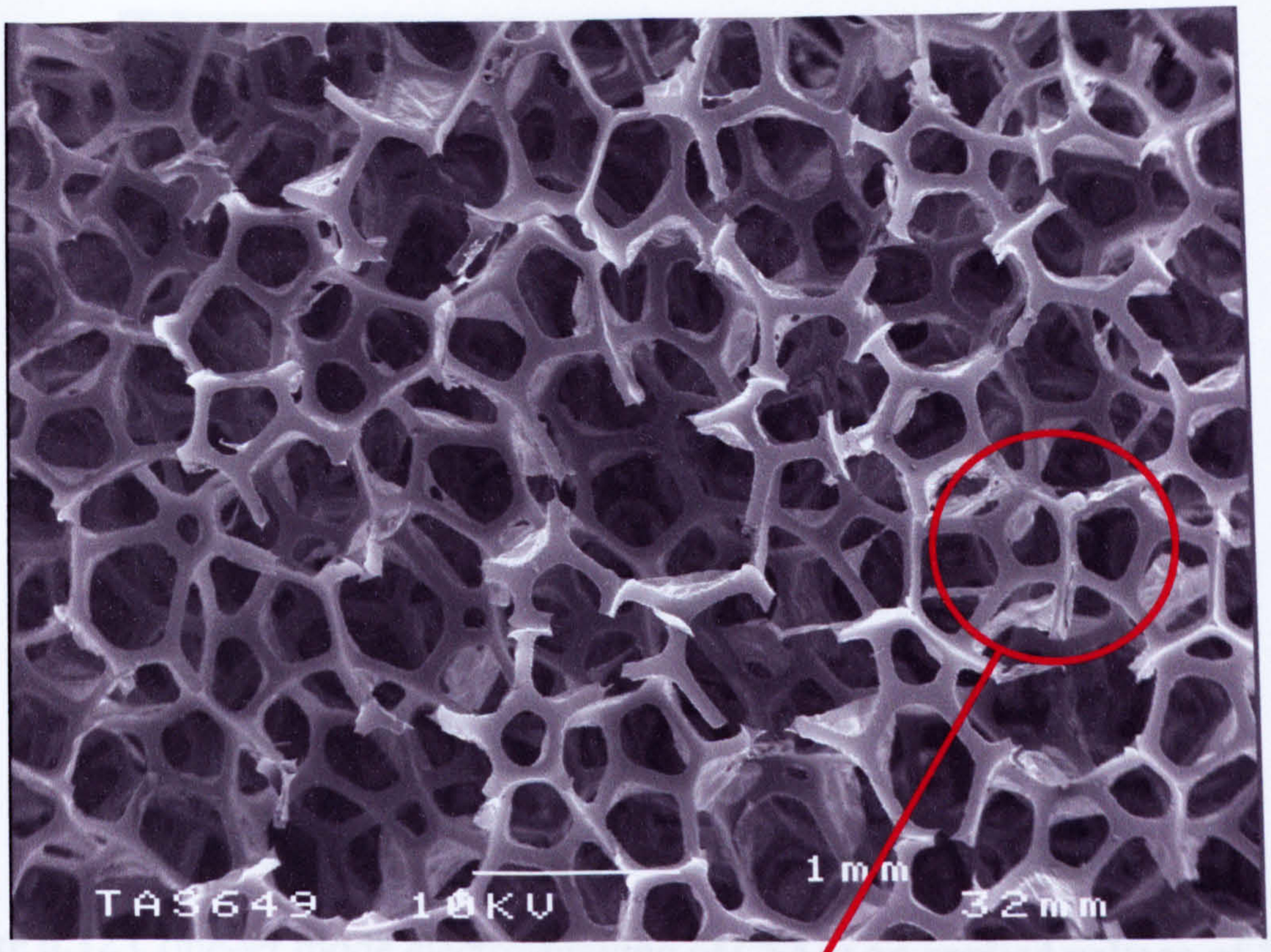

a

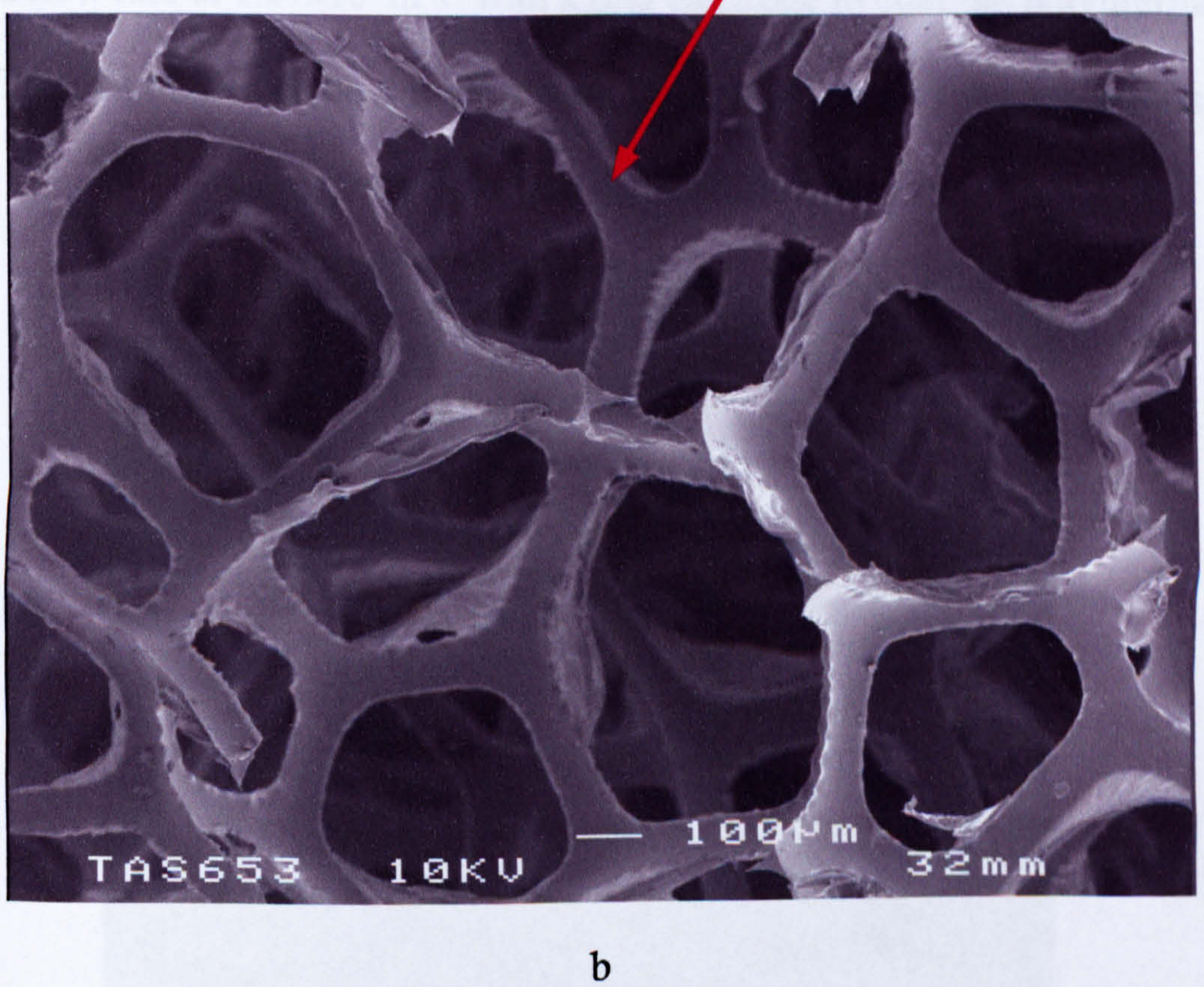

b

Figure 6.11 Scanning electron micrographs of the polyurethane foam used showing a) open-cell structure and b) struts

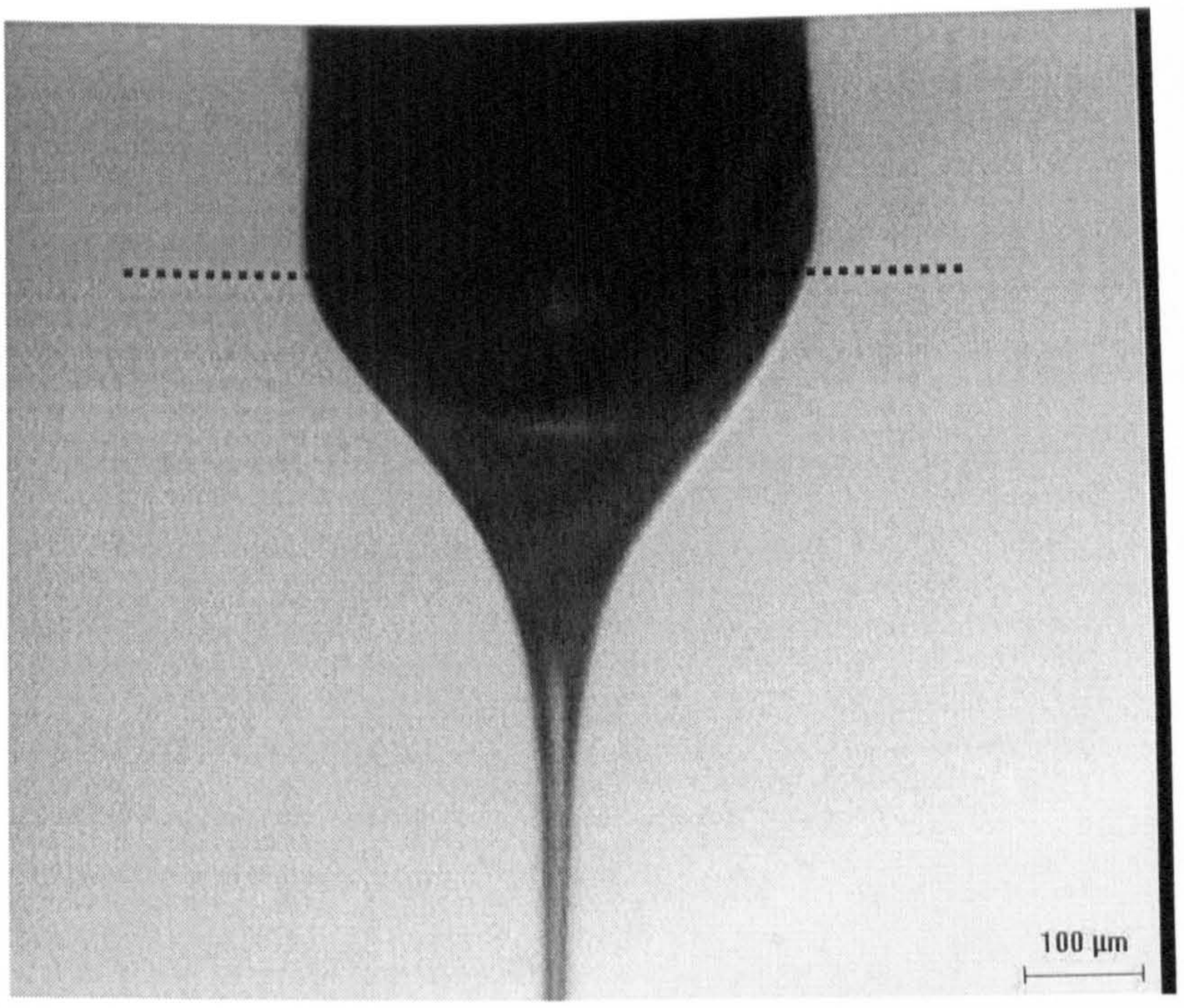

Figure 6.12 Cone-jet mode electrospraying of CS5 at an applied voltage of 10kV and a flow rate of $1.67 \times 10^{-9} m^3 s^{-1}$ with a ring electrode to coat the polyurethane foam. The exit of the needle is indicated by the dotted line and the conditions used are given in section 6.6.2 of Chapter 6.

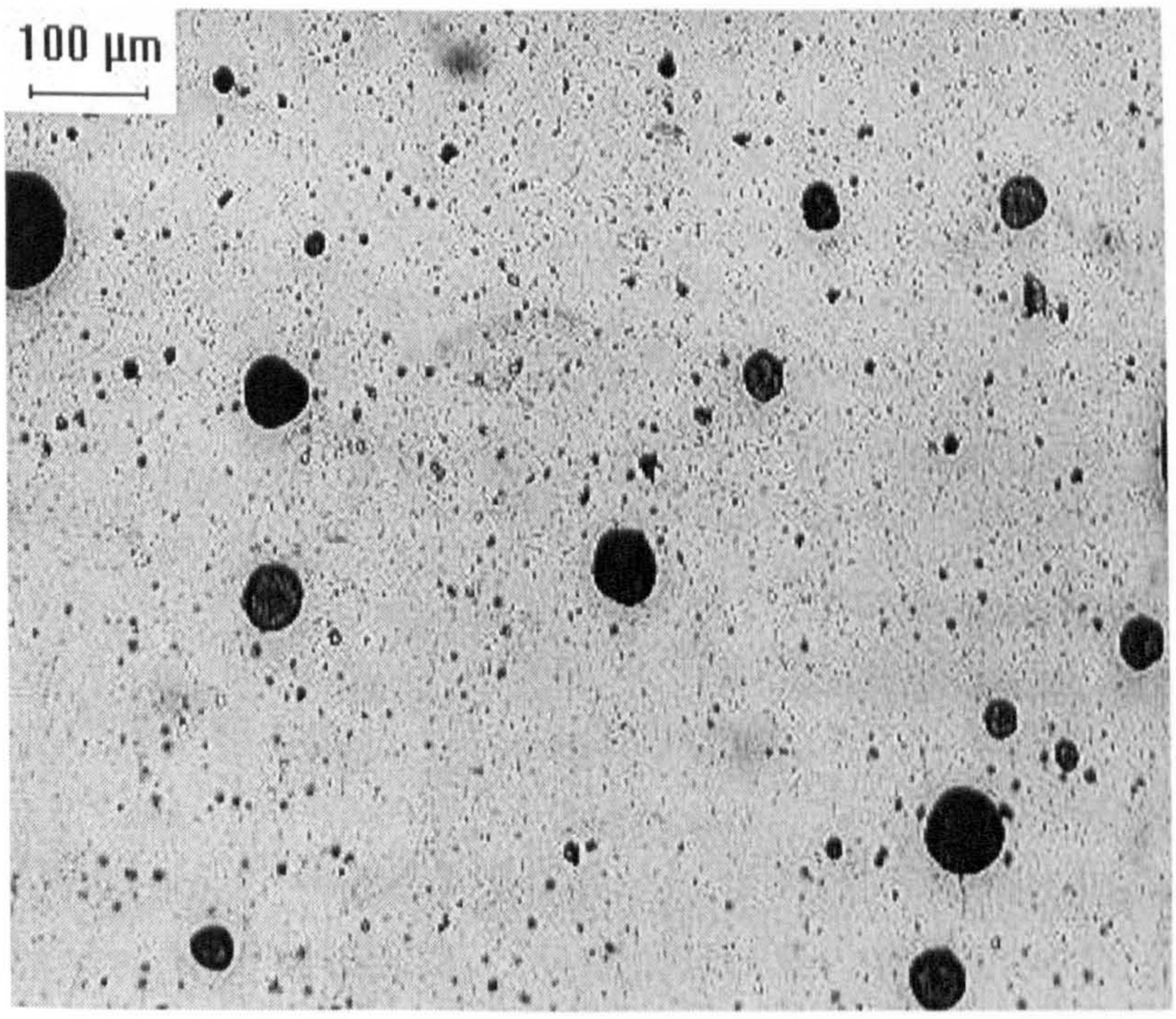

Figure 6.13 Optical micrograph of the alumina relics obtained by cone-jet mode electrostatic atomization of CS5 with a ring electrode as shown in **Figure 6.12**.

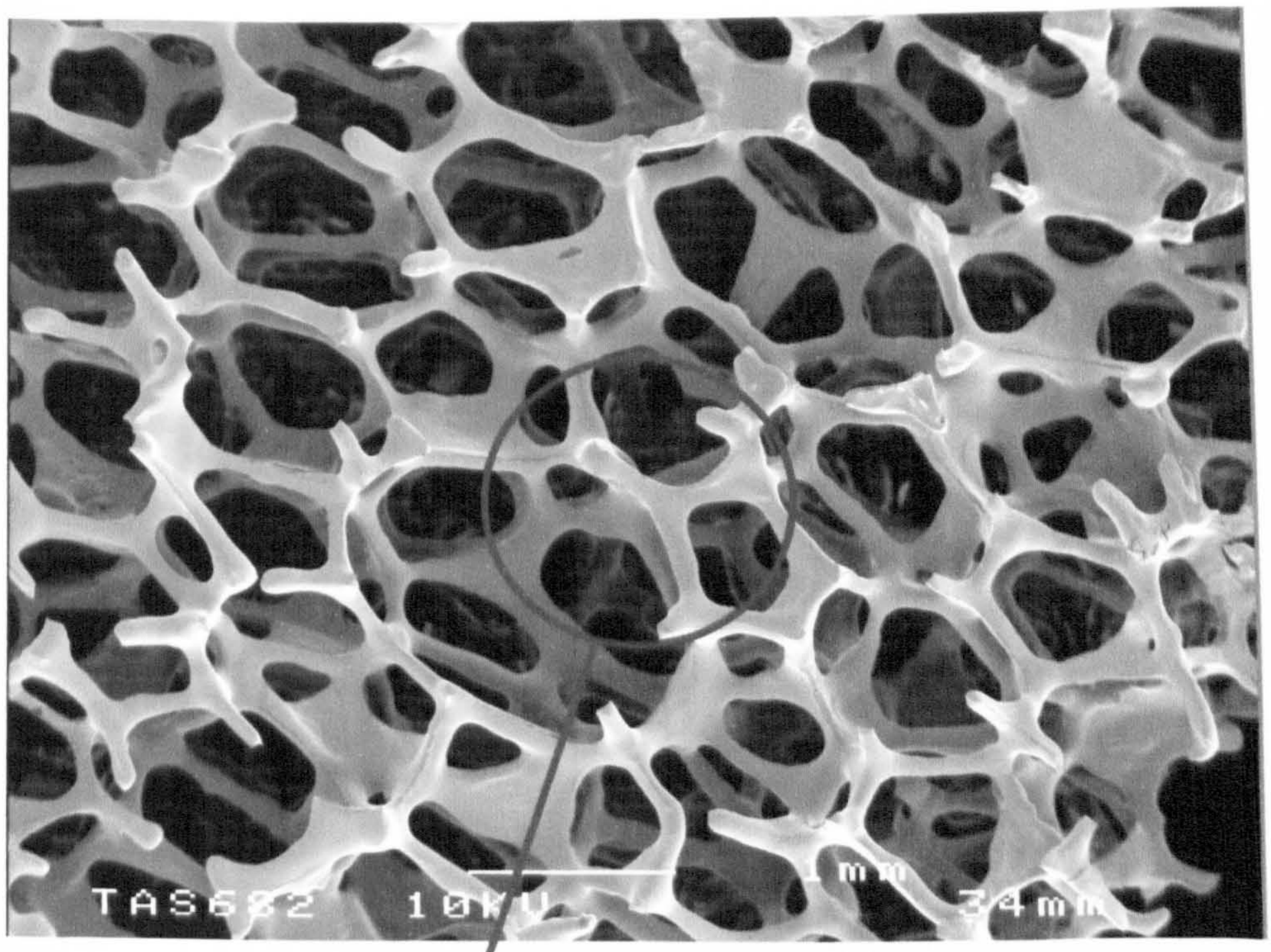

a

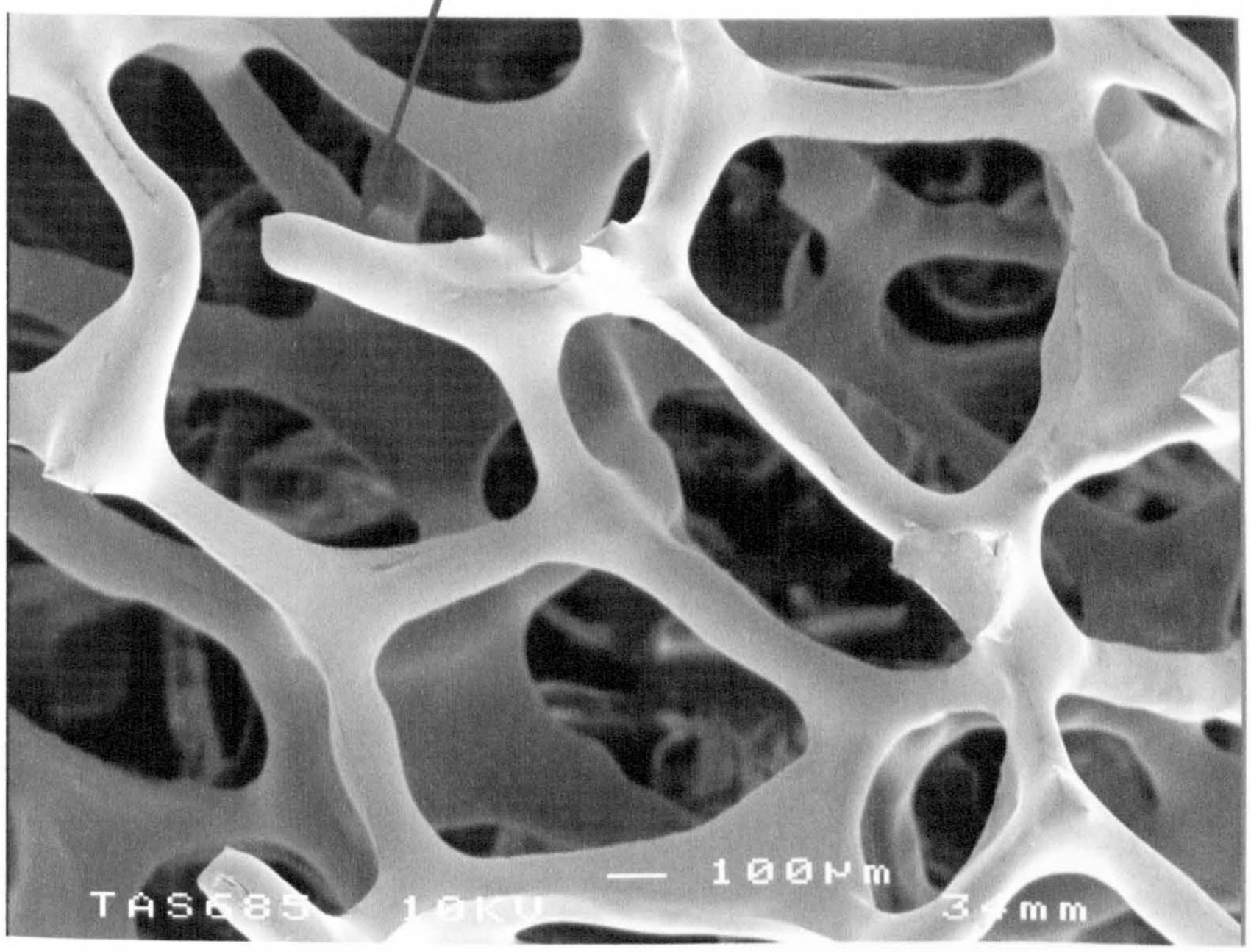

b

Figure 6.14 Structure of alumina foam produced by pyrolyzing electrosprayed polyurethane foam: a) open-cell structure and b) struts

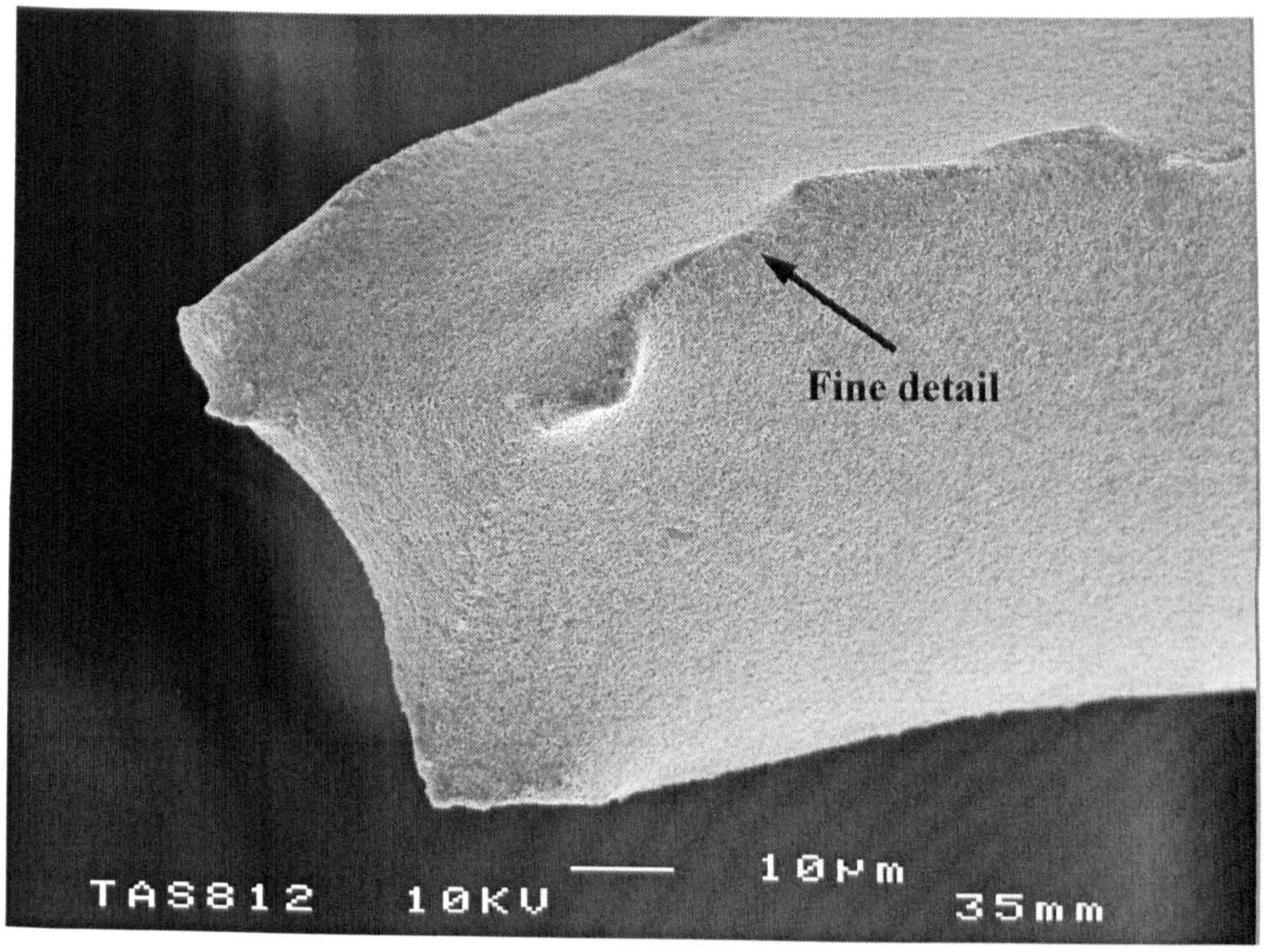

Figure 6.15 Image of a strut in the electrosprayed alumina foam showing fine detail

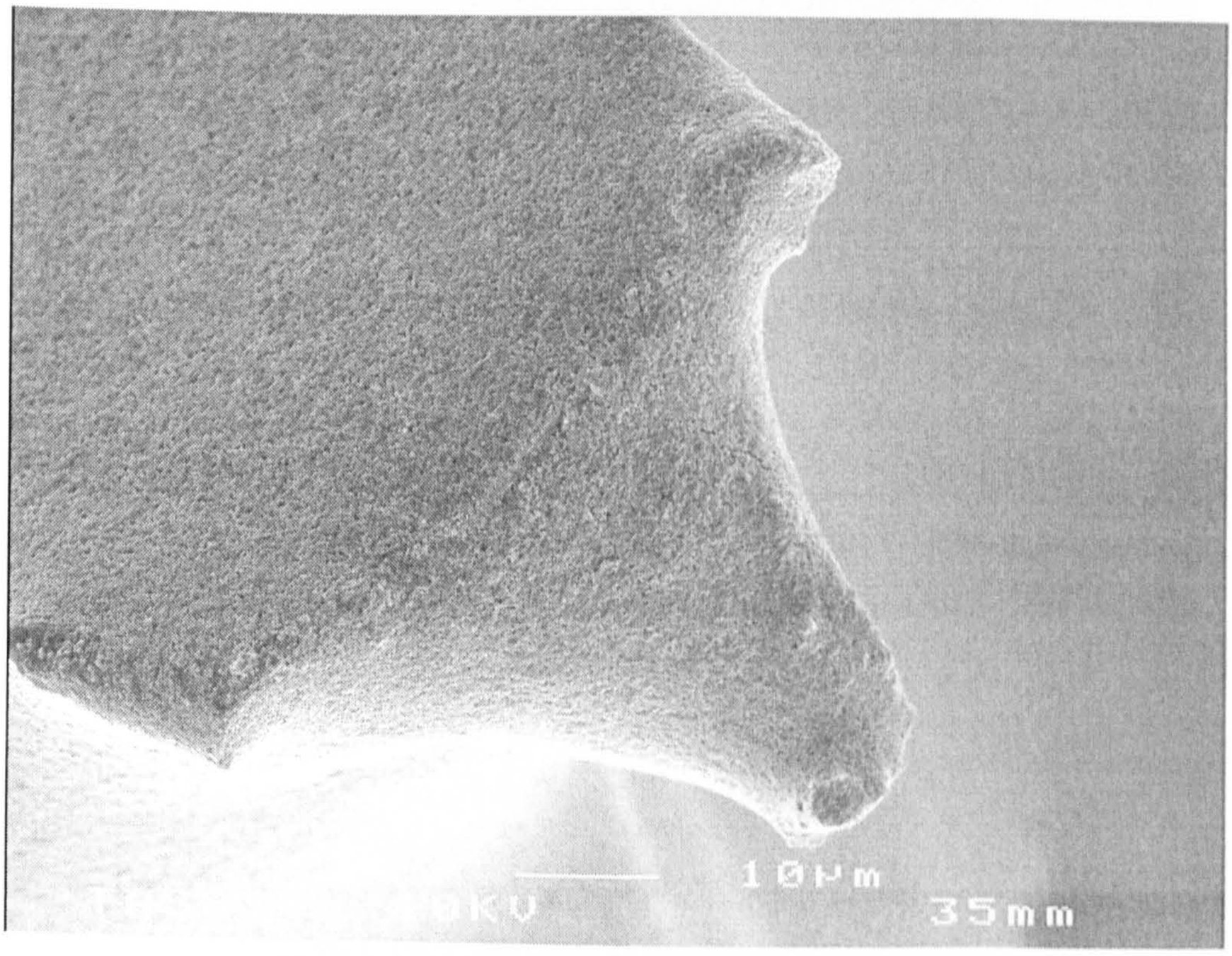

Figure 6.16 Fractured strut cross-section of alumina foam produced using the electrospraying route. It does not show a central void.

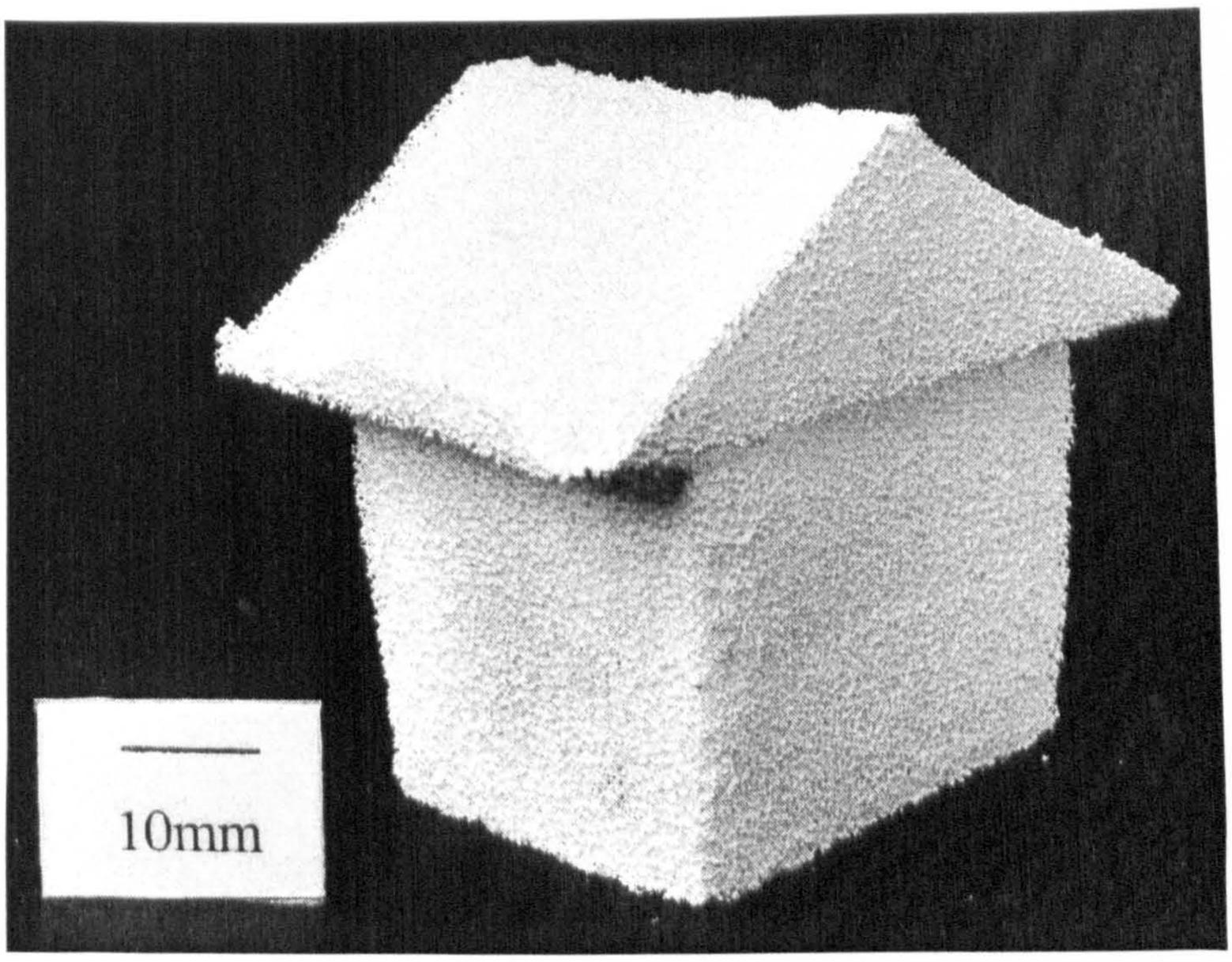

a

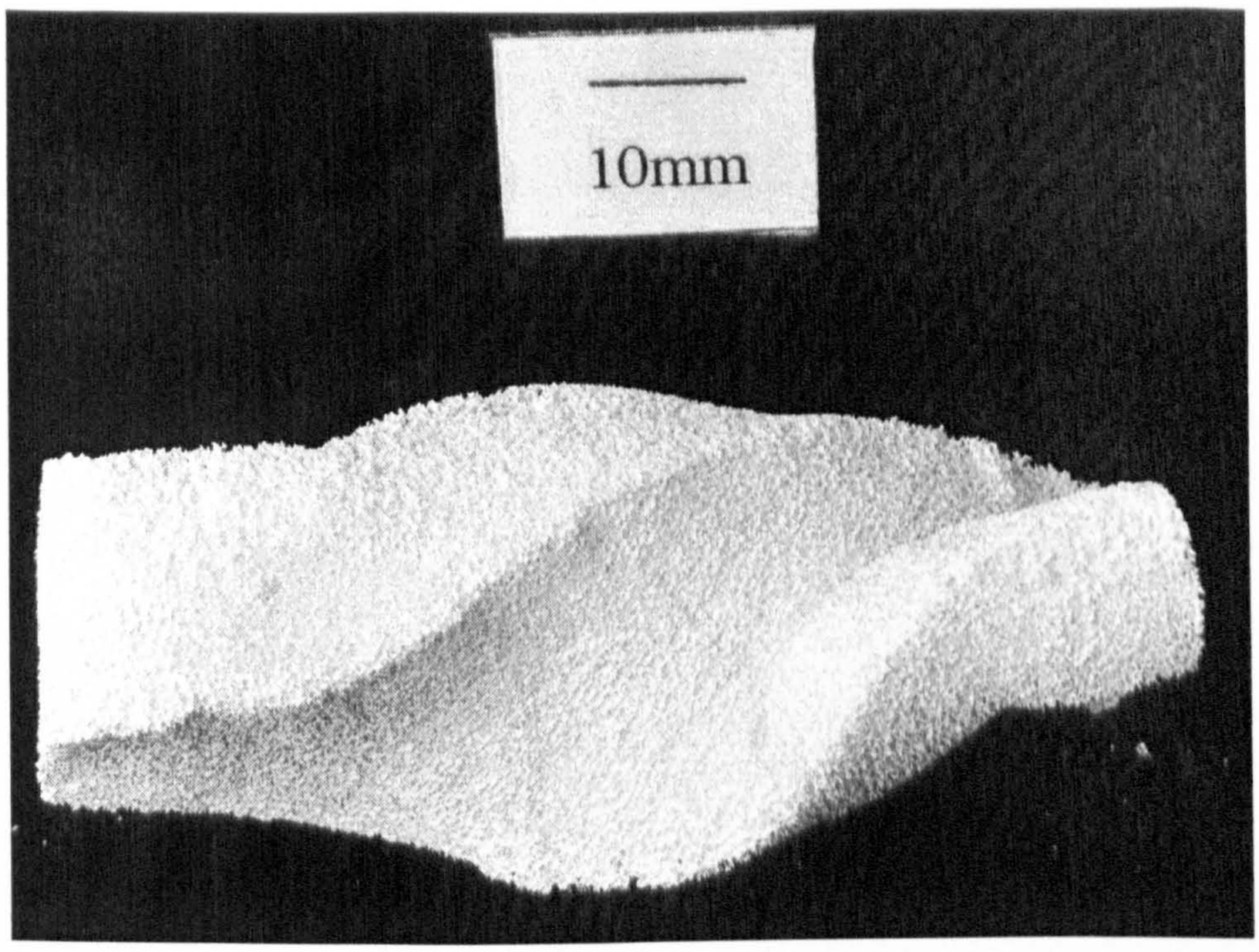

b

Figure 6.17 a) A hollow porous house produced by assembling electrosprayed alumina foam subsequently pyrolyzed at 1200^0C and b) a porous twisted alumina artefact produced by deformation, electrospraying and subsequent pyrolysis at 1200^0C

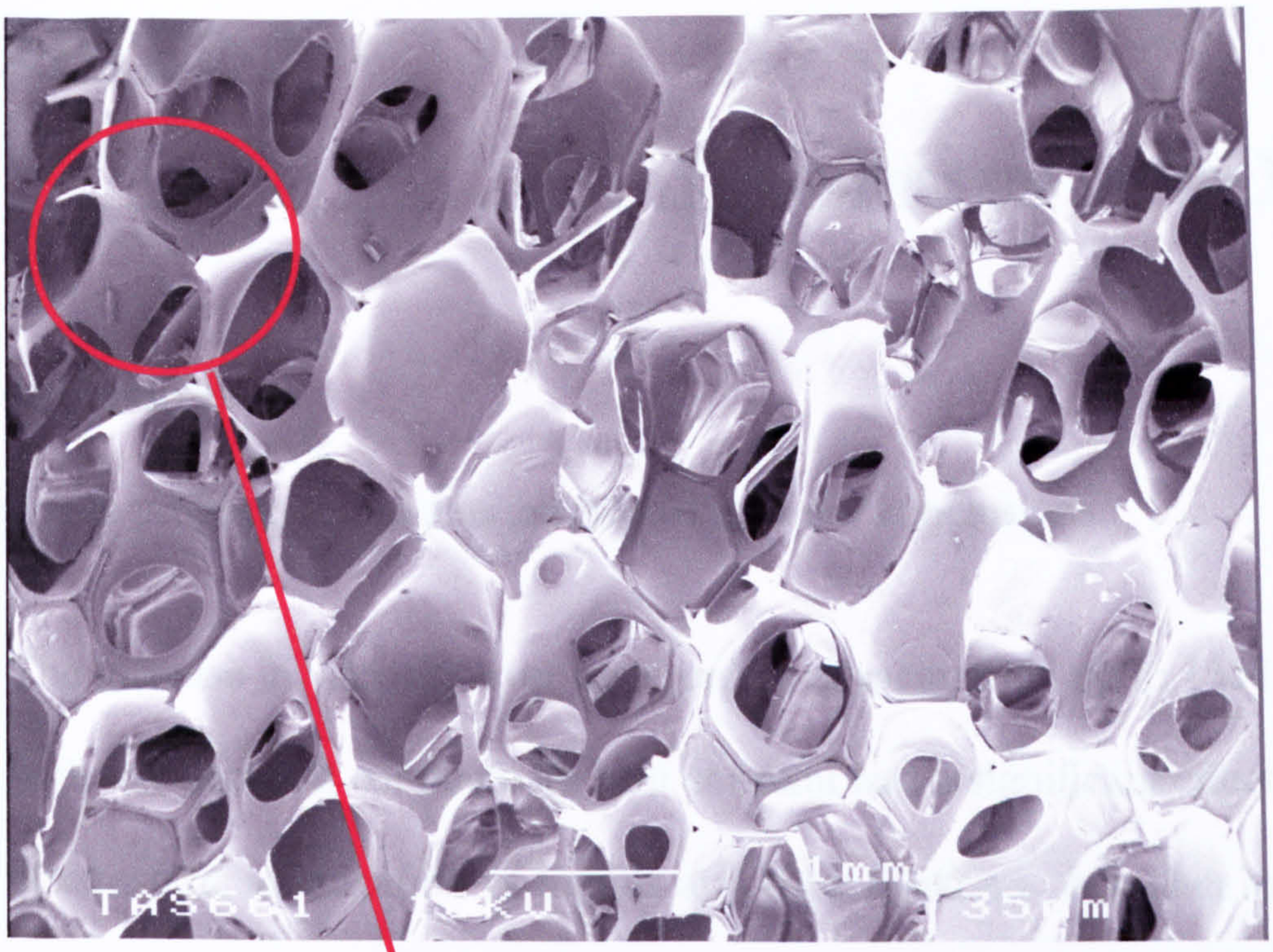

a

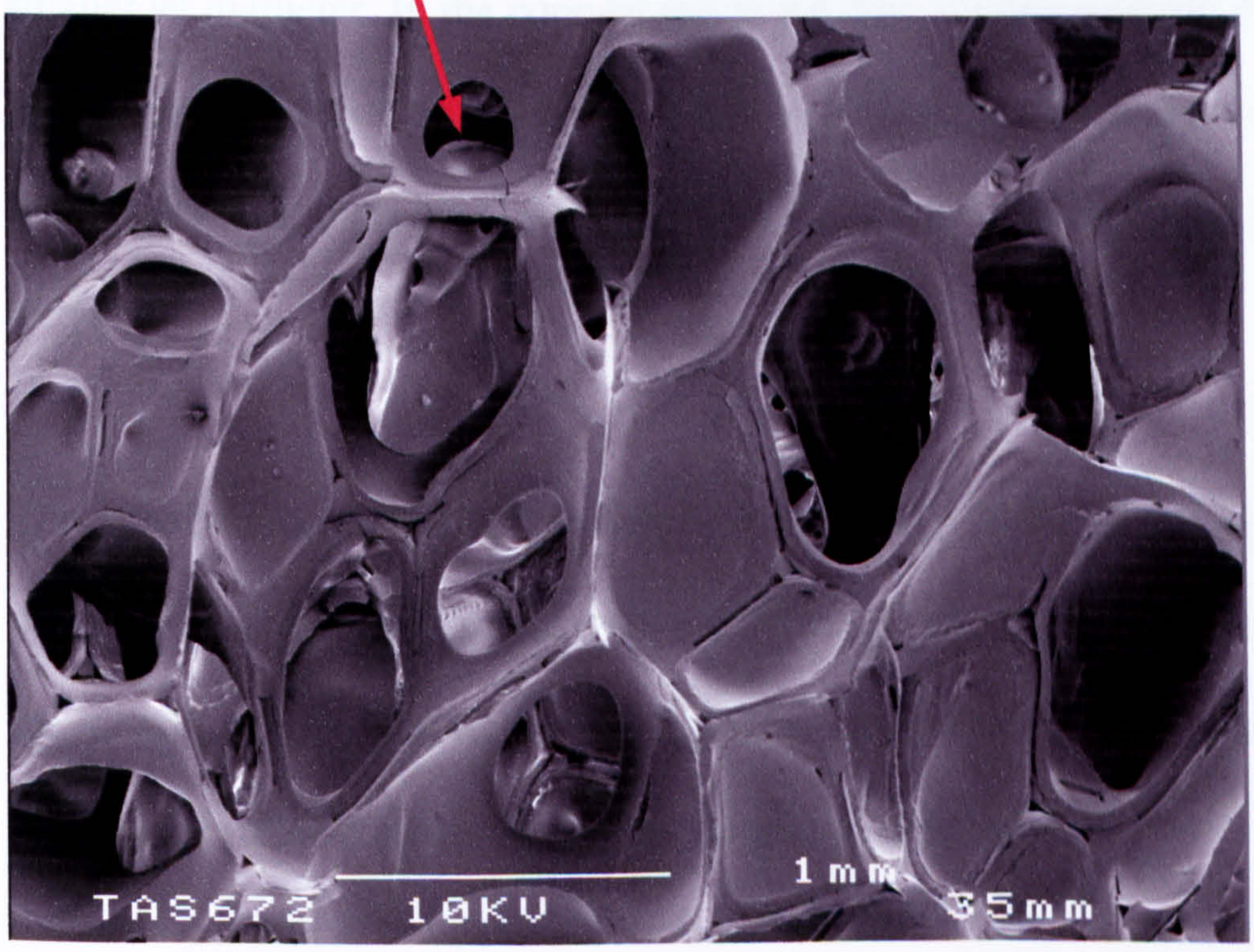

b

Figure 6.18 Ceramic foam prepared from CS5 by soaking for 3600s and pyrolyzing at 900^0C

CHAPTER 7

Conclusions and Further Work

7.1 Conclusions

This research program resulted in the following major conclusions.

1. The increase in viscosity over three orders of magnitude up to 1338 mPa s with the electrical conductivity held constant had a significant effect on the electrostatic atomization of liquids and their mixtures. A higher viscosity helped to produce stable cone-jet mode electrostatic atomization with a smaller jet diameter. In the cone-jet mode the size of relics and the droplets from which the relics originated increased significantly due to the increase in viscosity and, moreover, produced a wider size-distribution of relics and droplets.

2. The construction of applied voltage – flow rate – mode of atomization maps for ceramic suspensions over a wide range of flow rate has enabled the identification of the right combination of applied voltage and flow rate suitable for stable cone-jet mode electrostatic atomization.

3. The use of a point-like ground electrode helps to guide the ceramic suspension droplets towards a focal point.

4. Electrostatic atomization of ceramic suspensions in the cone-jet mode using pico-flow rates and a point-like ground electrode allows the

controlled deposition of fine ceramic relics (size<35μm) with a narrow size distribution. The major process control parameters are the applied voltage and flow rate, with the former decreasing the jet diameter and the latter increasing the jet diameter more significantly. Therefore, in the cone-jet mode there exists a small envelope which is suitable for producing the finest relics in a ceramic print.

5. A novel computer-controlled method of depositing ceramic droplets, according to a pre-determined architecture was developed. Thus ceramic electrostatic atomization printing (CEAP) allows a ceramic suspension flowing through a needle to be subjected to electrostatic atomization in the cone-jet mode and by using a point-like ground electrode the resulting spray can be focused and printed on a substrate placed between the needle and the ground electrode. The substrate was moved with the aid of a 2-axis computer controlled stepper motor driven system which enabled the creation of different ceramic architectures. At an applied voltage of 10kV, droplet relics in the print were in the size range 30-60μm.

6. Ceramic electrostatic atomization printing enables the printing of characters, combinations of characters and single tracks.

7. The electrostatic atomization rig was modified to incorporate three needles and three ground electrodes to enable simultaneous printing of multiple tracks.

8. Open-cell ceramic foams with a very high volume of porosity were produced by electrospraying polyurethane foam with a ceramic slurry. The fine ceramic slurry droplets produced by electrostatic atomization penetrated the polyurethane template replicating even its finest detail. Unlike in the ceramic slurry immersion method, the struts of the ceramic foams produced did not contain a central hole or cracks.

9. Sprayed foams were assembled and also subjected to deformation prior to pyrolysis to produce structures and artefacts, respectively.

7.2 Future work

Considering the research carried out in this thesis and the outcomes produced, the following recommendations for future work are made.

For a deeper understanding of the effect of liquid viscosity on the electrostatic atomization process more investigations should be carried out using silicone oils. These liquids have a very low evaporation rate and viscosities can be varied from 1mPa s to 58000mPa s. Additives are not required for adjusting other crucial liquid parameters such as electrical conductivity, surface tension etc, as they are approximately similar for these oils over a wide range of viscosities. This type of investigation will also allow for the development of scaling laws for estimating the jet diameter incorporating viscosity as a variable. The existing scaling law (equation 4.2 in Chapter 4) does not consider viscosity.

Operational maps should be drawn, for a range of liquids which are of interest to the aerosol community, for ceramic suspensions varying the volume fraction of powder and for different ceramics. As illustrated by the work carried out in Chapter 5 of this thesis, these maps can incorporate a wide range of flow rates and applied voltages i.e. from $10^{-6}m^3s^{-1}$ to $10^{-15}m^3s^{-1}$ and 0-30kV. The equipment necessary is now available in our electrostatic atomization laboratory. These maps are vital for tailoring the process control necessary to achieve a given droplet and relic size.

An in-depth study needs to be carried out with the use of a high speed camera *cum* laser system to observe phenomena at the apex of the cone and on the edges of the cone during electrostatic atomization with the increase of flow rate and applied voltage. A similar investigation should be carried out using various ground electrode configurations. Variations in droplet/relic size distributions must be studied as a function of electrode. These investigations will help in setting up a basis for modelling the process.

The electric fields encountered during electrostatic atomization of a ceramic suspension needs to be measured and modelled for various electrode configurations. The distribution of relics in the X-Y space can then be better understood as the charge/mass ratio of the droplets is a key factor in the process which responds to the electric field.

Ceramic electrostatic atomization printing has to be investigated more with respect to focussing the spray and reducing scatter. With a demand on

generating finer and finer droplets (and relics), this is a difficult proposition. The use of a gas stream or a laser to direct the droplets to their destination is suggested.

Exploring the possibilities of 2-D and 3-D printing with ceramic electrostatic atomization printing technology is suggested. Functional ceramic and metal tracks are features which can be printed this way. 3-D ceramic structures such as walls and pillars should be printed and compared with the 3D structures formed using jet-printer technology. The registration of accuracy of the droplets in ceramic electrostatic atomization printing has to be evaluated experimentally with respect to the z-axis in particular. A study of the velocity of printing and acceleration/deceleration of the device is required to generate a deeper understanding of the mechanics of the process.

The use of electrospraying ceramics for forming functional gradient micro-tubes and ceramic foams is an exciting possibility. Feasibility studies should be also carried out for using this technique to make micro-tube insulators for micro-electronics and graded foams for aerospace.

Ceramic electrostatic atomization printing and electrospraying can be useful in biomedical research. Electrospraying collagen and various polymeric materials as scaffolding for implants and cell growth should be investigated.

REFERENCES

Agarwala, M.K., Bandyopadhyay, A., Van Weeren, R., Langrana, N.A., Safari, A., Danforth, S.C., Jamalabad, V.R., Whalen, P.J., Donaldson, R. and Pollinger, J., 1996a, *Proc. Solid Freeform Fabrication Symposium,* Austin: University Of Texas at Austin, pp. 326-334.

Agarwala, M.K., Bandyopadhyay, A., Van Weeren, R., Safari, A., Danforth, S.C., Langrana, N.A., Jamalabad, V.R. and Whalen, P.J., 1996b, *Amer. Ceram. Soc. Bull.*, **75**, pp. 60-65.

Allahverdi, M., Danforth, S.C., Jafari, M. and Safari, A., 2001, *J. Euro. Ceram. Soc.*, **21**, pp. 1485-1490.

Allen A.M. and Sachs, E.M., 2000, *Metals And Materials-Korea,* **6**, pp. 589-594.

Amstead, B.H., Ostwald, P.F. and Begeman, M.L., 1969, *Manufac. Processes, 8th edition*, Wiley, NY.

Ashby, F. M., 1983, *Metall. Trans. A,* **14**, pp. 1755-1769.

Ashley, S., 1993, *Mechanical Engineering*, **115**, pp. 50-53.

Atwood, C.L., Maguire, M.C., Pardo, B.T. and Bryce, E.A., 1996, *Sampe Journal,* **32**, pp. 55-60.

Bagwell, R.B. and Messing, G.L., 1996, *Key Eng. Mat.*, **115**, 45-64.

Bailey A.G., 1988, *Electrostatic spraying of liquids*. Research Studies Press.

Bandyopadhyay, A., Panda, R.K., Janas, V.E., Agarwala, M.K., Danforth, S.C. and Safari, A., 1997, *J. Amer. Ceram. Soc.*, **80**, pp. 1366-1372.

Bandyopadhyay, A., Panda, R.K., Mcnulty, T.F., Mohammadi, F., Danforth, S.C. and Safari, A., 1998, *Rapid Prototyping J.*, **4**, pp. 37-49.

Bao X., Nangrejo M.R., and Edirisinghe M.J., 2000, *J of Mat. Sci.*, **35**, pp. 4365-4372.

Bao, X., Nangrejo, M.R. and Edirisinghe, M.J., 1999, *J. Mat. Sci.* **34**, 2495-2505.

Beaman, J.J., Barlow, J.W., Bourell, D.L., Crawford, R.H., Marcus, H.L. and Mcalea, K.P., 1997, Solid Freeform Fabrication: A New Direction In Manufacturing, *Massachusetts: Kluwer Academic Publishers*, pp. 1-49 and pp. 121-165.

Berry, E. Brown, J.M., Connell, M., Craven, C.M., Efford, N.D., Radjenovic A. and Smith, M.A., 1997, *Medical Engineering And Physics*, **19**, pp. 90-96.

Beuth, J. and Klingbeil, N., 2001, *J. Min. Met. and Mat. Soc.*, **53**, pp. 36-39.

Bibb, R., Freeman, P., Brown, R., Sugar, A., Evans, P. and Bocca, A., 2000, *Proc. Inst. Mech. Eng. Part H – J. Eng. Med.*, **214**, pp. 589-594.

Birmingham, B.R., Tompkins, J.V., Harrison S.L. and Marcus, H.L., 1996, *Proc. 2nd Int. Conf. Beam Proc. Adv. Mat.,* Srivatsan T.S. and Moore, J.J. Eds, Warrendale: Minerals, Metals And Materials Society, pp. 105-117.

Blazdell P.F. and Evans, J.R.G. 2000, *J. Mat. Proc. Tech.*, **99**, pp. 94-102.

Blazdell, P.F., Evans, J.R.G., Edirisinghe, M.J., Shaw, P. and Binstead, M.J., 1995, *J. Mat. Sci. Lett.,* **14**, pp. 1562-1565.

Borra, J.P., Camelot, D.M.A., Marijnissen, J.M.C. and Scarlett, B., 1996, *J. Aerosol Sci.* **27**, 1, pp. S181-S182.

Borra, J.P., Tombette, Y. and Ehouarn, P., 1999, *J of Aerosol Sci.* **30**, pp. 913-925.

Bose, S., Suguira, S. and Bandyopadhyay, A., 1999, *Scripta Materialia*, **41**, pp. 1009-1014.

Bourell, D.L., Marcus, H.L., Barlow, J.W. and Beaman, J.J., 1992, *Int. J. Powder Metall.*, **28**, pp. 369-381.

Bourriau, J., 1981, *Pottery from the Nile Valley before the Arab Conquest*, Cambridge, pp.15-18.

Brenzy, R. and Green, D. J., 1992, *Mat. Sci. and Tech.*, **11**, pp. 467-516.

Brezny, R. and Green, D. J., 1993a, *J. Amer. Ceram. Soc.*, **71**, pp. 145-1152.

Brezny, R., 1993b, *J. Am. Ceram. Soc.*, **76**, pp. 2185-2192.

Brockmeyer, J. W. and Pizzirusso, J. F., 1988, *J. Mat. Eng.*, **105**, pp. 39-41.

Brockmeyer, J. W., 1982, *U. S. Pat. No. 4343704*, Aug. 10.

Brockmeyer, J. W., 1986, *U. S. Pat. No. 4610832*, Sep. 9.

Brockmeyer, J. W., Aubrey, L. S. and Dore, J. E., 1989, *U. S. Pat. No: 4885263*, Dec. 5.

Brown, D. D. and Green, D. J., 1994, *J. Amer. Ceram. Soc.*, **77**, pp. 1467-1472.

Bunnell, D.E., Das, S., Bourell, D.L., Beaman, J.J. and Marcus, H.L. 1986, *Proc. Solid Freeform Fabrications Symp.*, Marcus, H.L., Beaman, J.J., Beaman, D.L., Bourell, Cannon, W.R., Morris, J.R., and Mikeska, K.R., *Adv. in Cera.*, Blum, J.R. and Cannon, W.R., Eds. *Amer. Ceram. Soc.*, **19**, Columbus, Ohio, pp. 161-174.

Carrion, A., 1997, *Rapid Prototyping J.*, **3**, pp. 99-115.

Cawley, J.D., 1997, *Proc. Int. Gas Turb. and Aeroengine Cong. and Exhib.*, Orlando, Florida, USA, New York: American Society of Mechanical Engineers, **1-6.**

Cawley, J.D., 1999, *Curr. Opinion in Sol. St. and Mat. Sci.*, **4**, 483-489.

Cawley, J.D., Heuer, A.H., Newman, W.S. and Mathewson, B.B., 1996, *Amer. Ceram. Soc. Bull.*, **75**, pp. 75-79.

Chandra, S., Di Marzo, M., Qiao Y.M. and Tartarini, P. 1996, *Fire Safety J.*, **27**, pp. 141-158.

Chao, W. J. and Chou, K. S., 1996, *Key Eng. Mater.*, **115**, pp. 93-108.

Chartier, T., Chaput, C., Doreau F. and Loiseau, M., 2002, *Euro. Ceram. Vii, Pt 1-3, Key Engineering Materials*, **206**, pp. 293-296.

Chen D-R., Pui D.Y. and Kaufman S.L., 1995, *J of Aerosol Sci.* **26**, pp. 963-977.

Chen, C.H., Edmond, M.H.J., Kelder, E.M., Meester, B. and Schoonman, J. 1999, *J of Aerosol Sci.* **30**, pp. 959-967.

Chen, D.R. and Pui, D.Y.H., 1997, *J. Aerosol Sci. and Tech.*, **27**, 367-380.

Chen, Y., Bartzos, D., Lu, Y., Niver, E., Pilleux, M.E., Allahverdi, M., Danforth, S.C., and Safari, A., 2001, *Microwave and Optical Tech. Lett.*, **30**, pp. 305-307.

Chu, T.M.G., Halloran, J.W., Hollister S.J. and Feinberg, S.E., 2001, *J. Mat. Sci. – Mat. in Med.*, **12**, pp. 471-478.

Cima, M.J., Yoo, J., Khanuja, S., Rhynerson, M. and Nammour, D., 1995, *Proc. Solid Freeform Fabrications Symp.*, In Proc. Solid Freeform Fabrication Symp., H.L. Marcus, J.J. Beaman, D.L. Beaman, D.K. Bourell, J.W. Barlow and R.H. Crawford, Eds., University Of Texas At Austin, pp. 479-488.

Cloupeau, M. and Prunet-Foch, B., 1989, *J of Electrostatics* **22**, pp. 135-159.

Cloupeau, M. and Prunet-Foch, B., 1990, *J of Electrostatics* **25**, pp. 165-184.

Cloupeau, M. and Prunet-Foch, B., 1994, *J of Aerosol Sci* **25**, pp. 1143-1157.

Colombo P., 2002, *Key Eng. Mater.*, **206-213**, pp. 1913-1918.

Colombo, P., Griffoni, M. and Modesti, M., 1998, *J. Sol-Gel Sci. Tech.*, **13**,195-199.

Conley, J.G. and Marcus, H.L., 1977, *J. Manuf. Sci. and Eng. Trans ASME*, **119**, pp. 811-816.

Coward, T.J., Watson R.M., and Wilkinson, I.C., 1999, *Int. J. Prosthodont*, **12**, pp. 20-27.

Crump, S.S., 1991a, *Intel. Desi. and Manuf. for Prototy.*, Bachi, A. and Beaman, J.J., Eds. American Society of Mechanical Engineers, New York, **50**, pp. 53-60.

Crump, S.S., 1991b, *Proc. 2nd Int. Conf. On Rapid Prototy.*, Dayton, Ohio, pp. 354-357.

Curodeau, A., Sachs E. and Caldarise, S., 2000, *J. Biomed. Mat. Res.*, **53**, pp. 525-535.

Dao, Q., Frimodig, J.C., Le, H.N., Li, X.Z., Putnam, S.B., Golda, K., Foyos, J., Das, S., Wohlert, M., Beaman, J.J. and Bourell, D.L., 1999, *Mat. & Des.* **20**, pp. 115-121.

Doreau, F., Chaput, C. and Chartier, T., 2000, *Adv. Eng. Mat.*, **2**, pp. 493-496.

Dörre, E. and Hübner,H., 1927, Alumina : processing, properties, and applications, Springer-Verlag.

Dullien, F. A. L., 1979, *Porous media fluid transport and pore structure*, Academic Press, NY, USA, pp. 1-159.

Edirisinghe, M.J., 1997, *Mater. World*, **5**, pp. 138-140.

Edirisinghe, M.J., 1998, *Proc. 1998 Tms Fall Meeting*, T.S. Srivatsan And K.A.

Fernandez de la Mora J. and Loscertales I.G., 1994, *J of Fluid Mech.* **260**, pp. 155-184.

Fernandez de la Mora J., Navascues J., Fernandez F. and Rosell-Llompart J. 1990, *J of Aerosol Sci.* **21**, 1, pp.673-676.

Fitzgerald, T. J., Michaud, V.J. and Mortensen, A., 1995, *J. Mater. Sci.*, **30**, pp. 1037-1045.

Ganan-Calvo, A.M., 1994, *J of Aerosol Sci.* **25**, pp. 309-310.

Ganan-Calvo, A.M., 1999, *J of Aerosol Sci.* **30**, pp. 863-872.

Ganan-Calvo, A.M., Davila, J. and Barrero, A., 1994, *4^h Int. Aerosol Conf. Los Angeles, Califonia* **1**, pp. 44-45.

Ganan-Calvo, A.M., Davila, J. and Barrero, A., 1997, *J of Aerosol Sci.* **28**, pp. 249-275.

Ganan-Calvo, A.M., Lasheras J.C., Davila, J. and Barrero, A., 1994 *J of Aerosol Sci.* **25**, pp. 1121-1142.

Geiger, M., Steger, W., Greul, M. and Sindel, M., 1994, *Earp Newsletter 3,*

Aarhus, A. and Malik, A.K., 1986, *Manufac. Sci.*, Ellis Harwood, Chichester, UK.

Gibson, L. J. and Ashby, M. F., 1988, *Cellular Solids*, Pergamon Press, NY, USA, pp. 1-167.

Glardon, R., Karapatis, N., and Romano, V., 2001, *Annals-Manufac.Tech.*, **50**, pp. 133-136.

Glowacki, B.A., 2000, *Supercond. Sci. Terch.*, **13**, pp. 1-8.

Gomez A. and Tang K., 1991, *Proc. 5th Int. Conf. ICLASS-91, Gaithersburg MD, USA* pp. 805-812.

Gomez A. and Tang K., 1994, *Phys. Fluids A.* **6**, pp. 404-414.

Gomez, A., Bingham, D., de Juan, L. and Tang, K., 1998, *J of Aerosol Sci.* **29**, pp. 561-574.

Grace J.M. and Marrijnissen J.M.C., 1994, *J of Aerosol Sci.* **25**, pp. 1005-1019.

Greco, A., Licciulli, A. and Maffezzoli, A., 2001, *J. Mat. Sci.*, **36**, pp. 99-105.

Greul, M. and Lenk, R., 2000, *Indust. Ceram.*, **20**, pp. 115-117.

Greul, M., 1996, *Mat. Tech.*, **11**, pp. 140-142.

Greul, M., Pintant, T., and Greulich, M., 1995, *Computers In Industry*, **28**, pp. 23-28.

Grida I. *Private communication.*

Griffin, A., Mcmillin, S., Griffin C. and Barton, K., 1997, *Proc. The 7th Int. Conf. On Rapid Prototyping,* Lightman, A.J., Chartoff, R.P., Agarwala M.K. and Pring, F. Eds. University of Dayton, USA, pp. 355-359.

Griffin, E.A., Mumm, D.R. and Marshall, D.B., 1996, *Amer. Ceram. Soc. Bull.*, **75**, pp. 65-68.

Griffith, M.L. and Halloran, J.W., 1996, *J. Amer. Ceram. Soc.*, **79**, pp. 2601-2608.

Griffith, M.L. and Halloran, J.W., 1997, *J. Appl. Phys.*, **81**, pp. 2538-2546.

Griffith, M.L., Schlienger, M.E., Harwell, L.D., Oliver, M.S., Baldwin, M.D., Ensz, M.T., Essien, M., Brooks, J., Robino, C.V., Smugeresky, J.E., Hofmeister, W.H., Wert, M.J. and Nelson, D.V., 1999, *Mat. and Des.*, **20**, pp. 107-113.

Grigoriev, D.A., Edirisinghe, M.J., Bao, X., Evans, J.R.G. and Luklinska, Z.B. 2001, *Phil. Mag. Lett.* **81**, pp. 285-291.

Hagiwara, H. and Green, D. J., 1987, *J. Amer. Ceram. Soc.*, **70**, pp. 811-815.

Hagiwara, H. and Green, D. J., 1988, *Advanced Ceramics 11.*, Elsevier Appl. Sci., NY, USA, Part **7**, pp. 105-120.

Hartman, R.P.A., Borra, J-P, Brunner, D.J., Marijnissen, J.C.M. and Scarlett, B., 1999a, *J of Electrostatics.* **47**, pp. 143-170.

Hartman, R.P.A., Brunner, D.J., Camelot, D.M.A., Marijnissen, J.C.M. and Scarlett, B., 1999b, *J of Aerosol Sci.,*. **30**, pp. 823-849.

Hartman, R.P.A., Brunner, D.J., Camelot, D.M.A., Marijnissen, J.C.M. and Scarlett, B., 2000, *J of Aerosol Sci.* **31**, pp. 65-95.

Hartman, R.P.A., Marijnissen, J.C.M. and Scarlett, B., 1997, *J of Aerosol Sci.* **28**, pp. S527-S528.

Hayati I., Bailey A.I. and Tadros T.F., 1987, *J of Coll. and Interf. Sci.* **117** (1) pp. 205-221.

Hayati I., Bailey A.I. and Tadros Th. F., 1987, *Nature* **319**, pp. 41-43.

Hebner, T.R., Wu, C.C., Marcy, D., Lu, M.H. and Sturm, J.C., 1998, *App. Phys. Lett.*, **72**, pp. 519-521.

Heinzl, J. and Hertz, C.H., 1985, *Electr. and Electron Phy.*, **65**, pp. 91-171.

Helferich, R. L. and Schenck, R. C., 1989, *U. S. Pat. No. 4871485,* Oct. 3.

Higashitani, K., Yoshida, K., Tanise N. and Murata, H., 1993, *Coll. Surf. A: Phsysiochem. Eng.*, **81**, pp. 167-175.

Hilmas, G., 1996, *Mat. Tech.*, **11**, pp.226-228.

Holland, I. J., 1963, *U. S. Pat. No. 3097930* July 16.

Hutmacher, D.W. Schantz, T. Zein, I. Ng, K.W. Teoh S.H. and Tan, K.C. 2001, *J. Biomed. Mats. Res.*, **55**, pp. 203-216.

Hutmacher, D.W., Zein, I., and Teoh, S.H., 2000, *Proces. and Fab. Adv. Mat. Viii,* D.A. Khor, T.S. Srivatsan, M. Wang, W. Zhou, F. Boey Eds., *World Sci. Publ.* pp. 201-206.

Innocentini, M. D. M., Sepulveda, P., Salvini, V.R. and Pandolfelli, V. C., 1998, *J. Amer. Ceram. Soc.*, **81**, pp. 3349-3352.

Inui, T. and Otowa, T., 1985, *Appli. Cataly.*, **14**, pp. 83-93.

Ishizaki, K., 1995, A Hot *J. Por. Mat.*, pp. 1219-227.

Ishizaki, K., Komarneni, S. and Nanko, M., 1998, *Por. Mat.: Pro. Tech. and App.*, Kluwer Academic, Dordrecht, Netherlands, pp. 181-223.

Jackson, G. and Meredith, W., *U. S. Pat. No 4547469*, Oct. 15, 1985.

Jackson, T.R. Liu, H. Patrikalakis, N.M. Sachs E.M. and Cima, M.J. 1999, *Mat. and Des.*, **20**, pp. 63-75.

Jaworek, A. and Krupa, A. 1996, *J. Aerosol Sci.*, **27**, pp. 75-82.

Jaworek, A. and Krupa, A. 1998, 3rd Int. Conf. Multiphase Flow, Lyon, France, pp. 1-8.

Jaworek, A. and Krupa, A. 1999, *J of Aerosol Sci.* **30**, pp. 873-893.

Jaworek, A., Machowski, W., Krupa, A. and Balachandran, W., 1999,. *Insti. of Phy. (UK) Conf Series.* **163**, pp. 109-114.

Keeling, M.R., 1981, *Phys. Technol.*, **12**, pp. 196-203.

Kelly, A.J., 1990, *J. Aerosol Sci. and Tech.*, **12**, pp.526-537.

Kelly, A.J., 1994, *J. Aerosol Sci..*, **25**, pp.1159-1177.

Khoshnevis, B., Bukkapatnam, S., Kwon, H. and Saito, J., 2001, *Rapid Prototyping Journal*, **7**, pp. 32-41.

Kim, K. and Turnbull, R.J., 1976, *J. App. Phys.*, **47**, pp.1964-1969.

King, B.H., Dimos, D., Yang, P. and Morissette, S.L., 1999, *J. Electroceramics*, 3, pp. 173-178.

Klebe, R., 1988, *Exp. Cell. Res.*, **179**, pp. 362-373.

Klein, L. C. and Woodman, R. H., 1996, *Key Eng. Mater.*, **115**, pp. 109-124.

Klosterman, D. A. Chartoff, R.P. Osborne, N.R. Graves, G.A. Lightman, A. Klostermann, D. Chartoff, R. Osborne, N. and Graves, G. 1997, *Ceram. Eng. Sci. Proc.*, **18**, pp. 113-120.

Knitter, R., Bauer, W., and Gohring, D., 2001a, *Adv. Eng. Mat.*, **3**, pp. 49-54.

Knitter, R., Gohring, D., Risthaus, P. and Hausselt, J., 2001b, *Microsystem Tech.*, **7**, pp. 85-90.

Kochan D. and Himmer, T., 1999, *Ceram. Forum Int.*, **76**, pp. 5-9.

Kochan, D., 1992, *Computers In Industry*, **20**, pp. 133-140.

Kodama, H., 1981, *Rev. Sci. Intr.*, **52**, pp. 1770-1773.

Kruth, J.P. Leu, M.C. and Nakagawa, T. 1998, *Cirp Annals*, **47**, pp. 525-540.

Kruth, J.P., 1991, *Annals of the CIRP*, **40**, pp. 603-614.

Kuhn, L. and Myers, R.A., 1979, *Amer. Scientist*, **240**, pp. 120-132.

Kulkarni, P. and Dutta, D., 1999, *J. Manuf. Sci. and Eng.-Trans. ASME*, **121**, pp. 93-103.

Lange, F. F. and Miller, K. T., 1987, *Adv. Ceram. Mat.*, **2**, pp. 827-831.

Lange, F.F., 1984, *J. Amer. Ceram. Soc.*, **66**, pp. 83-89.

Lannguth, K., 1995, *Ceram. Inern.*, **21**, pp. 237-242.

Lannguth, V. R., Innocentini, M. D. M. and Pandolfelli, V. C., 2000, *Amer. Ceram. Soc. Bull.*, **79**, pp. 49-54.

Lau W.W.Y. and Burns, C.M. 1973, *J. Coll. Interf. Sci.* **45**, pp. 295-302.

Law, S.E., 1989, *IEEE Trans.*, **25**, pp.1081-1087.

Le, H.P., 1998, *J. Imaging Sci. Tech.*, **42**, pp. 49-62.

Leach, R.H., Pierce, R.J., Hickman, E.P., Mackenzie M.J. and Smith, H.G., 1993, *The Printing Ink Manual,* 5th Edn., *Chapman And Hall, London*, pp.14-85.

Lee, F.C., Mills R.N. and Tulke F.E., *J. Res. Develop.*, 1984, **28**, pp. 307-313.

Lee, J.H., Prud'homme, R.K., and Aksay, L.A., 2001, *J. Mat. Res.*, **16**, pp. 3536-3544.

Lee, S.J., Jung, I.Y., Lee, C.Y., Choi S.Y. and Kum, K.Y., 2001, *Dental Traumatology*, **17**, pp. 114-119.

Lee, S-F.F., Sachs E. and Cima, M., 1995, *Rapid Prototyping J.*, **1**, pp. 24-37.

Lehmann O. and Stuke, M., 1995a, *Science*, **270**, pp. 1644-1646.

Lehmann O. and Stuke, M., 1995b, *J. De Physique Iv*, 5, pp. C5-601-C5-605.

Lehmann, O., and Stuke, M.,1994, *Mat. Lett.*, **21**, pp. 131-136.

Lemmo, A.V. Rose D.J. and Tisone, T.C. 1998, *Current Opinion In Biotech.*, **9**, pp. 615-617.

Levy, R.A. Godvri S. and Crawford, R.H. 1994, *Amer. J. Neuroradiol*, **15**, pp. 473-477.

Leyland, N.S., Evans, J.R.G. and Harrison, D.J., 2002, *J. Euro. Ceram. Soc.*, **22**, pp. 1-13.

Licciulli, A., Greco A. and Maffezzoli, A., 2000, *Indus. Ceram.*, **20**, pp. 97-99.

Lindberg, R.A., 1990, *Processes and Mat. of Manufac.* 4th Edn., Allyn and Bacon, Boston, pp.18-20.

Litborn, E., Stjernström M. and Roeraade, 1998, *J. Anal. Chem.*, **70**, 4847-4852.

Lloyd W.J. and Taub, H.H. 1988, *In: Output Hardcopy Devices,* R.C. Durbeck And Sherr, S. Eds, *Academic Press, Inc.,*. Boston USA, pp. 311-370.

Lous, G. M., Cornejo, I.A., Mcnulty, T.F., Safari, A., and Danforth, S.C., 2000, *J. Amer. Ceram. Soc.*, **83**, pp. 124-128.

Luttgens, U., Dulcks, Th. and Rollgen, F.W., 1992, *Surface Sci.*, **266**, pp.197-203.

Ma W.Y. and He, P.R., 1999, *J. Mater. Proc. Tech.*, **90**, pp. 191-197.

Mair, G., 1993, *Mastering Manufac.*, MacMillan, London.

Maxwell J. and Pegna, J., 1998, *Proc. Solid Freeform Fabrication,* H.L. Marcus, J.J. Maxwell, J.L., Pegna, J., Messia, D.V., *Applied Physics A-Materials Science And Processing*, **67**, pp. 323-329.

McALEA, K., Forderhase, P., Hejmadi, U. and Nelson, C., 1997, *Proc. 7th Int. Conf. Rapid Prototyping* Lightman, A.J., Chartoff, R.P., Agarwala M.K. and Pring, F., Eds., San Francisco, California, USA, Dayton: University Of Dayton, pp. 23-33.

Meek, T., Blake, R. and Gregory, T., 1985, *Ceram. Eng. Sci. Proc.*, **6**, pp. 1161-1170.

Meesters, G.M.H., Vercoulen, P.H.W., Marijnissen, J.C.M. and Scarlett, B. 1992, *J of Aerosol Sci.* **23**, pp. 37-49.

Melcher, J.R., 1963, *Field coupled surface waves*. Cambridge, Mass. M.I.T. USA.

Melican, M.C. Zimmerman, M.C. Dhillon, M.S. Ponnambalam, A.R.

Melvin, L.S. and Beaman, J.J., 1992, *Proc. Solid Freeform Fabrication 3rd Symposium* Marcus, H.L. Beaman, K.J. Barlow, J.W. Bournell D.L. and Craw, R.H. Eds, University Of Texas At Austin, pp. 118-123.

Mestel A.J., 1998, *J of Fluid Mech.*, **312**, pp. 313-326.

Montanaro, L., Jorand Y., Fantozzi G. and Negro A., 1998, *J. Euro. Ceram. Soc.*, **18**, pp. 1339-1350.

Morissette, S.L., Lewis, J.L., Clem, P.G., Cesarano, J. and Dimos, D.B., 2001, *J. Amer. Ceram. Soc.*, **84**, pp. 2462-2468.

Morozov, V.N., Ya, Tamara. and Kallenbach, N.R. 1998, *Int. J of Mass Spect. and Ion Proc.* **178**, pp. 143-159.

Motoki, H., *U. S. Pat. No. 4084980*, April **18**, pp. 1978.

Mott M. and Evans, J.R.G. 1999, *Mat. Sci. Eng.*, **271**, pp. 344-352.

Mott M. and Evans, J.R.G. 2001, *J. Amer. Ceram. Soc.*, **84**, pp. 307-313.

Mott, M. Song J.H. and Evans, J.R.G. 1999, *J. Amer. Ceram. Soc.*, **82**, pp. 1653-1658.

Nakajima, H., 1990, *U. S. Pat. No. 4965230*, Oct. 23.

Nangrejo M.R., Bao X. and Edirisinghe M.J., 2000 *J of Mat. Sci. Lett.*, **19**, pp. 787-789.

Nangrejo, M.R., Bao, X. and Edirisinghe, M.J., 2001, *J. Cell. Poly.*, **20**, pp.17-36.

Nelson, J.C., Vail, N.K., Barlow, J.W., Beaman, J.J., Bourell, D.L., and Marcus, H.L., 1995, *Industrial And Engineering Chemistry Research*, **34**, pp. 1641-1651.

Nettleship, I., 1996, *Key Eng. Mat.*, **115**, pp. 305-324.

Neukermans A., 1973, *J of Appl. Phy.* **44**, pp. 4769-4770.

Noakes T.J., Pavey I.D., Bray D. and Rowe R.C., 1986, US patent No 4829996.

Nur, H.M., Song, J.H., Evans, J.R.G. and Edirisinghe, M.J., 2002, *J. Mater. Sci: Mat. in Electronics*, **13**, pp. 213-219.

Okuda, H. and Kelly, A.J., 1996, *J of Phy. of Plas.* **3**, pp. 2191-2196.

Oldenburg, K.R. Zhang, J-H. Chen, T. Maffia, A. Blom, K.F. Combs A.P. and Chung, T.D.Y. 1998, *J. Biomolecular Screening*, **3**, pp. 55-62.

Önnerfjord, P. Nilsson, J. Wallman, L. Laurell T. and Marko-Varga, G., 1998, *Anal. Chem.*, **70**, pp. 4755-4760.

Ono, I. Abe, K. Shiotani S. and Hirayama, Y., 2000, *Journal Of Craniofcial Surgery*, **11**, pp. 527-537.

Otzuka, M. and Akiyama, T., 1995, Vincenzinizini, Techna., Italy, pp. 2431-2438.

Parkin, C.S., 1973, *J. Fluid Mech.*, **32**, pp.187-193.

Pegna, J., 1997, *Autom. in Constr.*, **5**, pp. 427-437.

Peng, H. X., Fan, Z. and Evans J. R. G., 2000, *Ceram. Intern.*, **26**, pp. 887-895.

Petzold, R. Zeilhofer H.F. and Kalender, W.A. 1999, *Comput. Med. Imaging And Graphics*, **23**, pp. 277-284.

Pham, D.T. and Gault, R.S., 1998, *Int. J. Mach. Tools Manuf.*, **38**, pp. 1257-1287.

Pham, D.T. and Wang, X., 2000a, *Proc. Int. Mech. Eng. B. J. Eng. Manuf.*, pp. 214, 425-430.

Pham, D.T., 2000b, *Proc. Int. Mech. Eng. C J. Mech. Eng. Sci.*, **214**, pp. 635-640.

Pham, D.T., Dimov S.S., and Gault, R.S., 1999, *Int. J. Adv. Manuf. Tech.*, **15**, pp. 674-682.

Philipse, A. P. and Schram, H., 1991, *J. Amer. Ceram. Soc.*, **74**, pp. 728-732.

Porter, N.L. Pilliar R.M. and Grynpas, M.D. 2001, *J. Biomedical Mat. Res.*, **56**, pp. 504-515.

Pryor, M. J. and Gray, T. J., 1977, *U. S Pat. No. 4056586,* Nov. 1.

Ramsey, B.J. Evans P.S.A. and Harrison, D. 1997, *J. Electronic Manufact.*, **7**, pp. 63-67.

Rangarajan, S., Qu, G., Venkataraman, N., Safari, A. and Danforth, S.C., 2000, *J. Amer. Ceram. Soc.*, **83**, pp.1663-1669.

Ravault, F. E. G., 1974.*U. S Pat. No. 3845181,* Oct. 29,

Ravault, F. E. G., 1975. *U.S Pat. No. 3907579,* Sep. 23,

Rayleigh Lord F., 1878, *Proc. Lon. Math. Soc.* **11**, pp. 4-13.

Rayleigh, J.W.S. 1882, *Philos. Mag.*, **14**, pp. 184-186.

Risthaus, P., Gohring, D. and R. Knitter, 2002, *Euro Ceram. Vii, Pt1-3, Key Eng. Mat.*, **206**, pp. 337-340.

Rosell-Llompart, J. and Fernandez de la Mora, J. 1994, *J of Aerosol Sci.* **25**, pp. 1093-1119.

Sachs, E. Cima, M. Cornie, J. Brancazio, D. Bredt, J. Curodeau, A. Fan, T. Khanuja, S. Lauder, A. Lee J. and Michaels, S. 1993, *Cirp Annals,* **42**, pp. 257-260.

Sachs, E. Cima, M. Williams, P. Brancazio D. and Cornie, J. *1992, J. Eng. Ind.,* **114**, pp. 481-488.

Sachs, E.M. 2000.*Us Patent 6036777, March 14,*

Safari, A. and Danforth, S.C., 1999, *Ferroelectrics*, **231**, pp. 731-745.

Safari, A., 1999, *Mat. Res. Innovat.*, **2**, pp. 263-269.

Safari, A., Danforth, S.C., Panda, R., and Mcnulty, T., 1998, *J Korean Phy. Soc.*, **32**, S1733-S1736.

Saggio-Woyansky, J., Scott, C. E. and Minnear, W. P., 1992, *Amer. Ceram. Soc. Bull.*, **71**, pp. 1674-1682.

Sakka, S., Kozuka, H. and Adachi, T., 1993, *Ceramic Trans.*, **31**, pp. 27-40.

Salata, O.V., Hull, P.J. and Dobson, P.J. 1997. *J of Adv. Mat.* **9**, pp. 413-417.

Salvin V.R., Innocentini M.D.M. and Pandolfelli V.C., 2000, *Amer. Ceram. Soc. Bull.*, **79**, pp. 49-54.

Sato, M., Takahashi, H., Awazu, M., and Ohshima, T. 1999, *J of Electrostatics*. **46**, pp. 171-176.

Schneider, J.M., Lindblad, N.R., Hendricks, C.D. and Crowley, J.M., 1976, *J. Appl. Phys*, **38**, 2599-2605.

Schnider J.M., Lindblad N.R., Hendricks C.D. and Crowley J.M. 1967, *J of Appl Phys.* **38**, pp. 2599-2605.

Schwartzwalder K., Somers H. and Somers A.V., 1963. US Patent 3,090,094 of May 21,

Schweizer J.W., and Hanson D.N., *J of Coll. and Interf. Sci.* **35** (3) pp. 417-423.

Sepulveda, P. and Binner, J. G. P., 1999, *J. Euro. Cerami. Soc.*, **19**, pp. 2059-2066.

Sepulveda, P., 1997, *Amer. Ceram. Soc. Bull.*, **76**, pp. 61-65.

Shapiro, M. S., 1992, *Light Metals, The Minerals, Metals And Materials Society*, Virginia, USA, pp. 895-898.

Shepherd, P.R. Evans, P.S.A. Ramsey B.J. and Harrison, D.J. 1997, *Electronics Lett.*, **33**, pp. 483-484.

Sheppard, L. M., 1993, *Ceram. Trans.*, **3**, pp. 13-23.

Sherman, A. J., Tuffias, R. H. and Kaplan, R. B., 1991, *Amer. Ceram. Soc. Bull.*, **70**, pp. 1025-1029.

Simchi, A., Petzoldt, A. and Pohl, H., 2001, *Int. J. Powder Metall.*, **37**, pp. 49-61.

Smith, D.P.H. 1986, *IEEE Trans. Ind Appl.* **IA-22**, pp. 527-535.

Song J.H., Edirisinghe M.J. and Evans J.R.G. 1999, *J of the Amer. Ceram. Soc.* **82**, pp. 33-74.

Stitzel, J.D., Bowlin, G.L., Mansfeild, K., Wnek, G.E. and Simpson, D.G. 2000, *Int. SAMPE Tech. Conf.* **32**, pp. 205-211.

Stoker, N.G. Mankovich N.J. and Valentino, D. 1992, *J. Oral And Maxillofacial Surgery*, **50**, pp. 466-471.

Subramanian, P.K. and Marcus, H.L., 1995, *Mater. Manuf. Processes*, 10, 689-706.

Subramanian, P.K., Zong, G. and Marcus, H.L., *Solid Freeform Fabrication Proceedings*, Marcus, H.L., Beaman, J.J., Barlow, J.W., Bourell, D. L. and Crawford, R.H., Eds, 1992, pp. 63-71.

Sun L. and Shaw, L.L. 1999a, *Metal. and Mat. Trans. A*, **30**, pp. 2549-2551.

Sun, L. Crocker, J.E. Shaw L.L. and Marcus, H.L. 1999b, *MRS Symp. Proc.*, **542**, pp. 37-44.

Sundermann, E., 1973. *U. S. Pat. No. 3745201*, July 10,

Tang, K. and Gomez, A., 1994, *Phys. Fluids*, **7**, 2317-2332.

Tang, K. and Gomez, A., 1995, *J of Coll. and Interf. Sci.* **175**, pp. 326-332.

Tang, K. and Gomez, A., 1996, *J of Coll. and Interf. Sci.* **184,** pp. 500-511.

Tantry, P. K., Misra, S. N. and Shashi M. A. L., 1993, *Ceram. Trans.*, **31**, pp. 89-99.

Tay B.Y. and Edirisinghe M.J. 2002, *Proc. of the Royal Soc.* **458,** 2039-2051.

Tay, B.Y. and Edirisinghe, M. J. 2001, *J of Mat. Res.* **16,** pp. 373-384.

Taylor, G.I., 1964 *Proc. of the Royal Soc.* **280,** pp. 383-397.

Teng K.F. and Vest, R.W. 1987, *IEEE Trans. Comp. Hybrids and Manuf. Tech.*, **12**, pp. 545-549.

Teng K.F. and Vest, R.W. 1988, *IEEE Trans. Comp. Hybrids And Manuf. Tech.*, **11**, pp. 291-297.

Teng, W.D., Huneiti, Z.A., Machowski, W., Evans, J.R.G., Edirisinghe, M.J. and Balachandran, W. 1997, *J of Mat. Sci. Lett.* **16**, pp. 1017-1019.

Tohver, V., Morissette, S.L., Lewis, J.A., Tuttle, B.A., Voigt, J.A., and Dimos,

Trygg, L., 1994, *Int. J. Human Factors In Manuf.*, **4**, pp. 321-338.

Trouton, F.T.,1906, *Proc. of the Royal Soc. A.* **77**, pp. 426-440.

Tseng, A.A. and Tanaka, M., 2001, *Rapid Prototyping J.*, **7**, pp. 6-17.

Tulliani J-M., Montanaro L., Bell T.J. and Swain M.V, 1999, *J. Amer. Ceram. Soc.* **82**, pp. 961-968.

Turnbull, R.J., 1992, *IEEE Trans. Appl.* **28**(6), pp. 1432-1438.

Tyberg. J. and Bohn, J.H., 1999, *Mat. and Design*, **20**, pp. 77-82.

Uhland, S.A. Holman, R.K. Cima, M.J. Sachs E. and Enokido, Y. 1999, *MRS Symp.Proc.*, **542**, pp. 153-158.

Uziel, Y. 1997, *SME Technical Paper 98-117-2*, pp. 1-8.

Vail, N.K. Swain, L.D. Fox, W.C. Aufdlemorte, T.B. Lee G. and Barlow, J.W. 1999, *Mat. and Design*, **20**, pp. 123-132.

Vail, N.K., and Barlow, J.W., *Solid Freeform Fabrication Proceedings*, Marcus, H.L., Beaman, J.J., Barlow, J.W., Bourell, D. L. and Crawford, R.H., Eds, 1992, pp. 124-130.

Vander J. Sloten, R. Van Audekercke and G. Van Der Perre, 2000, *Ind. Ceram.*, **20**, pp. 109-112.

Vedula V.R., Green D.J. and Hellman J.R., 1999,. *J. Amer. Ceram. Soc.*, **82**, pp. 961-968.

Vedula, V. R., Green D. J. and Hellman J. R., 1998, *J. Euro. Ceram. Soc.*, **18**, pp. 2073-2080.

Velenga, S.J. and Klinkenberg, A., 1965, *Chem. Eng. Sci.*, **20**, pp. 923-948.

Volpato, N., Childs, T.H.C., Stewart, T.D. and Watson, P., *J. Eng. Manuf.*, 2001, **215**, pp. 873-876.

Vonnegut, B. and Neubauer, R.L. 1952, *J of colliod Sci.* **7**, pp. 616-622.

Wallenberger, F.T., *Science*, 1995, **267**, pp. 1274-1275.

Walton, A.J. Stevenson, J.T.M. Haworth, L.I. Fallon, M. Evans, P.S.A.

Wang, L.W., Yanez, J., Sigmund, W.M., and Aldinger, F. 2000, *Ind. Ceram.*, **20**, pp. 93-94.

Wanke, M.C. Lehmann, O. Muller, K. Wen Q.Z. and Stuke, M. *Science*, 1997, **275**, pp. 1284-1286.

Webb, P.A. 2000, *J. Med. Eng. & Techn.*, **24**, pp. 149-153.

Weber, C., 1931, Zum Zerfall eines Flussigkeitsstrahle. Z fur Angrew Math, *Und. Mech.*, **11**, pp. 136-143.

White H.J., 1963, *Industrial Electrostatic Precipitation*. Addison-Wesley pub. Company INC.

Wu, M.L., Zhao, W.H., Tang, Y.P., Li, D.C. and Lu, B.H., 2001, *Rapid Prototyping Journal*, **77**, pp. 268-274.

Xiang, Q.F. Evans, J.R.G. Edirisinghe M.J. and Blazdell, P.F. 1997, *Proc. Inst. Mech. Eng: J. Eng. Manuf.*, **211b**, pp. 211-214.

Xiong, Z. Yan, Y.N. Zhang R.J. and Sun, L. *Scripta Mater.*, 2001, **45**, pp. 773-779.

Yan, Y.N., Zhang, R.J., Hong, G.D., and Yuan, X.M., 2000, *Mat. and Design*, **21**, pp. 93-99.

Yang, P., Dimos, D., Rodriguez, M.A., Huang, R.F., Dai, S. and Wilcox, D., 1999, *MRS Symp. Proc.*, **542**, pp. 159-164.

Yarwood, J. C., Dore, J. E. and Preuss, R. K., 1978.*U. S, Pat. No. 4075303*, Feb. 21.

Yarwood, J. C., Dore, J. E. and Preuss, R. K., *U. S. Pat. No. 3962081*, June 8, 1976.

Yoshino, I. and Iwami, I., 1980. *U. S. Pat. No. 4207113.*

Young, J.S., Fox, S.R., and Anseth, K.S., 1999, *J. Manuf. Sci. & Eng. – Trans ASME,* **121**, pp. 474-477.

Yuen, M.C., 1968, *J.Fluid Mech.,* **33**, pp. 151-165.

Z.W.Zhao and L. Laperriere, 2000, *Int. J. Prod. Res.*, **38**, pp. 69-83.

Zein, I. Hutmacher, D.W. Tan K.C. and Teoh, S.H. 2002, *Biomaterials*, **23**, pp. 1169-1185.

Zeleny J., 1914, *Phy. Rev.* **3**, pp. 69-91.

Zeleny J., 1915, *Proc. Camb. Phil. Soc.* **18**, pp. 71-83.

Zeleny J., 1917, *Phy. Rev.* **10**, pp. 1-16.

Zhang, Y.M. Han, J.C. Zhang, X.H. He, X.D. Li Z.Q. and Du, S.Y. 2001, *Mat. Sci. and Eng.*, **299**, pp. 218-224.

Zhao, X. Evans, J.R.G. Edirisinghe M.J. and Song, J.H. 2002, *J. Mat. Sci.*, **37**, pp. 1987-1992.

Ziemian, C.W., and Crawn, P.M., 2001, *Rapid Prototyping J.*, **7**, pp. 138-147.